

Univerza v Ljubljani

Fakulteta za elektrotehniko

Bor Kos

# Numerično določanje elektromagnetnih količin v človeškem telesu za preventivno in terapevtsko uporabo

DOKTORSKA DISERTACIJA

Mentor: izr. prof. dr. Tadej Kotnik

Somentor: doc. dr. Peter Gajšek

Ljubljana, 2013



University of Ljubljana

Faculty of Electrical Engineering

Bor Kos

# Numerical computation of electromagnetic fields in the human body for preventive and therapeutic applications

DOCTORAL DISSERTATION

Mentor: prof. Tadej Kotnik, Ph. D.

(University of Ljubljana, Slovenia)

Peter Gajšek, Ph. D.

Ljubljana, 2013



## Preface

---

The present PhD thesis is the result of numerical modeling and algorithm development carried out during the PhD study period at the Laboratory of Biocybernetics, Faculty of Electrical Engineering, University of Ljubljana. The work on human exposure to electromagnetic fields was performed in collaboration with the Institute of Non-Ionizing Radiation, Ljubljana. The results of the presented work have been published in the following papers in international scientific journals:

**Paper 1:** Kos B, Valič B, Kotnik T and Gajšek P 2011 Exposure assessment in front of a multi-band base station antenna *Bioelectromagnetics* **32** 234–42

**Paper 2:** Kos B, Valič B, Miklavčič D, Kotnik T and Gajšek P 2011 Pre- and post-natal exposure of children to EMF generated by domestic induction cookers *Phys Med Biol* **56** 6149–60

**Paper 3:** Kos B, Valič B, Kotnik T and Gajšek P 2012 Occupational exposure assessment of magnetic fields generated by induction heating equipment—the role of spatial averaging *Phys Med Biol* **57** 5943–53

**Paper 4:** Miklavčič D, Snoj M, Zupanic A, Kos B, Cemazar M, Kropivnik M, Bracko M, Pecnik T, Gadzijevec E and Sersa G 2010 Towards treatment planning and treatment of deep-seated solid tumors by electrochemotherapy *Biomed Eng Online* **9** 8

**Paper 5:** Kos B, Zupanic A, Kotnik T, Snoj M, Sersa G and Miklavčič D 2010 Robustness of treatment planning for electrochemotherapy of deep-seated tumors *J Membr Biol* **236** 147–53

**Paper 6:** Edhemovic I, Gadzijevec E M, Breclj E, Miklavčič D, Kos B, Zupanic A, Mali B, Jarm T, Pavliha D, Marcan M, Gasljevec G, Gorjup V, Music M, Vavpotic T P, Cemazar M, Snoj M and Sersa G 2011 Electrochemotherapy: a new technological approach in treatment of metastases in the liver *Technol Cancer Res Treat* **10** 475–85

**Paper 7:** Zupanic A, Kos B and Miklavčič D 2012 Treatment planning of electroporation-based medical interventions: electrochemotherapy, gene electrotransfer and irreversible electroporation *Phys Med Biol* **57** 5425–40

Unless otherwise noted, all illustrations are the author's own work.



## Acknowledgements

---

I am greatly indebted to my mentor Tadej Kotnik, who has introduced me into the world of science with invaluable advice, guidance and examples, for which I am deeply grateful. Thanks for teaching me how to write scientific papers and grants and for all the fruitful discussions, be they work-related or not.

Thanks to Peter Gajšek, who was always encouraging me to do more and better research while trusting my initiative and ideas.

I would also like to thank my parents, for proofreading the manuscript and for always being supportive and encouraging me to do more.

Thanks to all the great colleagues at the Laboratory of Biocybernetics. Special thanks to those of you with whom I have had the pleasure of working on some of the papers included in this thesis, and thanks to all the rest for making it a friendly and welcoming workplace.



## Table of contents

---

Preface .....	V
Table of contents .....	IX
Abstract .....	XIII
Razširjen povzetek v slovenskem jeziku .....	XV
Uvod .....	XV
Bioelektromagnetika .....	XV
Električni pojavi v živih celicah .....	XVI
Raziskave varnosti elektromagnetnih sevanj .....	XVIII
Elektroporacija – pojav pri visokih električnih poljih .....	XIX
Metode .....	XX
Rezultati in diskusija .....	XXI
Poklicna izpostavljenost večpasovnim baznim postajam .....	XXI
Izpostavljenost otrok magnetnim poljem indukcijskih kuhališč .....	XXIV
Prostorsko povprečenje izmerjenih vrednosti pri vrednotenju izpostavljenosti .....	XXV
Načrtovanje zdravljenja za terapije na osnovi elektroporacije in analiza robustnosti .....	XXVII
Zaključek .....	XXXIII
Izvirni prispevki k znanosti .....	XXXIV
Poklicna izpostavljenost večpasovnim baznim postajam .....	XXXIV
Izpostavljenost občutljivih skupin magnetnim poljem indukcijskih kuhališč .....	XXXIV
Metoda za prostorsko povprečenje izmerjenih magnetnih polj .....	XXXV
Metoda za načrtovanje zdravljenja globoko ležečih tumorjev .....	XXXV
Inovativne vizualizacije za načrtovanje zdravljenja z metodami na osnovi elektroporacije .....	XXXV
Introduction .....	1

## Table of contents

Bioelectromagnetics – the science of interaction of electromagnetic phenomena with biological matter	1
Physiological electromagnetism – the endogenous electromagnetic fields in humans.....	4
The cellular membrane.....	4
Transmembrane transport in general .....	5
Membrane potential.....	6
Research of safety of electromagnetic fields in humans.....	8
Electromagnetic fields safety standards.....	8
Mechanisms of interaction.....	9
Biological effects.....	11
Electroporation - interaction at very high electric fields .....	12
The electroporation phenomenon.....	12
Tissue during the application of electroporation pulses.....	14
Electroporation applications in medicine.....	14
Treatment planning at tissue level .....	15
Aims.....	17
Research papers .....	19
Paper 1 .....	22
Paper 2.....	32
Paper 3.....	46
Paper 4.....	58
Paper 5.....	68
Paper 6.....	76
Paper 7.....	88
Discussion .....	105
Discussion of EMF safety related papers.....	105
Exposure to multi-band base station antennas .....	105
Exposure of children to magnetic fields from induction cookers .....	107

The role of spatial averaging of measured fields in exposure assessment..... 109

Discussion of electroporation and treatment planning papers..... 111

    Towards treatment planning..... 111

    Robustness of treatment planning..... 112

    Treatment of liver metastasis with ECT ..... 114

    Treatment planning of other electroporation based treatments and advanced visualizations ..... 115

Conclusion and future work ..... 119

Original contributions ..... 121

    Occupational exposure to multi-band base-station antennas ..... 121

    Determination of exposure of sensitive groups to fields generated by induction cookers..... 121

    Method for spatial averaging of measured magnetic fields ..... 121

    Method for treatment planning of deep-seated tumours..... 122

    Novel visualizations for electroporation-based treatment planning ..... 122

References..... 123



## Abstract

---

Bioelectromagnetics is defined as the study of interactions of electromagnetic phenomena with living matter. Electromagnetic fields in the macroscopic world are governed by laws compiled into the famous four Maxwell's equations. Even though the equations are very compact and elegant in the written form, solving them analytically is impossible in all but the simplest of cases. Since measurements inside the human body are difficult and invasive, the best available possibility for determining electromagnetic quantities inside the human body is by using numerical methods.

In the present doctoral dissertation, I first give a brief history of the research on bioelectromagnetics, then present the endogenous electric phenomena of human cells. In the continuation I outline the basic mechanisms of interactions of exogenous electromagnetic fields with the human body and their biological effects. Next, I present the biological effects of electromagnetic fields in the body, that the exposure standards aim to prevent. I briefly discuss the possibility of electromagnetic fields causing and recap the main findings, which indicate that highly exposed could have a higher probability of developing cancer. The interaction at very high applied electric fields is dominated by the phenomenon of electroporation, which causes an increase in the permeability of the cellular membrane.

In the scientific papers included in this thesis, I set out to determine electromagnetic quantities in the human body using the finite-difference time-domain method and the finite element method for preventive and therapeutic applications. In the area of preventive applications, I focus on determining occupational exposure to multi-band base station antennas, determining the exposure of children and pregnant women to magnetic fields generated by induction cookers, and determining occupational exposure to induction heating equipment with the evaluation of spatial averaging of measured fields. In the area of therapeutic applications, I focus on treatment planning for electroporation-based treatments, but mainly on electrochemotherapy treatment planning for treatment of deep-seated tumours. I also analyse the robustness of the developed treatment plans and the sensitivity of the treatment to small errors during treatment execution. For presenting the treatment plans in an user-friendly way, I have developed several novel visualisation techniques, which focus on clearly presenting the most crucial data relevant to the success of the treatment.

The work on safety of human exposure has built upon some issues that were not thoroughly defined in the exposure guidelines. The 2010 ICNIRP guidelines have brought the change in the quantity used as a

## Abstract

basic restriction at low frequencies (*in situ* electric field instead of current density used in the old Guidelines), and an increase in the reference levels for magnetic fields. Results show that the change in the basic restrictions and the reference levels didn't introduce the risk of overexposure, even where sensitive groups such as children and pregnant women are considered. Spatial averaging can also be used instead of more time- and cost-demanding numerical determination of exposure for determining exposure compliance in cases where the magnetic fields in free space are slightly above the reference levels and the magnetic fields are highly inhomogeneous.

Numerical methods have also been successfully applied to the challenge of producing treatment plans for electroporation-based treatments. Numerical modelling allows for the production of robust treatment plans with automatic optimization of electrode voltages and positions, which allow the performing physicians to have confidence in the success of the treatment. This could eventually lead to more difficult cases being treated, where other options for efficacious treatment are limited. The developed methods and visualisations should also enable physicians to be less dependent on engineers and with appropriate software solutions should be able to prepare treatment plans themselves.

## Razširjen povzetek v slovenskem jeziku

---

### Uvod

#### **Bioelektromagnetika**

Bioelektromagnetika je veda, ki preučuje medsebojne vplive elektromagnetnih pojavov (polj, napetosti in tokov) z živimi organizmi. Eden izmed prvih raziskovalcev električnih pojavov – Luigi Galvani – je v 18. stoletju opazil, da lahko električne iskre povzročijo gibanje žabjih nog (Galvani 1791). Njegovo teorijo o obstoju živalske elektrike je sicer zavrnil njegov sodobnik Alessandro Volta (Piccolino 1998), vendar je ta prvi poskus vseeno nakazal, da ima elektrika pri živih bitjih pomembno vlogo. Do sodobnih raziskav elektromagnetnih pojavov v človeškem organizmu je seveda moralo preteči še veliko časa. Kljub napredku v napravah in merilnih tehnikah je neposredno merjenje elektromagnetnih količin v telesu zahtevno in invazivno, zato se v praksi uporablja le približek, elektromagnetne količine pa se merijo v fantomih. Fantomi so približki človeškega telesa, napolnjeni s prevodno tekočino ali gelom, z električnimi lastnostmi, podobnimi človeškemu telesu. Z ustreznimi merilnimi sondami je mogoče v prevodni tekočini izmeriti elektromagnetna polja in iz tega sklepati na polja v človeškem telesu.

Namesto neposrednih ali posrednih meritev v človeškem telesu pa je mogoče elektromagnetne količine neposredno izračunati, saj so znani fizikalni zakoni, ki v makroskopskem svetu opisujejo obnašanje elektromagnetnih pojavov. Eden najpomembnejših prispevkov na tem področju je bilo poenotenje vseh dotedanjih rezultatov poskusov v Maxwellove enačbe, ki popolnoma opišejo medsebojno odvisnost električnega, magnetnega in elektromagnetnega polja. Kljub matematično elegantnemu zapisu štirih Maxwellovih enačb pa je njihovo reševanje zahtevno in razen v najbolj preprostih primerih analitične rešitve ne obstajajo. Zato je za reševanje pogosto treba uporabiti eno izmed numeričnih metod. Pri določanju vpliva elektromagnetnih polj na ljudi sta najbolj pogosto uporabljani metoda končnih elementov (*FEM - finite element method*) in metoda končnih diferenc v časovnem prostoru (*FDTD – finite-difference time-domain*) (Hand 2008).

Pri metodi končnih elementov se prostor razdeli na elemente, kjer se neznana količina aproksimira s preprosto matematično funkcijo. Reševanje parcialnih diferencialnih enačb se tako prevede v reševanje večjega števila algebraičnih enačb. Mreža se lahko z gostoto prilagodi oblikam geometrije problema, tako da so kompleksne strukture opisane natančno, pri enostavnih pa se prihrani pri zahtevnosti izračuna

(potrebe po spominu in računskih ciklih). Metoda končnih diferenc v časovnem prostoru uporablja končne diference drugega reda za izražanje parcialnih odvodov po prostorskih koordinatah. S preskakovalnim algoritmom se v prvem ciklu izračuna električno polje iz magnetnega, v naslednjem ciklu pa magnetno polje iz električnega. Z ustrezno izbiro časovnega koraka je algoritem numerično stabilen in omogoča natančne in numerično učinkovite izračune širjenja elektromagnetnega polja v prostoru.

V zadnjih nekaj desetletjih se je izredno razmahnila uporaba novih tehnologij, ki bodisi za komunikacijo, bodisi kot stranski produkt, proizvajajo elektromagnetna polja. Tako je narasla tudi izpostavljenost prebivalstva umetnim virom EMS, še posebej pa delavcev, ki delajo v bližini nekaterih vrst naprav. Z rastjo uporabe tehnologij se je seveda pojavilo tudi vprašanje, ali imajo lahko te tehnologije kakšen škodljiv vpliv na človeški organizem. Raziskave o vplivu elektromagnetnih polj na ljudi so potekale na dva temeljna načina. Pri laboratorijskih poskusih s prostovoljci so določali mejne vrednosti, pri katerih lahko ljudje občutijo neželene učinke, in na podlagi teh rezultatov so bile tudi določene trenutne smernice za zaščito pred elektromagnetnimi sevanji. Hkrati pa so potekale tudi epidemiološke raziskave, pri katerih so poskušali raziskovalci povezati izpostavljenost določenim virom sevanja s povečanjem tveganja za nastanek določenih bolezni.

Sočasno z razvojem tehnologij, ki jih uporabljamo v vsakodnevnem življenju, je potekal tudi razvoj različnih načinov uporabe elektromagnetnih pojavov za terapevtske namene. Nekatere aplikacije, ki se že uporabljajo v klinikah, so npr. elektrokirurški noži (Jackson 1970), pospeševanje celjenja zlomov (Canè *et al* 1993), lajšanje bolečin (Trock *et al* 1994), zdravljenje tumorjev z radiofrekvenčno ablacijo (Curley *et al* 1999), vnos učinkovin preko kože (Levin *et al* 2005) ter zdravljenje tumorjev z elektrokemoterapijo (Sersa *et al* 2008).

### **Električni pojavi v živih celicah**

Za raziskovanje elektromagnetnih pojavov v človeškem organizmu je treba podrobneje poznati vlogo električnih pojavov pri biokemičnih procesih v celicah, ki so osnovne organizacijske enote živih bitij. Evkariotske in prokariotske celice so obdane s tanko membrano, sestavljeno iz fosfolipidnih molekul, ki so sestavljene iz hidrofobnih (vodo-odbijajočih) maščobnih repov ter hidrofilnih (vodo-privlačnih) fosfatnih glav. Zaradi svoje kemične strukture se fosfolipidi v vodnem okolju sami orientirajo v dvosloj, kjer so hidrofobni repi združeni v njegovi notranjosti, hidrofilne fosfatne glave so na obeh zunanjih površinah dvosloja v stiku z vodo. Dvosloj navadno tvori zaključene ploskve (vezikle), ki so napolnjeni in obdani z vodnim okoljem. Biološka celica je tak vezikel, ki vsebuje vse biomolekule in strukture, ki jih celica potrebuje za svoje delovanje, lipidni dvosloj, ki obdaja celice, pa se imenuje celična membrana.

Celična membrana je zelo tanka (5-7 nm) ter ne prepušča električno nabitih ionov in večjih molekul. V živih celicah so v membrano vgrajene tudi številne beljakovine; te opravljajo funkcije receptorjev, sodelujejo pri prenosu snovi preko celične membrane in sestavljajo celični skelet, ki daje celicam obliko. S pomočjo celične membrane in membranskih beljakovin celice vzdržujejo urejeno in nadzorovano okolje in nadzorujejo prehajanje snovi preko membrane z različnimi mehanizmi. Difuzija je gibanje snovi ali energije iz področja z višjo koncentracijo v področje z nižjo koncentracijo, torej v nasprotni smeri koncentracijskega gradienta. Majhne nenabite molekule lahko prehajajo celično membrano z difuzijo, z večanjem njihove molekulske mase pa postaja difuzija praktično nemogoča. Ionski kanali so pore v celični membrani, ki jih tvorijo posebne beljakovine. Kanali omogočajo selektivno prehajanje električno nabitih ionov in so tipično selektivni, torej omogočajo prehajanje samo enemu tipu iona ali molekule. Številni kanali so lahko tudi aktivni, kar pomeni, da se lahko odpirajo ali zapirajo v odzivu na določene dražljaje (vezava ustrezne molekule, ustrezna transmembranska napetost ali mehanski dražljaji). Črpalke so posebne beljakovine in v nasprotju s kanali omogočajo črpanje tudi v smeri koncentracijskega gradienta. Ker je tak proces podoben valjenju kamna v hrib, potrebujejo črpalke za svoje delovanje energijo. Zadnji mehanizem prehajanja membrane predstavlja endo- oziroma eksocitoza. Pri endocitozi se majhen del membrane iz površine celice uviha, kar ustvari majhen žep. Ko se ustje žepka zapre, se ta odcepi od celične membrane v obliki vezikla, celična membrana pa se zmanjša za površino, ki jo predstavlja vezikel. V nobenem trenutku pa ne pride do stika notranjosti vezikla ali zunajcelične tekočine s citosolom. Eksocitoza je podoben postopek, ki poteka v obratni smeri.

Z zgoraj naštetimi mehanizmi celice vzdržujejo ustrezno sestavo citosola. Zaradi delovanja aktivnih črpalk in ionskih kanalov se v celicah vzpostavi neravnovesje določenih ionov znotraj celice v primerjavi z zunajceličnim prostorom ( $K^+$  ter  $H^+$  ioni so bolj pogosti znotraj celic,  $Na^+$  ter  $Ca^+$  ioni pa zunaj celic). Posledica procesov uravnavanja koncentracij ionov pa je, da se citosol v mirovanju nahaja na nižjem električnem potencialu od zunanosti. To razliko potencialov različni avtorji imenujejo *membranski potencial*, *transmembranski potencial*, *membranska napetost* ali *transmembranska napetost*. Po definiciji napetosti kot razlike dveh električnih potencialov je s fizikalnega gledišča najbolj ustrezen izraz *transmembranska napetost*. Tipična membranska napetost človeških celic je v intervalu med -20 ter -200 mV (Levin 2012). Ker so električni naboji v celicah mobilni, se naberejo na površini celične membrane, podobno kot naboji na ploščnih kondenzatorjih, in v membrani ustvarjajo močno električno polje v razponu od 4 do 40 MV/m. Transmembranska napetost opravlja tudi zelo pomembno funkcijo celične in medcelične komunikacije, pri čemer je najbolj znan primer širjenje akcijskega potenciala po membrani živčnih celic. Ta pojav lahko sprožijo tudi zunanja elektromagnetna polja, kar bom opisal v naslednjem

razdelku, če pa je vsiljena transmembranska napetost zaradi zunanjega električnega polja dovolj visoka, nastanejo v membrani pore, ki začasno povečajo njeno prepustnost. Ta proces se imenuje elektroporacija.

### **Tveganja zaradi izpostavljenosti elektromagnetnim poljem in sevanjem**

Sistematične raziskave in določanje standardov za omejevanje izpostavljenosti elektromagnetnim sevanjem so se začeli z ustanovitvijo mednarodne komisije za neionizirna sevanja (INIRC) leta 1977. V letu 1992 se je komisija preimenovala v mednarodno komisijo za varstvo pred neionizirnimi sevanji (ICNIRP). Ta komisija je leta 1998 izdala prve Smernice o omejevanju izpostavljenosti elektromagnetnim sevanjem, ki pokrivajo frekvence od 1 Hz do 300 GHz (ICNIRP 1998). V istem časovnem obdobju je sekcija za elektromagnetno varnost pri IEEE pripravila prvo izdajo standarda IEEE C95.1 (IEEE 1992), ki so ga kasneje še dvakrat posodobili (IEEE 1999, 2006). Kasneje je ICNIRP izdala posodobljene smernice za statična magnetna polja ter nizke frekvence (ICNIRP 2009, 2010). Namen standardov in smernic je zagotoviti take življenjske in delovne pogoje, da ni možnosti za nastanek zaznavnih učinkov ali neželenih vplivov na zdravje. Tako IEEE kot ICNIRP standardi poznajo dva nivoja zaščite. Pri prvem nivoju gre za meritve elektromagnetnih sevanj v praznem prostoru, kjer se izmerjene vrednosti primerjajo z referenčnimi vrednostmi. Drugi nivo pride v veljavo šele, kadar so referenčne vrednosti iz prvega nivoja presežene. Takrat je treba določiti dozimetrične količine v telesu (električno polje, gostota toka, stopnja specifične absorpcije, gostota pretoka moči), ter jih primerjati z mejnimi vrednostmi. Kadar so mejne vrednosti presežene, je treba ukrepati in zmanjšati izpostavljenost. V nadaljevanju bom povzel glavne mehanizme interakcije elektromagnetnih polj in sevanja s človeškim telesom in njihove fiziološke učinke.

Elektromagnetna polja imajo različne učinke glede na frekvenco. Pri izpostavljenosti statičnemu električnemu polju se prosti naboji v telesu razporedijo, dokler se ne izniči notranje polje v telesu. Magnetno polje pa prehaja človeško telo praktično nespremenjeno in ne vpliva na telo. Pri zelo velikih gostotah magnetnega pretoka (preko 8 T) se zaradi magnetnohidrodinamičnih učinkov v krvnem obtoku lahko poveča krvni tlak. Premikanje preko gradienta magnetnega polja lahko zaradi magnetne indukcije povzroči vrtoglavico, slabost ali kovinski okus v ustih.

Pri nizkih frekvencah (do približno 10 MHz) zunanje električno polje še vedno povzroča prerazporeditev nabojev, ki pa se zaradi periodičnega izmenjevanja smeri električnega polja gibljejo (Miklavčič *et al* 1999). Prerazporejanje nabojev, ki sledi zunanjemu električnemu polju, tako tvori električni tok. Magnetno polje tako kot pri statičnem primeru prehaja skozi telo, vendar se po Faradayjevem zakonu indukcije v telesu inducira električno polje v sklenjenih zankah. V odvisnosti od površine zank raste tudi inducirano električno polje.

Pri visokih frekvencah (od 100 kHz do 300 GHz) sta električno in magnetno polje sklopljena in se lahko širita v prostor. Elektromagnetna polja v tem frekvenčnem razponu so običajno namenoma ustvarjena za komunikacijo. Pri visokih frekvencah prosti naboji ne morejo dovolj hitro slediti spremembam električnega polja, zato višjefrekvenčna sevanja lahko prodrejo v telo. Človeško telo je relativno dober prevodnik, vendar vseeno prihaja do izgub, zato se del elektromagnetne energije v telesu sprošča kot toplota, ki povzroča segrevanje tkiv. V odvisnosti od frekvence pa vdorna globina elektromagnetnega polja pada in se zato vedno večji delež energije sprošča bližje površini telesa. Pri frekvencah nad 10 GHz se praktično vsa energija absorbira na površini telesa.

Odvisno od frekvence imajo elektromagnetna polja tudi različne zaznavne in neželene vplive. Pri nizkih frekvencah lahko električna polja v telesu povzročijo neposredno stimulacijo vzdražnih celic, kar lahko povzroči bliskanje v vidnem polju, stimulacijo ali modulacijo centralnega živčnega sistema ali stimulacijo perifernega živčevja ter povezanih mišic. Pri visokih frekvencah lahko sproščena toplota povzroči prekomerno segrevanje posameznih izpostavljenih tkiv ali dvig celotne telesne temperature.

Vprašanje, ali lahko izpostavljenost elektromagnetnim sevanjem poveča tveganje za nastanek raka, v javnosti pogosto sproža debate in zaskrbljenost. Kljub številnim raziskavam, ki so bile narejene v zadnjih tridesetih letih, enoznačnega odgovora na to vprašanje še ni. Čeprav pogosto ne dosežejo statistične značilnosti ali imajo metodološke probleme, so številne raziskave pokazale povišano tveganje za nastanek otroške levkemije, kadar so otroci dalj časa izpostavljeni gostoti magnetnega pretoka preko  $0.3 \mu\text{T}$ . Zaradi teh rezultatov je mednarodna agencija za raziskave raka IARC leta 2002 uvrstila nizkofrekvenčna magnetna polja v kategorijo 2B možnih kancerogenov (IARC 2002). Tudi izpostavljenost mobilnim telefonom je močno narasla. Mednarodna raziskava INTERPHONE je pokazala povečano tveganje za nastanek nekaterih možganskih tumorjev pri uporabnikih, ki so mobilni telefon uporabljali več kot 30 minut dnevno (INTERPHONE Study Group 2010). Tudi starejša švedska raziskava je pokazala korelacijo med uporabo mobilnih in brezžičnih domačih telefonov in možganskimi tumorji (Hardell *et al* 2007, 2011). V podobni raziskavi, ki se je osredotočila na otroke, niso odkrili povezave (Aydin *et al* 2011). Zaradi naštetih rezultatov je IARC razvrstila sevanje mobilnih telefonov v kategorijo 2B (IARC In preparation).

### **Elektroporacija – pojav pri visokih električnih poljih**

Pri obravnavi učinkov elektromagnetnih sevanj na ljudi je pomembno poudariti, da so jakosti električnega polja v telesu relativno majhne (do nekaj 10 V/m), čeprav je lahko izpostavljenost polju zelo dolgotrajna. Kadar pa v tkivo dovedemo električno polje z zelo visokimi jakostmi (nad 10000 V/m), seveda za zelo kratek čas, saj bi sicer tkivo zgorelo, v celicah pride do elektroporacije. Elektroporacija je

pojavnost, pri katerem se v celični membrani zgodijo strukturne spremembe, ki povečajo njeno prepustnost za različne ione in molekule. Tako lahko snovi, ki sicer ne morejo prehajati celične membrane, vstopajo ali izhajajo iz celice in se tako izognejo običajnim mehanizmom celičnega transporta. Pojav je bil prvič opisan leta 1958 (Stämpfli 1958, Coster 1965). Šele kasneje pa so pojav uspešno uporabili za uničevanje celic (Hamilton and Sale 1967), spremembo prehodnosti celične membrane (Neumann and Rosenheck 1972) in vnos DNK v celice (Neumann *et al* 1982).

Najbolj pogosta in najširše sprejeta teoretična razlaga za povišanje prepustnosti celične membrane med elektroporacijo je, da visoka vsiljena transmembranska napetost v njej povzroči nastanek vodnih por. Por zaradi majhne velikosti in kratke časovne obstojnosti še niso uspeli slikati s katero od tehnik mikroskopiranja, ki omogočajo največje povečave. Kljub temu pa rezultati simulacij lipidnih dvoslojev z molekularno dinamiko potrjujejo teorijo njihovega nastanka. Molekularna dinamika kaže, da pride z visokim električnim poljem preko membrane do vdora vodnih molekul v hidrofobno plast dvosloja. Ob dovolj velikem električnem polju se ustvari preko membrane vodni most, ki mu sledi preurejanje fosfolipidnih molekul, ki spremenijo orientacijo, tako da se njihove hidrofilne glave obrnejo proti ustvarjenemu vodnemu mostu. Pore v membrani nastanejo v nekaj nanosekundah, v živih celicah pa lahko ostane membrana prepustna še več minut po prenehanju električnih pulzov (Pakhomov *et al* 2007, Pucihar *et al* 2008).

Pri elektroporaciji celic obstajata dva značilna praga električne poljske jakosti, ki razmejujeta različne učinke elektroporacije. Če so celice izpostavljene prešibkemu električnemu polju, se ne zgodi nobena sprememba. Kadar so celice izpostavljene nad *reverzibilnim pragom*, se ustvarijo pore, ki povečajo prehodnost membrane, vendar se v dovolj hitrem času vnovič zaprejo, da celice preživijo. Kadar so celice izpostavljene nad *ireverzibilnim pragom*, si celice ne morejo več opomoči in odmrejo. Pri še višjih električnih poljih ali predolgih časih izpostavljenosti pa dvig temperature povzroči termične poškodbe.

Za učinkovito elektroporacijo brez pretiranega segrevanja se večinoma uporabljajo električni pulzi krajši od 1 ms, tipična dolžina pulzov pa je 50 ali 100  $\mu$ s, amplitude električnega polja pa segajo od 100 V/cm (mišične celice, oociti) do 20 kV/cm (bakterije).

## Metode

V tem razdelku bom predstavil osnovne metode gradnje modelov človeškega telesa za numerično določanje elektromagnetnih količin in programsko opremo, ki sem jo uporabljal pri izračunih z uvodoma omenjenima numeričnima metodama. Gradnja anatomsko pravih modelov najpogosteje temelji na

tomografskih medicinskih slikah (računalniška tomografija ali magnetno resonančno slikanje). Prvi korak pri gradnji modelov je segmentacija, oz. določanje tkiv v aksialnih prerezih. Razmak med prerezi (debelina rezin) in ločljivost slik določata končno ločljivost modela. Po segmentaciji se izdelata tridimenzionalni model, ki je lahko sestavljen iz vertikalno povezanih dvodimenzionalnih krivulj, iz kvadrov (»vokslov«) ali iz nepravilnih tridimenzionalnih teles. Zahtevnost gradnje in uporabe modelov se pri različnih aplikacijah razlikuje, načeloma pa je najbolj zahtevna in tudi najbolj natančna gradnja modelov iz nepravilnih tridimenzionalnih teles.

Pri raziskavah sem uporabil več različnih modelov odraslih, otrok in nosečnic. Modeli odraslega moškega, odrasle ženske in dveh otrok (*Virtual family*) so osnovani na magnetno resonančnih slikah (Christ *et al* 2010), modela odraslega moškega in ženske na osnovi kriosekcije (Visible Human Project) (Ackerman 1998), modele nosečnice na osnovi magnetno resonančnih in ultrazvočnih slik ploda združenih z računalniško generiranim modelom ženske (Femnum) (Bibin *et al* 2010, Daz 2010) ter model nosečnice iz združenih računalniško tomografskih slik trebušnega predela nosečnice (Shi and Xu 2004) in prerezov telesa ženske iz projekta Visible Human Project (Ackerman 1998), ki smo ga sestavili s programskim paketom iSeg (Zurich MedTech AG, Zürich, Švica). Za raziskave načrtovanja zdravljenja z elektrokemoterapijo sem uporabil pacientu prilagojena modela, zgrajena na podlagi računalniško tomografskih in magnetno resonančnih slik. Modela vključujeta ciljne tumorje in okoliško zdravo tkivo – žile, jetra, mišice in maščobno tkivo. Segmentirane rezine vertikalno povežemo (Sel *et al* 2007), v geometrijo pa nato dodamo ustrezno število elektrod. Med dovajanjem elektroterapijskih pulzov se spreminja prevodnost tkiva, kar sem fizikalno modeliral z uporabo sekvenčnega modela.

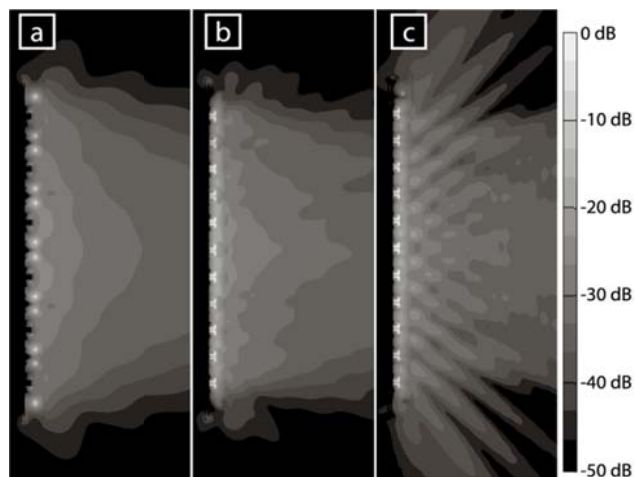
Pri izračunih z metodo FDTD sem uporabil implementacijo FDTD v programskem paketu SEMCAD X (Schmid & Partner Engineering AG, Zürich, Švica), ki omogoča učinkovite in hitre izračune, poleg tega pa so bili rezultati pridobljeni s tem paketom že večkrat validirani z meritvami. Pri izračunih z metodo končnih elementov sem uporabil implementacijo v programskem paketu COMSOL Multiphysics (Comsol AB, Stockholm, Švedska) v povezavi s programskim paketom Matlab (Mathworks, Natick, Massachusetts, ZDA).

## Rezultati in diskusija

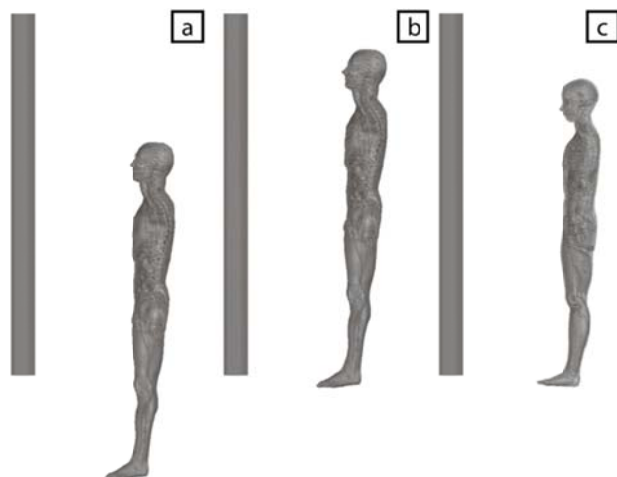
### **Poklicna izpostavljenost večpasovnim baznim postajam**

Čeprav je bilo objavljenih že veliko študij, v katerih so preučevali izpostavljenost delavcev v neposredni bližini baznih postaj mobilne telefonije (Martinez-Burdalo *et al* 2005, van Wyk *et al* 2005, Alanko *et al*

2008, Cooper *et al* 2002, Coray and Krahenbuhl 2003, Joseph and Martens 2005, Joseph *et al* 2008), pa še nobena raziskava ni preučila primera sočasne izpostavljenosti poljem več frekvenc, do kakršnih pride neposredno pred antenami večpasovnih baznih postaj. Takšne bazne postaje omogočajo prostorsko in cenovno učinkovito sočasno delovanje več sistemov mobilne telefonije. V doktorskem delu sem raziskal izpostavljenost pred večpasovno anteno bazne postaje.



**Slika 1:** izračunana efektivna vrednost električnega polja pred anteno bazne postaje pri (a) 900 MHz, (b) 1800 MHz ter (c) 2100 MHz. Vrednost 0 dB ustreza električni poljski jakosti 1000 V/m. Največje električno polje je v okolici sevalnih elementov, ki so v vsakem okencu na levi strani. Elektromagnetno sevanje se širi v smeri proti desni.



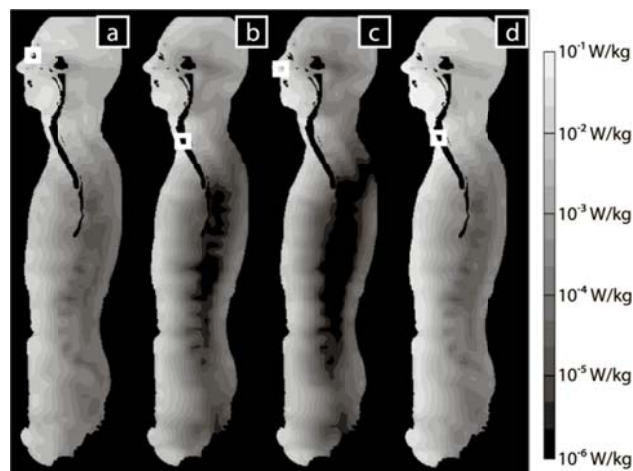
**Slika 2:** različni položaji modelov človeka pred anteno: (a) moški v položaju, kjer je bolj izpostavljena glava; (b) moški v položaju, pri katerem je maksimalno izpostavljeno celotno telo; (c) ženska. V prečni osi so bili vsi modeli poravnani z osjo antene. Oddaljenost od antene smo merili od sprednjega dela prsnega koša v prečnem prerezu do površine pokrova antene.

Izračunane vrednosti električnega polja v prostem prostoru so se dobro ujemale z rezultati meritev na enaki anteni, ki so objavljeni v literaturi (Toivonen *et al* 2009). Tudi vrednosti stopnje specifične absorpcije v fantomu napolnjenem s prevodno tekočino so se dobro ujemale, zato smo lahko model uporabili za izračune izpostavljenosti ljudi pri različnih oddaljenostih modela od antene.

Eden glavnih prispevkov raziskave je bila tudi primerjava dveh algoritmov za seštevanje prispevkov lokalizirane stopnje specifične absorpcije vsake izmed frekvenc. Smernice ICNIRP predvidevajo seštevanje prispevkov pri izpostavljenosti več frekvencam po naslednji formuli:

$$\sum_{i=1}^n \frac{SAR(f_i)}{SAR_L} \leq 1,$$

kjer je  $SAR(f_i)$  stopnja specifične absorpcije pri frekvenci  $f_i$  in  $SAR_L$  mejna vrednost SAR. Vsota poteka po vseh frekvencah, ki so prisotne v določenem primeru izpostavljenosti. V raziskavi sem primerjal dve metodi seštevanja: preprosto metodo, kjer se seštejejo samo najvišje vrednosti izpostavljenosti pri vsaki frekvenci, ter metodo, pri kateri se vrednosti seštevajo v vsaki točki v modelu in nato poišče maksimum.



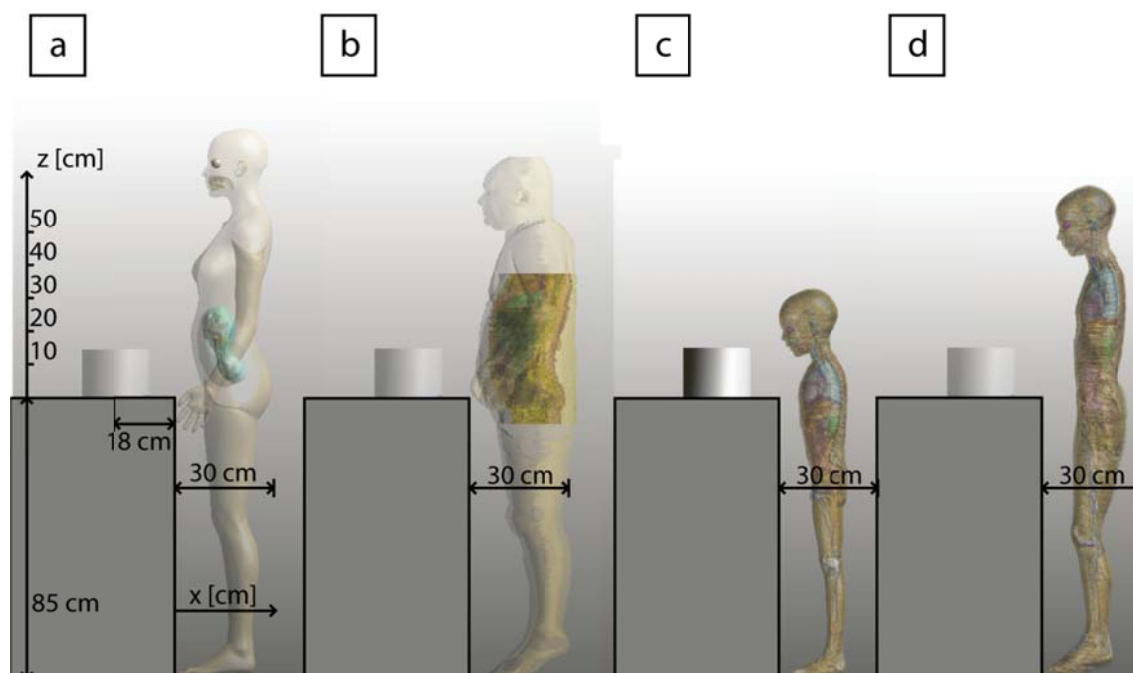
**Slika 3:** Seštevanje stopnje specifične absorpcije. Beli kvadratici označujejo najvišjo vrednost SAR pri (a) 900, (b) 1800, (c) 2100 MHz, ter (d) sešteto maksimalno vrednost pri vseh frekvencah. Slika ilustrira problem uporabe vsote maksimalnih vrednosti, saj so lokalni maksimumi vsake izmed frekvenc na različnih lokacijah in se zato na seštevajo popolnoma.

Pri preprostem seštevanju lahko v primerjavi s točkovnim seštevanjem pride do precenjevanja izpostavljenosti. Moji rezultati so pokazali precenjevanje v razponu od 2 do 55 %. V praksi je zato primerno uporabljati preprosto metodo seštevanja, saj je izguba natančnosti relativno majhna, hkrati pa točkovno seštevanje zahteva tudi hranjenje obsežne baze izračunov in zamudno iskanje maksimuma pri vsakem možnem razmerju oddajnih moči in oddaljenosti od antene.

### Izpostavljenost otrok magnetnim poljem indukcijskih kuhališč

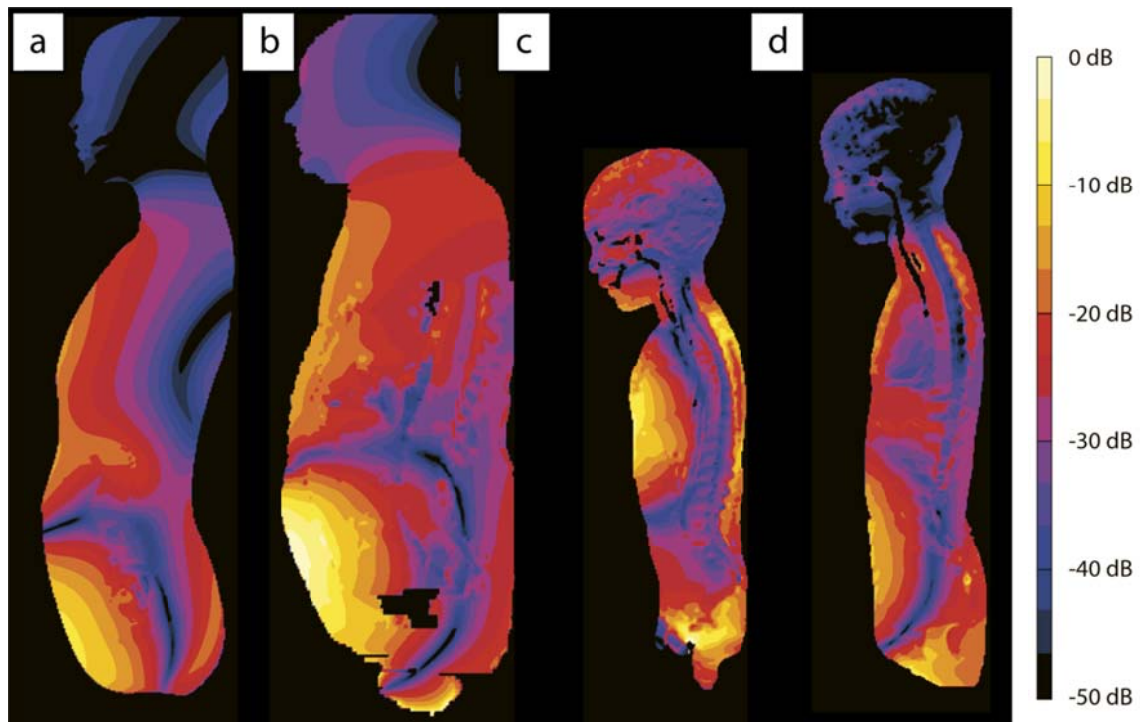
Ker so se raziskave izpostavljenosti elektromagnetnim poljem zgodovinsko pretežno osredotočale na polja omrežnih frekvenc pri nizkih frekvencah in na frekvence, ki jih uporabljajo sistemi za brezžično komunikacijo (900 MHz do 2450 MHz), je ostalo frekvenčno območje srednjih frekvenc med 1 kHz in 1 MHz pretežno neraziskano. Prav v tem frekvenčnem področju pa delujejo vedno bolj priljubljena indukcijska kuhališča, ki tipično delujejo na frekvencah med 20 kHz in 100 kHz, ter dosegajo priključne moči do 7 kW. Naprave na Evropskem tržišču morajo sicer ustrezati mednarodnim standardom, vendar ima standard za dovoljena magnetna polja relativno blage zahteve. Zahteva namreč merjenje gostote magnetnega pretoka 30 cm od roba naprave. Na sliki 4 je ilustriровано, da se pri običajni uporabi kuhališča telo dejansko nahaja precej bliže.

Da bi raziskali izpostavljenost magnetnim poljem indukcijskih kuhališč, smo izmerili magnetna polja, ki jih ustvarja tako kuhališče med delovanjem. Na podlagi meritev smo prilagodili numerični model kuhališča, dokler nismo dosegli dobrega ujemanja med rezultati numeričnega modela in izmerjenimi vrednostmi. Dobljeni model kuhališča smo nato uporabili za določanje inducirane električne polja in gostote toka v telesu.



**Slika 4:** postavitve modelov nosečnic (a in b) ter otrok (c in d) pred indukcijskim kuhališčem. Pri običajnem položaju za kuhališčem je človek bistveno bliže od 30 cm, kolikor predvideva trenutno veljavni standard.

Izračunane gostote toka in električne poljske jakosti v telesu kažejo, da pri napravi, ki smo jo modelirali, ne prihaja do preseganja mejnih vrednosti. Tudi sprememba vrednotenja mejnih vrednosti in povišanje referenčnih vrednosti v smernicah ICNIRP iz leta 2010 v primerjavi s prej veljavnimi smernicami iz leta 1998 ne prinese preseganja mejnih vrednosti. Kljub temu se pri nosečnicah pojavljajo najvišje vrednosti izračunane gostote toka in električne poljske jakosti ravno v trebušnem predelu in v področju maternice in ploda (slika 5).



**Slika 5:** Inducirano električno polje v telesu (a) nosečnice v 26. tednu, (b) nosečnice v 30. tednu, (c) 11-letne deklice ter (d) 6-letnega dečka. Velikosti modelov niso v razmerju. Vrednost 0 dB predstavlja 100 mV/m.

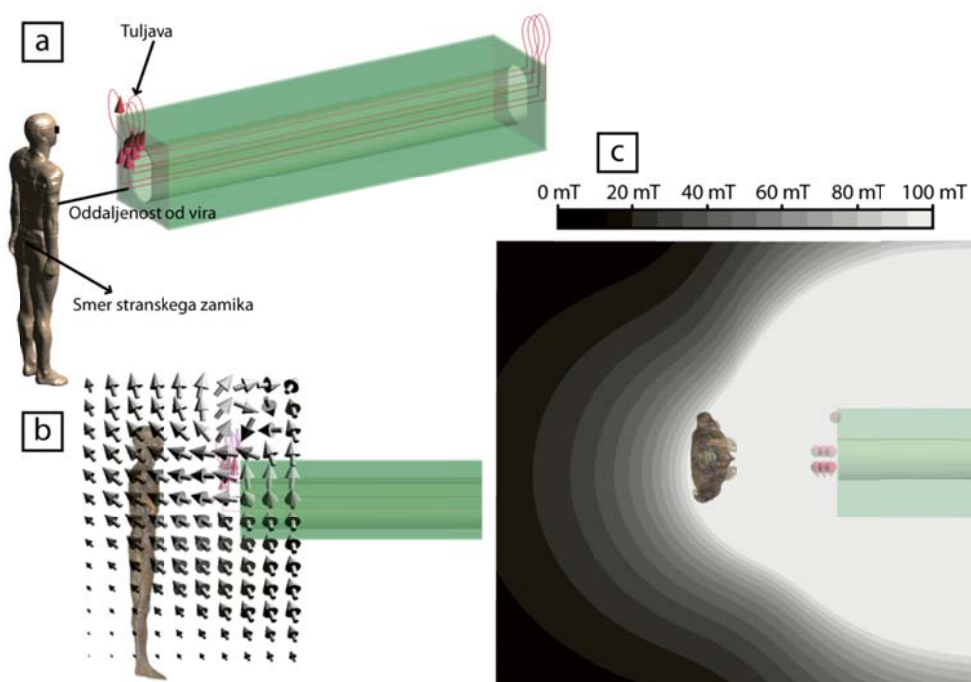
Čeprav mejne vrednosti niso bile presežene v nobenem primeru, pa je bistveno opozoriti, da so bila magnetna polja, ki jih je ustvarjalo izmerjeno kuhališče, bistveno nižja od zahtev standarda, zato bi lahko na trgu obstajale tudi naprave z veliko močnejšimi stresanimi polji. Uporabniki takih naprav bi lahko bili ob uporabi neprimerne posode prekomerno izpostavljeni.

### **Prostorsko povprečenje izmerjenih vrednosti pri vrednotenju izpostavljenosti**

Kljub temu da industrijske aplikacije indukcijskega segrevanja pogosto uporabljajo zelo velike delovne moči, pa v literaturi ni veliko podatkov o izpostavljenosti delavcev takim virom. Ena izmed redkih publikacij na to temo podaja le izmerjene vrednosti magnetnega polja v praznem prostoru (Floderus *et al* 2002). Pri delovnih močeh preko 1 MW je preseganje mejnih vrednosti zelo verjetno, vendar so pri takih

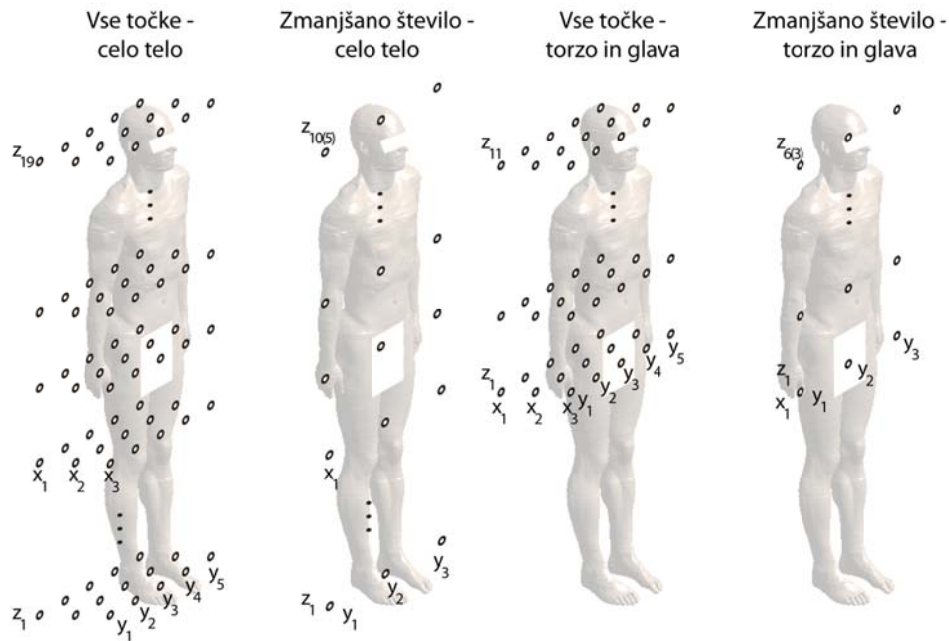
napravah prisotna tudi druga tveganja, kot so nevarni plini, nevarnost električnega šoka in visoke temperature obdelovancev ali tekoče kovine, zato je gibanje v okolici teh naprav strogo omejeno.

Pri naši raziskavi smo se osredotočili na tunelsko peč za indukcijsko popuščanje z delovno močjo 10 kW. Zaradi prostorskih omejitev tovarne morajo delavci opravljati kontrolo kvalitete v neposredni bližini vhoda v tunelsko peč, zato so izpostavljeni nehomogenim poljem, ki na nekaterih mestih presegajo referenčne vrednosti. Zaradi enostavnejšega vrednotenja izpostavljenosti smo želeli preveriti primernost prostorskega povprečenja, ki ga omenjajo smernice ICNIRP, vendar v njih ni natančneje definirano (Jokela 2007, ICNIRP 2010).



**Slika 6:** Postavitev modela človeka v bližini tunelske peči. (a) označene osi oddaljenosti od vira ter stranskega zamika, (b) smer magnetnega polja v bližini vira, (c) efektivna vrednost gostote magnetnega pretoka okoli naprave.

Za preverjanje vpliva različnega števila točk za povprečenje in njihove postavitve po telesu smo si zamislili šest različnih konfiguracij, ki vsebujejo od 9 do 285 točk. Poleg različnega števila točk smo preverjali tudi dve različni metriki: aritmetično, pri kateri je povprečje enako vsoti vseh točk deljeno s številom točk ter kvadratično, pri kateri je povprečje enako korenu iz vsote kvadratov vseh točk deljeno s številom točk.



**Slika 7:** Shematski prikaz različnih postavitve točk za povprečenje. Pri polnem številu točk so te med seboj oddaljene 10 cm, pri zmanjšanem pa so razdalje večje. Pri zmanjšanih postavitvah so točke postavljene zgolj na površini telesa, ki je bližje viru.

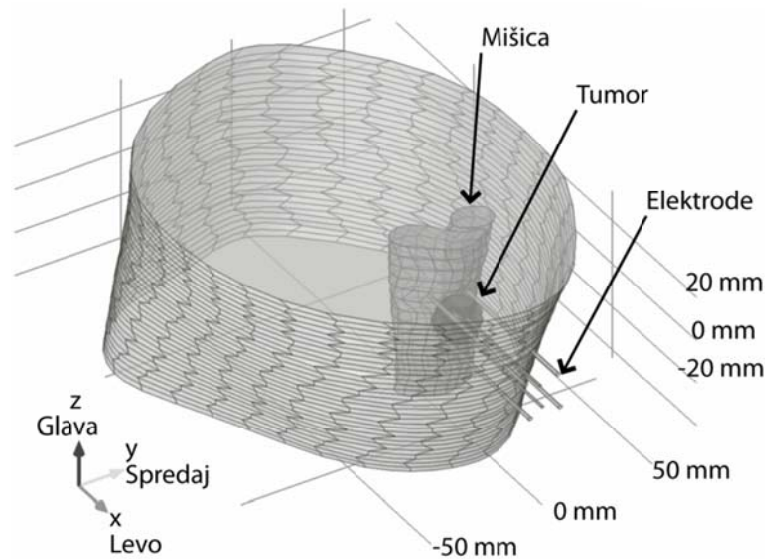
Rezultati kažejo, da so za praktično uporabo bolj primerne postavitve z manjšim številom točk, čeprav dosežejo znižanje izmerjenega polja le za faktor 2. Pri postavitvah z večjim številom točk je lahko faktor zmanjšanja tudi večji od 5, vendar se takrat pojavi velika verjetnost, da bomo prekomerno izpostavljeno delovno mesto ocenili kot primerno. Pri uporabi zmanjšanih postavitve, ki pokrivajo le torzo in glavo, je resda večja verjetnost, da bomo delovno mesto, ki sicer ni prekomerno izpostavljeno, ovrednotili kot prekomerno obremenjeno, vendar je vseeno manjša, kot če bi uporabili samo največjo izmerjeno vrednost.

Metoda povprečenja izmerjenih magnetnih polj je primerna za uporabo pri majhnih oddaljenostih od vira polja (20 do 100 cm). Pri manjših oddaljenosti je magnetno polje zelo nehomogeno in bi s povprečjem tvegali prekomerno izpostavljenost. Pri večjih oddaljenostih pa so magnetna polja že praktično homogena in zato prostorsko povprečenje nima veliko smisla. Takrat je bolj primerno uporabiti kar neposredno referenčne vrednosti ali numerično določanje dozimetričnih količin.

### **Načrtovanje zdravljenja za terapije na osnovi elektroporacije in analiza robustnosti**

V nadaljevanju bom povzel raziskave in razvoj načrtovanja zdravljenja z elektrokemoterapijo. Pri zdravljenju površinskih tumorjev z elektrokemoterapijo lahko kirurgi uporabljajo standardne postopke (Mir *et al* 2006), ki brez posebnih priprav dosegajo objektivni odgovor v več kot 80 % primerov (Mali *et*

al 2013). Pri prehodu na zdravljenje globlje ležečih tumorjev pa se pojavi potreba po načrtovanju zdravljenja za bolj zanesljivo zagotavljanje pokritja celotnega tumorja z dovolj velikim električnim poljem. Prvi primer zdravljenja globoko ležečega tumorja z elektrokemoterapijo pri ljudeh je bil opravljen na Onkološkem inštitutu v Ljubljani. Za terapijo smo pripravili načrt zdravljenja z naslednjim postopkom. Računalniško tomografske slike so bile razgrajene in na podlagi obrisov tumorja, bližnjih mišic in zunanosti noge je bil zgrajen tridimenzionalni model (slika 8).

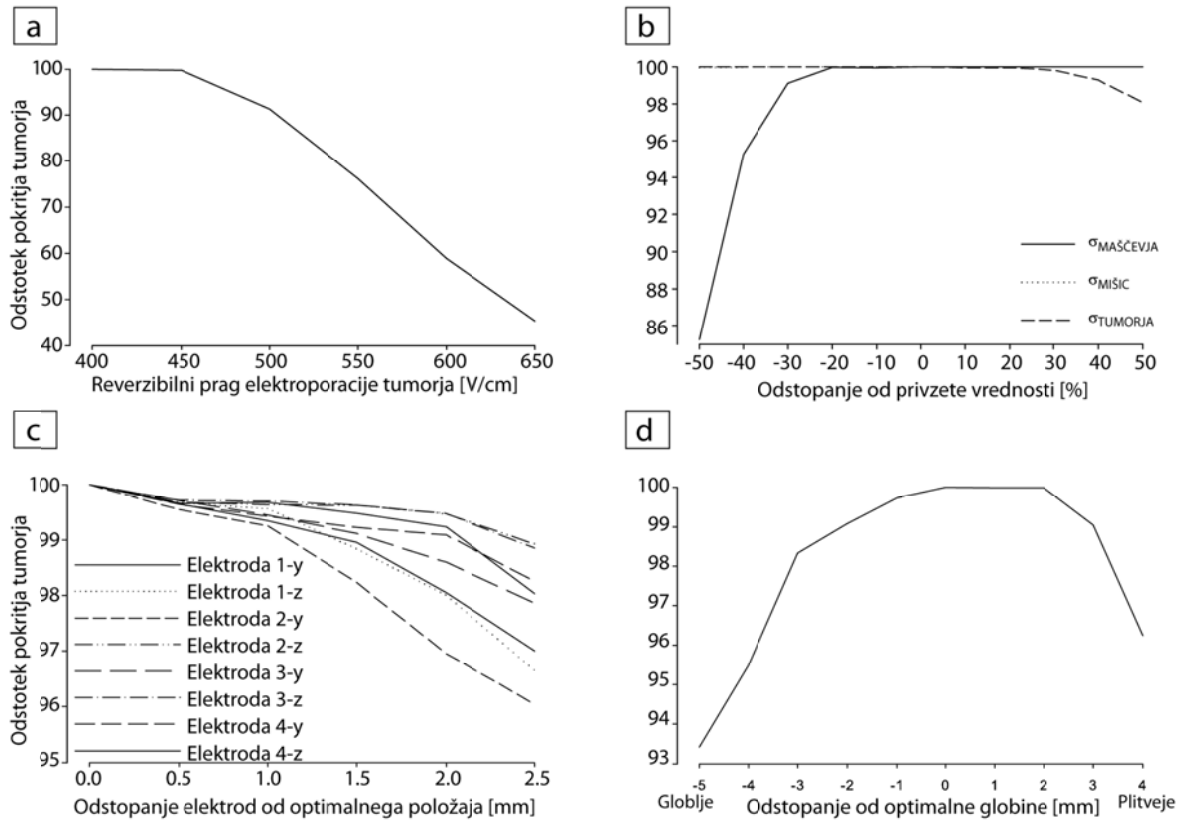


**Slika 8:** model noge (rdeče) s tumorjem in vstavljenimi elektrodami. Tumor (zelena) je ležal v neposredni bližini mišice (modra). Na sliki so vstavljene štiri elektrode, pripravljen pa je bil tudi načrt s petimi elektrodami.

Model noge smo uporabili za izračune pokritosti tumorja z električnim poljem in optimizacijo položajev elektrod in napetosti med elektrodami. Tako pripravljen načrt zdravljenja so nato uporabili kot vodilo pri izvajanju terapije. Načrt je sicer predvideval uporabo petih elektrod, pri čemer bi bila ena elektroda vstavljena v središče tumorja, vendar to v praksi ni bilo izvedljivo, saj tumor ni bil fiksno pritrjen in se je zato izmikal poskusom nabadanja. Po terapiji se je tumor sicer prvotno zmanjševal, po dveh mesecih pa je znova začel rasti, zato so ga kirurško izrezali. Kljub le delnemu uspehu se je metoda izkazala kot nezahtevna za paciente in uporabna. Naknadna analiza je pokazala, da je najverjetnejši vzrok za nepopolni uspeh nekoliko večja razdalja med elektrodami od pričakovane, zaradi česar je bil manjši delež tumorja izpostavljen prešibkemu električnemu polju.

Enak model noge smo nato uporabili za raziskavo robustnosti načrtov zdravljenja narejenih z našo metodo. Pri raziskavi robustnosti smo preverjali padce pokritosti tumorja v odvisnosti od majhnih sprememb (napak) v vhodnih podatkih modela. Te spremembe so bile naslednje: odstopanje od pravega

položaja, prenizka napetost ter napake v električnih lastnostih tkiv. Slednje so imele največji vpliv na učinkovitost terapije. Največji padec pokritosti smo opazili, kadar je dejanski prag elektroporacije višji od praga, ki je bil uporabljen za načrtovanje zdravljenja (slika 9).

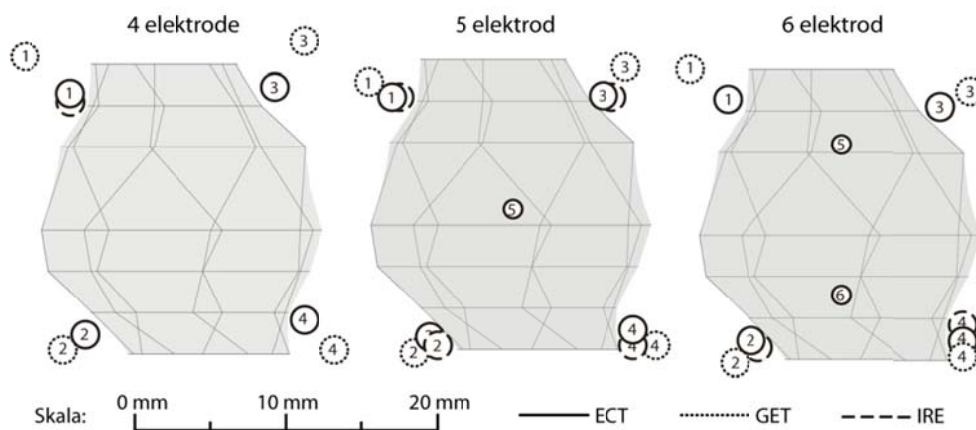


**Slika 9:** Padec pokritosti tumorja v odvisnosti od (a) reverzibilnega praga elektroporacije, (b) spremembe razmerja med prevodnostjo tumorja in okolice, (c) premikov posamezne elektrode, (d) preglobokga oziroma preplitvega vstavljanja elektrod.

Pomemben vpliv ima tudi razmerje med prevodnostjo tumorja in okoliškega tkiva. Če je to razmerje v realnosti večje od razmerja, uporabljenega pri izračunu, lahko pokritost tumorja upade. Odstopanje posameznih elektrod od optimalnih položajev ima sicer majhen vpliv, vendar se pri odstopanju vseh elektrod hkrati učinkovitost zelo hitro zmanjšuje. Globina vstavljanja elektrod je prav tako pomembna, kadar so dimenzije tumorja primerljive z dimenzijami aktivnega dela elektrod. Če so elektrode vstavljene pregloboko ali preplitvo, se lahko učinkovitost prav tako zmanjša. Pri odstopanju napetosti med posameznim parom za manj kot 200 V se učinkovitost zmanjša minimalno, kar nakazuje, da so nekateri deli tumorja pokriti z več kot enim parom elektrod.

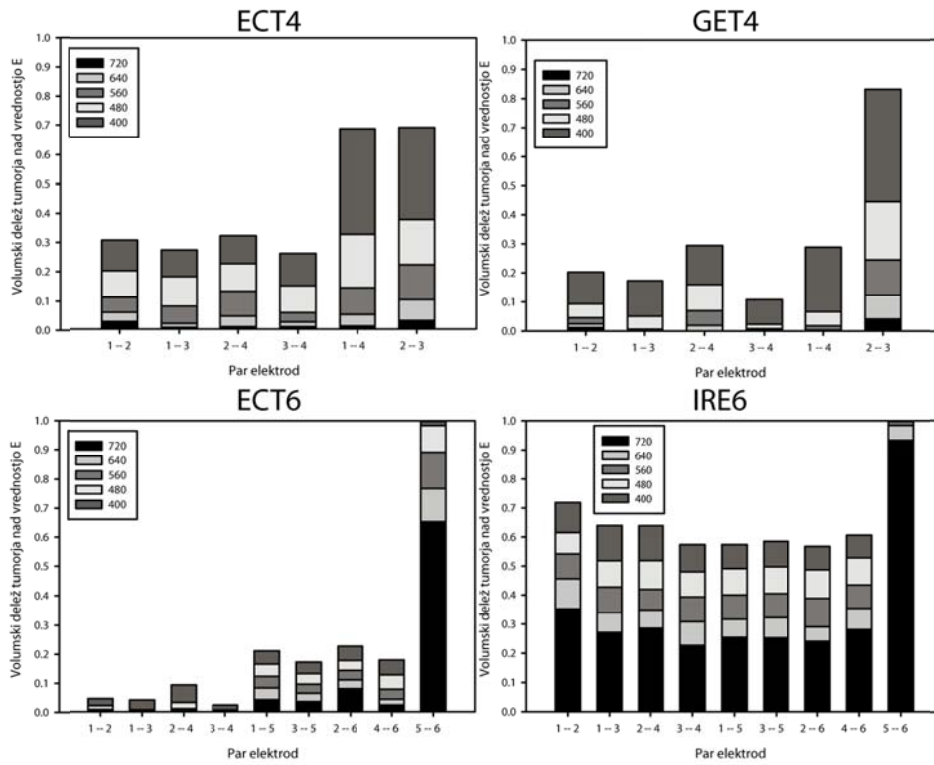
Isti primer tumorja v nogi smo uporabili tudi pri zadnji raziskavi, pri kateri smo razširili metodo za načrtovanje zdravljenja tudi na druge metode na osnovi elektroporacije: ireverzibilno ablacijo in gensko

elektrotransfekcijo. Različne metode imajo različne zahteve po pokritju ciljnega tkiva z električnim poljem. Elektrokemoterapija zahteva pokritje celotnega ciljnega tkiva z električnim poljem nad reverzibilnim pragom. Ireverzibilna ablacija potrebuje pokritje ciljnega tkiva nad ireverzibilnim pragom, genska elektrotransfekcija pa pokritje ciljnega tkiva nad reverzibilnim pragom, vendar pod ireverzibilnim pragom. Pri raziskavi smo uporabili enake optimizacijske algoritme, kot v predhodnih primerih, vendar smo vsaki metodi posebej priredili kriterijsko funkcijo. Tako je enak optimizacijski algoritem vrnil bistveno različne napetosti in postavitve elektrod.

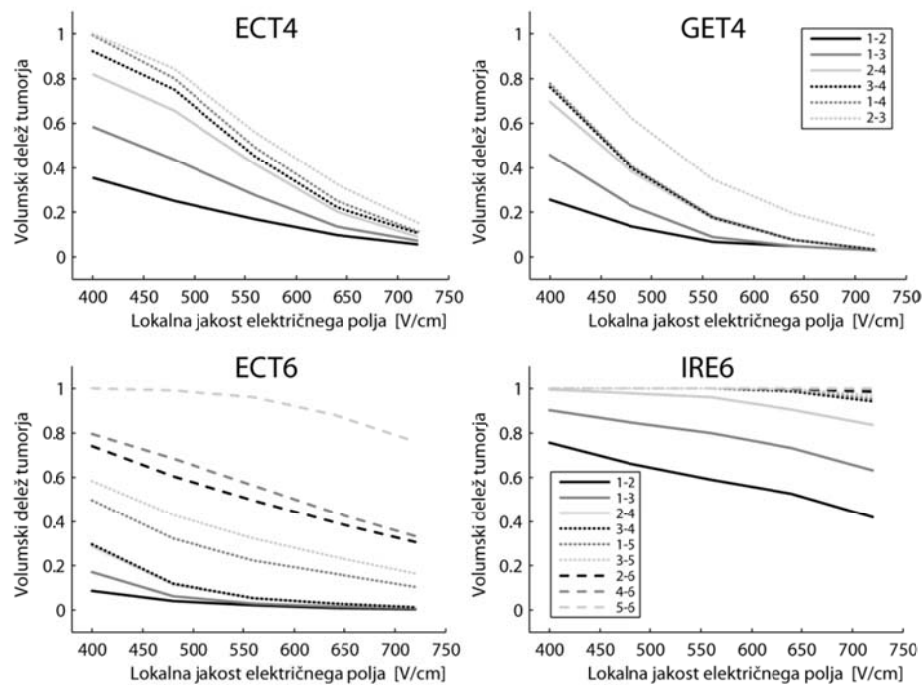


**Slika 10:** Optimizirane postavitve elektrod za različne vrste terapije

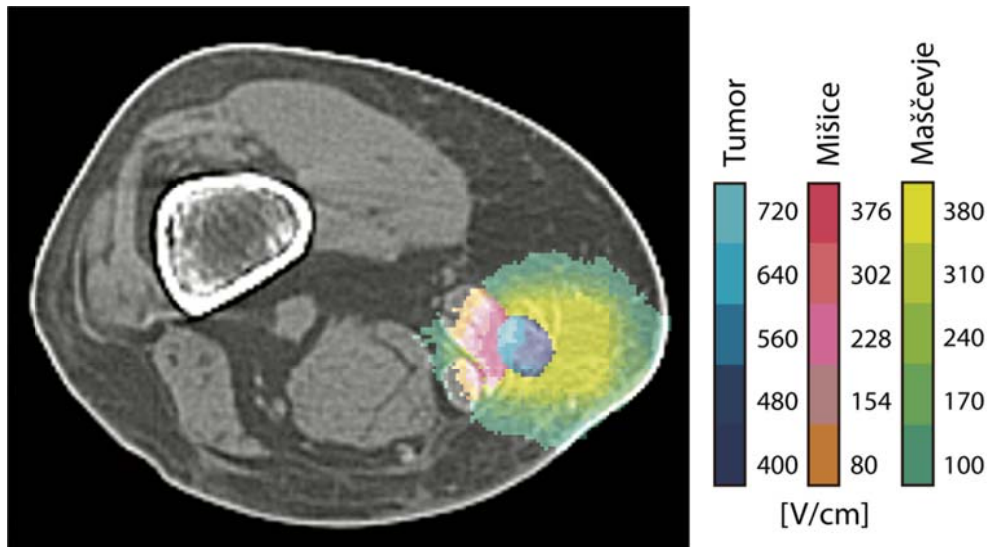
Pri veliki količini podatkov, posebno pri tridimenzionalnih problemih se pogosto pojavi problem z vizualizacijo podatkov, zato smo za lažjo orientacijo in medsebojno primerjavo razvili tri nove načine predstavljanja načrtov zdravljenja.



Slika 11: Grafi prispevkov posameznih parov elektrod.



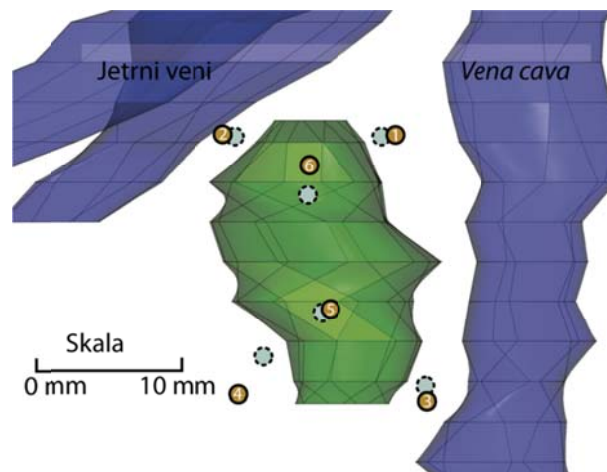
Slika 12: Krivulje kumulativne pokritosti z električnim poljem



**Slika 13:** Prečni prerez elektroporacije. Na sliki je označena električna poljska jakost v različnih tkivih.

Na sliki 11 so prikazani primeri grafa prispevkov posameznih parov elektrod, iz katerega je mogoče razbrati, koliko vsak par elektrod prispeva k celotni pokritosti ciljnega tkiva z električnim poljem nad reverzibilnim in ireverzibilnim pragom elektroporacije. Na sliki 12 so prikazane krivulje kumulativne pokritosti z električnim poljem, ki prikazujejo naraščanje pokritosti celotnega ciljnega tkiva z električnim poljem nad določeno vrednostjo. Krivulje omogočajo tudi hitro oceno robustnosti načrta, saj je iz njih razvidno, po kolikšnem številu pulzov je dosežena pokritost celotnega ciljnega tkiva z dovolj velikim električnim poljem. Slika 13 pa prikazuje prerez elektroporacije, kjer so stopnje elektroporacije glede na doseženo jakost električnega polja prikazane na rezinah izvornih medicinskih slik. S pregledovanjem več rezin lahko dobimo predstavo o učinkovitosti elektroporacije v treh dimenzijah in hkrati hitro odkrijemo morebitna področja, kjer je uspešnost zdravljenja vprašljiva.

Metode načrtovanja zdravljenja smo uspešno prenesli tudi na primere zdravljenja metastaz raka debelega črevesa na jetrih. V klinični študiji, ki poteka na Onkološkem inštitutu, smo uspešno pozdravili primer tumorja v jetrih, ki je bil za klasične terapije izredno problematičen. Pri tumorjih, ki ležijo v neposredni bližini glavnih jetrnih žil je namreč izrezovanje nemogoče ali težavno, uporaba terapij na osnovi segrevanja tkiva pa onemogočena zaradi hladilnega učinka velikih žil. Z uporabo metod za načrtovanje zdravljenja smo pripravili načrt, ki so ga nato intra-operativno izvedli.



**Slika 14:** Položaj tumorja med glavnimi jetrnimi venami in veno cavo z označenimi položaji elektrod: načrtovani položaji so označeni z oranžnimi krožci, rekonstruirani položaji med zdravljenjem pa s črtanimi modrimi krožci.

Po dveh mesecih se je tumor glede na radiološke izvide zmanjšal in pacient se je odločil za kirurško odstranitev, saj točnega stanja tumorja iz slik ni bilo mogoče razbrati. Po uspešni operaciji in histološki preiskavi se je izkazalo, da v tumorju ni bilo živih rakavih celic. Kljub odstopanjem od prvotno načrtovanih položajev elektrod je bil načrt zdravljenja dovolj robusten, da je zagotovil uspešno terapijo.

## Zaključek

Numerični metodi končnih diferenc v časovnem prostoru in končnih elementov sem uporabil za določanje elektromagnetnih količin za preventivne in terapevtske namene. Zaradi neprestane rasti uporabe novih tehnologij je določena mera izpostavljenosti elektromagnetnim sevanjem neizogibna. V neposredni bližini virov EMS je določanje natančne porazdelitve polj zahtevno zaradi kompleksne geometrije virov, porazdelitve elektromagnetnih polj in njihove nehomogenosti. Moje raziskave na področju zaščite pred prekomerno izpostavljenostjo EMS so se osredotočale na nekatera v literaturi manj raziskana področja in manj natančno definirana določila smernic za omejevanje izpostavljenosti. Smernice iz leta 2010 so prinesle spremembo v definiciji mejnih vrednosti pri nizkih frekvencah (inducirano električno polje namesto gostote toka) in povišano referenčno vrednost za magnetna polja. Moji rezultati kažejo, da spremembe v smernicah niso prinesle tveganja za prekomerno izpostavljenost niti pri bolj občutljivih skupinah, kot so nosečnice in otroci. Kadar so magnetna polja v praznem prostoru nehomogena in v bližini ali malo nad referenčnimi vrednostmi, je sprejemljivo uporabiti prostorsko povprečenje namesto bolj zahtevnega določanja izpostavljenosti z numeričnimi izračuni. Prihodnje raziskave se bodo osredotočale na še neraziskane nove tehnologije in izpostavljenost pri

različnih položajih telesa, predvsem na velike prevodne zanke, ki jih lahko sklenejo roke in noge s telesom ali okoljem.

Numerične metode so se prav tako odlično izkazale pri načrtovanju zdravljenja z različnimi terapijami na osnovi elektroporacije. Numerično modeliranje omogoča izdelavo robustnih načrtov zdravljenja z optimiziranimi položaji elektrod in napetostmi med elektrodami. Predhodno pripravljene načrte zdravljenja omogočajo zdravnikom zaupanje v uspeh terapije. V prihodnosti bo to lahko vodilo k povečanemu številu uspešnih primerov, posebej kadar so druge možnosti zdravljenja omejene. Novo razvite metode vizualizacije bodo omogočile razvoj enostavnih in razumljivih programskih rešitev za načrtovanje zdravljenja, ki ne bodo zahtevale obsežnega inženirskega znanja in znanja uporabe numeričnih metod. V prihodnosti bo treba z novimi raziskavami zapolniti vrzeli v znanju o vplivu elektroporacijskih pulzov na tkiva in določanje reverzibilnih in ireverzibilnih pragov različnih tkiv. Cilj je tudi prehod iz določanja zgolj elekričnega polja in uporabe preprostih pragov za določanje učinkovitosti na modele na osnovi verjetnosti za uspešno elektroporacijo. Taki modeli bodo omogočali nadaljnje izboljšave optimizacijskih algoritmov, boljše napovedi učinkovitosti zdravljenja in formalno validacijo načrtovanja zdravljenja.

## Izvirni prispevki k znanosti

---

### **Poklicna izpostavljenost večpasovnim baznim postajam**

Čeprav so bile objavljene številne raziskave poklicne izpostavljenosti visokofrekvenčnim elektromagnetnim sevanjem baznih postaj za mobilno telefonijo, se nobena ni osredotočila na primer izpostavljenosti večpasovnim baznim postajam. Take antene postajajo vedno pogostejše, saj operaterjem ponujajo prostorsko in časovno učinkovito rešitev uporabe več sistemov sočasno. Z metodo FDTD sem določil izpostavljenost pred večpasovno anteno, ki deluje na tipičnih frekvencah mobilne telefonije (900, 1800 in 2100 MHz), ter raziskal različne pristope k vrednotenju sočasne izpostavljenosti več frekvencam.

### **Izpostavljenost občutljivih skupin magnetnim poljem indukcijskih kuhališč**

Otroci v vseh stopnjah razvoja, predvsem pa pred rojstvom, so v primerjavi z odraslimi bolj občutljivi na različne fizikalne dejavnike; toda glede njihove občutljivosti na EMS takšna razlika še ni bila nedvoumno dokazana, pa tudi še ne ovržena. Da bi prišli do zanesljivih rezultatov, je bistvenega pomena zagotoviti dovolj natančno poznavanje izpostavljenosti v najrazličnejših konfiguracijah elektromagnetnih polj, frekvenc in telesa nosečnic in otrok. V ta namen sem izvedel študijo izpostavljenosti ploda in otrok

poljem, ki jih ustvarjajo vedno bolj priljubljena indukcijska kuhališča. Z numeričnimi izračuni sem določil inducirano električno polje v različnih tkivih (celotni plod, živčni sistem ploda, maternica, posteljica) in raziskal spremembe v tolmačenju, ki so jih prinesle posodobljene smernice ICNIRP.

### **Metoda za prostorsko povprečenje izmerjenih magnetnih polj**

Kadar so izmerjene jakosti magnetnega polja na delovnem mestu višje od referenčnih vrednosti, to ne pomeni nujno, da je delovno mesto čezmerno izpostavljeno. Ustrežanje standardom za omejevanje izpostavljenosti se lahko dokaže s primerjavo numerično določenih dozimetričnih količin v telesu z mejnimi vrednostmi. Ker so ti postopki zahtevni za izvedbo in terjajo tudi veliko časa, bi prostorsko povprečenje izmerjenih magnetnih polj lahko bilo praktična alternativa. Preveril sem različne postavitve točk za povprečenje in primerjal oceno izpostavljenosti glede na povprečno vrednost z oceno izpostavljenosti glede na numerično določene količine v telesu. Rezultati kažejo, da je ob pravilnem izboru postavitve točk prostorsko povprečenje upravičeno.

### **Metoda za načrtovanje zdravljenja globoko ležečih tumorjev**

Pri načrtovanju zdravljenja z elektroterapijo uporabljamo anatomsko pogojene, pacientu prilagojene modele, ki omogočajo numerično določanje električne poljske jakosti v tumorju in zdravih okoliških tkivih. Za doseganje učinkovitosti je ključnega pomena popolno pokrivanje ciljnega tkiva z električnim poljem, katerega jakost presega prag reverzibilne elektroporacije. Kljub ustreznemu pokrivanju ciljnega tkiva v numeričnem modelu prihaja pri dejanski izvedbi terapije do številnih majhnih napak in odstopanj od načrta. Zato je treba zagotoviti ustrezno robustnost načrta zdravljenja, tako da bo zdravljenje uspešno kljub odstopanju od parametrov, ki je v določeni meri neizogibno. V svojem delu sem zato preveril občutljivost načrta zdravljenja na primeru, ki je bil uporabljen tudi v kliničnem posegu. Preveril sem občutljivost načrta zdravljenja na majhne napake v legi posameznih elektrod in vseh elektrod hkrati, na spremembe električne prevodnosti tkiv ter na napake v dovedenih napetostih.

### **Inovativne vizualizacije za načrtovanje zdravljenja z metodami na osnovi elektroporacije**

Vizualizacija in predstavitev kompleksnih tridimenzionalnih podatkov je zahtevna. Ker numerični modeli za načrtovanje zdravljenja obsegajo take podatke, sem razvil več inovativnih pristopov za vizualizacijo električnih polj v ciljnem in okoliških tkivih. Nove vizualizacije ponujajo pogled na podatke s poudarkom na različne pomembne lastnosti in tako omogočajo enostavno primerjavo različnih rešitev ter olajšajo iskanje morebitnih šibkih točk pripravljenih načrtov zdravljenja.



## Introduction

---

### Bioelectromagnetics – the science of the interaction of electromagnetic phenomena with biological matter

Bioelectromagnetics can be defined as the study of interactions of electromagnetic quantities – fields, voltages and currents – with living matter. The study of electricity actually originated from the studies of Luigi Galvani in the 18th century (Galvani 1791). Although his initial hypothesis on the existence of animal electricity inherent to living beings was later refuted by Alessandro Volta (Volta 1800, Piccolino 1998), his discovery that sparks can stimulate frog legs to move was ground-breaking at the time. This experiment showed that electricity plays an important role in the functioning of living organisms.

Today, the physical laws that govern the behaviour of electric, magnetic and electromagnetic fields (EMF) are known, with the most important contribution being from James Clerk Maxwell in his Treatise on Electricity and Magnetism, published in 1873 (Maxwell 1873). He managed to compile the results and findings of all the then known experiments in electricity and condense these findings into four famous equations that fully describe the behaviour of the electric, magnetic and electromagnetic fields. Although Maxwell's equations are very elegant in their differential notations (see Box 1 below), solving them analytically is a difficult task and is in fact possible only in the simplest of cases. Since measurements inside the human body are difficult and invasive, it is generally only possible to approximate the quantities inside the human body by performing measurements on phantoms, which are simplified models of the human body filled with a liquid or gel approximating the dielectric properties of human tissues.

The task of solving Maxwell's equations in geometries that have some resemblance to the complex structures of human biology therefore had to wait for the development of sufficiently powerful computers and suitable numerical techniques. The two approaches that are most commonly used for computations in determining human exposure to electromagnetic fields are the finite element method (FEM) and the finite-difference time-domain method (FDTD) (Hand 2008). My work described in this thesis was largely based on these two methods. The finite element method was first proposed by Richard L. Courant in 1943 (Courant 1943, Pelosi 2007), when he proposed the piece-wise linear approximation of the unknown quantity on the sides of triangles with simple polynomial functions. The triangular mesh

## Introduction

can be adapted in density and shape to conform to the geometry of the problem, thus allowing for higher accuracy in critical regions and lower use of computational resources (memory and number of computational cycles) in regions of lesser variability.

The finite-difference time-domain method can be traced back to 1966, when Kane Yee (Yee 1966) first presented the “leapfrog algorithm”. This sequentially solves the differential equations first for the electric field, using second order finite differences for determining the derivatives of the magnetic field, then in the next step solves for the magnetic field, using second order finite differences for determining the derivatives of the electric field. This algorithm for the sequential solving of two interdependent components of the electromagnetic field is stable with an appropriate choice of time-step length and allows for the computation of the propagation of electromagnetic fields in three-dimensional models.

### Box 1: Maxwell's equations



James Clerk Maxwell (1831-1879)

$$\begin{aligned}\nabla \cdot E &= \frac{\rho}{\epsilon_0} \\ \nabla \cdot B &= 0 \\ \nabla \times E &= -\frac{\partial B}{\partial t} \\ \nabla \times B &= \mu_0 J + \mu_0 \epsilon_0 \frac{\partial E}{\partial t}\end{aligned}$$

The first equation is Gauss' law describing that electric field lines originate in positive charges and end in negative charges. The second is Gauss' law for magnetism, which states that no magnetic “charges” exist. Instead, magnetic fields are generated by dipoles, which means that magnetic field lines have no beginning or ending, and instead form loops. The third equation is named Faraday's law and states that the changing magnetic field causes the induction of electric fields in closed loops. The final equation is the corrected Ampere's law, which states that magnetic fields are produced by moving charges as well as changes in the electric field. Image engraving by G. J. Stodart from a photograph by Fergus of Greenack.

Since Maxwell's time, there has also been an amazing explosion of new technologies using electricity for driving motion, producing light and heat, as well as for processing and transferring information. Consequently, the exposure of humans to EMF of various frequencies has been steadily increasing. With increasing exposure there has also been increasing interest in the potential effects of these fields on the functioning of the human body. Research into possible adverse effects proceeded along two lines. The first was population-based epidemiological studies, where the goal is to determine whether the exposure to a certain agent causes increases in the incidence of certain diseases or physiological effects. The other direction of research was direct laboratory experiments with volunteers, where thresholds for perception of electromagnetic fields were determined. Laboratory experiments form the basis for the setting of safety guidelines and should prevent all detectable effects in the majority (at least 95 %) of the population.

Simultaneously with the development of new technologies and research into their safety, the research of the use of electricity for therapeutic purposes advanced rapidly. Using various frequencies, time courses of the fields and different modes of application, several different therapeutic endpoints can be achieved. Among the applications already in clinical use are electro-surgery (Jackson 1970), acceleration of fracture healing (Canè *et al* 1993), pain reduction (Trock *et al* 1994), treatment of lesions with radiofrequency ablation (Curley *et al* 1999), transport of substances through the skin (Levin *et al* 2005), and treatment of tumours with electrochemotherapy (Sersa *et al* 2008).

In the following sections I first briefly describe the cells, their membranes, and their natural electromagnetic activity. Next, I give a brief overview of the mechanisms of the interaction of external – non contact – electric, magnetic and electromagnetic fields with the human body and the effects that these interactions can cause. Standards for the protection of population and workers exposed to EMF are presented next, along with a brief history of these standards. In the penultimate section of the introduction, I present the electroporation phenomena which occur when cells are exposed to very high pulsed electric fields, and also some of the therapeutic applications of electroporation. The motivation for performing treatment planning for these therapeutic applications is presented next, along with the typical steps of such treatment planning procedures based on established methods used e.g. in radiotherapy. The introduction ends with a brief outline of the aims of this doctoral thesis.

# Physiological electromagnetism – the endogenous electromagnetic fields at a cellular level

## The cellular membrane

As an important part of biochemistry, electricity naturally plays an important role in the molecular processes that occur in cells. All living cells, prokaryotic as well as eukaryotic, are encapsulated in a thin molecular membrane composed of phospholipids. These lipids have hydrophobic (water-repellent) tails composed of long chains of hydrocarbons and hydrophilic (water-attracting) phosphate heads. Due to their chemical nature, the phospholipids in an aqueous environment naturally form a double layer with the hydrophobic tails gathered together on the inside and the hydrophilic heads on the outside of the bilayer, and this bilayer typically forms a closed surface (a vesicle) filled and surrounded by the aqueous medium (Alberts *et al* 2009). A biological cell is such a vesicle, but with interior containing all the biomolecules and structures necessary for the cell's functioning and with the bilayer referred to as the *plasma membrane*.

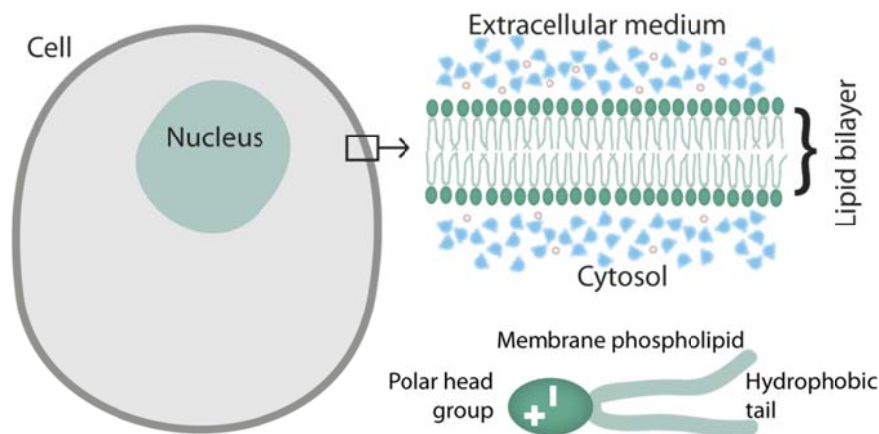


**Figure 1:** A schematic drawing of an animal cell. The nucleus contains the genetic material, while the cytoplasm contains the organelles and other cellular mechanisms needed for the cell's functioning. On the right, a close-up cross-section of a lipid bilayer is shown. The aqueous environment inside and outside the ~5 nm thick lipid bilayer is in contact with the hydrophilic heads of the phospholipids.

The plasma membrane is very thin (5-7 nm) and highly non-permeable to charged ions and larger molecules. In living cells, it also contains a large number of proteins which perform various functions, serving as receptors, mediators of trans-membrane transport and building the cytoskeleton that gives the cell its shape. With the help of the plasma membrane, the cells maintain a highly controlled environment

in the cytosol, which contains various types of ions and molecules, cellular molecular machinery and organelles with specific functions. The membrane bilayer itself has distinct outer and inner layers which are composed of different molecules.

### Transmembrane transport in general

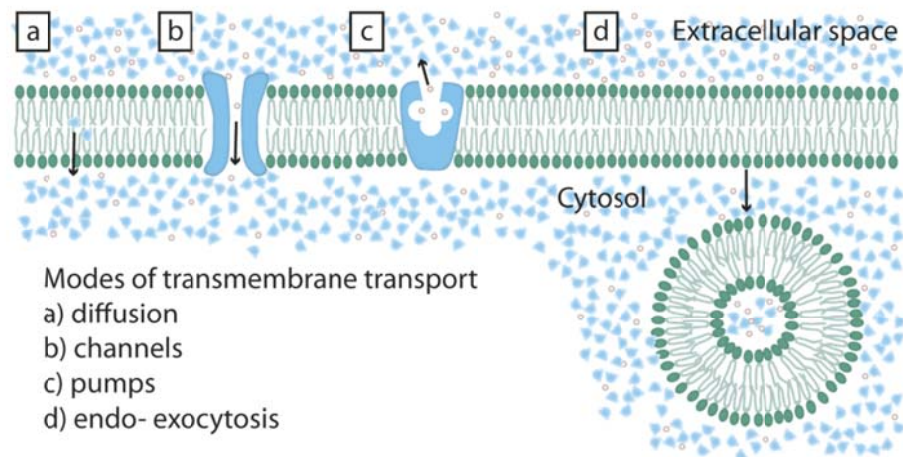


**Figure 2:** Transmembrane transport illustrated. The figure shows the four main modes of transmembrane transport, which are described below.

#### **Diffusion**

Diffusion is the movement (of energy or matter) from an area of higher concentration to an area of lower concentration. In mathematics, the gradient of a scalar field is a vector field that points in the direction of the greatest *increase* of the scalar field. Therefore the diffusion can also be described as the movement along the concentration gradient vector, but opposite to its direction. Small uncharged molecules such as molecular oxygen and carbon dioxide can diffuse across the membrane. Water and ethanol, although polar, can still cross the cellular membrane, albeit at a lower rate. With increasing molecular size, the rate of diffusion rapidly decreases, so that e.g. glucose hardly crosses the cellular membrane at all. Charged molecules however, no matter how small, cannot cross the cellular membrane without the help of special molecules or molecular mechanisms described below.

#### **Channels**

Channels are formed by special proteins that embed themselves into the cellular membrane and form an aqueous pore, which allows the passive diffusion of ions and some small organic molecules. The channel proteins are very selective as to which molecules they allow passage, which essentially means that there are specialized channels for every molecule or ion that needs to be transported. Many channels are also gated,

## Introduction

which means that they can be either open or closed depending on some condition, such as the presence of a certain molecule (ligand), mechanical stress, or in a certain range of the transmembrane voltage.

### **Pumps**

Pumps are specialized proteins that can actively transfer specific molecules across the cell membrane in any direction, even in the direction of increasing concentration (which cannot be achieved by diffusion through either the bilayer itself or passive channels in the bilayer). This enables the cells to actively generate and maintain an imbalance of certain molecules or ions outside and inside the cell. Although the pumps can transfer molecules and ions in the direction of increasing concentration, this process, like rolling a stone uphill, requires energy.

### **Endo- and exocytosis**

For even larger molecules or certain highly reactive chemicals that could damage the cell interior, the remaining mechanism is endocytosis. Although strictly speaking, endo- and exocytosis are not mechanisms of trans-membrane transport, since the transferred material doesn't cross the membrane, but remains on the same side of the membrane bilayer and isolated from the cytosol, this important mechanism of cellular transport is described here for the sake of comprehensiveness. This mechanism is based on small indentations (inverted bubbles) forming in the cellular membrane. The indentation then deepens until it forms an enclosed sphere, which detaches from the rest of the cellular membrane and forms a small vesicle that can then move to its destination inside the cytosol. The same mechanism can also operate in the reverse direction (termed exocytosis), essentially expunging the vesicle contents from the inside of the cell into the extracellular space without the contents ever coming into contact with the cytosol.

### **Membrane potential**

Most cells have active machinery in their membranes that maintains and regulates the balance of ions between their outsides and insides. This allows the cells to keep the concentration of certain ions higher in the cell than in the extracellular space (e.g.  $K^+$  ions and  $H^+$  ions are more abundant inside the cells). At the same time, the cells keep the concentration of certain ions higher in the extracellular space than in the cytosol (e.g.  $Na^+$  and  $Ca^{2+}$  ions are more abundant outside the cells), i.e. the cells prefer some ions to be outside their membranes and other ions to be inside. The imbalance between  $K^+$  and  $Na^+$  ionic concentrations is generated by the sodium-potassium pump (Na-K ATPase), and  $K^+$  leak channels allow some  $K^+$  ions to leak out of the cell again. This brings the cytosol to a lower electric potential compared to the extracellular medium, and the potential difference between the cytosol and the extracellular medium is variously termed *membrane potential*, *transmembrane potential*, *membrane voltage*, and

*transmembrane voltage*. Since voltage is defined as the difference of electric potentials between two points, the term *transmembrane voltage* is the most appropriate from the physics perspective.

The transmembrane voltage or TMV is typically between -20 mV and -200 mV in typical human cells (Levin 2012). Since the charges that generate the TMV are mobile both inside and outside the cell, they converge and accumulate right next to the plasma membrane, similarly to the charges on the electrodes of a plate capacitor. Given that the typical thickness of the cellular membrane is around 5 nm (Alberts *et al* 2009), the TMV causes electric fields in the range of 4-40 MV/m.

The TMV serves a crucial function in multicellular organisms as it is used by various cells for cellular communication across short and long distances. The best known mechanism where the TMV serves as the main means of signalling is in nerve cells, where the interplay of voltage-gated channels and pumps allows the signal to travel along the length of the nerve cell without attenuation at much higher speeds than could be achieved by chemical signalling alone. In the case of nerve cells, the mechanism that triggers the propagation of the signal or the *firing* of the neuron is the depolarisation, i.e. the reduction, of the TMV below a certain threshold. This electrical effect on the nerve cells can also be caused by a sufficiently strong external EMF, as discussed in the following section. The dynamic behaviour of neurons is the essential mechanism that enables rapid responses to the environment and allows for the complex computational capacity of the brain as well as the rapid and precise control of muscle movement. Other important mechanisms that require membrane transport are e.g. light detection and photosynthesis.

When a cell is exposed to an external electric field, the charges inside the cell migrate under the influence of the electric field until the electric field caused by their redistribution neutralises the external field in the cytosol. This causes an additional component of the transmembrane voltage, termed *induced transmembrane voltage*, which superimposes on the physiological transmembrane voltage (which is also referred to as the *resting transmembrane voltage*). If the total transmembrane voltage exceeds a certain critical threshold value, which is in the range of several hundred mV, with its exact value dependent on the composition of the membrane and various other parameters, the cell membrane becomes permeabilized in a phenomenon known as electroporation. This phenomenon and some of its applications are described in more detail below.

## Research into risk assessment of electromagnetic fields in humans

### **Electromagnetic fields safety standards**

Systematic research on the effects of EMF on human health began with the formation of the International Non-Ionizing Radiation Commission (INIRC) in 1977 and its successor, the International Commission for Non-Ionizing Radiation Protection (ICNIRP) in 1992. At roughly the same time the section for electromagnetic safety of the Institute of Electrical and Electronics Engineers (IEEE) prepared the first edition of the IEEE C95.1 standard in 1991 (IEEE 1992). This standard was further revised in the years 1999 (IEEE 1999) and 2006 (IEEE 2006), and it was the first standard to set limits for human exposure to non-ionizing EMF. In 1998 the currently still valid ICNIRP Guidelines for Limiting Exposure to Time-varying Fields from 1 Hz to 300 GHz (ICNIRP 1998) were published, which are similar to the IEEE standard in many aspects. New Guidelines on Limits of Exposure to Static Magnetic Fields (ICNIRP 2009) were published in 2009. In the following year new Guidelines for Limiting Exposure to Time-varying Fields from 1 Hz to 100 kHz (ICNIRP 2010) were published, which revised a part of the original 1998 Guidelines. The aim of these standards is to ensure such living and working conditions as to prevent any kind of perceptible effect or injury. The standards are only aimed at preventing well-documented immediate effects since no compelling evidence for delayed effect exists so far. The standards offer a two-layer approach to preventing overexposure. The first layer is the determination of EMFs (electric field, magnetic field, magnetic flux density) in an unperturbed (empty) space and comparison with the reference levels, while the second layer is the determination of internal electromagnetic quantities and comparison with basic restrictions. The evaluation of the second layer is only necessary if the reference values from the first layer are exceeded, and in the case of overexposure with respect to basic restrictions the Guidelines imply that action is required. For easier understanding of the safety standards, I first present an overview of the interaction mechanisms of electromagnetic fields at different frequencies with the human body and then describe the resulting physiological effects.

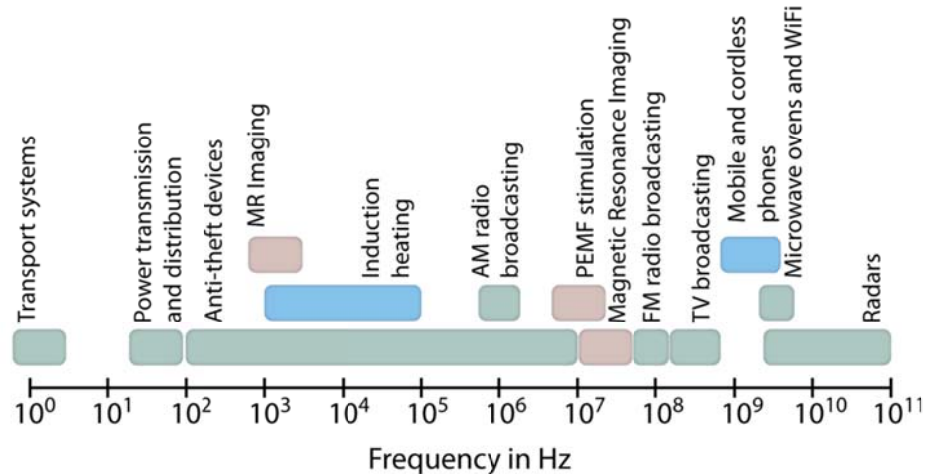


**Figure 3:** The use of the electromagnetic spectrum by different technologies.

### Mechanisms of interaction

The interaction between exogenous electromagnetic fields and the human body can roughly be split into interaction with static fields, interaction with low frequency fields (up to roughly 10 MHz), and interaction with high frequency fields (from roughly 100 kHz to roughly 300 GHz). In the frequency range where the two bands overlap, characteristic effects of both types can be observed. The discussion of electromagnetic fields in this thesis will generally be limited to frequencies below 300 GHz, as introduced by the safety standards (ICNIRP 1998, IEEE 2006). Above 300 GHz, the interactions are governed by the particle-like nature of the EMF (photons), and will not be discussed within this thesis.

### Static fields

In the case of static fields, it is more appropriate to use the term static electric and static magnetic field separately. Namely, at zero frequency, the electric and magnetic fields are decoupled, meaning that one does not affect the other.

The static electric field causes the free charges which are abundant in the human body to transfer towards the outer boundary of the body in a way that negates the internal electric field. This process is very fast and presents a very high damping of the external field (Polk and Postow 1996).

In contrast, the static magnetic field is almost unaffected by the human body, therefore it passes through it unchanged and consequently also does not produce any effects on the human body. At magnetic flux densities in excess of 8 T, however, some effects do arise. Due to the effects of magnetohydrodynamics, the magnetic field has an influence on the charged molecules in the bloodstream or, e.g., in the vestibular labyrinth fluid of the ear (Roberts *et al* 2011), caused by the Lorenz force on moving charged particles.

## Introduction

This causes a measurable rise in systolic blood pressure (ICNIRP 2009), but the effect is transient and disappears when the magnetic field is removed.

Moving in a strong static magnetic field gradient can also induce an effect, due to the Faraday's law of induction. For gradients exceeding 0.5 T/m, the induced electric fields can be strong enough to stimulate excitable cells and can result in feelings of nausea, vertigo, or a metallic taste in the mouth (ICNIRP 2009).

### **Low frequency fields**

In the low frequency range (up to roughly 10 MHz), the electric and magnetic fields are still mostly decoupled and can be considered separately in the majority of cases. The electric field causes the accumulation of charges on the surface of the body, which similarly to the static case neutralise the external electric field inside the body. However, due to the periodic changes of most external fields, the accumulated charges move in sync with the external field, thereby generating an electric current.

At low frequencies, magnetic fields pass through the human body unimpeded, but time-varying fields induce electric fields due to Faraday's law of induction. The electric fields are induced in loops, and the larger the loop (bounded by a continuous conductive area within the body), the larger the induced electric field.

### **High frequency fields**

At frequencies from 100 kHz to 300 GHz, the electric and magnetic fields can also radiate into space, and the electric and magnetic field are coupled. Thus, it is appropriate to speak about electromagnetic fields. Electromagnetic fields in this frequency range are usually intentionally transmitted from antennas, most commonly for communication purposes. At these frequencies, the charges in the human body cannot follow the rapid changes in the external electric field, and consequently this field can penetrate into the human body and persist within it. Because the human body is a relatively good conductor at higher frequencies, it absorbs the energy carried by the electromagnetic field, which then causes heating of the tissues.

Depending on the frequency, there are different patterns of heating (ICNIRP 1998). From 100 kHz to 20 MHz the absorption in the trunk diminishes and increased absorption can occur in the neck and legs. Between 20 MHz and 300 MHz whole-body resonance can occur, since body size becomes comparable with the wavelength of the external electromagnetic field, which can lead to a peak in absorption. Larger bodies experience resonance at lower frequencies, and smaller bodies (e.g. children) at higher frequencies (Bakker *et al* 2010). At still higher frequencies, the penetration depth of the electromagnetic fields

decreases with frequency, which causes more energy to be deposited near the surface of the body and leads to local heating of the skin and subcutaneous tissues. At frequencies above 10 GHz, all energy is deposited at the surface of the body, comparable to optical radiation.

## **Biological effects**

### ***Stimulation of excitable cells***

When induced electric fields are strong enough to produce a considerable voltage along the length of an excitable cell (typically tens of mV), this can result in the cell's excitation. Although the excitation of a single cell generally does not cause any perceptible effect in the human body, the induced electric fields can excite several hundred cells simultaneously while a similar effect can also result from propagation of the signal from one excitable cell to another. The cells most susceptible to this kind of excitation are the electrically excitable cells in the retina, for which the excitation threshold can be as low as 20 mV/m (Saunders and Jefferys 2007). Since the retina is considered a part of the central nervous system, the standards for human exposure are set to prevent the possibility of excitation of these cells (ICNIRP 2010). The threshold for peripheral nerve stimulation is about 6 V/m (Reilly 2002) at low frequencies, and increases at frequencies above 1 kHz, since there is less time for the charge accumulation that leads to stimulation. The threshold for direct stimulation of muscle cells is about a factor of 10 higher than that for nerve cells, so in practice the stimulation of motor neurons occurs sooner and causes muscle cell stimulation through their normal pathways, while the threshold for direct muscle stimulation is not reached.

### ***Heating***

Human cells are sensitive to temperature and most of them operate with highest efficiency at 37 °C, the typical body core temperature. When temperature is increased by less than 1 °C, no significant detrimental effects can be observed, and the threshold for considerable thermal damage is 43 °C (ICNIRP 1998). Higher temperatures can be tolerated if they are present for a short time (Dewey 1994), i.e. the threshold for thermal damage is higher if the elevated temperatures are only present briefly.

With exposure to electromagnetic fields, it is necessary to separate the effects of whole-body heating and local heating. The former is manifested as the rise of the core body temperature and is usually more prominent at lower frequencies. Localized heating occurs mostly near the surface of the body and can cause localized temperature rises. This can be especially problematic in tissues which have poor capacity for thermal regulation due to low blood perfusion – most notably the eye (Taflove and Brodwin 1975,

Hirata 2005, Laakso 2009) – or are especially sensitive to temperature changes, e.g. the testes (Setchell 1998).

### **Possible adverse effects at below-threshold exposures**

In the last three decades, many studies have been published on the possible increase of childhood leukaemia incidence in children exposed for longer periods to power line frequency (for both 50 and 60 Hz) magnetic flux densities exceeding 0.3  $\mu\text{T}$  (Kheifets *et al* 2010). Although the studies usually have some methodological drawbacks regarding the precise determination of actual exposure of the cases, or fail to reach statistical significance, they have repeatedly and consistently reported odds ratios for childhood leukaemia in the range of 1.4-2. This prompted the International Agency for Research on Cancer at the World Health Organisation to classify power line magnetic fields as category *2B possible carcinogens* in the year 2002 (IARC 2002). The classification *possible carcinogen* means that there is some evidence for carcinogenesis in humans, while there is limited corroboration in animal studies or understanding of mechanisms that could lead to such effects.

Simultaneously, there have also been efforts to evaluate the potential carcinogenicity of high-frequency EMF, particularly those emitted by mobile phones. The Interphone study was a large international epidemiological study and it showed increased odds ratio for certain brain tumours in heavy users of mobile phones (INTERPHONE Study Group 2010). An older study from Sweden also indicated the association between mobile and cordless phone use and brain tumours (Hardell *et al* 2007, 2011). Another study which focused on children did not find any association between the use of mobile phones and brain tumours (Aydin *et al* 2011). A Danish cohort study on the use of mobile phones (Frei *et al* 2011) also didn't find any statistically significant association between mobile phone use and cancer, although that study has been criticised due to some methodological issues (Philips and Lamburn 2011). Based on the results of these epidemiological studies, radiofrequency EMF have also been classified as group 2B possible carcinogens by the IARC in 2012 (IARC In preparation).

## Electroporation - interaction at very high electric fields

### **The electroporation phenomenon**

When the induced transmembrane voltage is sufficiently high – hundreds of mV, depending on cell type and physiological conditions – the cellular plasma membrane undergoes a molecular-level transformation that renders it permeable to various ions and molecules. This effect allows various substances that

otherwise cannot enter or exit the cells to bypass the normal mechanisms of trans-membrane transport and directly cross the cellular membrane. After the effect was first described (Stämpfli 1958, Coster 1965), it was discovered that it can be used to kill cells (Hamilton and Sale 1967), change the permeability of the plasma membrane (Neumann and Rosenheck 1972) and even transfer DNA into cells (Neumann *et al* 1982).

The most widely accepted theoretical explanation for the observed rise in membrane permeability to ions and molecules is that the induction of sufficiently large TMV causes aqueous pores to form in the membrane. Although nobody has yet managed to image these pores, their existence is nevertheless corroborated to quite a large extent by molecular dynamics (MD) simulations. These simulations show that with the application of electric field across the membrane, molecules of water are first drawn through the hydrophobic part of the plasma membrane, forming a water bridge across it. This causes the adjacent phospholipids to reorient so that their hydrophilic heads face the water bridge forming metastable aqueous pores across the membrane. Such pores are formed within a few nanoseconds, but their resealing can last for seconds or even minutes after the external field ceases (Pakhomov *et al* 2007, Pucihar *et al* 2008).

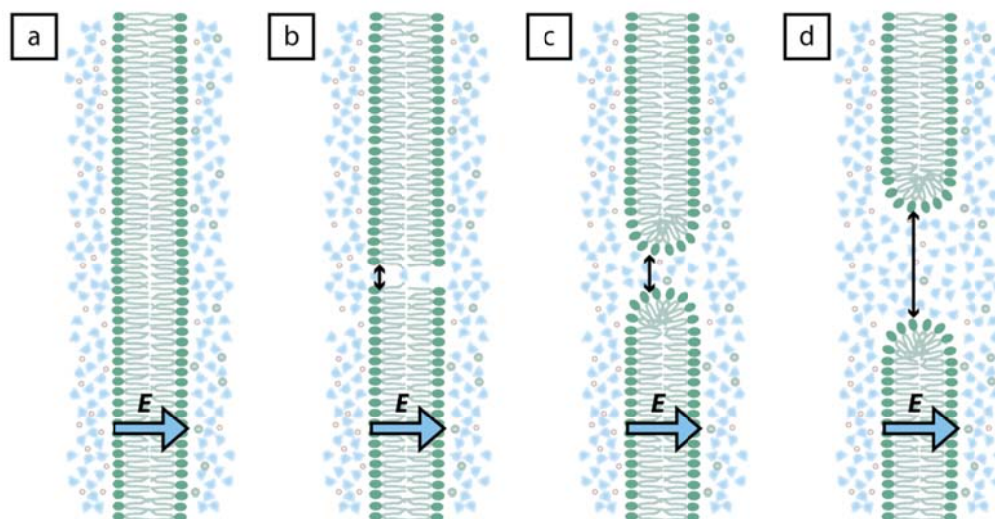


**Figure 4:** Pore formation during electroporation: a) Lipid bilayer without pores b) water drawn through the hydrophobic layer by the electric field, c) phospholipid reorientation, d) formation of a metastable aqueous pore.

If the electric field to which the cells are exposed is too low, no effects occur, as the transmembrane voltage is too low to cause electroporation. If the applied electric field is higher than the so-called

## Introduction

*reversible electroporation threshold*, the pores form, but reseal sufficiently rapidly to preserve cell functionality. Above the *irreversible electroporation threshold*, the cells can no longer recover and therefore lose their viability. For even higher electric fields, and/or excessively long exposures, temperature rise caused by the delivery of the electric energy results in thermal damage.

Pulses that are efficient in inducing reversible electroporation without substantial heating have durations below 1 ms, typically between 50 and 100  $\mu$ s, and amplitudes between 100 V/cm (muscle cells, oocytes) and 20 kV/cm (bacteria). The reversible and irreversible electroporation thresholds depend on the cell size, shape, as well as on the duration of the pulses (Pucihar *et al* 2011), with the general rule that the pulse amplitude required for electroporation increases as the duration decreases (Pucihar *et al* 2011). In continuation, I will present the electroporation effects on tissues, which are relevant to treatment planning for electroporation-based treatments.

### **Tissue during the application of electroporation pulses**

Cells in tissues are organised in a three-dimensional matrix consisting of different types of cells and an extracellular scaffold, which helps give cells their shape and function. Different tissues have different water contents and different levels of blood perfusion, which leads to different tissues having markedly different electrical characteristics (Duck 1990, Gabriel *et al* 1996). The varying electrical properties have an important influence on the electric field distribution, and since the most reliable predictor of electroporation in tissues is the *in situ* electric field (Miklavcic *et al* 1998), the electric properties of tissues during electroporation have to be considered. One of the most important considerations is that tissue conductivity increases during electroporation pulse application (Sel *et al* 2005, Cukjati *et al* 2007) in an electric field-dependent rise of bulk tissue conductivity. The theoretical explanation for this conductivity increase is that pores formed during electroporation serve as additional conductive pathways for the electric current, which is otherwise forced to flow only in the extracellular space. The factor of conductivity increase during the pulse is around 3 (Cukjati *et al* 2007, Kranjc *et al* 2012), but the bulk conductivity increase after pulse application is lower than that (Ivorra *et al* 2009).

### **Electroporation applications in medicine**

Electroporation has several applications in clinical medicine. The most established application is *electrochemotherapy (ECT)*, which uses reversible electroporation to enhance the entry and thus cytotoxic effectiveness of chemotherapeutic drugs (Mir *et al* 1991, Sersa *et al* 2008). For successful ECT, the whole tumour volume has to be exposed to electric fields above the *reversible* electroporation threshold.

The second application – *non-thermal ablation by irreversible electroporation (IRE)* – uses irreversible electroporation to directly cause cell death in the target tissue (Daniels and Rubinsky 2009, Garcia *et al* 2010). To this end, IRE requires the whole target volume to be exposed to electric fields above the *irreversible* electroporation threshold. The advantage of IRE with respect to other ablation techniques is that it leaves the extracellular structures in the tissue largely unaffected, which accelerates recovery and reduces scarring. Therefore, avoiding thermal damage becomes an important consideration. It should be noted that the benefits of IRE also apply to ECT to an even greater extent, since the treatment is less aggressive and also has a lower probability of causing tissue damage.

The third application – *gene electrotransfer (GET)* – uses reversible electroporation to introduce DNA into the target tissue. This is applicable both in gene therapy, where a non-defective human gene replaces the function of a defective gene (Anderson 1998), and in DNA vaccination, where a pathogen DNA is introduced, and by its expression triggers an acquisition of immune response to this pathogen (Donnelly *et al* 1997). A promising example of GET use is introducing cytokine encoding genes to stimulate the human immune system to attack and destroy the cancerous cells (Heller and Heller 2010, Cemazar *et al* 2010). The efficiency of GET increases with the target volume exposed to *reversible* electroporation, while *irreversible* electroporation must be avoided to preserve the target tissue.

### **Treatment planning at tissue level**

In the previous section I have presented the various approaches for using electroporation-based treatments in medicine. Since the requirement on using sufficiently strong electric fields is very stringent and failure to adequately treat even small volumes of cancerous tissues can cause tumor regrowth, it is sensible to perform treatment planning in advance (Pavliha *et al* 2012). Since biological tissues are typically very complex in shape and structure, determining the electric field distribution is a complex task that requires the use of numerical methods. In the work presented in this thesis the finite element method was applied and it is also commonly used by other authors in the field (Mahmood and Gehl 2011, Garcia *et al* 2011). Patient-specific treatment planning involves several steps: medical imaging, image segmentation, model building, numerical simulations with optimization, and validation. *Medical imaging* is usually performed before physicians decide to use an electroporation-based treatment. For the purpose of model building it is preferable if the medical images are tomographic (i.e. showing several cross-sections or slices of the region of interest), which can be achieved by using magnetic resonance or computed tomography imaging. *Image segmentation* involves examining the medical images to determine which areas on each slice belong to particular tissue types and then delineating the target area to be treated. *Model building* entails using the segmented images to reconstruct a three-dimensional model

## Introduction

which is representative of the patient's original anatomy and is usable as the input model for numerical simulation software. In this step, the appropriate values have to be assigned to the electrical parameters of all the tissues in the model. *Numerical simulation with optimization* is the step where the electric field distribution in the tissue is determined numerically. If several electrode pairs are used for pulse delivery the simulation has to be performed for each electrode pair separately and the total coverage determined. In order to perform optimization, suitable cost functions need to be defined, which allow the optimization algorithm to compare different solutions against each other. *Validation* entails the examination of the performed treatment plan by the performing physician and the monitoring of pulse delivery during the treatment, as well as monitoring the effects of the treatment in the follow-up.

## Aims

---

The aims of this doctoral thesis were to apply numerical methods in novel approaches for answering some outstanding questions in the area of exposure of workers and more sensitive members of the population to some hitherto unexplored sources or exposure scenarios. In the second direction of research, the papers are focused on developing techniques and processes for treatment planning of electroporation-based therapies.

On the subject of exposure to electromagnetic fields, the first aim was to explore the topic of simultaneous exposure to sources emitting multiple frequencies, with a particular focus on exploring different approaches for evaluating combined exposure. The second aim was to explore exposure to the stray fields generated by equipment for induction heating and for this aim we performed two studies. The first study focused on whether standards-compliant induction cookers normally intended for use by adults could cause overexposure in more sensitive groups such as children and pregnant women. The second study tried to answer whether spatial averaging of measured magnetic fields can be appropriate for determining exposure in cases where magnetic fields are highly inhomogeneous and where some measurements are above the reference levels, while others are below the reference levels.

On the subject of electroporation treatment planning, the aim was to develop techniques and algorithms for performing patient-specific treatment plans. The techniques were first developed and deployed for the treatment of a deep-seated melanoma metastasis in the patient's thigh. Along with the development of the methods for treatment planning, the aim was to also verify the robustness and practical applicability of the treatments. Finally, the algorithms for treatment planning, which were first developed for treatment planning of ECT, were extended to also apply to IRE and GET treatment planning. Along with the development of methods for computation and optimization of treatment plans, advanced visualizations were developed which intend to present the large amounts of data generated by the computation in a user-friendly and accessible way.



## Research papers

---

The research papers are presented in a chronological fashion with the papers pertaining to the two groups (dosimetry of human exposure to electromagnetic fields and electroporation treatment planning) following each other. In the area of the use of numerical modelling for dosimetric / preventive applications, we first explored the subject of multiband base-station antennas (Kos *et al* 2011a). Since the introduction of third-generation mobile networks, which coexist with older second-generation networks, the widespread adoption of multiband antennas was necessary, due mostly to spatial restrictions – the operators needed to install equipment operating in a different frequency range at existing sites. Such multiband antennas consist of independent systems for multiple-frequency transmission integrated into one antenna housing. According to the upcoming worker safety regulations, such antennas would need to be evaluated for occupational exposure. Our main interest was to evaluate the interaction of the three contributions in relation to the total exposure. We wanted to explore whether the contributions were completely additive, meaning that the sum of the maximum possible exposure from each frequency can be used for comparison with the basic restrictions, or if the total exposure is considerably lower than the sum of maximum possible exposures. The results indicated that the sum of maximum possible exposures from each frequency is not overly conservative, since it overestimates the real total exposure by a maximum of 50 % and a minimum of 5 %.

The second paper focused on one of the less explored frequency regions in terms of exposure and also investigated a more at-risk group, namely pregnant women and children (Kos *et al* 2011b). The exposure we considered was a device of increasing popularity – the induction cooker. They are energy efficient electrical cookers, which work by heating the cooking vessel with inductive heating using magnetic fields from 20 kHz to 100 kHz. We compared the exposure relative to the basic restrictions in the original ICNIRP guidelines and the newer 2010 ICNIRP guidelines. We found that the exposure reached a higher percentage of the original guidelines than the new guidelines, but in all cases, the exposure was below the basic restrictions in the realistic cases examined.

In the third paper, we continued the theme of induction heating, albeit this time in an industrial application (Kos *et al* 2012). Since there were no published data available on the exposure to such equipment in terms of the numerical dosimetry of fields inside the human body, we investigated the case of such inhomogeneous exposure. Additionally, we wanted to explore the possibility of using the spatial

averaging of measured fields in determining compliance, to essentially allow work in areas where measured magnetic flux density in free space exceeds the reference levels, but the real exposure in terms of basic restrictions and fields inside the human body could conceivably still be below the basic restriction. We found that for distances greater than 20 cm from the source this is indeed the case, since the inhomogeneous fields don't cause the basic restrictions to be exceeded. Further than a metre from the source, such averaging is again not very applicable, since the fields become so homogeneous that the averaging has less of an effect.

In the second group of papers, pertaining to treatment planning for electroporation-based treatments, we started by preparing a treatment plan for the first reported case of treatment of deep seated tumours using needle electrodes and intravenous bleomycin (Miklavcic *et al* 2010). The patient had a melanoma metastasis in the thigh and we prepared a treatment plan for guidance of the patient's treatment. Although only a partial response of the treated tumour was achieved, this nevertheless paved the way for numerical treatment planning in more patients and based on the gathered data, the two following studies were also performed.

In the second paper, we investigated the robustness of such a treatment plan in the light of inevitable errors that can occur during electroporation treatment (Kos *et al* 2010). We used the model of the tumour in the thigh described in the aforementioned paper to compute the deviation from the optimal result (i.e. coverage with sufficiently strong electric fields) depending on possible errors in the positioning of the electrodes, lower-than-specified applied voltages and variations in tissue parameters (such as conductivity and electroporation threshold).

The third paper (Edhemovic *et al* 2011) contains a report of the successful application of lessons learned in previous research, reported in the first two papers. In this paper, we reported the use of the applied procedures for treatment planning in the treatment of an otherwise untreatable metastasis of colorectal carcinoma in the liver. The treatment was very successful, as the whole treated tumour was confirmed to be non-viable by histological analysis.

The last paper in the second group (Zupanic *et al* 2012) used the same anatomy as the first two papers in this group, however in this paper we investigated the optimal positioning of electrodes for different treatment goals, i.e. electrochemotherapy, tissue ablation by irreversible electroporation and gene electrotransfer for gene therapy. The three approaches require different cell responses and therefore different profiles of applied electric fields. In order to achieve that, we designed a different cost function for each treatment modality and used these cost functions with a genetic optimization algorithm to

optimize electrode positions and applied voltages using different numbers of electrodes. As anticipated, the optimization algorithm returned markedly different results for the three different treatment modalities. To aid in the representation of the developed treatment plans, we also developed three new visualisations to provide insight into the data given by the model.

## Paper 1

**Title:** Exposure Assessment in Front of a Multi-Band Base Station Antenna

**Authors:** Kos Bor, Valič Blaž, Kotnik Tadej, Gajšek Peter

**Publication:** Bioelectromagnetics

**DOI:** 10.1002/bem.20640

**Year:** 2011

**Volume:** 32

**Number:** 3

**Pages:** 234-242

## Exposure Assessment in Front of a Multi-Band Base Station Antenna

Bor Kos,<sup>1,2</sup> Blaž Valič,<sup>2</sup> Tadej Kotnik,<sup>1</sup> and Peter Gajšek<sup>2\*</sup>

<sup>1</sup>Faculty of Electrical Engineering, University of Ljubljana, Ljubljana, Slovenia

<sup>2</sup>INIS – Institute of Non-ionizing Radiation, Ljubljana, Slovenia

This study investigates occupational exposure to electromagnetic fields in front of a multi-band base station antenna for mobile communications at 900, 1800, and 2100 MHz. Finite-difference time-domain method was used to first validate the antenna model against measurement results published in the literature and then investigate the specific absorption rate (SAR) in two heterogeneous, anatomically correct human models (Virtual Family male and female) at distances from 10 to 1000 mm. Special attention was given to simultaneous exposure to fields of three different frequencies, their interaction and the additivity of SAR resulting from each frequency. The results show that the highest frequency—2100 MHz—results in the highest spatial-peak SAR averaged over 10 g of tissue, while the whole-body SAR is similar at all three frequencies. At distances >200 mm from the antenna, the whole-body SAR is a more limiting factor for compliance to exposure guidelines, while at shorter distances the spatial-peak SAR may be more limiting. For the evaluation of combined exposure, a simple summation of spatial-peak SAR maxima at each frequency gives a good estimation for combined exposure, which was also found to depend on the distribution of transmitting power between the different frequency bands. *Bioelectromagnetics* 32:234–242, 2011. © 2010 Wiley-Liss, Inc.

**Key words:** occupational RF exposure; multi-band base station; finite-difference time-domain method; whole-body SAR; spatial-peak SAR

### INTRODUCTION

Maintenance workers and technicians in the mobile communications industry often have to work in the vicinity of mobile communication base station antennas and it is not always possible to turn off all transmitters at a site. Occasionally, other workers also have to perform their tasks close to base station antennas, sometimes without the knowledge of the base station operator. Because the strongest fields are found near base station antennas, an exposure assessment is needed for all those who may come close to them. With the Directive 2004/40/EC coming into effect, all employers in the European Union will be required to assess the levels of electromagnetic fields (EMF) to which their workers are exposed. Because multi-band antennas for mobile communications are ever more widespread, in this study we present a study on how electromagnetic sources of this type interact with the human body, with the focus on compliance testing with basic restrictions.

Exposure limits are defined in the International Commission on Non-Ionizing Radiation Protection (ICNIRP) Guidelines [ICNIRP, 1998] and the Institute of Electrical and Electronics Engineers (IEEE) standard C95.1 [IEEE, 2006]. In the frequency band of Global System for Mobile Communications (GSM) and Universal Mobile Telecommunications System (UMTS)

mobile networks ranging from 900 to 2100 MHz, both use the specific absorption rate or SAR—the measure of absorbed power per mass of tissue—as the dosimetric quantity. Since SAR in a human body cannot be measured non-invasively, experimental assessment has to be performed on phantoms—plastic shells approximating the shape of the human body filled with conductive liquid [CENELEC, 2002]. A robotic measurement setup is usually used to scan the volume of the phantom for highest SAR values. As an alternative, numerical assessment allows investigating SAR in a more realistic, heterogeneous model of the body, with finite-difference time-domain (FDTD) method being the most commonly used [Hand, 2008]. Several 3D heterogeneous anatomical models have been constructed either from cryosection [Ackerman, 1998] or

Grant sponsor: Slovenian Research Agency (Project L7-2231).

\*Correspondence to: Peter Gajšek, INIS, Pohorskega bataljona 215, SI-1000 Ljubljana, Slovenia. E-mail: peter.gajsek@inis.si

Received for review 10 February 2010; Accepted 16 November 2010

DOI 10.1002/bem.20640

Published online 22 December 2010 in Wiley Online Library (wileyonlinelibrary.com).

from images of high-resolution computed tomography or magnetic resonance imaging [Dimbylow, 1997; Christ et al., 2010].

A number of studies on near-field exposure to base station antennas have been published, ranging from measurement of fields [Cooper et al., 2002] and numerical calculation of SAR and EMF [Martinez-Burdalo et al., 2005; van Wyk et al., 2005; Lacroux et al., 2008] to estimation formulas based on antenna parameters [Faraone et al., 2000; Thors et al., 2008]. All of these studies have investigated the exposure to one frequency at a time. In realistic settings, however, there are often several transmitters at one site, operating at different frequencies simultaneously. The most interesting case is three-band antennas, which combine all the three common mobile communication frequencies (900, 1800, and 2100 MHz) in a single panel antenna and are widely used by network providers. Because the EMF of all three frequencies are radiated simultaneously in both space and time, a combined exposure evaluation gives a more complex and complete picture than if the exposure to each frequency is assessed alone.

In this study, we present a model of a commercially available three-band antenna and its interaction with different heterogeneous human models. We also assess the most important factors limiting the safety distance and compare our results with previously published data. The goals of this study were to investigate two different approaches for evaluating simultaneous exposure to multiple frequencies: to evaluate their practical usability, and to determine their influence on the final compliance regions for base station antennas.

## MATERIALS AND METHODS

### Numerical Computation

We used the SEMCAD X version 14 (Schmid & Partner Engineering, Zurich, Switzerland) platform for modeling and simulations. The FDTD is very suitable for evaluating human exposure to radiofrequency EMF as the computational cost rises linearly with the size of the problem. In all cases, the human body and the box phantom were discretized to a resolution of  $2 \text{ mm} \times 2 \text{ mm} \times 2 \text{ mm}$  as a suitable trade-off between accuracy and computational cost [Gosselin et al., 2009]. In FDTD simulations, the number of cells per wavelength in the medium has an effect on wave propagation speed and field attenuation. At the highest frequency used in our simulations (2100 MHz), the tissue with the smallest number of cells per wavelength is the gallbladder (8.5 cells per wavelength). However, the number of cells per wavelength in tissues closer to the surface,

such as muscle, skin, fat etc., which get the bulk of EMF exposure, is higher than 9.5. Each simulation was run for 20 periods of the central frequency to ensure that the wave propagated throughout the entire computational domain as well as to allow the simulation to reach a steady state.

### Antenna Model and Validation

A three-band panel base station antenna (Kathrein 742 265, Kathrein; Scala Division, Medford, OR) was evaluated. It has two sets of radiating elements, one for 900 MHz GSM with six radiating elements, and another for 3G UMTS at 2100 MHz and GSM at 1800 MHz with 11 radiating elements. All the three bands can be used simultaneously by using appropriate combiners. We modeled the geometry based on an actual antenna that has been taken out of use and dismantled; we were able to model the array and the internal structure as shown in Figure 1. The metal parts were modeled as perfect electric conductors, while the internal plastic parts and the radome were modeled as lossy dielectric material ( $\epsilon_r = 4.3$ ,  $\sigma = 0.001 \text{ S/m}$ ). The radiating elements were excited in the simulation at the direct location of the connecting cables and the feeding network was not modeled, which means that the internal losses were not included in the simulation. The antenna under investigation has a double cross-polarization of  $+45^\circ$  and  $-45^\circ$ , which provides diversity in a space-efficient manner. This means that many significant parts of the antenna are at a  $45^\circ$  angle to the main axes of the antenna, which required the spatial discretization of the computational grid to be relatively fine—the smallest steps were  $<0.5 \text{ mm}$ .

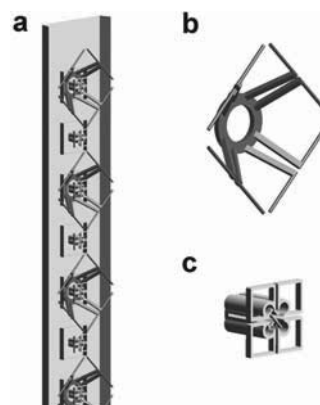


Fig. 1. Internal structure of the antenna. Top half of the antenna array is shown on the left (a); GSM 900 radiating element (b) and GSM 1800/UMTS radiating element (c) are shown on the right. Internal plastic parts for structural reinforcement were included in the model but are not shown in this figure.

Two excitation schemes were evaluated and compared to published measurement results [Toivonen et al., 2009]. The accuracy of the antenna model in free space was also evaluated by comparing calculated far-field radiation patterns with the far-field data from the antenna manufacturer. In the first scheme, all radiating elements were excited with the same signal, using a voltage source at 1 V amplitude as used previously by Gosselin et al. [2009]. In the second scheme, however, the elements were excited at a constant phase, but at relative amplitudes of 0.54, 0.78, 1, 1, 0.78, and 0.54 (as reported by van Wyk et al. [2005]), with the relative amplitude 1 applied to the elements in the center of the antenna (two center-most elements at 900 MHz and three center-most elements at 1800 and 2100 MHz). After the simulation, the resulting fields were normalized to 1 W radiated power. Both excitations used a constant phase between the elements because more accurate phase distribution between the elements was not available.

Before calculating SAR in the human models, we had validated our antenna model. Several simulations were performed and compared with published measurements, first in free space, and then with a box phantom (500 mm × 800 mm × 200 mm) as detailed in the CENELEC 50383 standard [CENELEC, 2002]. For the free-space simulations, the FDTD grid was padded with 800 mm of background in the direction of the main beam, and to  $4\lambda$  in the other directions. The  $E$  field was then calculated and the maximum value of  $E_{RMS}$  was obtained in the planes parallel to the antenna surface at distances of 10, 100, 300, and 600 mm; this method corresponds very well to the plane sweep measurement described in CENELEC [2002] and Toivonen et al. [2009].

Localized spatial-peak SAR (henceforth:  $SAR_{10g}$ ) in the box phantom fluid was calculated at the aforementioned distances between the phantom and the antenna and compared to measurements of the same antenna published in the literature [Toivonen et al., 2009]. The relative permittivities of the phantom fluid were 38.1, 39.4, and 34.8 for GSM 900, GSM 1800, and UMTS, respectively, and the electric conductivities were 0.99, 1.4, and 1.56 S/m for GSM 900, GSM 1800, and UMTS, respectively. For each point examined, a cube was used as the averaging volume for  $SAR_{10g}$  with an algorithm according to the IEEE C95.3 standard [IEEE, 2002].

### Human Model

We used the Virtual Family male and female anatomical human models [Christ et al., 2010]. They represent an average European male and female, with a height of 1.74 and 1.6 m, respectively, and a mass of 70

and 58 kg, respectively. The body mass indexes of the two models are very similar: 23.1 for the male model and 22.7 for the female. Tissue parameters were evaluated from the well-known parametric model [Gabriel et al., 1996b] for each center frequency used in the simulations.

The simulations were performed for three separate setups at five different distances between the antenna and body measured in the normal direction from the front of the antenna radome. The male model was simulated in two positions: (i) with the head near the center of the antenna, so as to represent the worst case for  $SAR_{10g}$  in the head, and (ii) with the body at the same height as the antenna, to represent the worst case for whole-body SAR (henceforth:  $SAR_{wb}$ ). The female model was positioned in a manner similar to the second male position.

In all cases, the body was positioned facing the antenna, oriented in such a way that the distance between the antenna and the body was perpendicular to the antenna's long axis and was kept as constant as possible. The distances are therefore shortest at the nose, and longer, for example, at the neck and the legs. The only exception to this is the feet, which are turned forward in the model; the toes are therefore closer to the antenna than the rest of the body. The different positions of the human models in front of the antenna are illustrated in Figure 2.

### Evaluating Combined Exposure

The ICNIRP Guidelines [ICNIRP, 1998] give the following formula for determining whether the basic restrictions have been exceeded in the case of combined

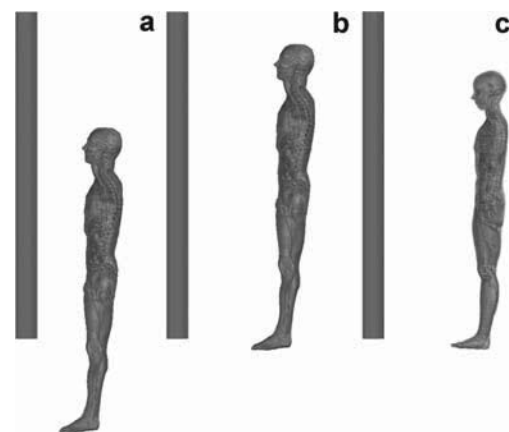


Fig. 2. Illustration of the different positions of the models in front of the antenna. Positions 1 (a) and 2 (b) of the male model are shown on the left. The female model was positioned similar to male 2, with the feet at the same height (c).

exposure:

$$\sum_i \frac{\text{SAR}_i(f_i)}{\text{SAR}_L(f_i)} \leq 1$$

where  $\text{SAR}_i$  is SAR caused by the field at frequency  $f_i$  and  $\text{SAR}_L$  is the basic restriction. The guidelines specify that the effects of the fields of different frequencies should be examined for additivity, and if they are found to be additive, the maximum value of SAR at each frequency should be used. With  $\text{SAR}_{\text{wb}}$ , this is the only possibility, as it is an integrated value over the whole body.  $\text{SAR}_{10\text{g}}$ , however, is aimed at preventing small localized heat stress in tissues. If there are several hot-spots in the body, all of them caused by the same frequency and all below the basic restriction, the exposure is within the limits. However, if the hot-spots are caused by different frequencies, then each of them being below the basic restriction is not necessarily sufficient because the sum in the formula above could still exceed 1.

To evaluate the combined exposure and explore the additivity of  $\text{SAR}_{10\text{g}}$  in the case of the three-band base station antenna in more detail, we summed the  $\text{SAR}_{10\text{g}}$  values voxel by voxel using the following algorithm. First, an FDTD simulation for each frequency present in the case under investigation was run. To enable the results to be added in a simple manner, without requiring further interpolation of data, the same computational grid was used in all simulations. Next, the  $\text{SAR}_{10\text{g}}$  values were extracted and normalized to the total power of each frequency. The contributions from each frequency were then added together voxel by voxel. Finally, the maximum  $\text{SAR}_{10\text{g}}$  was determined from the sum of all contributing frequencies and this was compared with the basic restrictions.

We used the efficient averaging algorithm based on IEEE C95.3 standard [IEEE, 2002], which is

included in the SEMCAD package. In comparison to the more general requirement that the tissue over which the SAR is averaged only has to be contiguous, the averaging volume in the IEEE standard is more precisely defined (a cube) and thus more broadly comparable. The averaging speed is also crucial because very big meshes are required to simulate whole humans, and in order to find the global maxima the algorithm has to be applied to each voxel in the simulation.

In evaluating the combined effects of the three different frequencies, it is necessary to keep in mind that in general, the different bands will have different total radiated powers. In total, eight different distributions of radiated power among the three frequencies were investigated, with the ratios of power between GSM 900, GSM 1800 and UMTS being the following, respectively: 1–1–1, 1–2–2, 1–2–5, 2–3–5, 2–3–1, 2–2–5, 5–3–2, and 5–3–5. To enable a direct comparison between results with a different total radiated power, we normalized all results to 1 W.

## RESULTS

### Antenna Model Validation

In order to validate our numerical model, we compared the simulated free-space far-field pattern with the manufacturer’s data, and good agreement was obtained for the non-uniform excitation scheme: the differences in the vertical half-power beamwidth were  $0.5^\circ$ ,  $0.1^\circ$ , and  $0^\circ$  at 900, 1800, and 2100 MHz, respectively, and the differences in the maximum gain were 1.1, 0, and 1.8 dB at 900, 1800, and 2100 MHz, respectively. Furthermore, we compared the results of our simulations to previously published data [Toivonen et al., 2009], both for free-space maximum  $E_{\text{RMS}}$  and for  $\text{SAR}_{10\text{g}}$  inside a standardized box phantom. The results are presented in Table 1. With respect to

TABLE 1. Comparison Between Simulated and Measured Values

Distance (mm)	GSM 900			GSM 1800			UMTS		
	Meas. <sup>a</sup>	Sim.	Diff. (%)	Meas. <sup>a</sup>	Sim.	Diff. (%)	Meas. <sup>a</sup>	Sim.	Diff. (%)
$E_{\text{max}}$ (V/m RMS)									
10	46.7	56.5	21	54.9	62.7	14	65.2	80.9	24
100	32.2	38.3	19	40.3	40.4	0	46.2	49.9	8
300	20.3	27.3	34	24.7	32	30	29.8	31.4	5
600	17	21	24	18.7	23.5	26	21.7	22.3	3
$\text{SAR}_{10\text{g}}$ (W/kg)									
10	0.230	0.236	2	0.235	0.260	11	0.355	0.474	33
100	0.058	0.086	49	0.088	0.098	11	0.202	0.241	20
300	0.017	0.030	76	0.066	0.060	–9	0.047	0.062	32
600	0.012	0.020	70	0.020	0.027	36	0.035	0.045	28

The presented  $E$  values are the maximum measured or simulated  $E_{\text{max}}$  (V/m RMS) in a plane sweep measurement at different distances from the antenna, while the SAR values represent the maximum measured or simulated  $\text{SAR}_{10\text{g}}$

<sup>a</sup>Published in Toivonen et al. [2009].

the non-uniform excitation scheme, the results for the first excitation (with all amplitudes equal to 1) were, on average, 15% lower for the  $E$  field, and up to 40% lower for SAR. The non-uniform excitation scheme was finally selected for the human model calculations and the uncertainty analysis was based on that excitation scheme. The uncertainties of the antenna model are discussed below. The simulated field is shown on the slice plot in Figure 3. The slices pass through the middle of the antenna and present a side view of the panel.

### Error Analysis

Among all 24 data points, comparing simulations and measurements in Table 1, the largest error of our simulations was 2.6 dB, while the error was smaller than 2 dB in more than 80% of the cases. Based on these errors and the uncertainty of the original measurement setup (approximately 1 dB for extended uncertainty, based on a similar setup described by Kuster et al. [2006]), a conservative estimate of the errors of the model is 3.2 dB, systematically in the direction of overestimating the actual exposure. The contributions to the uncertainty are the following: unknown excitation scheme used in the actual antenna (i.e., differences in power fed to each element and also each element's relative phase); internal losses in the real antenna that reduce the total radiated power by an unknown amount; difference in matching between different elements at the same frequency; and the unknown effect of the proximity of conductive bodies on the feeding network and power distribution between different radiating elements.

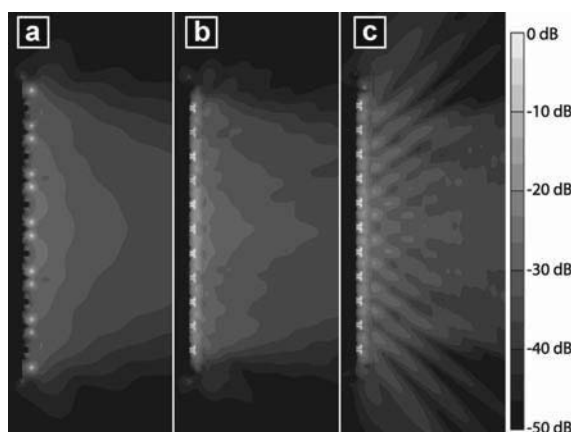


Fig. 3.  $E_{\text{RMS}}$  in the center plane of the antenna at 1 W total radiated power. From left to right are fields at (a) 900 MHz, (b) 1800 MHz, and (c) 2100 MHz. The scale is in dB, and 0 dB corresponds to 1000 V/m.

*Bioelectromagnetics*

The values of SAR in the human model are further influenced by uncertainties in tissue dielectric parameters [Gabriel et al., 1996a] and to a small extent by the number of FDTD cells per wavelength in the FDTD simulation (only at 2100 MHz). The number of FDTD cells per wavelength does increase the numerical propagation speed error by a small amount [Taflove and Hagness, 2005]; however, it is still small with respect to the uncertainties in dielectric properties of body tissue [Gabriel et al., 1996a], in particular its permittivity. The uncertainties in permittivity have a greater effect when  $\text{SAR}_{10\text{g}}$  values are low compared to the  $\text{SAR}_{\text{wb}}$ , or when the errors are involved in tissues that form a large part of the model (e.g., muscle) [Mason et al., 2000; Gajsek et al., 2001a,b].

### Human Exposure

The results for human exposure are presented in Table 2, which lists the percentage of basic restriction per 1 W of transmitted power.  $\text{SAR}_{10\text{g}}$  in the UMTS frequency band reaches the highest level—5.41%/W at 10 mm from the antenna for the male model in position 2.  $\text{SAR}_{10\text{g}}$  is the highest at 2100 MHz in most other cases as well. This is expected since the body absorbs higher frequencies in a smaller volume; thus, for a similar total absorbed power, the average power in a constant volume is larger.

For  $\text{SAR}_{\text{wb}}$ , all the three frequencies result in a similar exposure. Since the antenna in the study is larger than the human models used in the study, the energy is absorbed almost uniformly across the whole body. Therefore, the localized  $\text{SAR}_{10\text{g}}$  is the more restrictive constraint up to distances of about 200 mm. At larger distances,  $\text{SAR}_{\text{wb}}$  is the more limiting factor. The results of combined exposure are presented in Table 3. The comparison of the two summation approaches in Table 4 shows that the largest difference between them is 55% for the female model at 200 and 500 mm from the antenna (50–30–20% power ratio). The median value of all the computed differences (they are not normally distributed) was 18.5%, with the 25th and 75th percentile being 11% and 27%, respectively.

In the case of occupational exposure to base station antennas, some tissues have a higher average exposure than others. While the maximum peak values are always found in the tissues closest to the surface of the body, such as skin or muscle, some internal organs also receive a high exposure relative to their mass. We have computed SAR statistics for each different tissue in the model, and the highest mean SAR values over the entire tissue were found in the cornea, larynx, penis, sclera, thyroid gland, and testes. These tissues all have a low total mass, so the average SAR over the

**TABLE 2. Simulated Values of SAR in % of Basic Restriction (10 W/kg for SAR<sub>10g</sub> and 0.4 W/kg for SAR<sub>wb</sub>) per Watt of Total Radiated Power**

Distance (mm)	GSM 900 only			GSM 1800 only			UMTS only		
	Male 1	Male 2	Female	Male 1	Male 2	Female	Male 1	Male 2	Female
<b>SAR<sub>10g</sub></b>									
10	2.25	2.96	1.45	3.18	3.25	2.99	3.81	5.41	3.04
100	1.15	1.27	1.03	2.33	1.79	1.60	2.94	1.74	1.65
200	0.87	1.13	0.96	1.08	1.77	1.03	1.10	1.37	1.11
500	0.48	0.55	0.56	0.65	0.58	0.51	0.62	0.63	0.64
1000	0.26	0.31	0.42	0.40	0.45	0.41	0.47	0.37	0.39
<b>SAR<sub>wb</sub></b>									
10	1.66	2.33	2.95	1.52	2.18	2.45	1.68	2.30	2.45
100	1.28	1.75	2.36	1.21	1.77	2.05	1.15	1.63	1.70
200	1.10	1.58	2.06	1.00	1.39	1.55	0.93	1.28	1.50
500	0.71	0.96	1.32	0.69	0.98	1.13	0.67	0.94	1.04
1000	0.43	0.59	0.81	0.43	0.63	0.69	0.38	0.51	0.57

The values for SAR<sub>10g</sub> and SAR<sub>wb</sub> at each frequency are shown separately

whole tissue can reach more than 50% of the maximum SAR<sub>10g</sub>.

## DISCUSSION

We have presented a calculation of the occupational exposure in front of a multi-band base station antenna. Prior to calculating exposure in anatomical human models, we have conducted an extensive validation of the model by comparing our results to previously published studies. This comparison shows that our approach gives a good estimation of the SAR inside a standardized phantom [CENELEC, 2002], even at close distances. The fact that the results are biased toward overestimating the exposure is related to the choice of excitation of the separate antenna elements. Namely, we have chosen a symmetrical, non-uniform excitation amplitude at different radiating elements, as described by van Wyk et al. [2005], rather than an identical amplitude at each element, with the goal of obtaining better results in the closest vicinity of the antenna. Another source of discrepancy is the fact that the internal feeding network of the antenna was not modeled and, therefore, the internal losses of the antenna are not taken into account. Since the measurements [Toivonen et al., 2009] were normalized to 1 W input power to the antenna, and our simulations are normalized to 1 W total radiated power, the difference between the two should be taken into account. However, since the exact internal losses are unknown, they cannot be separated from other sources of errors in the evaluation.

At larger distances, the SAR<sub>wb</sub> is the more limiting factor in our results as well as in previously published literature [Thors et al., 2008; Gosselin et al.,

2009], especially when large antennas are considered. The close distance between the antenna and the body affects the impedance of the radiating elements and thus the matching. The resulting change in the antenna feed structure has been studied previously, and has been found to influence the calculated values of SAR [Joseph and Martens, 2005; van Wyk et al., 2005]. Our validation (Table 1) shows that the model does not underestimate the SAR even at the smallest antenna-phantom distances. The largest difference between measurements and our simulated results was 2.6 dB, which may be partly caused by less than ideal matching of the radiating elements (average SWR was 1.58, 1.5, and 4.5 at 900, 1800 and 2100 MHz, respectively).

The results of the simulations performed on the anatomical model show that the occupational exposure to a single frequency is the highest at 2100 MHz for localized SAR<sub>10g</sub>, but for the SAR<sub>wb</sub> none of the frequencies plays such a dominant role, with all three frequencies contributing very similarly to exposure in each of the three cases examined. The differences between exposures for the male (position 2) and the female model in SAR<sub>10g</sub> are not very large, but the female does have a higher exposure for SAR<sub>wb</sub>. This can be explained by the smaller weight of the female model; although the total power absorbed by the female is slightly lower than by the male, the ratio of power to mass, and thus SAR<sub>wb</sub>, is larger in the end.

In evaluating the simultaneous exposure, we compared two different summation approaches: a simple method of summation of the maxima, and a much more demanding voxel-by-voxel summation. The largest difference in the results caused by the difference in the summation approach is 55% in the female model

240 Kos et al.

**TABLE 3.** Comparison of Voxel-by-Voxel Summation at Different Ratios of Transmitted Power Power (GSM 900–GSM 1800–UMTS 2100)

Distance (mm)	Combined SAR <sub>10g</sub> (power ratio)							
	1–1–1	1–2–2	1–2–5	2–3–5	2–3–1	2–2–5	5–3–2	5–3–5
Male 1								
10	2.42	2.70	3.11	2.84	2.38	2.88	2.04	2.43
100	1.89	2.18	2.46	2.24	1.80	2.24	1.55	1.84
200	0.83	0.88	0.96	0.90	0.80	0.90	0.77	0.83
500	0.44	0.47	0.49	0.46	0.48	0.47	0.42	0.42
1000	0.32	0.36	0.40	0.37	0.31	0.36	0.27	0.31
Male 2								
10	3.27	3.34	3.95	3.55	3.16	3.68	3.15	3.30
100	1.52	1.61	1.65	1.60	1.54	1.58	1.42	1.48
200	1.07	1.08	1.09	0.99	1.26	1.02	1.12	1.00
500	0.52	0.52	0.55	0.53	0.51	0.54	0.51	0.52
1000	0.36	0.38	0.37	0.37	0.37	0.36	0.34	0.34
Female								
10	2.06	2.33	2.54	2.36	2.03	2.34	1.72	1.99
100	1.21	1.36	1.46	1.37	1.20	1.35	1.03	1.16
200	0.73	0.78	0.88	0.82	0.69	0.84	0.65	0.74
500	0.42	0.47	0.53	0.49	0.39	0.50	0.36	0.42
1000	0.28	0.32	0.34	0.32	0.28	0.32	0.29	0.27
Distance (mm)	Combined SAR <sub>wb</sub>							
	1–1–1	1–2–2	1–2–5	2–3–5	2–3–1	2–2–5	5–3–2	5–3–5
Male 1								
10	1.62	1.61	1.64	1.63	1.59	1.64	1.62	1.64
100	1.22	1.20	1.18	1.20	1.23	1.19	1.24	1.22
200	1.01	0.99	0.97	0.98	1.02	0.98	1.04	1.01
500	0.69	0.69	0.68	0.68	0.70	0.68	0.70	0.69
1000	0.42	0.41	0.40	0.41	0.42	0.41	0.42	0.41
Male 2								
10	2.27	2.26	2.27	2.27	2.25	2.28	2.28	2.28
100	1.72	1.71	1.68	1.70	1.74	1.69	1.73	1.71
200	1.42	1.39	1.35	1.37	1.44	1.37	1.47	1.42
500	0.96	0.96	0.95	0.96	0.97	0.95	0.96	0.96
1000	0.58	0.57	0.55	0.56	0.59	0.55	0.58	0.57
Female								
10	2.62	2.55	2.51	2.55	2.62	2.56	2.70	2.64
100	2.04	1.98	1.87	1.94	2.10	1.93	2.14	2.04
200	1.70	1.63	1.58	1.63	1.71	1.64	1.79	1.73
500	1.17	1.14	1.10	1.13	1.18	1.13	1.21	1.17
1000	0.69	0.67	0.63	0.66	0.71	0.65	0.73	0.69

All results are shown in % of basic restriction (10 W/kg for SAR<sub>10g</sub> and 0.4 W/kg for SAR<sub>wb</sub>) and are normalized to 1 W total radiated power.

(at 200 and 500 mm distances). This shows that for similar designs of collinear multi-band base station antennas, where the radiating elements of different frequencies are packed close together, the peaks of energy absorption tend to be located at similar spots in the human body, also at different frequencies. The combined SAR<sub>10g</sub> exposure is dominated by the highest frequency present—in this case, 2100 MHz. The additivity is also illustrated in Figure 4, where a separate comparison between each frequency band and a combined exposure is presented. Since the difference

between the voxel-by-voxel summation and the much simpler summation of maxima is relatively small, the simple approach can be recommended for investigations of compliance with the basic restrictions. The voxel-by-voxel summation requires much more storage and computational power. To calculate the maximum SAR for a different ratio of powers at the antenna, it is necessary to store the data for SAR for the whole-body volume for each frequency (for FDTD, this represents a 3D array with as many elements as the number of tissue voxels), and then find the maximum element of the

TABLE 4. Overestimation of Combined SAR by the Simple Summation Approach

Distance (mm)	Combined SAR <sub>10g</sub> (power ratio), %							
	1-1-1	1-2-2	1-2-5	2-3-5	2-3-1	2-2-5	5-3-2	5-3-5
Male 1								
10	27	20	11	17	25	15	40	26
100	13	7	4	7	13	7	20	15
200	22	19	11	16	26	15	27	21
500	33	30	23	30	22	26	33	35
1000	18	11	7	11	18	11	26	19
Male 2								
10	18	21	15	20	11	19	12	20
100	5	4	2	4	5	4	7	6
200	33	37	32	46	18	38	22	37
500	13	13	10	12	14	11	13	13
1000	5	3	2	3	5	4	7	6
Female								
10	21	16	11	15	23	14	30	21
100	17	10	7	10	18	11	29	20
200	41	34	21	28	47	26	55	39
500	34	22	12	19	40	19	55	36
1000	43	27	16	25	45	26	43	48

voxel-wise sum of these arrays weighted by appropriate radiated powers. Additionally, these SAR values will be true for only one orientation of the body and may not necessarily be the same in a different orientation.

For the presented antenna, the worst-case exposures can be evaluated for each distance from the antenna (both SAR<sub>10g</sub> and SAR<sub>wb</sub>) and from these, the maximum total radiated power that will not cause the basic restrictions to be exceeded can be determined. Taking into account the estimated error of 3.6 dB, these powers are 8, 15, 21, 33, and 54 W at 10, 100, 200, 500,

and 1000 mm, respectively. It is important to note that these are actual transmitted powers at the antenna and they should take into account the losses in the antenna feed cables, internal losses in the antenna, and losses in combiners and other equipment at a base station site.

In the case of combined, multi-band exposure, as well as for single frequencies, the SAR<sub>wb</sub> is the more limiting factor at larger distances (above 200 mm), while SAR<sub>10g</sub> becomes more restrictive at smaller distances. Similar results were obtained in previous studies [Martinez-Burdalo et al., 2005; Gosselin et al., 2009], although they only examined exposure to one frequency at a time.

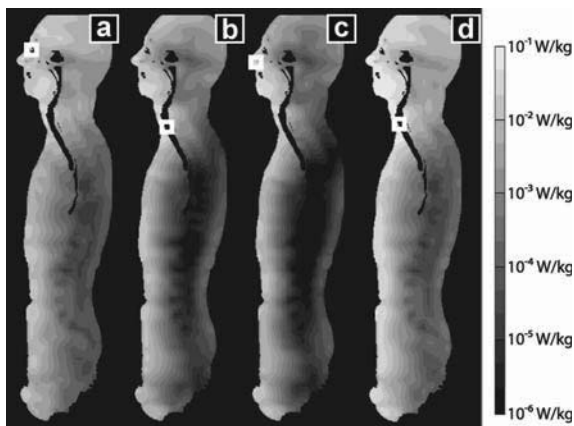


Fig. 4. SAR<sub>10g</sub> in the male model at 500 mm from the antenna. From left to right are: (a) 900 MHz, (b) 1800 MHz, (c) 2100 MHz, and (d) voxel-by-voxel combined SAR values for all three frequencies. The white squares indicate the location of the maximum values of SAR<sub>10g</sub>. The ratios of power for each frequency are 1-1-1, and the total radiated power of all frequencies is 3 W.

CONCLUSIONS

In evaluating simultaneous exposure to several frequencies emitted by a multi-band antenna, where there are several linear arrays one within the other, a simple summation of highest spatial-peak SAR values for each frequency provides a good, slightly conservative approximation of the real combined SAR. Using this approach, it is also very easy to calculate the exposure levels for different transmitting powers of the antenna in different real-life situations, so this should be the preferable method in assessing occupational exposure according to current legislation.

ACKNOWLEDGMENTS

The authors would like to thank Mobitel for providing access to the antenna presented in this work.

## REFERENCES

- Ackerman MJ. 1998. The visible human project. *Proc IEEE* 86:504–511.
- CENELEC. 2002. Basic standard for the calculation and measurement of EMF strength and SAR related to human exposure from radio base stations and fixed terminal stations for wireless telecommunications systems (110 MHz–40 GHz). European Standard EN 50383. Brussels, Belgium; CENELEC.
- Christ A, Kainz W, Hahn E, Honegger K, Zefferer M, Neufeld E, Rascher W, Janka R, Bautz W, Chen J, Kiefer B, Schmitt P, Hollenbach H, Shen J, Oberle M, Szczerba D, Kam A, Guag J, Kuster N. 2010. The Virtual Family-development of surface-based anatomical models of two adults and two children for dosimetric simulations. *Phys Med Biol* 55:N23–N38.
- Cooper J, Marx B, Buhl J, Hombach V. 2002. Determination of safety distance limits for a human near a cellular base station antenna, adopting the IEEE standard or ICNIRP guidelines. *Bioelectromagnetics* 23:429–443.
- Dimbylow PJ. 1997. FDTD calculations of the whole-body averaged SAR in an anatomically realistic voxel model of the human body from 1 MHz to 1 GHz. *Phys Med Biol* 42:479–490.
- Faraone A, Tay RYS, Joyner KH, Balzano Q. 2000. Estimation of the average power density in the vicinity of cellular base-station collinear array antennas. *IEEE Trans Vehicular Tech* 49:984–996.
- Gabriel S, Lau RW, Gabriel C. 1996a. The dielectric properties of biological tissues: III. Parametric models for the dielectric spectrum of tissues. *Phys Med Biol* 41:2271–2293.
- Gabriel S, Lau R, Gabriel C. 1996b. The dielectric properties of biological tissues: II. Measurements in the frequency range 10 Hz to 20 GHz. *Phys Med Biol* 41:2251–2269.
- Gajsek P, Hurt WD, Zirix JM, Mason PA. 2001a. Parametric dependence of SAR on permittivity values in a man model. *IEEE T Bio-Med Eng* 48:1169–1177.
- Gajsek P, Zirix JM, Hurt WD, Walters TJ, Mason PA. 2001b. Predicted SAR in Sprague–Dawley rat as a function of permittivity values. *Bioelectromagnetics* 22:384–400.
- Gosselin MC, Christ A, Kuhn S, Kuster N. 2009. Dependence of the occupational exposure to mobile phone base stations on the properties of the antenna and the human body. *IEEE Trans Electromagn Compat* 51:227–235.
- Hand JW. 2008. Modelling the interaction of electromagnetic fields (10 MHz–10 GHz) with the human body: Methods and applications. *Phys Med Biol* 53:R243–R286.
- ICNIRP. 1998. Guidelines for limiting exposure to time-varying electric, magnetic, and electromagnetic fields (up to 300 GHz). *Health Phys* 74:494–522.
- IEEE. 2002. IEEE Recommended Practice for Measurements and Computations of Radio Frequency Electromagnetic Fields With Respect to Human Exposure to Such Fields, 100 kHz–300 GHz. IEEE Std C95. 3-2002 (Revision of IEEE Std C95.3-1991).
- IEEE. 2006. IEEE Standard for Safety Levels with Respect to Human Exposure to Radio Frequency Electromagnetic Fields, 3 KHz to 300 GHz. IEEE Std C95. 1-2005 (Revision of IEEE Std C95.1-1991).
- Joseph W, Martens L. 2005. Comparison of safety distances based on the electromagnetic field based on the SAR for occupational exposure of a 900-MHz base station antenna. *IEEE Trans Electromagn Compat* 47:977–985.
- Kuster N, Torres VB, Nikoloski N, Frauscher M, Kainz W. 2006. Methodology of detailed dosimetry and treatment of uncertainty and variations for in vivo studies. *Bioelectromagnetics* 27:378–391.
- Lacroux F, Conil E, Carrasco AC, Gati A, Wong MF, Wiart J. 2008. Specific absorption rate assessment near a base-station antenna (2,140 MHz): Some key points. *Ann Telecommun* 63:55–64.
- Martinez-Burdalo M, Martin A, Anguiano M, Villar R. 2005. On the safety assessment of human exposure in the proximity of cellular communications base-station antennas at 900, 1800 and 2170 MHz. *Phys Med Biol* 50:4125–4137.
- Mason P, Hurt W, Walters T, D'Andrea J, Gajsek P, Ryan K, Nelson D, Smith K, Zirix J. 2000. Effects of frequency, permittivity, and voxel size on predicted specific absorption rate values in biological tissue during electromagnetic-field exposure. *IEEE Trans Microwave Theor Tech* 48:2050–2058.
- Taflove A, Hagness SC. 2005. Computational electrodynamics: The finite-difference time-domain method. 3rd edition. Norwood, MA: Artech House.
- Thors B, Strydom ML, Hansson B, Meyer FJC, Karkkainen K, Zollman P, Ilvonen S, Tornevik C. 2008. On the estimation of SAR and compliance distance related to RF exposure from mobile communication base station antennas. *IEEE Trans Electromagn Compat* 50:837–848.
- Toivonen T, Toivo T, Puranen L, Jokela K. 2009. Specific absorption rate and electric field measurements in the near field of six mobile phone base station antennas. *Bioelectromagnetics* 30:307–312.
- van Wyk MJ, Bingle M, Meyer FJC. 2005. Antenna modeling considerations for accurate SAR calculations in human phantoms in close proximity to GSM cellular base station antennas. *Bioelectromagnetics* 26:502–509.

## Paper 2

**Title:** Pre- and post-natal exposure of children to EMF generated by domestic induction cookers

**Authors:** Kos Bor, Valič Blaž, Miklavčič Damijan, Kotnik Tadej, Gajšek Peter

**Publication:** Physics in Medicine and Biology

**DOI:** 10.1088/0031-9155/56/19/001

**Year:** 2011

**Volume:** 56

**Number:** 19

**Pages:** 6149-6160

## Pre- and post-natal exposure of children to EMF generated by domestic induction cookers

Bor Kos<sup>1</sup>, Blaž Valič<sup>2</sup>, Damijan Miklavčič<sup>1</sup>, Tadej Kotnik<sup>1</sup> and Peter Gajšek<sup>2,3</sup>

<sup>1</sup> Laboratory of Biocybernetics, Faculty of Electrical Engineering, University of Ljubljana, Tržaška 25, SI-1000 Ljubljana, Slovenia

<sup>2</sup> Institute of Non-Ionizing Radiation, Pohorskega Bataljona 215, SI-1000 Ljubljana, Slovenia

E-mail: bor.kos@fe.uni-lj.si, damijan.miklavcic@fe.uni-lj.si, tadej.kotnik@fe.uni-lj.si, blaz.valic@inis.si and p.gajsek@inis.si

Received 8 March 2011, in final form 27 July 2011

Published 30 August 2011

Online at [stacks.iop.org/PMB/56/6149](http://stacks.iop.org/PMB/56/6149)

### Abstract

Induction cookers are a type of cooking appliance that uses an intermediate-frequency magnetic field to heat the cooking vessel. The magnetic flux density produced by an induction cooker during operation was measured according to the EN 62233 standard, and the measured values were below the limits set in the standard. The measurements were used to validate a numerical model consisting of three vertically displaced coaxial current loops at 35 kHz. The numerical model was then used to compute the electric field ( $E$ ) and induced current ( $J$ ) in 26 and 30 weeks pregnant women and 6 and 11 year old children. Both  $E$  and  $J$  were found to be below the basic restrictions of the 2010 low-frequency and 1998 ICNIRP guidelines. The maximum computed  $E$  fields in the whole body were 0.11 and 0.66 V m<sup>-1</sup> in the 26 and 30 weeks pregnant women and 0.28 and 2.28 V m<sup>-1</sup> in the 6 and 11 year old children (ICNIRP basic restriction 4.25 V m<sup>-1</sup>). The maximum computed  $J$  fields in the whole body were 46 and 42 mA m<sup>-2</sup> in the 26 and 30 weeks pregnant women and 27 and 16 mA m<sup>-2</sup> in the 6 and 11 year old children (ICNIRP basic restriction 70 mA m<sup>-2</sup>).

(Some figures in this article are in colour only in the electronic version)

### 1. Introduction

Induction cookers (also referred to as induction hobs) are electrical cooking appliances that use intermediate-frequency magnetic fields to heat the cooking vessel directly without heating the contact surface of the appliance itself (Acero *et al* 2010). The magnetic field induces

<sup>3</sup> Author to whom any correspondence should be addressed.

eddy currents in the ferromagnetic base of the cooking vessel and thereby generates heat from resistive losses in the base of the vessel. The induction cookers typically operate in the frequency range between 20 and 100 kHz, and can deliver powers of up to 3.6 kW (Millan *et al* 2010). Their main advantages are rapid cooking times and higher energy efficiency compared to conventional (resistive) and glass-ceramic (infrared) cookers. With decreasing prices, induction cookers are gaining in popularity and up to 300 thousand units yearly are predicted for sale in Europe alone (ICNIRP 1998).

Exposure scenarios could also include children and pregnant women that belong to a particularly sensitive group of users. It is accepted that children are generally more vulnerable than adults to some environmental, physical and chemical influences (Mancini 2004, Grandjean and Landrigan 2006). It is plausible that such vulnerability could also exist for EMFs, although this conjecture has not yet been proven (Kheifets *et al* 2005). In particular, interesting is the case of pregnant women as with the typical position of a mother in front of the cooker, the foetus is at a very small distance to the source of magnetic field. Furthermore, children might also occasionally use domestic cooking appliances and their height would put their heads, and therefore their central nervous system, closer to the field source than adults.

There are as yet few reports available on the subject of human exposure to the magnetic fields generated by induction cookers. Two papers (Stuchly and Lecuyer 1987, Yamazaki *et al* 2004) report measurements of domestic induction cookers and conclude that the fields are below the ICNIRP reference levels. Viellard *et al* (2007) have also reported that measured fields are below the reference levels at 30 cm from the device, as measured according to the EN 62233 standard. However, closer to the devices, the magnetic field approaches and in some operating conditions that can plausibly occur even exceeds the reference levels for magnetic flux density.

In this paper, we present a numerical model of a domestic induction cooker and validate it with measurements. We use the model to perform simulations of induced current density and internal electric field according to the original ICNIRP (1998) and the revised low-frequency ICNIRP (2010) guidelines in two models of pregnant women and in two models of children—a 6 year old male and an 11 year old female.

## 2. Materials and methods

### 2.1. Measurement protocol

Two European standards have been published that deal with the measurement procedures for induction cookers: the first one was the CENELEC 50366: *Household and similar electrical appliances—electromagnetic fields—methods for evaluation and measurement* (CENELEC 2003), which was superseded by the IEC 62233: *Measurement methods for electromagnetic fields of household appliances and similar apparatus with regard to human exposure* in 2008 (IEC 2005). Both standards employ a technically equivalent measurement procedure in which the fields are measured at 30 cm from the front of the device in a vertical line. The field should be averaged over an area of 100 cm<sup>2</sup> to ensure that local maxima and inhomogeneities do not affect the measurements excessively. The averaged magnetic flux density in front of the device has to be below the 1998 ICNIRP guidelines reference levels for general public (ICNIRP 1998), which is 6.25  $\mu$ T for the range from 800 Hz to 150 kHz, which includes all the frequencies used in induction cookers.

The measurement was performed with a calibrated Narda ELT-400 field meter with a 100 cm<sup>2</sup> isotropic probe (both from Narda Safety Test Solutions GmbH, Pfullingen, Germany). The instrument was used in 'field strength' mode, which has a flat frequency response across

a wide frequency range of 1–400 kHz. The analogue output of the ELT-400 was connected to a Tektronix MSO4104 oscilloscope (Tektronix Inc., Beaverton, OR, USA), with the spectrum analysis performed using FFT. According to the currently valid domestic appliance standard (IEC 2005), measurements were performed at 30 cm from the front of the induction cooker, and additionally, the fields were also measured at shorter distances of 1, 5 and 10 cm from the front of the appliance, to enable a better validation of our numerical model. The heating power was set to maximum with the boost function activated. The field meter was mounted on a non-conductive tripod and the height was varied manually. The measurements were taken at 5 cm vertical spacings, from –25 to 45 cm relative to the level of the cooking surface. The measurements were performed with a full pot of water on the largest cooker with a maximum power setting (power-boost function activated). The RMS value of the magnetic flux density (denoted henceforth as  $B$ ) was recorded in each location. Separately, the frequency spectrum was recorded on the oscilloscope to determine the frequency content and enable adequate comparison with the basic restrictions.

Additionally, we have measured the low-frequency component of  $B$  using a calibrated Wandel & Golterman EFA-3 (now Narda Safety Test Solutions GmbH, Pfullingen, Germany) field meter with a  $B$  field probe and a low-pass filter with the cut-off frequency set to 3 kHz. The measurements show that the maximum value of  $B_{\text{RMS}}$  at 1 cm distance was less than  $2.2 \mu\text{T}$ . This justified the exclusion of the ELF component of the magnetic field from the dosimetric simulations, since this value represents less than 2.2% of the reference levels according to the 1998 ICNIRP guidelines and even less than that according to the 2010 guidelines, which have a higher reference level for general public exposure.

The main components of an induction cooker are the induction coils, which are placed below the cooking surface, the ferrite magnetic substrate and the cooking vessel, which acts as a part of the resonance circuit, absorbs the magnetic field energy and converts it into heat (Acero *et al* 2010). Yamazaki *et al* (2004) have developed a method for simple characterization of the magnetic field of an induction cooker by a single magnetic dipole moment (i.e. one that can be modelled by a single current loop), but we opted for a more detailed model consisting of three vertically displaced, concentric current loops. The middle current loop presents the main (source) coil, while the upper and lower current loops, with the currents flowing in a counter-phase to the main loop, present the eddy currents in the base of the pot and in the ferrite flux guides below the main coil, respectively (Koller and Novak 2009). A comparison of such a three-loop model to the simpler single-loop model showed that in the former, the differences between simulations and measurements are smaller, in particular close to the cooker, which is the region of interest for this study (data not shown).

## 2.2. Human models

Two anatomical models of pregnant women were used in the study. The first model was made by our group by combining segmented computed tomography images of a 30 weeks pregnant woman (Shi and Xu 2004) with cross-sectional images of a female from the Visible Human database obtained from cryosection (Ackerman 1998). The original image set of Shi and Xu included only the thoracic region from below the pubic symphysis to above the liver and was extended with homogeneous upper and lower body parts using the iSeg segmenting software (Zurich Med Tech, Zurich, Switzerland). The slice thickness of the model is 7 mm in the central region, and 3 mm in the upper and lower homogeneous parts. The height of the model is 158 cm and the weight is 93 kg, giving body-mass index of 37, which classifies the subject as obese. The total weight of the model is close to the weight of the original subject as reported by Shi and Xu (2004), while the height of the original subject was not reported. The

**Table 1.** Dielectric properties of foetal tissues used in the simulations.

Tissue	Conductivity	Source
Foetal bladder	0.22	(Gabriel <i>et al</i> 1996b)
Foetal gray matter	0.34	(Lu <i>et al</i> 1996)
Foetal cerebro-spinal fluid	1.60	(Grimnes and Martinsen 2008)
Foetal eye	1.50	(Gabriel <i>et al</i> 1996b)
Homogeneous foetal body	0.44	(Lu <i>et al</i> 1996)
Foetal heart	0.65	(Gabriel <i>et al</i> 2009)
Foetal lung	0.22	(Lu <i>et al</i> 1996)
Foetal stomach	0.54	(Gabriel <i>et al</i> 1996b)
Umbilical cord	0.70	(Gabriel <i>et al</i> 1996b)
Amniotic fluid	1.50	(Gabriel <i>et al</i> 1996b)
Uterus	0.53	(Gabriel <i>et al</i> 1996b)
Skeleton of foetus	0.30	(Gabriel <i>et al</i> 2009)
Placenta	0.70	(Gabriel <i>et al</i> 1996b)

model consists of a total of 29 different tissues, and the utero-foetal unit is segmented into the following tissues: uterus, placenta, homogeneous foetal body and the skeleton of foetus. The volumes of the abdominal organs are realistic. The volume of the liver (2049 cm<sup>3</sup>) is larger than average (Dello *et al* 2011), while the volume of the spleen (218 cm<sup>3</sup>) is very close to the mean value reported by Spielmann *et al* (2005).

The second pregnant female was built by combining MRI image data (Bibin *et al* 2010) with a homogeneous three-dimensional computer-generated model of a female (Daz 3D Studio, [www.daz3d.com](http://www.daz3d.com)). The height of the model is 167 cm and the total weight is 48 kg, giving a body-mass index of 17.

The total weights of the foetuses are 0.92 and 1.48 kg for the 26 and 30 weeks pregnant models, respectively. This is very close to the median values, which are 0.89 and 1.53 kg for 26 and 30 weeks, respectively, according to a formula for foetal weight for the European ethnic group (Gardosi *et al* 1995). While the weight of the foetuses is very near the median, the weight of the mothers is either on the underweight or obese side of the spectrum.

The anatomical models of children were the 6 year old boy and 11 year old girl from the Virtual Family (Christ *et al* 2010). All models were voxelled with a resolution of  $2 \times 2 \times 2$  mm<sup>3</sup>, to provide a high spatial resolution of the results for extraction.

The electric conductivities of tissues were taken from various sources. The values used for foetal conductivities are shown in table 1. Where available, we used directly measured values for foetal tissues measured at 100 kHz, as reported by Lu *et al* (1996). They measured the values from aborted foetuses after 15 weeks of gestation. For the foetal body, we used the measurements from muscle tissue reported by Lu *et al* (1996). Measurements of the dielectric properties of placenta, amniotic fluid and umbilical cord have been reported recently by Peyman *et al* (2011); however, they measured only at frequencies above 200 MHz. Below this frequency, no such data exist; however, the conductivities of umbilical cord and placenta are close to the conductivity of blood, while the conductivity of amniotic fluid is close to that of cerebrospinal fluid. These values have been used previously at low frequencies (Hand *et al* 2006, Dimbylow 2007).

### 2.3. Numerical computations

We used the magneto quasi-static low-frequency solver implemented in SEMCAD X v 14.4 (SPEAG, Zurich, Switzerland). The solver is based on the Biot–Savart law

$$\mathbf{A}_0(\mathbf{r}) = \frac{\mu_0}{4\pi} \int_{\Omega} \frac{\mathbf{j}_0(\mathbf{r}')}{|\mathbf{r} - \mathbf{r}'|} d\mathbf{r}' \quad (1)$$

in which it assumes a constant magnetic permeability  $\mu_0$  throughout the domain of integration  $\Omega$  and computes the vector magnetic potential  $\mathbf{A}_0$  generated by the source current  $\mathbf{j}_0$ . In the lossy domain (i.e. in the regions where electric conductivity  $\sigma$  is nonzero), the electric field  $\mathbf{E}$  is then computed from the equation

$$\nabla \cdot (\sigma \mathbf{E}) = -j\omega \nabla \cdot (\sigma \mathbf{A}_0). \quad (2)$$

This equation is obtained from the more general charge continuity equation under the assumption  $\sigma \gg \omega\epsilon$  (where  $\omega$  is the angular frequency and  $\epsilon$  is the dielectric permittivity), which is valid for most body tissues.

### 2.4. Exposure scenarios

Each model was positioned standing upright with the nearest point of the body being 180 mm from the centre of the cooker, while in the lateral direction, the centres of the cooker and the body were aligned. Vertically, the models were positioned 850 mm lower than the level of the induction cooker, which represents a typical height of domestic kitchen work surfaces, as can be seen in figure 1. This choice of positioning represents an exposure scenario at least

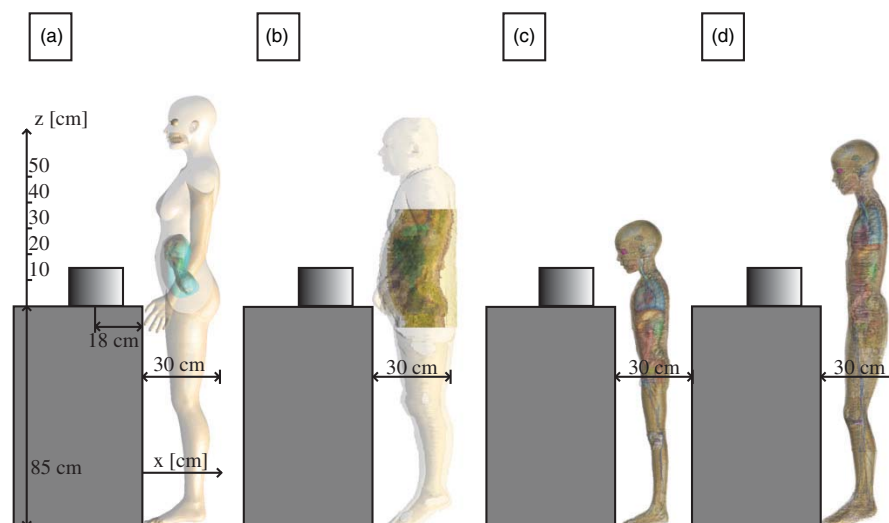


**Figure 1.** Side view of the exposure setup for the human models. The models are (a) a 50 kg, 26 weeks pregnant female (Bibin *et al* 2010), (b) a 90 kg, 30 weeks pregnant female (Shi and Xu 2004), (c) a 19 kg, 6 year old male (Christ *et al* 2010) and (d) a 36 kg, 11 year old female (Christ *et al* 2010). In all cases, the models are positioned with the feet at floor level, 85 cm lower than the level of cooking surface and with the closest point at 0 cm from the front of the appliance. The heights ( $z$ ) and distance ( $x$ ) of measurements corresponding to figure 2 are also indicated.

**Table 2.** Uncertainty budget of the measurements and numerical dosimetry.

Uncertainty sources	Tolerance (dB)	Distribution	Divisor	$c_i$	Uncertainty (dB)	Source
Measurements of $B$ field						
Reference field source	1.21	N ( $k = 2$ )	2	1	0.37	Calibration
$B$ -field probe nonlinearity	0.56	R	1.73	1	0.32	Calibration
Probe anisotropy	0.78	R	1.73	1	0.45	Calibration
Probe frequency dependence	1.12	R	1.73	1	0.42	Calibration
Reproducibility	0.5	N ( $k = 1$ )	1	1	0.5	Estimate
Numerical dosimetry						
Discretization of tissues	2.88	R	1.73	1	1.66	(Bahr <i>et al</i> 2007)
Conductivity of tissues	1.93	R	1.73	1	1.12	(Gabriel <i>et al</i> 1996a)
Induction cooker model	0.55	R	1.73	1	0.32	Estimate
Total uncertainty ( $k = 1$ )					2.02	

as realistic as a position at a distance of 30 cm from the source that is used in measurements according to the IEC standard.

### 2.5. Error analysis and uncertainty budget

The uncertainty of the measurements and simulations was evaluated and an uncertainty budget was prepared, as shown in table 2. The uncertainty contributions of measurements were as follows: the inaccuracy of the reference field source, the probe's nonlinearity, anisotropy, frequency dependence and the reproducibility of the measurement procedure (calibration from an accredited traceable laboratory). The uncertainty contributions of numerical dosimetry were as follows: uncertainty in conductivities of tissues (Gabriel *et al* 1996a), imprecision in discretization of tissues and the accuracy of the cooker model. Thus, the total estimated uncertainty of the results in this paper is 2.02 dB ( $k = 1$ ) and the extended total uncertainty is 4.04 dB. This is still low compared to the variations in fields produced by similar appliances from different manufacturers and from misaligned or improper cookware; these factors can increase the magnetic fields up to a factor of 5 (Viellard *et al* 2007).

## 3. Results and discussion

### 3.1. Measurements and model validation

The values computed numerically in free space were averaged over 100 cm<sup>2</sup> to be comparable with the measurements of the Narda ELT-400. The comparison is shown in figure 2. The data show good agreement, particularly along the vertical at a 10 cm horizontal distance from the appliance, where several important regions of the human models are located (vital organs, utero-foetal unit). The difference between measurements and computations can be explained by the constant permeability used by the SEMCAD solver, which does not allow for exact modelling of the ferromagnetic base of the cooking pot and the ferrite flux guides which are normally found below the induction coils to improve the performance. However, the differences between measurements and simulation are much less than the differences in reported emissions from different devices (Viellard *et al* 2007), which means that the results should be applicable to a wide range of appliances.

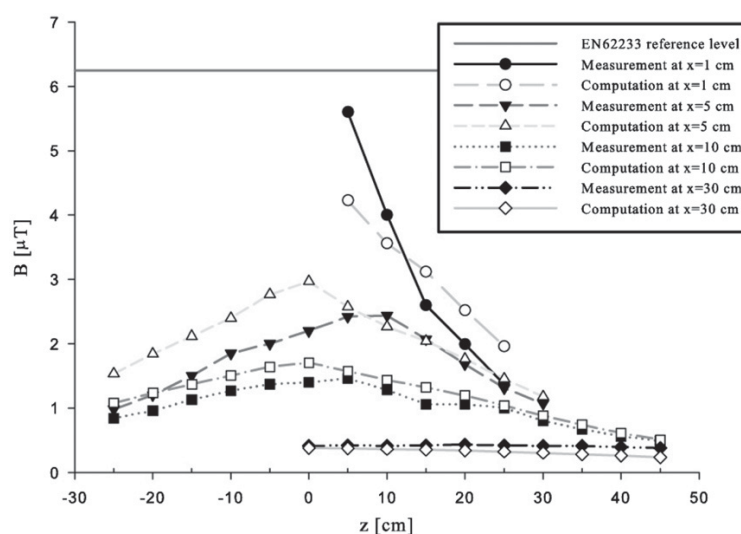


**Figure 2.** Comparison of the measured and calculated values of the RMS value of  $B$  averaged over  $100 \text{ cm}^2$  at different heights ( $z$ ) and horizontal distances from the appliance ( $x$ ).

**Table 3.** The spectral content of the  $B$ -field up to the fourth odd higher harmonic (all the even harmonics were below the noise level).

Harmonic order	Frequency (kHz)	BRMS ( $\mu\text{T}$ )	% of total RMS value <sup>a</sup>
1	35	1.500	99
3	105	0.170	11
5	175	0.082	5
7	245	0.034	2
9	315	0.016	1

<sup>a</sup> Total RMS value at this measurement point was  $1.53 \mu\text{T}$ .

The pot size with respect to the cooking area also has a strong effect on the stray fields. We measured this effect by using pots with diameters of 15, 20 and 25 cm on the same (21 cm) cooking area, and the measured values at a 5 cm horizontal distance from the appliance were  $4.5$ ,  $2.4$  and  $0.9 \mu\text{T}$ , respectively. A misalignment of the pot with respect to the centre of the cooking area increased the measured fields for the 20 and 25 cm pots by up to 20%, while the misalignment of the 15 cm pot did not result in a field increase.

During measurements we also examined the effect of operating several coils of the cooker simultaneously, but operating additional coils did not increase magnetic fields at any distance measured. This could be explained either by a built-in limitation on maximum power draw or by the configuration of resonant inverters, which reduces the maximum delivered power to each coil when several coils are operating simultaneously or increases the maximum power using the so-called 'boost mode' when only one coil is operating (Millan *et al* 2010).

The spectral content of the measured  $B$ -field at one of the measurement points is shown in table 3. Based on this measurement, the fundamental and first odd higher harmonics were

used in the computations. The 105 kHz frequency is at the higher end of the frequencies covered by the new (2010) ICNIRP guidelines, so its inclusion is justified.

### 3.2. Electric field and induced current in the human models

The internal electric fields and induced currents were computed in the four models and are shown in table 4. These results show that the internal electric field is far below the basic restrictions as imposed by the new low-frequency ICNIRP guidelines (2010), while the induced current density is significantly closer to its basic restriction as imposed by the original (1998) ICNIRP guidelines (in the new guidelines the restriction on the induced current density is absent). The only case in which this is not true is the 11 year old child, where the  $E$  field is a little less than 50% of the basic restriction. This occurs when low-conductivity voxels (in this case skin) form an electrical connection forming a large loop, which occurs between the hand and thigh in this specific model. The electric field in the low-conductivity region is consecutively very high. Such tissue loops can cause, albeit rarely, serious localized burns in MRI scans (Eising *et al* 2010). In the case of the MRI, however, the burns result from heating from the RF excitation field, which lies in the MHz frequency band. In the cases presented in this work, the internal electric fields are not strong enough to cause any tissue heating. Furthermore, at the frequencies studied in this work, protecting against excessive heating is not the objective of the exposure standards. It remains a question though whether such fields could cause nerve stimulation in areas of conductive tissue loops this large.

The 1998 guidelines specified that the current density should be averaged over an area of  $1 \text{ cm}^2$  perpendicular to the current direction, but the averaging was not applied in our computations, as it was previously shown that such averaging is poorly defined and open to conflicting interpretations (Dimbylow 2008, Zoppetti and Andreuccetti 2009). The new low-frequency guidelines specify an averaging volume for an internal electric field of  $2 \times 2 \times 2 \text{ mm}^3$ , and in our numerical approach, this was achieved by using a grid with the voxel size identical to the proposed averaging volume. Table 4 also shows data for the 99th percentile value of  $E$  and  $J$  fields in the central nervous system in the cases of children and in the utero-foetal unit in the cases of the pregnant women, as recommended by ICNIRP (2010). In the whole body, using the 99th percentile would push the estimate too low, the highest per cent accounts for more than 500 g of tissue in the case of the pregnant women. We therefore report the 999th permille, as it gives a more conservative result and is actually comparable between all models used in our study. Figure 3 shows a cross section of  $E$  through the centre of the body in all four models.

The induction cooker that was measured, produced less than  $0.5 \mu\text{T}$  at a distance of 30 cm, while the EN 62233 standard allows up to  $6.25 \mu\text{T}$ ; therefore, the appliance's magnetic field could be by up to a factor of 12 stronger and still be standard compliant. In comparison with the 1998 ICNIRP guidelines, the 2010 low-frequency guidelines have increased the reference levels for the  $B$ -field in the frequency range where the induction cookers operate from  $6.25 \mu\text{T}$  to  $27 \mu\text{T}$ . If the currently valid standard would be revised to the new reference level of  $27 \mu\text{T}$ , and the induction cooker producers would adapt their appliances to this change, the magnetic fields produced by these appliances could be up to a factor of 50 higher.

Our results indicate that the 999th permille (in a  $2 \times 2 \times 2 \text{ mm}^3$  voxel) would exceed the basic restrictions (ICNIRP 2010) if the source magnetic field strength would be increased by a factor of 45; the 999th permille of induced current density would exceed the basic restriction (ICNIRP 1998) if the source magnetic field strength would be increased by a factor of only 2.3. While the  $E$  field in the utero-foetal unit and the children's central nervous systems is generally low, and by more than two orders of magnitude below the basic restriction, the 99th percentile

**Table 4.** The computed values of the electric field ( $E$ ) and current density ( $J$ ) in the human models. The maxima are given for the whole body and the UFU (utero-foetal unit) for the pregnant women, and for the whole body and the CNS (central nervous system) in children.

	26 Weeks		30 Weeks		6 year old child		11 year old child	
	$E$ ( $V\ m^{-1}$ )	$J$ ( $mA\ m^{-2}$ )	$E$ ( $V\ m^{-1}$ )	$J$ ( $mA\ m^{-2}$ )	$E$ ( $V\ m^{-1}$ )	$J$ ( $mA\ m^{-2}$ )	$E$ ( $V\ m^{-1}$ )	$J$ ( $mA\ m^{-2}$ )
	<i>Values of dosimetric quantities at 35 kHz</i>							
Max WB	0.111	46	0.660	42	0.281	27	2.280	16
999th permille WB	0.038	27	0.080	18	0.099	14	0.065	10
Max CNS/UFU	0.028	46	0.078	23	0.039	4.4	0.009	1.0
99th centile CNS/UFU	0.024	29	0.032	18	0.021	2.3	0.005	0.54
	<i>Percentage of basic restriction<sup>a</sup></i>							
Max WB	2.3	65	14.0	60	6.0	39	48.2	22
999th permille WB	0.80	39	1.7	25	2.1	20	1.4	15
Max CNS/UFU	0.60	65	1.6	33	0.82	6.3	0.19	1.4
99th centile CNS/UFU	0.52	41	0.68	26	0.43	3.3	0.10	0.8
	<i>Values of dosimetric quantities at 105 kHz</i>							
Max WB	0.037	15	0.218	14	0.093	9.0	0.752	5.2
999th permille WB	0.012	9.1	0.026	5.8	0.017	4.7	0.021	3.4
Max CNS/UFU	0.009	15	0.026	7.7	0.013	1.4	0.003	0.32
99th centile CNS/UFU	0.008	10	0.011	6.1	0.007	0.76	0.002	0.18
	<i>Percentage of basic restriction<sup>b</sup></i>							
Max WB	0.26	7.2	1.54	6.7	0.66	4.3	5.32	2.5
999th permille WB	0.09	4.3	0.19	2.8	0.12	2.2	0.15	1.6
Max CNS/UFU	0.07	7.2	0.18	3.7	0.09	0.69	0.02	0.15
99th centile CNS/UFU	0.06	4.5	0.07	2.9	0.05	0.36	0.01	0.09
	<i>Combined percentage of basic restriction</i>							
Max WB	2.6	72	16	67	6.6	43	54	25
999th permille WB	0.89	44	1.9	28	2.2	23	1.5	16
Max CNS/UFU	0.67	72	1.8	37	0.91	7.0	0.21	1.6
99th centile CNS/UFU	0.57	46	0.75	29	0.48	3.7	0.11	0.86

<sup>a</sup>At 35 kHz, basic restriction for  $E$  is  $4.725\ V\ m^{-1}$  and for  $J$  it is  $70\ mA\ m^{-2}$ .

<sup>b</sup>At 105 kHz, basic restriction for  $E$  is  $14.175\ V\ m^{-1}$  and for  $J$  it is  $210\ mA\ m^{-2}$ .

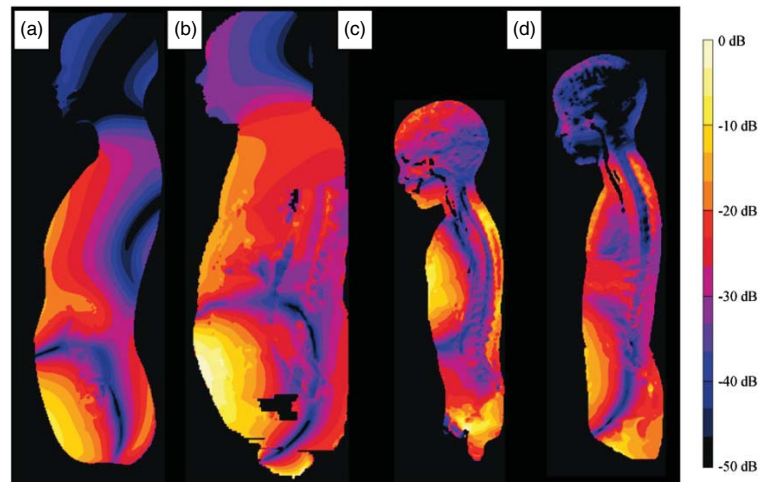


**Figure 3.** A cross section showing the  $E$  field values through the centre of the body. 0 dB represents  $0.1 \text{ V m}^{-1}$ . The models are (a) 26 weeks pregnant, (b) 30 weeks pregnant, (c) 6 year old child and (d) 11 year old child.

of the  $J$  field in the utero-foetal unit is relatively high, being only by a factor of 2.2 below the basic restrictions. These high values are located in the placenta in the case of 30 weeks pregnant and in the amniotic fluid in the case of 26 weeks pregnant. Taking into account the estimated extended ( $k = 2$ ) uncertainty, and the measured variation between different pots, the 95% confidence interval of the computed internal electric field spans the range from 0.2% up to 6% of the ICNIRP 2010 basic restrictions, while for the induced current density it spans the range from 3.8% up to 130% of the (now obsolete) ICNIRP 1998 basic restrictions. These confidence intervals can also realistically include the variations in fields produced by different appliance models.

#### 4. Conclusions

The results show that the magnetic fields produced by induction cookers do not cause the basic restriction for the internal electric field (ICNIRP 2010) to be exceeded in children and fetuses, even when the fields are increased by a factor of 5. Such an increase can realistically happen when the cookware is inappropriate for use on induction cookers and/or miss-aligned. Maximum exposure of a foetus is less than 2% of the new ICNIRP guidelines for limiting exposure to low-frequency electromagnetic fields, which makes exceeding the basic restriction unlikely. Furthermore, the 999th permille of the internal electric field in the whole body was less than 2.2% of the basic restriction in all cases, including children's central nervous system. The induced current density, however, is closer to its respective basic restriction (ICNIRP 1998) than the electric field and could exceed the basic restrictions even for induction cookers in compliance with the currently valid EN 62233 standard.

## Acknowledgments

The research was funded by the Slovenian Research Agency under various grants. The authors would like to thank Dr Xu of the Rensselaer Polytechnic Institute for providing us with the images of the 30 weeks pregnant woman.

## References

- Acero Jesus, Burdio J, Barragan L, Navarro D, Alonso R, Ramon J, Monterde F, Hernandez P, Llorente S and Garde I 2010 Domestic induction appliances *IEEE Ind. Appl. Mag.* **16** 39–47
- Ackerman M J 1998 The Visible Human Project *Proc. IEEE* **86** 504–11
- Bahr A, Bolz T and Hennes C 2007 Numerical dosimetry ELF: accuracy of the method, variability of models and parameters, and the implication for quantifying guidelines *Health Phys.* **92** 521
- Bibin L, Anquez J, de la Plata Alcalde J P, Boubekeur T, Angelini E D and Bloch I 2010 Whole-body pregnant woman modeling by digital geometry processing with detailed uterofetal unit based on medical images *IEEE Trans. Biomed. Eng.* **57** 2346–58
- CENELEC 2003 *EN 50366:2003 Household and Similar Electrical Appliances. Electromagnetic Fields. Methods for Evaluation and Measurement* (Brussels: CENELEC)
- Christ A *et al* 2010 The Virtual Family—development of surface-based anatomical models of two adults and two children for dosimetric simulations *Phys. Med. Biol.* **55** N23–38
- Dello S A W G, Stoot J H M B, van Stiphout R S A, Bloemen J G, Wigmore S J, Dejong C H C and van Dam R M 2011 Prospective volumetric assessment of the liver on a personal computer by nonradiologists prior to partial hepatectomy *World J. Surg.* **35** 386–92
- Dimbylow P J 2007 SAR in the mother and foetus for RF plane wave irradiation *Phys. Med. Biol.* **52** 3791–802
- Dimbylow P J 2008 Quandaries in the application of the ICNIRP low frequency basic restriction on current density *Phys. Med. Biol.* **53** 133–45
- Eising E G, Hughes J, Nolte F, Jentzen W and Bockisch A 2010 Burn injury by nuclear magnetic resonance imaging *Clin. Imaging* **34** 293–7
- Gabriel C, Peyman A and Grant E 2009 Electrical conductivity of tissue at frequencies below 1 MHz *Phys. Med. Biol.* **54** 4863–78
- Gabriel S, Lau R and Gabriel C 1996a The dielectric properties of biological tissues: II. Measurements in the frequency range 10 Hz to 20 GHz *Phys. Med. Biol.* **41** 2251–69
- Gabriel S, Lau R and Gabriel C 1996b The dielectric properties of biological tissues: III. Parametric models for the dielectric spectrum of tissues *Phys. Med. Biol.* **41** 2271–93
- Gardosi J, Mongelli M, Wilcox M and Chang A 1995 An adjustable fetal weight standard *Ultrasound Obstet. Gynecol.* **6** 168–74
- Grandjean P and Landrigan P 2006 Developmental neurotoxicity of industrial chemicals *Lancet* **368** 2167–78
- Grimmes S and Martinsen O G 2008 *Bioimpedance and Bioelectricity Basics* (Amsterdam: Elsevier)
- Hand J W, Li Y, Thomas E L, Rutherford M A and Hajnal J V 2006 Prediction of specific absorption rate in mother and fetus associated with MRI examinations during pregnancy *Magn. Reson. Med.* **55** 883–93
- ICNIRP 1998 Guidelines for limiting exposure to time-varying electric, magnetic, and electromagnetic fields (up to 300 GHz) *Health Phys.* **74** 494–522
- ICNIRP 2010 Guidelines for limiting exposure to time-varying electric and magnetic fields (1 Hz to 100 kHz) *Health Phys.* **99** 818–36
- IEC 2005 *EN 62233: Measurement Methods for Electromagnetic Fields of Household Appliances and Similar Apparatus with Regard to Human Exposure* (Geneva: International Electrotechnical Commission)
- Kheifets L, Repacholi M, Saunders R and van Deventer E 2005 The sensitivity of children to electromagnetic fields *Pediatrics* **116** e303–13
- Koller L and Novak B 2009 Improving the energy efficiency of induction cooking *Electr. Eng.* **91** 153–60
- Lu Y, Cui H, Yu J and Mashimo S 1996 Dielectric properties of human fetal organ tissues at radio frequencies *Bioelectromagnetics* **17** 425–6
- Mancini A 2004 Skin *Pediatrics* **113** 1114–9
- Millan I, Burdio J M, Acero J, Lucia O and Palacios D 2010 Resonant inverter topologies for three concentric planar windings applied to domestic induction heating *Electron. Lett.* **46** 1225–6
- Peyman A, Gabriel C, Benedickter H and Frohlich J 2011 Dielectric properties of human placenta, umbilical cord and amniotic fluid *Phys. Med. Biol.* **56** N93–8

- Shi C and Xu X G 2004 Development of a 30-week-pregnant female tomographic model from computed tomography (CT) images for Monte Carlo organ dose calculations *Med. Phys.* **31** 2491–7
- Spielmann A L, DeLong D M and Kliewer M A 2005 Sonographic evaluation of spleen size in tall healthy athletes *AJR Am. J. Roentgenol.* **184** 45–9
- Stuchly M A and Lecuyer D W 1987 Electromagnetic-fields around induction-heating stoves *J. Microw. Power Electromagn. Energy* **22** 63–9
- Viellard C, Romann A, Lott U and Kuster Niels 2007 B-field exposure from induction cooking appliances *IT'IS Report* (Zurich: IT'IS Foundation) <http://www.bag.admin.ch/themen/strahlung/00053/00673/03156/index.html>
- Yamazaki K, Kawamoto T, Fujinami H and Shigemitsu T 2004 Equivalent dipole moment method to characterize magnetic fields generated by electric appliances: extension to intermediate frequencies of up to 100 kHz *IEEE Trans. Electromagn. Compat.* **46** 115–20
- Zoppetti N and Andreuccetti D 2009 Review of open problems in assessing compliance with 2004/40/EC directive exposure limit values for low-frequency current density by means of numerical techniques *Radiat. Prot. Dosim.* **137** 247–51



## Paper 3

**Title:** Occupational exposure assessment of magnetic fields generated by induction heating equipment – the role of spatial averaging

**Authors:** Kos Bor, Valič Blaž, Kotnik Tadej, Gajšek Peter

**Publication:** Physics in Medicine and Biology

**DOI:** 10.1088/0031-9155/57/19/5943

**Year:** 2012

**Volume:** 57

**Number:** 19

**Pages:** 5943-5953

## Occupational exposure assessment of magnetic fields generated by induction heating equipment—the role of spatial averaging

Bor Kos<sup>1,2</sup>, Blaž Valič<sup>2</sup>, Tadej Kotnik<sup>1</sup> and Peter Gajšek<sup>2,3</sup>

<sup>1</sup> Laboratory of Biocybernetics, Faculty of Electrical Engineering, University of Ljubljana, Tržaška 25, SI-1000 Ljubljana, Slovenia

<sup>2</sup> Institute of Non-Ionizing Radiation, Pohorskega Bataljona 215, SI-1000 Ljubljana, Slovenia

E-mail: bor.kos@fe.uni-lj.si, blaz.valic@inis.si, tadej.kotnik@fe.uni-lj.si and peter.gajsek@inis.si

Received 16 April 2012, in final form 13 July 2012

Published 11 September 2012

Online at [stacks.iop.org/PMB/57/5943](http://stacks.iop.org/PMB/57/5943)

### Abstract

Induction heating equipment is a source of strong and nonhomogeneous magnetic fields, which can exceed occupational reference levels. We investigated a case of an induction tempering tunnel furnace. Measurements of the emitted magnetic flux density ( $B$ ) were performed during its operation and used to validate a numerical model of the furnace. This model was used to compute the values of  $B$  and the induced *in situ* electric field ( $E$ ) for 15 different body positions relative to the source. For each body position, the computed  $B$  values were used to determine their maximum and average values, using six spatial averaging schemes (9–285 averaging points) and two averaging algorithms (arithmetic mean and quadratic mean). Maximum and average  $B$  values were compared to the ICNIRP reference level, and  $E$  values to the ICNIRP basic restriction. Our results show that in nonhomogeneous fields, the maximum  $B$  is an overly conservative predictor of overexposure, as it yields many false positives. The average  $B$  yielded fewer false positives, but as the number of averaging points increased, false negatives emerged. The most reliable averaging schemes were obtained for averaging over the torso with quadratic averaging, with no false negatives even for the maximum number of averaging points investigated.

(Some figures may appear in colour only in the online journal)

### Introduction

Induction heating applications are very common in industrial processes, such as metal melting and refinement (Faerman *et al* 1997), as well as welding and hardening (Bayindir *et al* 2003).

<sup>3</sup> Author to whom any correspondence should be addressed.

They are also becoming more common in cooking, for both professional and domestic use (Acero *et al* 2010).

The fields used by induction heating equipment are alternating and can range in frequency from tens of Hz to hundreds of kHz (Bayindir *et al* 2003, Millan *et al* 2010). With the exception of the 50 and 60 Hz subrange of power line frequencies, this range is also among the least investigated in the scientific literature in terms of human exposure (Floderus *et al* 2002). Since the field strength required by induction heating applications is typically very high due to large power demands, from tens of kW to several MW (Floderus *et al* 2002), there is a significant possibility for fields exceeding the occupational reference levels as set out in the ICNIRP guidelines (ICNIRP 2010). With operations that require close proximity of a worker to a induction heating source, the worker is typically exposed to a highly nonhomogeneous field. When reference levels are exceeded, the ICNIRP guidelines, as well as the currently valid IEEE standards (IEEE 2006), require the determination of dosimetric quantities in the human body, and their comparison to the basic restriction. In the investigated frequency range, the most widely used reference level is the magnetic flux density ( $B$ ) and the basic restriction of the *in situ* electric field ( $E$ ), where the latter can only be determined non-invasively by means of numerical dosimetry (Bakker *et al* 2012, Hirata *et al* 2011), or by measurements on phantoms.

Numerical determination of dosimetric quantities in the human body is a complex task, and the most frequently used numerical methods all rely on staircasing (representation of curved surfaces by cubic voxels), resulting in the possibility of large errors. To reduce the staircasing errors, the ICNIRP guidelines recommend averaging over a volume of  $2 \times 2 \times 2 \text{ mm}^3$ , or using the 99th percentile value when investigating the tissue-specific  $E$ . We have previously used the whole body 999th permille (Kos *et al* 2011), while others have successfully employed spatial averaging of tissue conductivities to reduce drastic conductivity changes at the intra-tissue and tissue–air boundaries (Laakso and Hirata 2012).

In this study, we investigated the role of spatial averaging in the measurements of magnetic fields in empty space for classification of human exposure (overexposure versus compliance). Such averaging has been suggested in the literature (Jokela 2007, ICNIRP 2010), but to the authors' best knowledge, no attempt has yet been made to compare different averaging schemes in their predictive power regarding the classification of exposures. Here, we perform a comparison of six such schemes with the results of numerical dosimetry computed in the body serving as a reference.

We present a case of an induction tempering tunnel furnace where workers perform quality control checks near the entrance of the tunnel. We report the measurements and numerical simulations of the generated stray  $B$  and numerical simulations of induced  $E$  in the human body. Finally, we discuss the application of spatial averaging of  $B$  for determination of compliance with exposure guidelines.

## Materials and methods

### *Magnetic flux density measurements*

We performed measurements of the magnetic flux density ( $B$ ) generated by an induction tempering tunnel furnace using a calibrated ELT-400 instrument with the  $100 \text{ cm}^2$  probe (both from Narda STS, Pfullingen, Germany). Spot measurements of  $B$  were performed using the instrument's RMS detection mode that has a flat frequency response. The total uncertainty of the measurement setup determined in the frequency range from 6 Hz to 320 kHz is 2.3 dB. The tempering tunnel operates at 10 kHz and consists of three turns of wire, each running

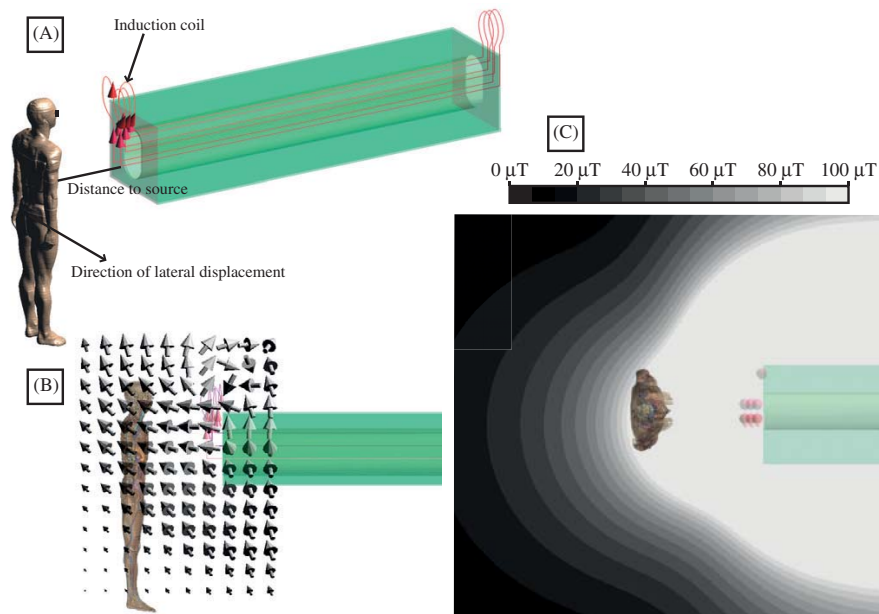


**Figure 1.** (A) Schematic view of the source geometry and positioning of the human model. The induction coil is composed of three turns carrying 2000 A of peak current. For the computations, the human model was positioned at five different distances to source and at three different lateral displacements. (B) Direction of the stray magnetic field. (C) Magnitude of the stray magnetic flux density. In all panels, the model is at 50 cm horizontal distance from the source.

horizontally around the tunnel 2.8 m long and 9 cm wide, and the adjacent turns separated vertically by 10 cm (figure 1(A)). The wires thus form a rectangular coil 3.06 m  $\times$  9 cm in cross-section (the wires extend some distance from the tunnel), with the magnetic field inside the coil generated predominantly in the vertical direction, and the stray magnetic field outside the furnace illustrated in figure 1(B).

The induction furnace is used for tempering hardened parts for drive shafts for the automotive industry. Due to the high precision and low tolerance of faulty parts required by automobile manufacturers, the parts undergo 100% inspection, which is done at the exit of the tempering tunnel to ensure any reject gets discarded as soon as possible in the manufacturing process. Additionally, due to space constraints for limiting factory floor footprint, the worker stations are positioned close to the source of the magnetic fields.

#### *Numerical simulations*

Using the SEMCAD X 14.6 software package (SPEAG, Zurich, Switzerland), a model of the source of magnetic field in the tunnel furnace was constructed based on the original manufacturer's technical drawings. The position and distance of the induction coil were determined with respect to the location where the quality control workers are typically stationed (figure 1). The model was then used to compute  $B$  in empty space at this location, as well as closer to the furnace. Since the probe used for magnetic-field measurements returned

**Table 1.** Body-averaging schemes in quantitative terms.

Averaging scheme	Back–front axis points	Right–left axis points	Vertical axis points	Total points
Whole body dense	3	5	19	285
Whole body reduced 1	1	3	10	30
Whole body reduced 2	1	3	5	15
Torso dense	3	5	11	165
Torso reduced 1	1	3	6	18
Torso reduced 2	1	3	3	9

$B$  averaged over three orthogonal circular 100 cm<sup>2</sup> surfaces, we developed an algorithm that performs the same type of averaging on the numerical results to provide comparability between the measured and the numerically computed  $B$ . More precisely,  $B$  was computed in a sphere with a radius of 5.64 cm (in approx. 42 000 voxels), the normal  $B$  was averaged over three orthogonal cross sections, and the total average  $B$  was computed as the norm of its three-dimensional vector.

The numerical computations of *in situ* electric fields ( $E$ ) were performed with the virtual family (Christ *et al* 2010) model ‘Duke’, i.e. the 34 year old male model. The model was positioned at a horizontal distance of 20, 30, 40, 50 or 100 cm from source (20 cm being the closest distance accessible to the workers in the case considered), and at a lateral displacement of 0, 20 or 50 cm to the right. The total number of different body positions was therefore 15. Vertically, the coil was positioned 120 cm above the feet of the model. Therefore, the area exposed to the highest  $B$  is the chest and head regions. The computation was performed at 10 kHz frequency using the low-frequency quasi-static solver implemented in SEMCAD X. Extended ( $k = 2$ ) total uncertainty of the dosimetric simulations was estimated to be 4 dB with details on the estimation given in a previously published work (Kos *et al* 2011). The human model was discretized to  $2 \times 2 \times 2$  mm<sup>3</sup> resolution, giving a total of 43 M-cells for the simulation. The resulting values of  $E$  were extracted for each tissue in the model (total of 77) and statistically analyzed to find their maximum, 99th percentile and mean values. We used the IT’IS database for dielectric properties of body tissues (Havgall *et al* 2011).

#### Averaging algorithms

The ICNIRP guidelines (ICNIRP 2010) suggest that determining only the maximum value of  $B$  at a certain position can be an overly conservative measure for determining compliance with the exposure limits. Spatial averaging of fields over the whole body, or parts of the body, is suggested by Jokela (2007) to give a less conservative and more realistic estimate of actual exposure. We have investigated six different spatial averaging schemes by varying the number of averaging points. Averaging introduces the possibility of false negatives, i.e. situations where the worker is overexposed, yet the averaged fields are below the reference level. Since the main goal of reference levels is to prevent any possibility of overexposure, false negatives have to be avoided. On the other hand, false positives, where the averaged fields exceed the reference levels, while the actual exposure is below the basic restrictions, would imply that the averaging algorithm is overly conservative, albeit less conservative than the use of the spatial maximum value.

In total, six averaging schemes with varying number of averaging points (from 9 to 285 points) were investigated, as shown in table 1 and illustrated in figure 2. Thus, in the *whole body dense* scheme, the averaging was performed at 285 points forming a rectangular

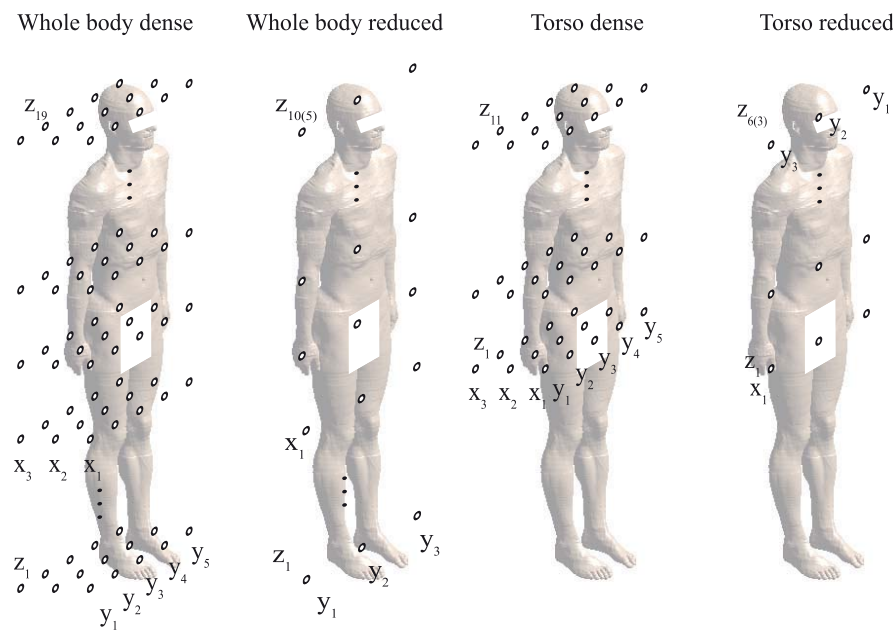


**Figure 2.** Body-averaging schemes illustrated. The whole body schemes covered the total body height of 180 cm, while the torso schemes covered only the 100 cm from the pelvis up. In the reduced schemes, the grid consisted of a single point along the front–back axis, located in the front plane of the body, since that plane is contributing the most to the total exposure.

grid with 3 points along the back–front ( $x$ ) axis, 5 points along the right–left ( $y$ ) axis, and 19 points along the vertical ( $z$ ) axis, with all points spaced equidistantly in 10 cm intervals. The procedure was similar for the *torso dense* scheme, with the legs region excluded and thus only 11 points along the vertical axis. With the *whole body reduced 1* and *torso reduced 1* averaging schemes, the points were spaced at 20 cm intervals, while with both *reduced 2* schemes, they were spaced at 20 cm intervals horizontally and at 40 cm intervals vertically.

Although the practical use of averaging with a number of points as high as 285 or 165 is questionable without some sort of automated measurement system, it was included for comprehensiveness.

For each scheme, 15 different body positions were investigated. In addition, we also investigated the differences between a simple arithmetic mean and a quadratic mean in spatial averaging, with the quadratic mean defined as

$$B_{\text{average}} = \sqrt{\frac{1}{n} \sum_{i=1}^n B_i^2}$$

and thus giving more importance to higher values. This yielded a total of 180 investigated combinations of averaging scheme, type of mean and body position.

**Table 2.** Measured magnetic flux density at five points in front of the assessed induction furnace. The reference value of ICNIRP (2010) at 10 kHz is 100  $\mu\text{T}$ .

Measurement spot	Measured $B$ ( $\mu\text{T}$ )	Computed $B$ ( $\mu\text{T}$ )	% error
1	350	224	−36%
2	117	70.5	−40%
3	116	176	52%
4	45	40.6	−10%
5	17	20	18%

## Results and discussion

### *Measurements of magnetic flux density*

The magnetic flux density ( $B$ ) was measured at five points in front of the tempering tunnel during its operation. As shown in table 2, at three of these points, the measured values of  $B$  exceeded the ICNIRP guidelines (ICNIRP 2010). Since workers need to perform some tasks at the points where an excessive field has been measured, according to these guidelines a more detailed assessment—dosimetric evaluation of *in situ* induced electric field ( $E$ )—needs to be performed.

In table 2, we also compare the measured and the computed values of  $B$  at the locations corresponding to the measurement points. Although some of the errors are relatively large, they are still within the uncertainty boundaries as specified by Kuster *et al* (2006). Therefore, it is appropriate to use the computed values of  $B$  for the investigation of the influence of spatial averaging.

### *Numerical computation of magnetic flux density and in situ electric fields*

The computed maximum and averaged fields at all investigated combinations of averaging scheme, type of mean and body position are shown in table 3, while a summary of the numerical dosimetry data is given in table 4. In our results, where the maximum  $B$  in the body does not exceed the ICNIRP reference levels, there are no cases of exposure exceeding the ICNIRP basic restrictions as indicated by the 99th percentile of  $E$ . Although Bakker *et al* (2012) have found some cases where such overexposure could occur, those were with child models exposed to homogeneous fields at the occupational reference levels. On the other hand, the maximum  $B$  yields many false positives and is thus an overly conservative predictor of overexposure, which is in agreement with the suggestions of the ICNIRP guidelines.

From the cross-referencing of tables 3 and 4, it is possible to identify the false negatives, i.e. the locations where the average  $B$  is below the reference level, while the induced  $E$  is above the basic restriction. There were three such false negatives in the 180 combinations investigated: at 40 cm distance in the aligned and 20 cm to-the-right positions, and at 20 cm distance in the 50 cm to-the-right position; all these false negatives were obtained using the whole-body-dense averaging scheme with the arithmetic mean. This indicates that whole-body averaging is inappropriate, particularly in highly nonhomogeneous fields.

Additionally, there were 17 false positives, with several locations where false positives were yielded only by the quadratic mean averaging, but not by the arithmetic mean. This is an expected result since the quadratic mean is more conservative, with the higher values given more importance.

**Table 3.** Computed values of averaged (*A*—arithmetic; *Q*—quadratic mean) and maximum (*M*) magnetic flux density (in  $\mu\text{T}$ ). Since the occupational reference level at 10 kHz is exactly 100  $\mu\text{T}$ , the numerical value of magnetic flux density is equal to the percentage of the reference level. The top row indicates the distances from the source to the frontal plane of the human body. Note that the maximum *B* values are the same in the aligned and 0.2 m right (R) position because the two positions share some measurement points which are located in the area with the strongest fields.

Scheme	Lateral position	Horizontal distance from source														
		20 cm			30 cm			40 cm			50 cm			100 cm		
		<i>A</i>	<i>Q</i>	<i>M</i>	<i>A</i>	<i>Q</i>	<i>M</i>	<i>A</i>	<i>Q</i>	<i>M</i>	<i>A</i>	<i>Q</i>	<i>M</i>	<i>A</i>	<i>Q</i>	<i>M</i>
Whole body dense	Aligned	190	291	1114	122	169	530	85	110	297	64	78	187	24	25	43
	0.2 m R	165	257	1114	111	155	530	81	104	297	61	75	187	23	25	43
	0.5 m R	80	113	476	65	86	315	53	66	213	44	53	149	20	22	41
Whole body reduced 1	Aligned	270	399	1114	164	225	530	111	142	297	80	98	187	27	29	43
	0.2 m R	236	368	1114	150	209	530	104	135	297	76	94	187	27	29	43
	0.5 m R	103	154	476	81	113	315	65	84	213	52	65	149	23	25	41
Whole body reduced 2	Aligned	284	390	830	177	229	445	120	148	266	86	102	174	28	30	42
	0.2 m R	249	359	830	161	214	445	112	141	266	83	99	174	28	30	42
	0.5 m R	111	157	400	83	115	279	66	87	196	53	67	141	23	25	40
Torso dense	Aligned	302	381	1114	187	220	530	127	142	297	92	100	187	30	31	43
	0.2 m R	261	337	1114	171	202	530	120	135	297	89	96	187	30	31	43
	0.5 m R	120	146	476	95	111	315	75	85	213	61	67	149	26	26	41
Torso reduced 1	Aligned	426	514	1114	253	289	530	165	182	297	116	124	187	35	35	43
	0.2 m R	371	474	1114	229	269	530	155	173	297	111	120	187	35	35	43
	0.5 m R	154	197	476	119	144	315	93	107	213	74	82	149	29	30	41
Torso reduced 2	Aligned	446	502	830	270	294	445	177	189	266	124	130	174	36	37	42
	0.2 m R	389	462	830	245	275	445	166	179	266	119	125	174	36	36	42
	0.5 m R	165	201	400	128	150	279	100	112	196	79	86	141	30	31	40

**Table 4.** Number of tissues with the 99th percentile of *in situ* electric field ( $E_{99\%}$ ) exceeding the basic restriction (BR), the highest of the  $E_{99\%}$  among all tissues, and its ratio to BR. The basic restriction at 10 kHz is  $2.7 \text{ V m}^{-1}$  for all tissues of the head and body (ICNIRP 2010).

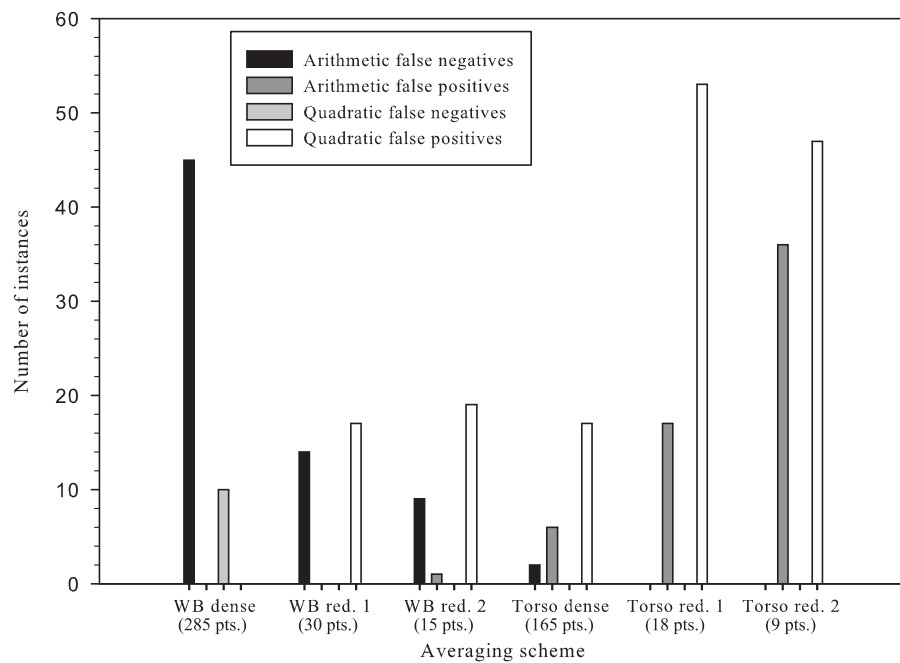
Distance (m)		0.2	0.3	0.4	0.5	1
Aligned	No of tissues over BR	33	12	2	0	0
	max $E_{99\%}$	$11.9 \text{ V m}^{-1}$	$6.07 \text{ V m}^{-1}$	$3.53 \text{ V m}^{-1}$	$2.23 \text{ V m}^{-1}$	$0.585 \text{ V m}^{-1}$
	max $E_{99\%}/\text{BR}$	439%	225%	131%	83%	22%
0.2 m right	Tissue with max $E_{99\%}$	Ear skin	Ear skin	Ear skin	Ear skin	Adrenal gland
	No of tissues over BR	28	10	1	0	0
	max $E_{99\%}$	$8.45 \text{ V m}^{-1}$	$4.63 \text{ V m}^{-1}$	$3.00 \text{ V m}^{-1}$	$2.10 \text{ V m}^{-1}$	$0.616 \text{ V m}^{-1}$
0.5 m right	max $E_{99\%}/\text{BR}$	313%	172%	111%	78%	23%
	Tissue with max $E_{99\%}$	Mucosa	Mucosa	Mucosa	Mucosa	Bone
	No of tissues over BR	3	0	0	0	0
0.5 m right	max $E_{99\%}$	$3.18 \text{ V m}^{-1}$	$2.49 \text{ V m}^{-1}$	$1.91 \text{ V m}^{-1}$	$1.48 \text{ V m}^{-1}$	$0.536 \text{ V m}^{-1}$
	max $E_{99\%}/\text{BR}$	118%	92%	71%	55%	20%
	Tissue with max $E_{99\%}$	Teeth	Mucosa	Mucosa	Mucosa	Bone

Table 4 also shows that the most overexposed tissues include mucosa, ear skin, bones and teeth. In this context, it should be noted that the restrictive ICNIRP limits aim to avoid stimulatory phenomena in the heart and the central nervous system, so overexposure of less susceptible tissues should not necessarily be viewed as a source of concern. Still, at the closest distance, the overexposed tissues also include white and gray matter, heart muscle and spinal cord.

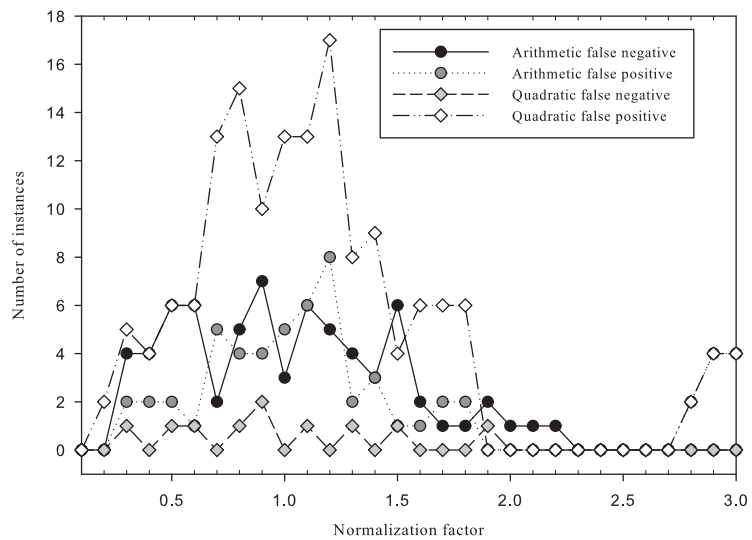
All the results presented in tables 3 and 4 were obtained with the current of 2000 A flowing in the induction coil. However, this current can be adjusted to the needs of the particular manufacturing process, resulting in proportionally changed values of  $B$  and consequently of  $E$ . This can affect the assessment of exposure, including the occurrence of false negatives and positives. To emulate the changes of induction coil current, we have scaled the values of  $B$  as given in table 3, and the resulting values of  $E$  as given in table 4, by factors ranging from 0.1 to 3 in increments of 0.1, and again compared the 99th percentile of  $E$  to the basic restrictions. Thus, we have investigated a total of 30 different power levels and corresponding changes of  $B$  and  $E$ . The total number of misclassifications was determined for each normalization factor, and the results are summarized with respect to the averaging scheme in figure 3, which suggests that irrespective of magnetic flux density, the quadratic averaging scheme generally produces the fewest false negatives.

Table 3 and figure 3 also show that in both arithmetic and quadratic averaging, as the number of averaging points increased, false negatives emerged and increased in number. The most reliable averaging schemes were obtained for averaging over the torso with quadratic averaging, with no false negatives even for the maximum number of averaging points investigated.

Figure 4 shows the data on misclassifications with respect to the scaling factor. This figure highlights that field averaging is the most important for the range of magnetic flux densities that induce *in situ* electric fields close (either below or above) to the basic restriction. For scaling factors below 0.3, the basic restriction is not exceeded in any tissue for any of the analyzed body positions, while above 1.9, the basic restriction is exceeded in at least one tissue for each body position except at the largest (100 cm) distance from the induction tunnel. As a consequence, for these scaling factors the number of misclassifications is very small, implying that for either sufficiently low or sufficiently high  $B$ , averaging can be avoided. In addition, averaging also becomes unnecessary at distances over 1 m from the tunnel, where  $B$



**Figure 3.** Misclassifications of exposure in different averaging schemes for the whole range of investigated scaling factors. The maximum  $B$  yielded 88 false positives and no false negatives.



**Figure 4.** Misclassifications of exposure as functions of the scaling factor.

becomes almost homogeneous, and its maximum value can be taken as a reliable indicator of exposure.

The case studied here is in some aspects quite specific, as it considers a single-source-type functioning at a single frequency. However, as can be seen in figures 1(B) and (C), the magnetic field in the location of the human body is rather similar, both in the aspect of its spatial distribution and its nonhomogeneity, to those in front of typical circular coils. In our case, we did not investigate the very nonhomogeneous fields at extremely close distances to the furnace, as such distances are in practice inaccessible to the workers; this may not be the case in many other magnetic field sources, for which the situation, including reasonable averaging methods, should be addressed by a separate study. The same conclusion applies for sources operating at considerably higher or lower frequencies.

### Conclusions

Magnetic fields generated by industrial induction furnaces can induce *in situ* electric fields exceeding the basic restriction according to the ICNIRP guidelines. For determination of occupational exposure, spatial averaging provides an adequate estimate, in the sense that it is protective, yet less conservative than the maximum value, which can lead to an excessive number of false positives. Quadratic averaging has a much lower likelihood of producing false negatives than simple arithmetic averaging, and averaging over the torso yields fewer false negatives than averaging over the whole body. Averaging is most important for magnetic fields that induce *in situ* electric fields close to the basic restriction, while for both significantly weaker or stronger fields the maximum value is a reliable indicator of exposure.

### Acknowledgment

This work was supported by the Slovenian Research Agency under grant number L7-2231.

### References

- Acero J, Burdío J M, Barragan L A, Navarro D, Alonso R, Ramon J, Monterde F, Hernandez P, Llorente S and Garde I 2010 Domestic induction appliances *IEEE Ind. Appl. Mag.* **16** 39–47
- Bakker J F, Paulides M M, Neufeld E, Christ A, Chen X L, Kuster N and van Rhoon G C 2012 Children and adults exposed to low-frequency magnetic fields at the ICNIRP reference levels: theoretical assessment of the induced electric fields *Phys. Med. Biol.* **57** 1815–29
- Bayindir N, Kukrer O and Yakup M 2003 DSP-based PLL-controlled 50–100 kHz 20 kW high-frequency induction heating system for surface hardening and welding applications RID B-4867–2008 *IEE Proc. B* **150** 365–71
- Christ A *et al* 2010 The Virtual Family—development of surface-based anatomical models of two adults and two children for dosimetric simulations *Phys. Med. Biol.* **55** N23–38
- Faerman L, Luzgin V, Petrov A and Rachkov S 1997 Highly efficient induction heating units for metallurgy and machine construction *Metallurgist* **41** 191–3
- Floderus B, Stenlund C and Carlgren F 2002 Occupational exposures to high frequency electromagnetic fields in the intermediate range (>300 Hz–10 MHz) *Bioelectromagnetics* **23** 568–77
- Hasgall P, Neufeld E, Gosselin M, Klingeböck A and Kuster N 2011 IT'IS Database for thermal and electromagnetic parameters of biological tissues [www.itis.ethz.ch/database](http://www.itis.ethz.ch/database)
- Hirata A, Takano Y, Fujiwara O, Dovan T and Kavet R 2011 An electric field induced in the retina and brain at threshold magnetic flux density causing magnetophosphenes *Phys. Med. Biol.* **56** 4091–101
- ICNIRP 2010 Guidelines for limiting exposure to time-varying electric and magnetic fields (1 Hz to 100 kHz) *Health Phys.* **99** 818–36
- IEEE 2006 IEEE standard for safety levels with respect to human exposure to radio frequency electromagnetic fields, 3 kHz to 300 GHz *IEEE Standard C95.1–2005 (Revision of IEEE Standard C95.1–1991)* doi:10.1109/IEEESTD.2006.99501

- Jokela K 2007 Assessment of complex EMF exposure situations including inhomogeneous field distribution *Health Phys.* **92** 531–40
- Kos B, Valič B, Miklavčič D, Kotnik T and Gajšek P 2011 Pre- and post-natal exposure of children to EMF generated by domestic induction cookers *Phys. Med. Biol.* **56** 6149–60
- Kuster N, Torres V B, Nikoloski N, Frauscher M and Kainz W 2006 Methodology of detailed dosimetry and treatment of uncertainty and variations for *in vivo* studies *Bioelectromagnetics* **27** 378–91
- Laakso I and Hirata A 2012 Reducing the staircasing error in computational dosimetry of low-frequency electromagnetic fields *Phys. Med. Biol.* **57** N25–34
- Millan I, Burdio J M, Acero J, Lucia O and Palacios D 2010 Resonant inverter topologies for three concentric planar windings applied to domestic induction heating *Electron. Lett.* **46** 1225–6

## Paper 4

**Title:** Towards Treatment Planning and Treatment of Deep-seated Solid Tumors by Electrochemotherapy

**Authors:** Miklavčič Damijan, Snoj Marko, Županič Anže, Kos Bor, Čemažar Maja, Kropivnik Mateja, Bračko Matej, Pečnik Tjaša, Gadžijev Eldar, Serša Gregor

**Publication:** Biomedical Engineering Online

**DOI:** 10.1186/1475-925X-9-10

**Year:** 2010

**Volume:** 9

**Number:** 10

**Pages:** 1-8

## RESEARCH

## Open Access

# Towards treatment planning and treatment of deep-seated solid tumors by electrochemotherapy

Damijan Miklavcic<sup>1</sup>, Marko Snoj<sup>2</sup>, Anze Zupanic<sup>1</sup>, Bor Kos<sup>1</sup>, Maja Cemazar<sup>2</sup>, Mateja Kropivnik<sup>2</sup>, Matej Bracko<sup>2</sup>, Tjasa Pecnik<sup>2</sup>, Eldar Gadzijev<sup>2</sup>, Gregor Sersa<sup>2\*</sup>

## Abstract

**Background:** Electrochemotherapy treats tumors by combining specific chemotherapeutic drugs with an intracellular target and electric pulses, which increases drug uptake into the tumor cells. Electrochemotherapy has been successfully used for treatment of easily accessible superficial tumor nodules. In this paper, we present the first case of deep-seated tumor electrochemotherapy based on numerical treatment planning.

**Methods:** The aim of our study was to treat a melanoma metastasis in the thigh of a patient. Treatment planning for electrode positioning and electrical pulse parameters was performed for two different electrode configurations: one with four and another with five long needle electrodes. During the procedure, the four electrode treatment plan was adopted and the patient was treated accordingly by electrochemotherapy with bleomycin. The response to treatment was clinically and radiographically evaluated. Due to a partial response of the treated tumor, the metastasis was surgically removed after 2 months and pathological analysis was performed.

**Results:** A partial response of the tumor to electrochemotherapy was obtained. Histologically, the metastasis showed partial necrosis due to electrochemotherapy, estimated to represent 40-50% of the tumor. Based on the data obtained, we re-evaluated the electrical treatment parameters in order to correlate the treatment plan with the clinical response. Electrode positions in the numerical model were updated according to the actual positions during treatment. We compared the maximum value of the measured electric current with the current predicted by the model and good agreement was obtained. Finally, tumor coverage with an electric field above the reversible threshold was recalculated and determined to be approximately 94%. Therefore, according to the calculations, a small volume of tumor cells remained viable after electrochemotherapy, and these were sufficient for tumor regrowth.

**Conclusions:** In this, the first reported clinical case, deep-seated melanoma metastasis in the thigh of the patient was treated by electrochemotherapy, according to a treatment plan obtained by numerical modeling and optimization. Although only a partial response was obtained, the presented work demonstrates that treatment of deep-seated tumor nodules by electrochemotherapy is feasible and sets the ground for numerical treatment planning-based electrochemotherapy.

**Trial registration:** EudraCT:2008-008290-54

\* Correspondence: [gsersa@onko-i.si](mailto:gsersa@onko-i.si)

<sup>2</sup>Institute of Oncology Ljubljana, Zaloška 2, SI-1000 Ljubljana, Slovenia

## Background

Electrochemotherapy is a type of tumor treatment that combines the use of specific chemotherapeutic drugs which have an intracellular target and low membrane permeability, with application of electric pulses to the tumors to increase drug uptake into cells. It provides good local tumor control when the two modalities combined are optimized; *i.e.* drug choice, distribution and concentration in the tumors, in addition to adequate electric pulse parameter selection and pulse delivery leading to cell membrane electroporation of the tumor tissue [1-4].

The drug used in electrochemotherapy needs to be adequately distributed in the tumor and present at a sufficient concentration. For treatment of small subcutaneous tumor nodules, such as melanoma metastases, intratumoral bleomycin or cisplatin administration is recommended, whereas for treatment of bigger tumor nodules, intravenous injection of bleomycin is used. Drug doses needed for treatment are provided in the published Standard Operating Procedures [5]. For optimal drug distribution within the tumor after intratumoral injection, only a few minutes are needed between the drug injection and electroporation of tumors. After intravenous bleomycin injection, at least 8 minutes are needed for the drug to be in a pharmacological peak in the tumor and the drug remains at a sufficient concentration for at least another 20 minutes [6].

The second prerequisite for successful electrochemotherapy is that the whole tumor mass is exposed to a sufficiently high electric field. This can be achieved by appropriate selection and placement of electrodes, and application of electric pulses of adequate amplitude. The distribution of the electric field after application of electric pulses by plate or needle electrodes has already been extensively elaborated for small tumor nodules [2]. These settings and electrodes provide efficient treatment of superficial tumor nodules up to 3 cm in diameter in a single electrochemotherapy session and have even been used to treat bone cancer [7-9]. However, to enable treatment of deep-seated tumors, a design of long needle electrodes and in particular their positioning with respect to the tumor is needed. If solid tumors of 3-4 cm diameter are located deep in the body, choosing electrical parameters that would result in a good clinical response and that would have no or minimal damage to normal tissue is of the utmost importance, especially in cases where tumors are located close to vital organs. Numerical modeling in treatment planning is the proposed approach that also allows verification of the electrical parameters based on the clinical response to electrochemotherapy [10].

In order to also develop electrochemotherapy for treatment of deep-seated tumors, the aim of our study was to treat a deep-seated melanoma metastasis in the

thigh of a patient by custom-made long needle electrodes. Based on treatment planning, the electric pulse parameters and positioning of electrodes were determined. The patient was treated accordingly by electrochemotherapy with bleomycin. The response to treatment was clinically, radiographically and histologically evaluated. Due to a partial response of the treated tumor (reduction in size by more than 50%), the metastasis was surgically removed after 2 months and pathological analysis was performed. Based on the data obtained, we re-evaluated the electrical treatment parameters in order to correlate the treatment plan with the clinical response of the electrochemotherapy-treated metastasis.

## Materials and methods

### Clinical data of the patient

A 51-year-old male Caucasian patient with a diagnosis of melanoma had been previously treated by electrochemotherapy with bleomycin given intravenously. The treated small superficial metastases on the right leg regressed completely after the treatment. In October 2008, a PET-CT was performed, which revealed a deep-seated metastasis in the right thigh (Figure 1). In December 2008, electrochemotherapy with long needle electrodes was performed using bleomycin given intravenously ( $15,000 \text{ IU/m}^2$ ) and electric pulses were delivered 10-12 minutes after injection. The study was approved by the national Ethics committee and institutional board. The patient signed an informed consent to participate in the study. The positioning of the electrodes

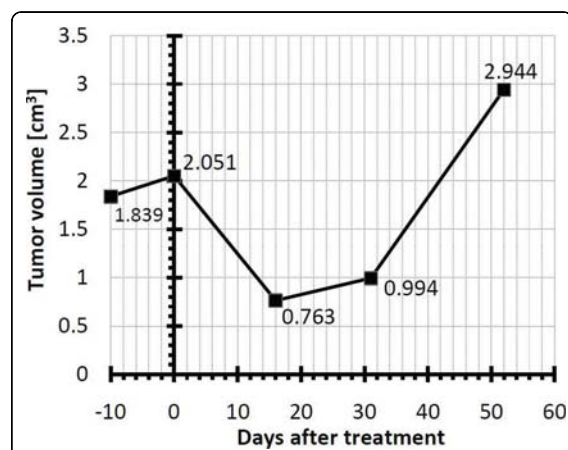


**Figure 1** Size of the melanoma metastasis determined by ultrasound. The figure shows the tumor size shortly before the treatment, at the time of the treatment itself and during the follow-up. Regrowth of the tumor was observed at day 31 and the tumor was excised at day 52.

was ultrasonographically guided. The treatment was performed in general anesthesia; in order to avoid strong muscle contractions induced by electric pulses the myorelaxant vecuronium bromide (Norcuron, Organon) was used. In February 2009, regrowth of the metastasis was observed by ultrasound. The metastasis was surgically removed by the end of February and a pathological analysis of the excised tissue was performed.

#### Numerical treatment planning

Based on the PET-CT radiographs, the position of the melanoma metastasis was determined. Its size was 20 × 14 mm in diameter and it was located in the right thigh, 20 mm under the skin. The location was estimated to be on or minimally invasive into thigh muscle fascia.

During preparation for electrochemotherapy, a slight growth of the metastasis was observed ultrasonographically (Figure 1). The anatomical model geometry used in the treatment planning procedure was obtained from CT images. All clinically relevant tissue structures (tumor, muscle, adipose tissue) were delineated and used to construct 3D geometry objects in the numerical computing environment Matlab (Mathworks, USA) by the planar contour method as previously described by [11] (Figure 2). The geometry of objects was then imported into the finite element analysis software Comsol Multiphysics 3.5 (COMSOL AB, Sweden). In the model, all tissues were considered homogeneous, the assigned conductivity values being: 0.2 S/m for the tumor, 0.018 S/m for adipose tissue, 0.135 S/m and 0.75

S/m for muscle tissue perpendicular and parallel to the muscle direction, respectively. These conductivity values were considered as approximations for DC values, and are extrapolated from measurements performed at 10 Hz. During the delivery of electric pulses, the conductivity of tissues changes as a consequence of electroporation. Measurements of conductivity during pulse application have shown that conductivity changes by a factor of around 3.5; therefore conductivity of electroporated tissue was increased by this factor, which agrees well with measurements taken on rat muscle and liver tissue and with the post-electroporation conductivity estimation performed by mathematical modeling for rabbit liver [12,13]. All conductivity values were chosen according to previous measurements of tumor and tissue conductivity and models of subcutaneous tumor and skin electroporation [12-14].

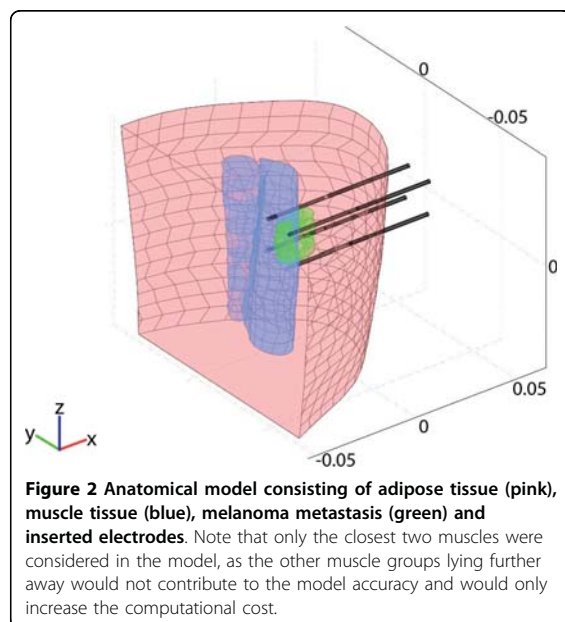
Numerical calculations were performed with Comsol. Electric field distribution in the tissue, caused by an electroporative pulse, was determined by solving the Laplace equation for static electric currents:

$$\nabla \cdot (\sigma \cdot \nabla \phi) = 0$$

where  $\sigma$  and  $\phi$  are tissue electric conductivity and electric potential, respectively. The boundary conditions used in our calculations were a constant potential on the surface of the electrodes and electrical insulation on all outer boundaries of the model. For tumors, the reversible electroporation threshold was considered to be 400 V/cm, for adipose tissue 100 V/cm, for muscle tissue 200 V/cm and 80 V/cm, in the perpendicular direction to muscle fibers and in the parallel direction, respectively. The irreversible threshold was set to 900 V/cm for all tissues.

In treatment planning, a numerical model of electroporation was used that did not take into account changes in tissue conductivity during electroporation. After the treatment, in order to compare the measured electric currents during electric pulse delivery and the currents predicted by the model, a model that took into account the changes in tissue conductivity was used. The conductivity dependencies on the electric field  $\sigma(E)$  of all tissues were approximated by a step function [14].

Electrode positions and voltages to be applied between individual electrodes were optimized using a genetic algorithm, described in more detail in previous studies [15,16]. In short, the algorithm optimized the position of each electrode ( $x, y, z$ ) - in discrete steps of 1 mm and the voltage between each pair of electrodes in discrete steps of 100 V. Feasible ranges of all these parameters were taken into account, as well as the specifications of the electric pulse generator (see below). First, a population of treatment plans (consisting of all electrode



positions and all used voltages) was randomly generated. The treatment plans then evolved over several hundred generations by mathematical operations cross-over and mutation according to the fitness function:

$$F = 100 \cdot V_{Trev} - 10 \cdot V_{Hirrev}$$

where  $F$  is fitness,  $V_{Trev}$  is the tumor volume subjected to the local electric field above the reversible threshold and  $V_{Hirrev}$  is the volume of healthy tissue subjected to a local electric field above the irreversible threshold. The weights in the fitness function were chosen to reflect the importance of the individual parameters for efficient ECT. Namely,  $V_{Trev}$  is crucial for efficient ECT; therefore its weight is larger (100) than the weight of  $V_{Hirrev}$ . The algorithm was stopped after 500 iterations - this number of iterations gave good solutions in previous studies [15,16] and the quality of the treatment plan was compared to previously set treatment plan requirements - when a sufficiently high quality treatment plan was achieved, *i.e.* the whole tumor was covered with a sufficiently high electric field and very little of the surrounding tissue was affected by the field. The optimization took 5 h on a Windows XP, 3.0 GHz, 2 GB RAM desktop computer.

#### Electrodes, pulse generator and pulse parameters

Four custom-made electrodes made of stainless steel, 1.8 mm in diameter with sharpened tips, insulated except for the upper 4 cm, were used. An additional 1.2 mm in diameter electrode was considered for direct insertion into the center of the tumor. The electrodes were connected to independently controlled generator outputs of the Cliniporator Vitae (IGEA, Carpi, Italy). The Cliniporator Vitae device is a pulse generator with 6 independently controlled and electrically insulated outputs each providing up to 3000 V, max current 50 A, delivering 8 rectangular electrical pulses (rise time 1  $\mu$ s) of 100  $\mu$ s duration at a pulse repetition frequency of 4 Hz [17]. The current and voltage are measured and logged with a precision better than 3%, which allows for pulse delivery control and post-treatment evaluation. Pulses were delivered 10-12 minutes after *i.v.* bolus injection of bleomycin.

## Results

### Optimized treatment plan

Treatment planning was performed for two different electrode configurations. The first configuration was with five electrodes with a central electrode inserted in the tumor and four electrodes distributed around the tumor, while the second configuration was with four electrodes outside the tumor (Figure 3). Although the five-electrode option was recognized as superior and was the primary choice for treatment, the central electrode could not be

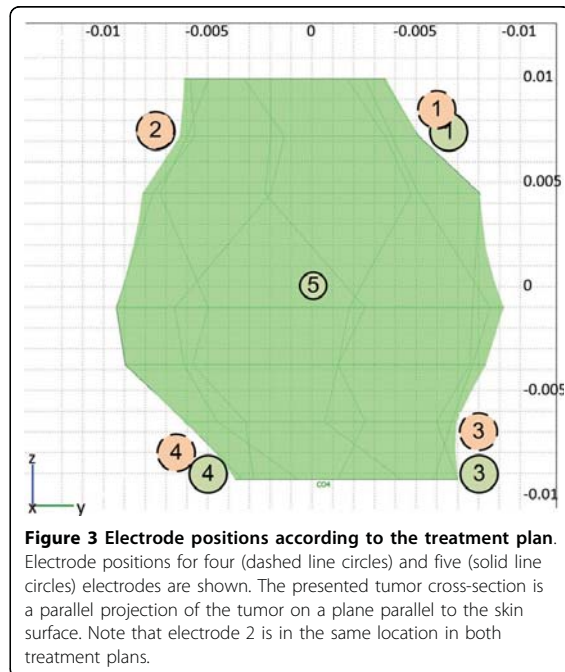


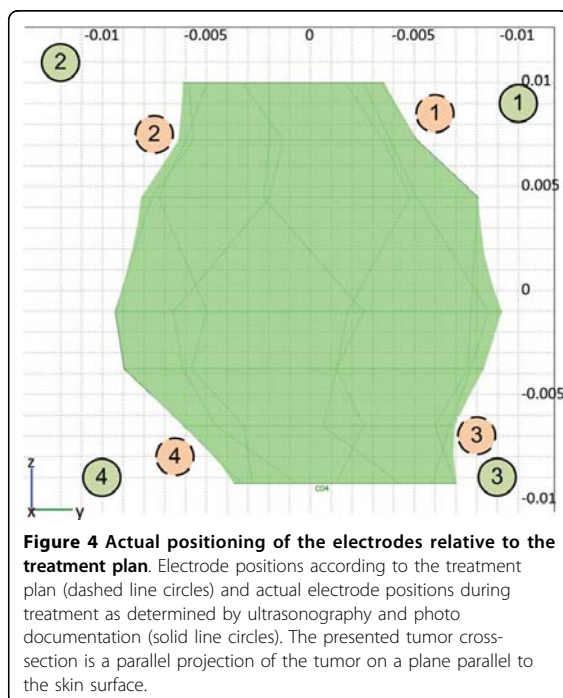
**Figure 3 Electrode positions according to the treatment plan.** Electrode positions for four (dashed line circles) and five (solid line circles) electrodes are shown. The presented tumor cross-section is a parallel projection of the tumor on a plane parallel to the skin surface. Note that electrode 2 is in the same location in both treatment plans.

inserted into the tumor as the tumor was very mobile, effectively “floating” in the surrounding adipose tissue. This mobility of the tumor also made it very difficult to rigorously follow the treatment plan for four electrodes, and as a result the electrodes were positioned farther away from the tumor than originally planned.

The results of optimization were electrode positions and minimum voltages for each electrode pair. Electrode positions outside the tumor were similar in both configurations, *i.e.* very close to the tumor surface; however the fifth electrode inside the tumor significantly reduced the required voltage to achieve efficient membrane electroporation of cells in the whole tumor, thereby also reducing damage to healthy tissue. The maximum voltages required were 3000 V and 2500 V in the four and five electrode configuration, respectively. The volume of irreversibly permeabilized healthy tissue according to the treatment plan was 13.8 cm<sup>3</sup> (of that 11.5 cm<sup>3</sup> adipose tissue and 2.33 cm<sup>3</sup> muscle tissue) in the four electrode configuration and 12.3 cm<sup>3</sup> (of that 10.4 cm<sup>3</sup> adipose tissue and 1.88 cm<sup>3</sup> muscle tissue) in the five electrode configuration. Depth of insertion was a few millimeters deeper than the tumor, slightly penetrating the muscle tissue.

### Treatment and response to the treatment

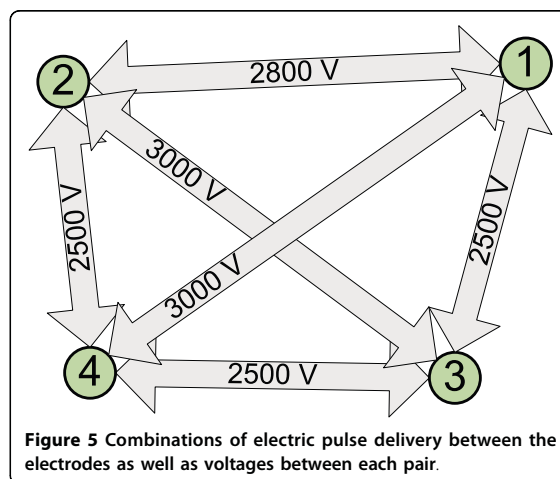
During the procedure, the four-electrode treatment plan was adopted. The electrodes were placed according to the treatment plan as depicted in Figure 4. Electrodes



were positioned under ultrasonographic guidance in the four outer corners of the tumor in the fat tissue, the deepest location being minimally inserted into the muscle (Figure 4). Eight pulses of 100  $\mu$ s each were delivered between each pair of electrodes. In total, 6 times 8 pulses were delivered to the tumor with amplitudes of 2800 V between electrodes (pair 1-2) 25 mm apart, 2500 V between electrodes (1-3, 2-4 and 3-4) 20 mm apart, and 3000 V between diagonal electrodes (1-4 and 2-3) (Figure 5). The currents recorded during electric pulse delivery were between 9 and 19 A.

The treatment was performed in general anesthesia and due to the myorelaxant given to the patient, only minor muscle contractions were observed. No other side-effects were noticed. The patient reported no discomfort after the treatment, and left the hospital after 2 days. The response to treatment with electrochemotherapy was followed ultrasonographically at regular time intervals (Figure 1). The first post-operative ultrasound showed a substantial decrease in the tumor volume (more than 50%), while the second showed a regrowth of tumor tissue.

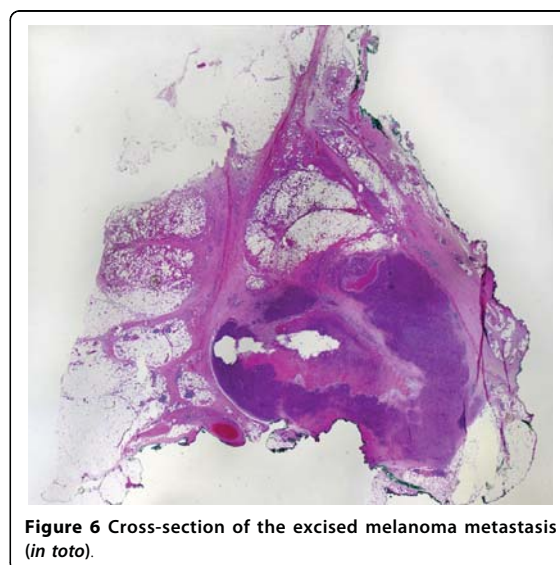
In February 2009, *i.e.* 52 days after electrochemotherapy was performed, the metastasis was excised. It was located 2 cm under the skin in the deep subcutaneous fat tissue, abutting on the muscle fascia. The size of the metastasis measured after excision (22  $\times$  15 mm) was determined on the pathological cross-section (Figure 6).



Histologically, the metastasis showed partial necrosis, estimated to represent 40-50% of the tumor. It was not possible to discriminate between spontaneous and induced necrosis. However, there was indirect evidence of the effect of electrochemotherapy; *i.e.* the presence of fat necrosis and obliterated blood vessels in the tissue around the tumor (Figure 7). These observations would not be expected in a fast-growing, untreated metastasis.

#### Numerical model validation

After the treatment, the geometry of the numerical model was updated according to measurements taken during the operating procedure and photo documentation of the treatment. Specifically, the four electrode positions in the model were changed according to these



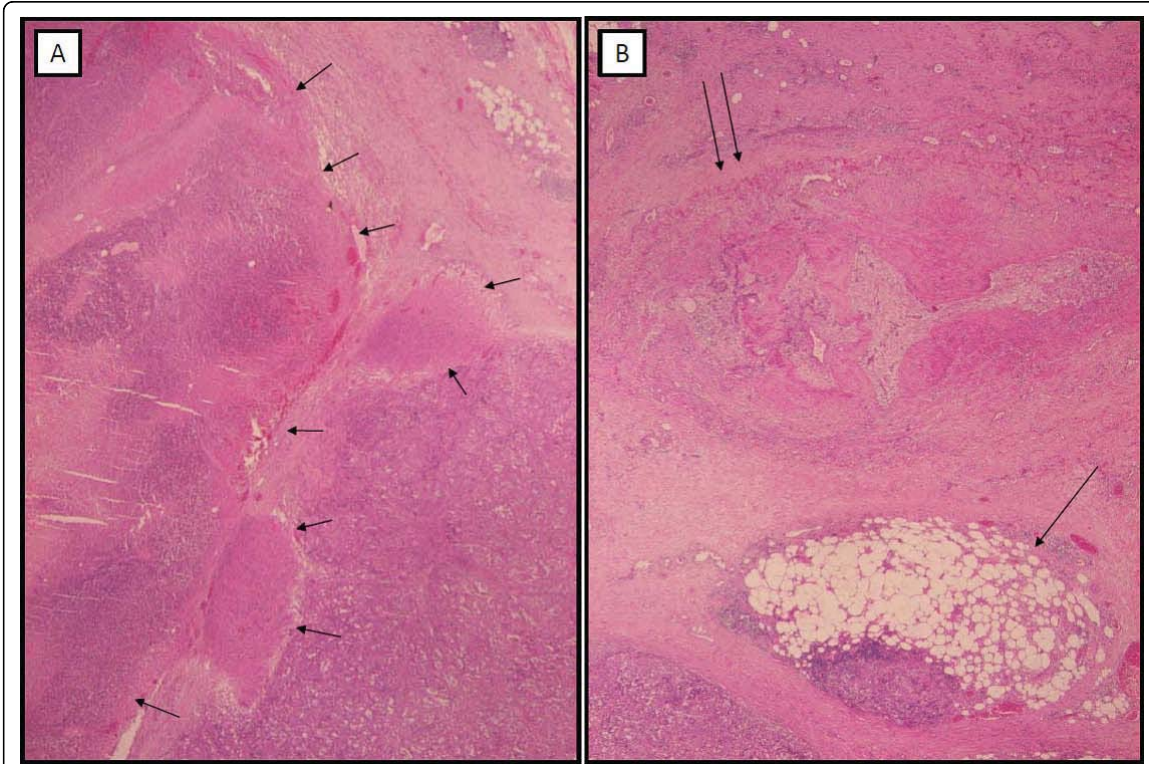


**Figure 7 Histology of melanoma metastasis treated by electrochemotherapy.** The tumor (A) shows partial necrosis (short arrows). In the surrounding tissue (B), fat necrosis (long arrow) and obliterated blood vessels (double arrow) are visible (H&E, original magnification 20X).

measurements (Figure 4). We compared the maximum value of the electric current measured by the Cliniporator Vitae during electric pulse delivery with the current predicted by the numerical model. Good agreement was obtained between the measurements and calculations, as presented in Table 1. Finally, tumor coverage with an electric field above the reversible threshold was recalculated using the revised geometry and the volume of the reversibly permeabilized tumor was determined to be approximately 94% (Figure 8).

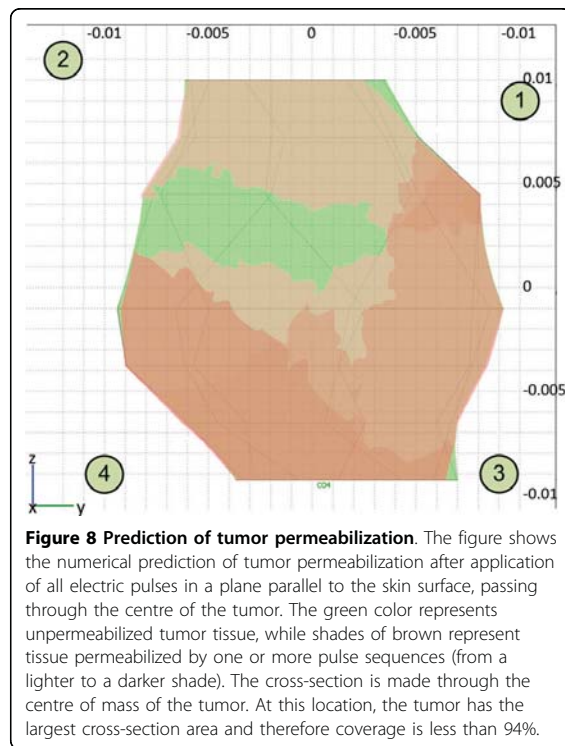
**Table 1 Agreement between maximum measured electrical currents and currents calculated in the numerical model**

Electrode pair	Measured current [A]	Calculated current [A]	Error [%]
1-2	16	16.2	1
1-3	18	17.3	-4
1-4	10	9.5	-5
2-3	19	17.2	-9
2-4	9	8.4	-7
3-4	9	8.0	-11

**Discussion**

We present here the first study of deep-seated tumor electrochemotherapy based on numerical treatment planning. Namely, electrochemotherapy was, until now only used for superficial and accessible tumor nodules, with an approximately 80% objective response rate [1,7,18-22]. In this, the first reported clinical case, a deep-seated melanoma metastasis in the thigh of the patient was treated by insertion of long needle electrodes around the tumor. A new electric pulse generator was used that provides higher voltages and currents and has six independently controlled insulated outputs, which thus allow for treatment of deeper-seated tumors by delivering electric pulses between different pairs of electrodes.

The electric conductivity values taken into account in the numerical model have been obtained from measurements done mostly on large animal tissues, which are not necessarily valid for human tissue as well [13]. Furthermore, these values are not valid for electroporated tissue, as electroporation increases tissue conductivity. In one of our previous studies, we measured the conductivity of rat muscle and liver tissue and the conductivity increased between 3.2-3.8 times for both tissue types [12]. Also,



comparing the measured and calculated electric current for rabbit liver resulted in an estimated conductivity increase of 3.6 [11]. In this study, an increase in conductivity of 3.5 as a result of electroporation was used for all tissues, a choice which seems to be at least partly validated by the agreement between the measured and calculated electric current in our study (Table 1).

In our post-treatment model, tissue electroporation thresholds for muscle and tumor were taken from previous studies in which these thresholds were determined by comparing *in vivo* measurements and numerical modeling of electroporation of different tissues [14,23,24]. In all these studies, the assumption was made that the values of the electric field, at which a change in tissue properties occur, coincides with the electroporation thresholds. This assumption was already considered both theoretically and practically in previous studies and can be considered as justified [25-27].

Two different electroporation models were used in our present study; the first which took into account changes in tissue properties and the second which did not, a simplification that made the calculation much faster. Both models predicted similar electroporation volumes (results not shown), while only the first model could predict the electric current density. As such, the second model was used for optimization-based treatment

planning and the first one for validation by comparing the measured and calculated electric currents.

According to the model used after the treatment, inaccuracies in positioning of the electrodes are most likely responsible for the inadequate electroporation of the entire tumor volume, although possible deviation from the assigned electrical conductivities and/or deviations from the assigned electroporation threshold for the tissues cannot be disregarded. Nevertheless, good agreement between the predicted and the measured delivered currents implies that the conductivity values chosen were very close to the real values. Under the assumption that the positioning of the electrodes was responsible for the inadequate tumor electroporation, calculations show that only a small percent of the tumor was not successfully electroporated (app. 6%); however this was enough for the tumor to survive and start growing again. While normally these relatively small errors in electrode positioning (Figure 4) would not lead to an unsuccessful treatment, the proximity of three different tissues with very different conductivities made the treatment very sensitive to electrode positioning. Adipose tissue that surrounded the tumor had by far the lowest conductivity, which meant that according to the voltage divider principle the electric field was largest in the adipose tissue around the tumor and not in the tumor [28].

## Conclusions

Electrochemotherapy of a deep-seated tumor was performed in a patient with the aim to verify the treatment approach, and the use of treatment planning in optimizing the positioning of the electrodes and electrical parameters. Although the configuration of five electrodes was recognized as the best in treatment planning, it was not possible to execute it due to "floating" of the tumor in the adipose tissue. The four-electrode position was thus used and at follow-up of the tumor growth, significant tumor reduction was observed (Figure 1). For effective treatment, however, all viable tumor cells have to be destroyed in order to prevent tumor regrowth. Therefore, as calculated in this tumor model, even a small percentage of remaining viable tumor tissue (6%) after electrochemotherapy was enough for tumor regrowth. Nevertheless, this clinical case demonstrates that treatment of deep-seated tumor nodules by electrochemotherapy is feasible and that optimization of the treatment approach by tumor numerical modeling is of significant help.

## Acknowledgements

This research was supported by the Slovenian Research Agency under various grants. We would also like to thank IGEA, Carpi (MO), Italy for providing us with the electrodes and Cliniporator VITAE. Written consent for publication was obtained from the patient.

**Author details**

<sup>1</sup>University of Ljubljana, Faculty of Electrical Engineering, Trzaska cesta 25, SI-1000 Ljubljana, Slovenia. <sup>2</sup>Institute of Oncology Ljubljana, Zaloska 2, SI-1000 Ljubljana, Slovenia.

**Authors' contributions**

DM, MS, MC, MK, TP, EG and GS were involved in treatment of the patient. MB performed pathology of the metastasis. DM, AZ and BK carried out medical image segmentation and performed numerical calculations. DM, AZ, BK and GS prepared the manuscript. All authors read and approved the final manuscript.

**Competing interests**

The authors declare that they have no competing interests.

Received: 3 November 2009 Accepted: 23 February 2010

Published: 23 February 2010

**References**

- Sersa G, Miklavcic D, Cemazar M, Rudolf Z, Pucihar G, Snoj M: **Electrochemotherapy in treatment of tumours.** *EJSO* 2008, **34**:232-240.
- Miklavcic D, Corovic S, Pucihar G, Pavselj N: **Importance of tumour coverage by sufficiently high local electric field for effective electrochemotherapy.** *EJC Suppl* 2006, **4**:45-51.
- Gothelf A, Mir LM, Gehl J: **Electrochemotherapy: results of cancer treatment using enhanced delivery of bleomycin by electroporation.** *Cancer Treat Rev* 2003, **29**:371-387.
- Larkin JO, Collins CG, Aarons S, Tangney M, Whelan M, O'Reilly S, Breatnach O, Soden DM, O'Sullivan GC: **Electrochemotherapy: aspects of preclinical development and early clinical experience.** *Ann Surg* 2007, **245**:469-479.
- Mir LM, Gehl J, Sersa G, Collins CG, Garbay JR, Billard V, Geertsen PF, Rudolf Z, O'Sullivan GC, Marty M: **Standard operating procedures of the electrochemotherapy: Instructions for the use of bleomycin or cisplatin administered either systemically or locally and electric pulses delivered by Cliniporator™ by means of invasive or non-invasive electrodes.** *EJC Suppl* 2006, **4**:14-25.
- Domenge C, Orłowski S, Luboinski B, De Baere T, Belehradec J-Jr, Mir LM: **Antitumor electrochemotherapy. New advances in the clinical protocol.** *Cancer* 1996, **77**:956-963.
- Marty M, Sersa G, Garbay JR, Gehl J, Collins CG, Snoj M, Billard V, Geertsen PF, Larkin JO, Miklavcic D, Pavlovic I, Paulin-Kosir SM, Cemazar M, Morsli N, Soden DM, Rudolf Z, Robert C, O'Sullivan GC, Mir LM: **Electrochemotherapy - An easy, highly effective and safe treatment of cutaneous and subcutaneous metastases: Results of ESOPE (European Standard Operating Procedures of Electrochemotherapy) study.** *EJC Suppl* 2006, **4**:3-13.
- Snoj M, Rudolf Z, Cemazar M, Jancar B, Sersa G: **Successful sphincter-saving treatment of anorectal malignant melanoma with electrochemotherapy, local excision and adjuvant brachytherapy.** *Anti-Cancer Drugs* 2005, **16**:345-348.
- Shimizu T, Nikaïdo T, Gomyo H, Yoshimura Y, Horiuchi A, Isobe K, Ebara S, Takaoka K: **Electrochemotherapy for digital chondrosarcoma.** *J Orthop Sci* 2003, **8**:248-51.
- Sel D, Macek-Lebar A, Miklavcic D: **Feasibility of employing model-based optimization of pulse amplitude and electrode distance for effective tumor electroporation.** *IEEE T Biomed Eng* 2007, **54**:773-781.
- Sel D, Cukjati D, Batiuskaite D, Slivnik T, Mir LM, Miklavcic D: **Sequential finite element model of tissue electroporation.** *IEEE T Biomed Eng* 2005, **52**:816-827.
- Cukjati D, Batiuskaite D, Andre F, Miklavcic D, Mir LM: **Real time electroporation control for accurate and safe in vivo non-viral gene therapy.** *Bioelectrochemistry* 2007, **70**:501-507.
- Gabriel C, Peymann A, Grant EH: **Electrical conductivity of tissue at frequencies below 1 MHz.** *Phys Med Biol* 2009, **54**:4863-4878.
- Pavselj N, Bregar Z, Cukjati D, Batiuskaite D, Mir LM, Miklavcic D: **The course of tissue permeabilization studied on a mathematical model of a subcutaneous tumor in small animals.** *IEEE T Biomed Eng* 2005, **52**:1373-1381.
- Corovic S, Zupanic A, Miklavcic D: **Numerical modeling and optimization of electric field distribution in subcutaneous tumors treated with electrochemotherapy using needle electrodes.** *IEEE T Plasm Sci* 2008, **36**:1665-1672.
- Zupanic A, Corovic S, Miklavcic D: **Optimization of electrode position and electric pulse amplitude in electrochemotherapy.** *Radiol Oncol* 2008, **42**:93-101.
- Campana LG, Mocellin S, Basso M, Puccetti O, De Salvo G, Chiarion-Sileni V, Vecchiato A, Corti L, Rossi CR, Nitti D: **Bleomycin-based electrochemotherapy: clinical outcome from a single institution's experience with 52 patients.** *Ann Surg Oncol* 2008, **16**:191-199.
- Bertacchini C, Margotti PM, Bergamini E, Ronchetti M, Cadossi R: **Irreversible electroporation systems for clinical use.** *Irreversible electroporation* Berlin: Springer VerlagRubinsky B 2010, 255-272.
- Quaglino P, Mortera C, Osella-Abate S, Barberis M, Illengo M, Rissone M, Savoia P, Bernengo MG: **Electrochemotherapy with intravenous bleomycin in the local treatment of skin melanoma metastases.** *Ann Surg Oncol* 2008, **15**:2215-2222.
- Heller R, Jaroszeski MJ, Reintgen DS, Puleo CA, DeConti RC, Gilbert RA, Glass LF: **Treatment of cutaneous and subcutaneous tumors with electrochemotherapy using intralesional bleomycin.** *Cancer* 1998, **83**:148-157.
- Sersa G, Cufer T, Cemazar M, Rebersek M, Zvonimir R: **Electrochemotherapy with bleomycin in the treatment of hypernephroma metastasis: case report and literature review.** *Tumori* 2000, **86**:163-165.
- Sersa G: **The state-of-the-art of electrochemotherapy before the ESOPE study: advantages and clinical uses.** *EJC Suppl* 2006, **4**:52-59.
- Semrov D, Miklavcic D: **Calculation of the electrical parameters in electrochemotherapy of solid tumours in mice.** *Comput Biol Med* 1998, **28**:439-448.
- Miklavcic D, Semrov D, Mekid H, Mir LM: **A validated model of in vivo electric field distribution in tissues for electrochemotherapy and for DNA electrotransfer for gene therapy.** *Biochim Biophys Acta* 2000, **1523**:73-83.
- Pavlin M, Miklavcic D: **Effective conductivity of a suspension of permeabilized cells: a theoretical analysis.** *Biophys J* 2003, **85**:719-729.
- Pavlin M, Kanduser M, Rebersek M, Pucihar G, Hart FX, Magjarevic R, Miklavcic D: **Effect of cell electroporation on the conductivity of a cell suspension.** *Biophys J* 2005, **88**:4378-4390.
- Ivorra A, Al-Sakere B, Rubinsky B, Mir LM: **In vivo electrical conductivity measurements during and after tumor electroporation: conductivity changes reflect treatment outcome.** *Phys Med Biol* 2009, **54**:5949-5963.
- Pavselj N, Miklavcic D: **Numerical modeling in electroporation-based biomedical applications.** *Radiol Oncol* 2008, **42**:159-168.

doi:10.1186/1475-925X-9-10

Cite this article as: Miklavcic et al: Towards treatment planning and treatment of deep-seated solid tumors by electrochemotherapy. *BioMedical Engineering OnLine* 2010 **9**:10.

**Submit your next manuscript to BioMed Central and take full advantage of:**

- Convenient online submission
- Thorough peer review
- No space constraints or color figure charges
- Immediate publication on acceptance
- Inclusion in PubMed, CAS, Scopus and Google Scholar
- Research which is freely available for redistribution

Submit your manuscript at  
www.biomedcentral.com/submit





## Paper 5

**Title:** Robustness of Treatment Planning for Electrochemotherapy of Deep-Seated Tumors

**Authors:** Kos Bor, Županič Anže, Kotnik Tadej, Snoj Marko, Serša Gregor, Miklavčič Damijan

**Publication:** Journal of Membrane Biology

**DOI:** 10.1007/s00232-010-9274-1

**Year:** 2010

**Volume:** 234

**Number:** 1

**Pages:** 147-153

## Robustness of Treatment Planning for Electrochemotherapy of Deep-Seated Tumors

Bor Kos · Anze Zupanic · Tadej Kotnik ·  
Marko Snoj · Gregor Sersa · Damijan Miklavcic

Received: 5 January 2010 / Accepted: 11 June 2010 / Published online: 2 July 2010  
© Springer Science+Business Media, LLC 2010

**Abstract** Treatment of cutaneous and subcutaneous tumors with electrochemotherapy has become a regular clinical method, while treatment of deep-seated tumors is still at an early stage of development. We present a method for preparing a dedicated patient-specific, computer-optimized treatment plan for electrochemotherapy of deep-seated tumors based on medical images. The treatment plan takes into account the patient's anatomy, tissue conductivity changes during electroporation and the constraints of the pulse generator. Analysis of the robustness of a treatment plan made with this method shows that the effectiveness of the treatment is not affected significantly by small single errors in electrode positioning. However, when many errors occur simultaneously, the resulting drop in effectiveness is larger, which means that it is necessary to be as accurate as possible in electrode positioning. The largest effect on treatment effectiveness stems from uncertainties in dielectric properties and electroporation thresholds of treated tumors and surrounding tissues, which emphasizes the need for more accurate measurements and more research. The presented methods for treatment planning and robustness analysis allow quantification of the treatment reproducibility and enable the setting of suitable

safety margins to improve the likelihood of successful treatment of deep-seated tumors by electrochemotherapy.

**Keywords** Electrochemotherapy · Electroporation · Treatment planning · Deep-seated tumor

### Introduction

Electrochemotherapy (ECT) is a treatment in which a specific chemotherapeutic drug having an intracellular target is combined with a strong pulsed electric field that increases cell membrane permeability—electroporation (Orlowski et al. 1988; Sersa et al. 1995). This increases the amount of molecules that enter cancer cells and have a cytotoxic effect. To achieve a complete response of the treated tumors, the electric field used for electroporation has to exceed a threshold value in the entire tumor volume (Miklavcic et al. 2006a; Sersa et al. 2008). In the last decade ECT has been successfully used for treatment of cutaneous and subcutaneous tumors, mainly melanoma (Campana et al. 2009; Marty et al. 2006). The success of ECT, its clinical applicability and recent development of more powerful electric pulse generators and new electrodes have resulted in the first clinical uses of ECT for treatment of deep-seated tumors (Miklavcic et al. 2010).

In the European Standard Operating Procedures of Electrochemotherapy (ESOPE) study a standard operating protocol was developed for ECT of cutaneous and subcutaneous tumors that provides physicians with a set of appropriate electrodes and electric pulse parameters depending on tumor size and location (Mir et al. 2006). This protocol, however, cannot be used for ECT of deep-seated tumors because of increased treatment complexity. Deep-seated tumors can be much bigger than cutaneous or subcutaneous

---

B. Kos · A. Zupanic · T. Kotnik · D. Miklavcic  
Faculty of Electrical Engineering, University of Ljubljana,  
Trzaska 25, 1000 Ljubljana, Slovenia

M. Snoj · G. Sersa  
Institute of Oncology, Zaloska 2, 1000 Ljubljana, Slovenia

D. Miklavcic (✉)  
Laboratory of Biocybernetics, Trzaska 25,  
1000 Ljubljana, Slovenia  
e-mail: damijan.miklavcic@fe.uni-lj.si

ones; their shape can be irregular; they can be in the vicinity of vital organs, damage to which has to be avoided; and the electric properties of the surrounding tissue as well as of the tumor can vary significantly. Since it is necessary to cover the entire volume of the tumor with electric field above the threshold to achieve a desirable effect, the choice of electrode position and voltages applied between the electrodes varies from case to case, which is why an individualized treatment plan, similar to radiotherapy treatment plans, is necessary (Bortfeld 1999). As the electric field distribution inside the target tissues is one of the most important predictors of electroporation (Miklavcic et al. 1998), the use of numerical models of electroporation has been proposed, in combination with optimization algorithms, as a means of ECT treatment planning (Corovic et al. 2008; Sel et al. 2007).

The treatment plan should be robust enough to prevent uncertainties both in the treatment planning stage and in the treatment itself from influencing the treatment outcome. The uncertainties include (1) all the input parameters for the numerical model (conductivity values for each tissue, electroporation thresholds and precision of the anatomical model) and (2) the difficulty in precisely positioning the electrodes (relative to each other and relative to the tumor). These uncertainties have to be carefully analyzed, and their significance for the success of the ECT treatment has to be evaluated.

Here, we present a method for creating a dedicated patient-specific treatment plan for deep-seated tumor ECT, its application on a case of melanoma metastasis in the thigh and a qualitative assessment of the treatment plan robustness.

## Methods

### Assembling a Patient-Specific Numerical Model

The first step in ECT treatment planning is the construction of a sufficiently detailed patient-specific model of the

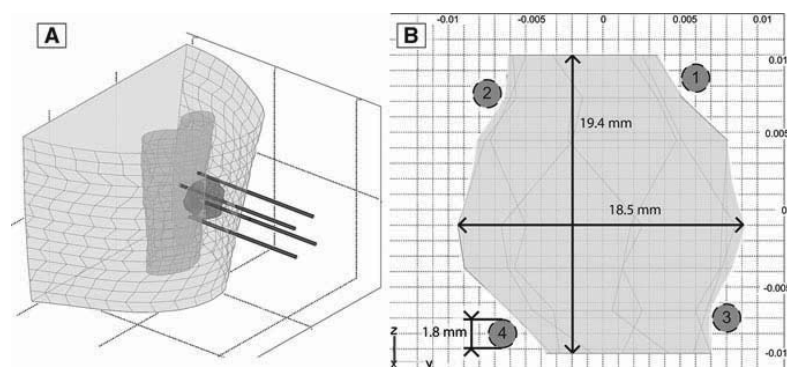
anatomy. Medical images (CT) of the region of interest were first segmented and then used to build a 3D geometry by approximating the segmented tissue with a closed spline curve and connecting the curves in the third dimension using Matlab (Mathworks, Natick, MA) as described previously (Sel et al. 2007). This geometry was then imported into COMSOL Multiphysics (COMSOL, Stockholm, Sweden), where finite-element analysis was performed.

In the presented case (Miklavcic et al. 2010) the geometry consisted of a melanoma metastasis in the right thigh, two nearby muscles (sartorius and gracilis) and surrounding adipose tissue. After the tissue geometry was built, the electrodes chosen for the treatment were added (in the presented case, four stainless-steel needle electrodes with a 30-mm exposed tip and the rest of the length insulated were used) (Fig. 1). As the skin is penetrated by the needle electrodes, its high impedance does not affect the calculations; therefore, it was not considered in the model along with other tissues located away from the tumor (e.g., femur and other thigh muscles). At the location of these tissues, the electric field strength is low and not significant for the treatment.

In the presented model, tumor, muscle and adipose tissue were modeled; their bulk conductivities were taken from the literature (0.135, 0.75, 0.2 and 0.02 S/m, for muscle in the direction perpendicular to muscle fibers, muscle in the direction parallel to muscle fibers, tumor and adipose tissue, respectively) (Gabriel et al. 1996; Haemmerich et al. 2009). These values present conductivities at a frequency of 10 or 50 Hz and have been previously used to accurately predict tissue electroporation and the total current delivered during electric pulses (Pavselj et al. 2005).

The mathematical model of electroporation used in the study is described in more detail by Sel et al. (2005). Briefly, the Laplace equation for static electric currents was used to calculate the electric field distribution in the model. A sequential model of electroporation was used, which takes into account the

**Fig. 1** **a** Model geometry. Four electrodes are inserted into the thigh (light gray) around the tumor (dark gray) according to the treatment plan. Also shown are two adjoining muscles that the electrodes penetrate by a few millimeters. **b** Electrode positions in the cross section perpendicular to the electrodes' axis, through the center of mass of the tumor



conductivity changes during electric pulse delivery due to electroporation (Cukjati et al. 2007; Ivorra et al. 2009). In the model, electroporation-increased tissue conductivities were increased by a factor of 3.5 (Cukjati et al. 2007) and the reversible thresholds for electroporation were considered to be 400 V/cm for tumor tissue, 100 V/cm for adipose tissue and 200 and 80 V/cm for muscle tissue in the direction perpendicular to muscle fibers and in parallel direction, respectively (Miklavcic et al. 2000; Corovic et al. 2010). The model assumes that the conductivities return to their initial values before the next pulse is delivered and does not differentiate between reversible and irreversible electroporation. Furthermore, the model considers only one pulse between each electrode pair because in order to model conductivity changes between each successive pulse in the regular eight-pulse train, the time course of conductivity after a pulse would have to be known.

#### Treatment Planning

The assembled numerical model was used together with a genetic algorithm, as previously described, to provide an optimal treatment plan (Corovic et al. 2008; Zupanic et al. 2008). When setting up the optimization, constraints had to be taken into account, e.g., feasible positions of the electrodes and specifications of the pulse generator (Cliniporator Vitae<sup>TM</sup>; IGEA, Carpi, Italy). Two treatment plans were generated: In the first, the position constraints were that the electrodes should be outside the tumor but <1 cm away, while in the second, there was an additional fifth electrode inserted in the center of the tumor. A lower number of electrodes did not yield a successful solution, and more were considered too difficult to position correctly. Due to problems with insertion of the central electrode during the actual treatment, the four-electrode plan was finally adopted (Miklavcic et al. 2010). The pulse generator constraints were the maximum available voltage (3,000 V) and current (50 A). In addition, only two electrodes at a time can have a set potential during electric pulse delivery. In the presented case the algorithm searched for the optimal positions of each of the four electrodes and the optimal voltage between each pair of electrodes. The optimization algorithm was set to maximize the volume of the tumor covered with electric fields over the reversible electroporation threshold and reduce the volume of nearby healthy tissue covered with fields over the irreversible electroporation threshold (Davalos et al. 2005; Rubinsky et al. 2007). Since the tumor coverage is essential for successful treatment, it was given 10 times more weight than damage to healthy tissue. The final number of parameters optimized for the treatment

was 15: depth of insertion of all electrodes,  $y$  and  $z$  positions of each electrode and voltage between each pair of electrodes.

#### Robustness Analysis

To assess the robustness of the presented treatment plan, we used the same numerical model as in the treatment planning and calculated the volume of tumor covered with an electric field over the reversible electroporation threshold, while varying a single model parameter at a time. In this parameterization study the parameters analyzed were the model inputs that were taken from the literature, such as electrical conductivity values and reversible electroporation thresholds for each tissue as well as the treatment planning parameters acquired from the optimization (electrode positions and voltages).

Every parameter was varied in five steps from the optimal position, and the percentage of tumor volume coverage was determined each time. Electrode positions perpendicular to the axis of insertion were varied in 0.5-mm steps away from the tumor in two perpendicular directions ( $y$ ,  $z$ ), depth of electrode insertion was varied in 1-mm steps in both directions (deeper and shallower penetration than optimal), voltages were varied in steps of 100 V below the optimal values, electrical conductivities were varied in steps of 10% of the values used in the model in both directions (higher and lower values than those used in the model) and electroporation thresholds were varied in steps of 50 V/cm above the values used in the model. All parameters, their baseline values and ranges are summarized in Table 1. The chosen parameters represent the uncertainties in the treatment procedure (positions) and tissue parameters (tissue conductivities and electroporation thresholds), while voltage can vary by up to 3% over the entire output voltage range (i.e., up to 90 V at the maximum 3 kV output). An additional motivation for investigating reductions in voltage was to verify the appropriateness of the optimization step and to determine if any electrode pair plays a critical role in ensuring total tumor coverage. Furthermore, it could be necessary to reduce the voltage in the clinical setting if the pulse generator is unable to provide the required current output due to technical limitations. This approach highlights the most critical parameters for the success of ECT and can also serve in determining the safety factors needed for treatment and predicting the ECT outcome.

#### Results and Discussion

We applied a genetic algorithm to optimize the positioning of four electrodes outside the tumor and necessary minimum

**Table 1** Summary of varied parameters, their respective baseline values and the ranges in which they were varied in the analysis

Parameter	Range	Baseline value
Depth of all electrodes	-5 to +5 mm	Treatment plan (Fig. 1)
Single electrode position	0-2.5 mm away from tumor	Treatment plan (Fig. 1)
Voltage between each electrode pair	0 to -500 V	Treatment plan (Fig. 1)
Tumor electroporation threshold	400-650 V/cm	400 V/cm
Fat conductivity	0.01-0.03 S/m	0.02 S/m
Tumor conductivity	0.1-0.3 S/m	0.2 S/m
Muscle conductivity <i>x, y</i> direction	0.075-0.203 S/m	0.135 S/m
Muscle conductivity <i>z</i> direction	0.375-1.125 S/m	0.75 S/m

Total number of parameters varied: 19

voltage to apply between each electrode pair. Current drawn from all electrode pairs was calculated, and we established that it was below the maximum 50-A current limit of the Cliniporator Vitae electroporation pulse generator. The optimized treatment plan was successful in covering the whole tumor volume with an electric field of no less than 400 V/cm, the estimated tumor electroporation threshold value; the details of the treatment plan are presented in Figs. 1 and 2 and Table 2. Figure 2 shows tumor coverage after each pulse application; it can be seen that the whole tumor is covered after the application of pulses to all six electrode pairs. It would be possible to cover the whole tumor with just two electrodes; however, the required voltage would be much higher, and the amount of healthy tissue damage would increase significantly. An additional benefit of using multiple electrodes is that many parts of the tumor are covered more than once and with different directions of the electric field, which has been shown to increase electroporation efficiency and molecular uptake (Rebersek et al. 2007).

According to our criteria, a solution is maximally fit when complete tumor coverage has been achieved and the volume of surrounding tissue above the irreversible electroporation threshold has been reduced to a minimum. In the case of using just two electrodes, a maximally fit

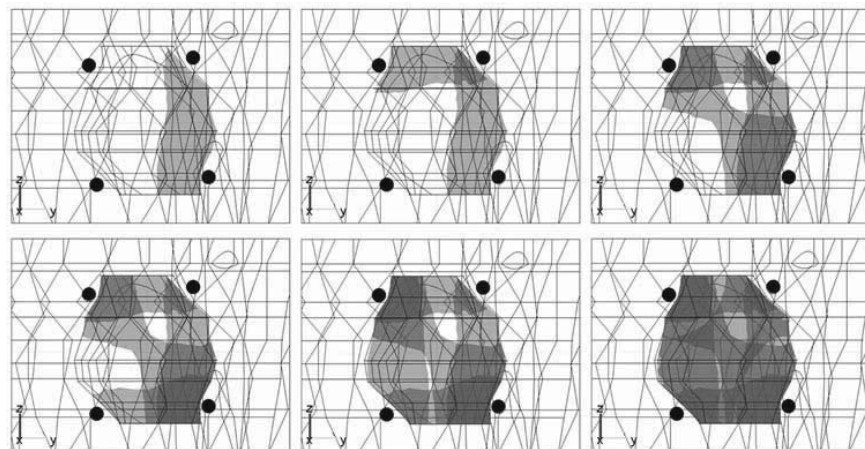
**Table 2** Voltage between each electrode pair according to the optimized treatment plan

Electrode pair	Voltage (V)
1-2	1,100
1-3	1,600
2-4	1,600
3-4	1,100
1-4	1,800
2-3	1,900

solution would be only marginally robust. Although robustness (of tumor coverage) could be increased, by, e.g., increasing the applied voltage, such an increase would be at the expense of fitness. In the case where there are more electrodes used, even a maximally fit solution (therefore the most sensitive to errors) is inherently more robust than using only two electrodes because some parts of the tumor are permeabilized more than once (Sersa et al. 1995).

In Figs. 3 and 4 we show the results of the robustness analysis. Lowering the voltage on one electrode pair by 300 V does not affect the tumor coverage at all (Fig. 3), while decreasing the voltage by 500 V causes a small volume (ranging 0.05-0.2%) to be below the threshold. This can be explained by the fact that most of the tumor

**Fig. 2** Tumor electroporation after application of each pulse in the sequence. Gray areas show where the electric field exceeded the threshold value



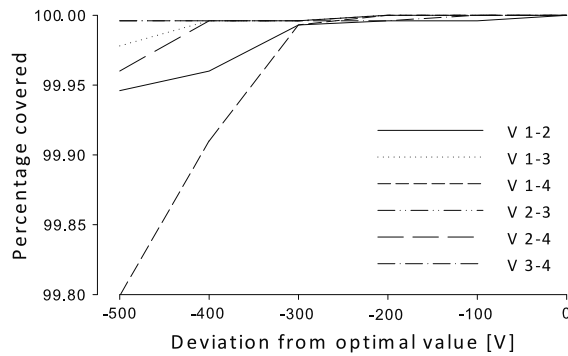


**Fig. 3** Robustness analysis: dependence of tumor coverage with an electric field over the electroporation threshold on different parameters. Effect of reducing voltage on a single electrode pair in steps of 100 V

volume is covered by more than a single pair of electrodes (Fig. 2). Therefore, a drop in effectiveness of one electrode pair does not affect the end result as dramatically as might be expected. The results also suggest that 100 V, which is

also the smallest adjustment step in the Cliniporator Vitae clinical pulse generator, for which this treatment plan was developed, is an appropriate step in voltage optimization of ECT.

The highest drop in tumor coverage was observed when increasing the tumor electroporation threshold (Fig. 4a); increasing the threshold to 650 V/cm reduces tumor coverage to just above 45%. The electroporation threshold is a critical parameter in many aspects. First, the thresholds are different for different tissues, and this fact is mostly attributed to differences in cell shapes and sizes between the tissues (Cemazar et al. 1998). Threshold measurements have so far been scarce (Miklavcic et al. 2000) and are further complicated by the fact that many tissues, among them larger tumors, are inherently heterogeneous and therefore probably exhibit a range of thresholds instead of just one. Furthermore, it is hard to cover a large volume of tissue with very high electric fields as the voltages and currents required would be higher than available from commercial pulse generators. All this calls for more research into the tissue electroporation thresholds and development of statistical

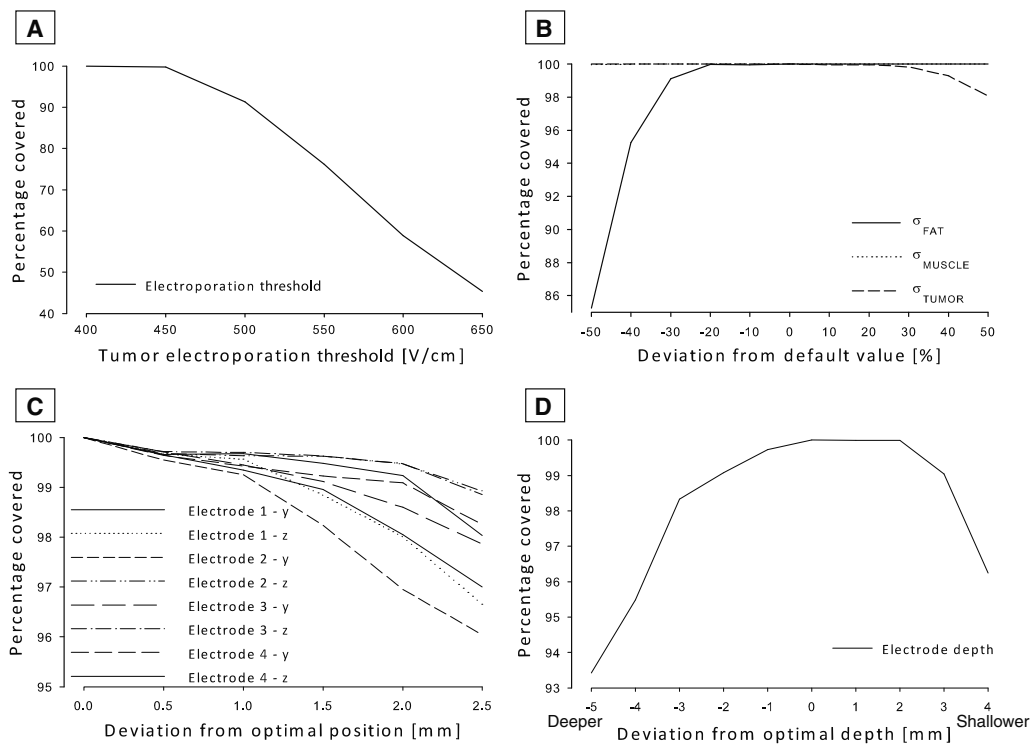


**Fig. 4** Robustness analysis: dependence of tumor coverage with an electric field over the electroporation threshold on different parameters. **a** Effect of deviations of tumor electroporation threshold in steps of 50 V/cm. **b** Effect of deviations of tissue conductivities from values used in treatment planning in steps of 10% of the values used.

**c** Effect of errors in electrode positions along a single axis in steps of 0.5 mm away from tumor surface. **d** Dependence on depth of insertion of all electrodes. Note that all plots do not share the same vertical scale

models of tissue electroporation (Goldberg and Rubinsky 2010) to improve the efficiency of ECT.

Deviations in tissue conductivity also affected the tumor coverage (Fig. 4b). More precisely, it is the ratio of conductivities between the tumor and surrounding (in this case adipose) tissue which is the (most) critical factor. When the conductivity of adipose tissue is lowered or, alternatively, the conductivity of the tumor is increased, the ratio of  $\sigma_{\text{TUMOR}}/\sigma_{\text{FAT}}$  is increased and the treatment effectiveness is reduced significantly. If this ratio is changed from 10 as in the original treatment plan to 20, tumor coverage is reduced to 85%, while if the ratio is reduced, the coverage is not affected but the robustness is increased. This stems from the fact that the lower conductivity of the surrounding tissue acts as an insulator, and it takes a larger part of the voltage between the electrodes according to the voltage divider principle (Pavselj and Miklavcic, 2009), which results in a decreased electric field and less successful electroporation. While tissue conductivities are not parameters that can be controlled by the optimization or the performing physician, it is necessary to note that data regarding low-frequency conductivities of human healthy and cancerous tissues are scarce, are difficult to measure and have values published by different authors/studies that vary significantly (Gabriel et al. 2009; Miklavcic et al. 2006b). It has been reported previously (Neal and Davalos 2009; Daniels and Rubinsky 2009) that inserting electrodes within the target region can greatly improve the electric field within the target region, while at the same time reducing the effect of the unknown conductivity ratio between target and surrounding tissue. When permitted by the nature of the treated tumor and the surrounding tissue, such a practice is a good way of eliminating some of the uncertainties present in this kind of ECT planning.

Electrode positions are also a critical parameter (Fig. 4c, d) since electrode insertion is the part of the procedure that is most prone to errors. Mispositioning a single electrode by 2 mm can already reduce tumor coverage from 100% to <97%. However, if all electrodes miss their target, the results are much more severely affected. When all electrodes are moved away from the tumor in a diagonal direction by 0.7 or 1.4 mm (effectively increasing the distance between the electrodes and the distance between the electrodes and the tumor), the tumor coverage decreases to 87 or 66%, respectively. The depth of insertion is also important, although we assumed at this point that all electrodes were placed at the same depth. Since the needle electrodes used in this case have a 3-cm noninsulated tip (comparable in size to the treated tumor) that delivers the pulses and the rest of the electrode length is insulated, inserting them either too deep or too shallow can cause significant reduction in tumor coverage, e.g., 6% when electrodes are inserted 5 mm too deep (Fig. 4d). These

results seem to be in contradiction with previous research (Corovic et al. 2008) that suggested that deeper insertion can be considered safe. However, in the previous calculations of Corovic et al. the tumors' physical size was small in relation to the length of the noninsulated (active) parts of the electrodes, whereas the size of the tumor in the current study was comparable to the noninsulated parts of the electrodes, which increases the possibility of missing the target. Our results suggest that it is necessary to be as accurate as reasonably possible in the operating theater, including use of medical imaging (e.g., ultrasound) for guidance in positioning electrodes. It would be possible to use longer electrodes (with longer active parts) to reduce this sensitivity; however, that would result in a significantly increased current, which the pulse generator might not be able to deliver.

A certain number of errors are likely to be made during the treatment, due to reasons mentioned previously. To ensure that the ECT outcome is not affected by these errors, a suitable safety margin should be employed during the treatment planning stage. The robustness analysis suggests that setting conservative values for dielectric properties (higher  $\sigma_{\text{TUMOR}}/\sigma_{\text{FAT}}$ ) and higher electroporation thresholds can increase the robustness of the treatment, but care must be taken to avoid excessive electric fields that would cause extensive healthy tissue damage.

Our results show that the presented method of treatment planning for deep-seated tumors by ECT is capable of producing efficient and robust treatment plans in the clinical setting. The robustness analysis indicates that further work is necessary to determine tissue electroporation thresholds and conductivity values, as well as enable accurate electrode positioning during ECT since these two parameters affect the treatment outcome to the highest degree. The presented work sets the ground for numerical treatment planning-based ECT of deep-seated solid tumors, quantifying its reproducibility and enabling the setting of suitable safety margins to improve the likelihood of successful treatment.

**Acknowledgement** This research was supported by the Slovenian Research Agency (ARRS) under various grants.

## References

- Bortfeld T (1999) Optimized planning using physical objectives and constraints. *Semin Radiat Oncol* 9:20
- Campana LG, Mocellin S, Basso M et al (2009) Bleomycin-based electrochemotherapy: clinical outcome from a single institution's experience with 52 patients. *Ann Surg Oncol* 16:191–199
- Cemazar M, Jarm T, Miklavcic D et al (1998) Effect of electric-field intensity on electroporation and electrosensitivity of various tumor-cell lines in vitro. *Electro Magnetobiol* 17:263–272

- Corovic S, Zupanic A, Miklavcic D (2008) Numerical modeling and optimization of electric field distribution in subcutaneous tumor treated with electrochemotherapy using needle electrodes. *IEEE Trans Plasma Sci* 36:1665–1672
- Corovic S, Zupanic A, Kranjc S et al (2010) In vivo electroporation detection based on magnetic resonance imaging, propidium iodide fluorescence and numerical modeling of anisotropic muscle tissue. *Med Biol Eng Comput* 48:637–648
- Cukjati D, Batuskaite D, Andre F et al (2007) Real time electroporation control for accurate and safe in vivo non-viral gene therapy. *Bioelectrochemistry* 70:501–507
- Daniels C, Rubinsky B (2009) Electrical field and temperature model of nonthermal irreversible electroporation in heterogeneous tissues. *J Biomech Eng* 131:071006
- Davalos RV, Mir LM, Rubinsky B (2005) Tissue ablation with irreversible electroporation. *Ann Biomed Eng* 33:223–231
- Gabriel S, Lau RW, Gabriel C (1996) The dielectric properties of biological tissues: II. Measurements in the frequency range 10 Hz to 20 GHz. *Phys Med Biol* 41:2251–2269
- Gabriel C, Peyman A, Grant EH (2009) Electrical conductivity of tissue at frequencies below 1 MHz. *Phys Med Biol* 54:4863–4878
- Goldberg A, Rubinsky B (2010) A statistical model for multidimensional irreversible electroporation cell death in tissue. *Biomed Eng Online* 9:13
- Haemmerich D, Schutt DJ, Wright AW et al (2009) Electrical conductivity measurement of excised human metastatic liver tumours before and after thermal ablation. *Physiol Meas* 30:459–466
- Ivorra A, Al-Sakere B, Rubinsky B et al (2009) In vivo electrical conductivity measurements during and after tumor electroporation: conductivity changes reflect the treatment outcome. *Phys Med Biol* 54:5949–5963
- Marty M, Sersa G, Garbay JR et al (2006) Electrochemotherapy—an easy, highly effective and safe treatment of cutaneous and subcutaneous metastases: results of ESOP (European Standard Operating Procedures of Electrochemotherapy) study. *EJC Suppl* 4:3–13
- Miklavcic D, Beravs K, Semrov D et al (1998) The importance of electric field distribution for effective in vivo electroporation of tissues. *Biophys J* 74:2152–2158
- Miklavcic D, Semrov D, Mekid H et al (2000) A validated model of in vivo electric field distribution in tissues for electrochemotherapy and for DNA electrotransfer for gene therapy. *Biochim Biophys Acta* 1523:73–83
- Miklavcic D, Corovic S, Pucihar G et al (2006a) Importance of tumour coverage by sufficiently high local electric field for effective electrochemotherapy. *EJC Suppl* 4:45–51
- Miklavcic D, Pavselj N, Hart FX (2006b) Electric properties of tissues. In: *Wiley encyclopedia of biomedical engineering*. John Wiley and Sons, New York
- Miklavcic D, Snoj M, Zupanic A et al (2010) Towards treatment planning and treatment of deep seated solid tumors by electrochemotherapy. *Biomed Eng Online* 9:10
- Mir LM, Gehl J, Sersa G et al (2006) Standard operating procedures of the electrochemotherapy: instructions for the use of bleomycin or cisplatin administered either systemically or locally and electric pulses delivered by the Cliniporator™ by means of invasive or non-invasive electrodes. *EJC Suppl* 4:14–25
- Neal RE, Davalos RV (2009) The feasibility of irreversible electroporation for the treatment of breast cancer and other heterogeneous systems. *Ann Biomed Eng* 37:2615–2625
- Orlowski S, Belehradek J, Paoletti C et al (1988) Transient electroporation of cells in culture—increased cytotoxicity of anticancer drugs. *Biochem Pharmacol* 37:4727–4733
- Pavselj N, Miklavcic D (2009) Numerical modeling in electroporation-based biomedical applications. *Radiol Oncol* 42:159–168
- Pavselj N, Bregar Z, Cukjati D et al (2005) The course of tissue permeabilization studied on a mathematical model of a subcutaneous tumor in small animals. *IEEE Trans Biomed Eng* 52:1373–1381
- Rebersek M, Faurie C, Kanduser M et al (2007) Electroporator with automatic change of electric field direction improves gene electrotransfer in vitro. *Biomed Eng Online* 6:25
- Rubinsky B, Onik G, Mikus P (2007) Irreversible electroporation: a new ablation modality—clinical implications. *Technol Cancer Res Treat* 6:37–48
- Sel D, Cukjati D, Batuskaite D et al (2005) Sequential finite element model of tissue electroporation. *IEEE Trans Biomed Eng* 52:816–827
- Sel D, Lebar AM, Miklavcic D (2007) Feasibility of employing model-based optimization of pulse amplitude and electrode distance for effective tumor electroporation. *IEEE Trans Biomed Eng* 54:773–781
- Sersa G, Cemazar M, Miklavcic D (1995) Antitumor effectiveness of electrochemotherapy with cis-diamminedichloroplatinum(II) in mice. *Cancer Res* 55:3450–3455
- Sersa G, Miklavcic D, Cemazar M et al (2008) Electrochemotherapy in treatment of tumours. *Eur J Surg Oncol* 34:232–240
- Zupanic A, Corovic S, Miklavcic D (2008) Optimization of electrode position and electric pulse amplitude in electrochemotherapy. *Radiol Oncol* 42:93–101

## Paper 6

**Title:** Electrochemotherapy: A New Technological Approach in Treatment of Metastases in the Liver

**Authors:** Edhemović Ibrahim, Gadžijev Eldar, Breclj Erik, Miklavčič Damijan, Kos Bor, Županič Anže, Mali Barbara, Jarm Tomaž, Pavliha Denis, Marčan Marija, Gašljević Gordana, Gorjup Vojka, Mušič Maja, Pečnik Vavpotič Tjaša, Čemažar Maja, Snoj Marko, Serša Gregor

**Publication:** Technology in Cancer Research and Treatment

**Year:** 2011

Volume: 10

Number: 5

**Pages:** 475-485

**Open Access Article**

The authors, the publisher, and the right holders grant the right to use, reproduce, and disseminate the work in digital form to all users.



Technology in Cancer Research and Treatment

ISSN 1533-0346

Volume 10, Number 5, October 2011

©Adenine Press (2011)

## Electrochemotherapy: A New Technological Approach in Treatment of Metastases in the Liver

www.tcrt.org

Electrochemotherapy is now in development for treatment of deep-seated tumors, like in bones and internal organs, such as liver. The technology is available with a newly developed electric pulse generator and long needle electrodes; however the procedures for the treatment are not standardized yet. In order to describe the treatment procedure, including treatment planning, within the ongoing clinical study, a case of successful treatment of a solitary metastasis in the liver of colorectal cancer is presented. The procedure was performed intraoperatively by inserting long needle electrodes, two in the center of the tumor and four around the tumor into the normal tissue. The insertion of electrodes proved to be feasible and was done according to the treatment plan, prepared by numerical modeling. After intravenous bolus injection of bleomycin the tumor was exposed to electric pulses. The delivery of the electric pulses did not interfere with functioning of the heart, since the pulses were synchronized with electrocardiogram in order to be delivered outside the vulnerable period of the ventricles. Also the post treatment period was uneventful without side effects. Re-operation of the treated metastasis demonstrated feasibility of the reoperation, without secondary effects of electrochemotherapy on normal tissue. Good antitumor effectiveness with complete tumor destruction was confirmed with histological analysis. The patient is disease-free 16 months after the procedure. In conclusion, treatment procedure for electrochemotherapy proved to be a feasible technological approach for treatment of liver metastasis. Due to the absence of the side effects and the first complete destruction of the treated tumor, treatment procedure for electrochemotherapy seems to be a safe method for treatment of liver metastases with good treatment effectiveness even in difficult-to-reach locations.

Key words: Electrochemotherapy; Liver metastases; Colorectal cancer.

### Introduction

Electrochemotherapy is a local treatment that uses electroporation of the tumors to increase uptake of cytotoxic drugs, such as bleomycin or cisplatin (1). In the case of bleomycin, up to a 1000-fold increase in cytotoxicity was observed (1-3). Currently electrochemotherapy is used in treatment of cutaneous and subcutaneous tumors of different histological types with response rate of 80% and long lasting complete responses of 70% (4, 5). The treatment has been predominantly used with palliative intent for melanoma metastases and other cutaneous tumors, whereas the colorectal liver metastases (CRLM) have not been treated yet. In a preclinical *in vitro* study on CMT-93 colorectal carcinoma cells it was demonstrated that exposure of cells to electric field potentiates cytotoxicity of bleomycin 500-fold (6).

**Abbreviations:** CRLM: Colorectal Liver Metastases; IVC: Inferior Vena Cava; Sg: Segment; MHV: Middle Hepatic Vein; LHV: Left Hepatic Vein; sRHV: Superior Hepatic Vein; US: Ultrasound; CEA: Carcinoembryonic Antigen; H&E: Haematoxylin and Eosin; ECG: Electrocardiogram.

**I. Edhemovic, M.D., M.Sc.<sup>1</sup>**  
**E. M. Gadzijev, M.D., Ph.D.<sup>1</sup>**  
**E. Breclj, M.D., Ph.D.<sup>1</sup>**  
**D. Miklavcic, Ph.D.<sup>2</sup>**  
**B. Kos, B.Sc.<sup>2</sup>**  
**A. Zupanic, Ph.D.<sup>2</sup>**  
**B. Mali, B.Sc.<sup>2</sup>**  
**T. Jarm, Ph.D.<sup>2</sup>**  
**D. Pavliha, B.Sc.<sup>2</sup>**  
**M. Marcan, B.Sc.<sup>2</sup>**  
**G. Gasljevic, M.D.<sup>1</sup>**  
**V. Gorjup, M.D., Ph.D.<sup>3</sup>**  
**M. Music, M.D., Ph.D.<sup>1</sup>**  
**T. Pecnik Vavpotic, B.Sc.<sup>1</sup>**  
**M. Cemazar, Ph.D.<sup>1</sup>**  
**M. Snoj, M.D., Ph.D.<sup>1</sup>**  
**G. Sersa, Ph.D.<sup>1\*</sup>**

<sup>1</sup>Institute of Oncology Ljubljana, Zaloska 2, SI-1000 Ljubljana, Slovenia

<sup>2</sup>University of Ljubljana, Faculty of Electrical Engineering, Trzaska 25, SI-1000 Ljubljana, Slovenia

<sup>3</sup>University Medical Center Ljubljana, Zaloska 2, SI-1000 Ljubljana, Slovenia

\*Corresponding author:  
 Prof. Gregor Sersa  
 E-mail: gsertsa@onko-i.si

Further development of electrochemotherapy is oriented into treatment of bigger as well as deep-seated tumors; in internal organs or at least 1 cm below the skin. The first reported case was treatment of deep-seated melanoma metastasis in the thigh (7), in which the treatment feasibility was demonstrated, but also a sensitivity study was performed which demonstrated that positioning of electrodes with respect to the initial treatment plan is important for the success of the treatment (8). The treatment of deep-seated tumors is now possible with the new electroporation device and the newly developed long-needle electrodes. In contrast to cutaneous tumor lesions, the abdominal tumors (such as metastases in the liver) are located in electrically highly conductive medium and the treatment region can be in close proximity of the heart. Therefore, the delivery of electroporation pulses should be synchronized with the refractory period of the cardiac cycle to minimize the probability of interaction of electric pulses with the heart function (9-11).

CRLM located in between inferior vena cava (IVC) and the main hepatic veins represent a challenge for a liver surgeon. Although the paracaval region and caudate process in the angle of the main hepatic veins inflow into IVC can be approached with segmental resection of segment 1 (Sg 1) it is often impossible to achieve a sufficient safety margin due to veins proximity. Available alternatives depend on the hepatic veins involved: if both, the middle (MHV) and left hepatic veins (LHV) are involved or the common trunk is involved, extended left hemihepatectomy together with Sg 1 (caudate lobe) is possible. When the superior right hepatic vein (sRHV) and MHV are involved and the LHV is unaffected, the right trisectionectomy may be performed (12, 13). It has become accepted as surgical standard that as much liver tissue as possible is preserved in treatment of CRLM (14). Another possibility; if both sRHV and common trunk are involved, in rare cases, when there are strong inferior and/or middle right hepatic veins present (15), the liver resection which includes left hemihepatectomy and Sg 8 and Sg 7 with preservation of Sg 5 and Sg 4 is possible. Using ablative method like RFA in this region has limitations because of the heat sink from cooling effect of hepatic veins (16-18).

Here we describe for the first time the treatment procedure of electrochemotherapy of CRLM, in a case of a patient with liver metastasis in between IVC and the origin of the main hepatic veins. We demonstrate the feasibility of the procedure and describe the procedure steps needed for electrochemotherapy, safety of the treatment and the treatment effectiveness.

### Material and Methods

#### Clinical Study

In the on-going Phase I/II study (EudraCT number 2008-008290-54; ClinicalTrials.gov (NCT01264952)) so far

8 patients were recruited: 5 patients with CRLM in both hemilivers planned for two-step surgical procedure and 3 patients with solitary metastasis on the MHV inflow to the IVC. The study was approved by Institutional Medical Board and Ethical Committee of the Republic of Slovenia.

#### Patient

The patient was a 55 years old lady who had been operated for sigmoid colon carcinoma (July 2007), stage pT3, N2 (6 positive out of 19 removed lymph nodes), M0. A R0 resection of the colon was performed, followed by 8 cycles of chemotherapy with Capecitabine. After 24 months a hypoechoic lesion close to IVC was found on ultrasound (US), measuring 24 × 21 mm. The lesion was confirmed to be a metastasis by the PET/CT and MRI scans. It was located in between the IVC and the main hepatic veins. The metastasis increased in a month to 35 × 20 mm. Due to its direct contact with IVC, MHV and sRHV, the metastasis was considered as non-resectable. Chemotherapy (capecitabine and oxaliplatin (XELOX) + bevacizumab) was introduced. After three cycles of chemotherapy, in the mid of November 2009, MRI using liver specific contrast Gd-EOB-DTPA showed partial downsizing of the lesion to 34 × 15 mm. It was still close to IVC and main hepatic veins; however there was a possibility that it could have become resectable. RFA was not considered as an option due to the proximity of the IVC and main hepatic veins and their cooling effect. The patient was offered an exploration and electrochemotherapy if the metastasis would still be found non-resectable during the surgery in the end of December 2009. The patient agreed and signed informed consent for electrochemotherapy.

#### Radiology of the Metastasis

Before electrochemotherapy, the liver metastasis was evaluated by contrast-enhanced Gd-EOB-DTPA MRI of liver. Pre contrast enhanced images included in- and opposed phase transversal images, T1W transversal images and T2W transversal and coronal images. Contrast enhanced images were obtained in late arterial (25 s), portal-venous (70 s) and late phase (5 and 20 min) in transversal and coronal planes. Post treatment the effect was evaluated by multislice contrast enhanced computed tomography (CT) in late portal phase (70 s), 5 mm slice reconstructions were made, in axial and coronal planes.

#### Treatment Planning

Prior to surgery and electrochemotherapy, numerical treatment planning was performed using a method established and reported earlier (7, 8, 19). Briefly, a 3-D model geometry was built based on segmented MRI images of the patient as described previously (20). The images were segmented into

## Electrochemotherapy of Liver Metastases

477

three tissues: liver, tumor and blood vessels, the IVC and the main hepatic veins. Next, several different electrode configurations were designed in consultation with the surgeon based on the limited number of possible access routes. Using an optimization algorithm coupled with a finite-element model of electroporation, the minimum required voltage for each electrode pair in each electrode configuration was computed to guarantee adequate electric field distribution in the tumor, as this is the major indication for successful electroporation (21). In contrast to previous work (7), a gradient optimization algorithm was used to optimize the voltages between each electrode pair, while positions of electrodes were determined by using the so-called forward modeling approach. Finally, the optimal design using 6 electrodes was used, as it provided the most robust treatment, and the surgeon was able to execute the plan.

### Electrochemotherapy

On the exposed liver the needle electrodes (1.2 mm in diameter with 4 cm non-isolated tip length) were inserted into the metastasis under US guidance. The positioning followed the provided treatment plan. The electrodes were connected to the electric pulse generator (Cliniporator *VITAE*, IGEA SpA, Carpi, Italy). Thereafter, the patient was given 15,000 U/m<sup>2</sup> of bleomycin (27.45 mg) intravenously in bolus. Eight electric pulses of 100  $\mu$ s duration were delivered between pairs of electrodes 8 min after the bleomycin injection, when the maximal pharmacological peak of bleomycin in the metastases was expected (22). The amplitudes and protocol of electric pulses delivery according to the treatment plan for this particular metastasis is given in Table I.

### ECG Synchronization

Delivery of electroporation pulses was synchronized with electrocardiogram (ECG); one pulse per heart-beat was delivered. Namely, Cliniporator *VITAE* provides an option for

synchronization of electroporation pulse delivery with ECG. The ECG triggering device AccuSync 42 (AccuSync Medical Research Corp., Milford, CT, USA) was used. The AccuSync is a 3-lead electrocardiograph which detects the R-wave from one of the preselected standard leads early on the ascending slope of the R-wave. ECG lead II was selected due to prominence of the R wave. This ECG signal was acquired independently of the regular ECG monitoring performed by the anesthesiologist. The Cliniporator *VITAE* is programmed to deliver a single electroporation pulse 50 ms after receiving a valid trigger from the AccuSync (provided that the latest R-R interval was within the 0.5-3.5 s range) thus avoiding the so-called vulnerable period of the ventricles, the T wave. Both the ECG signal used for synchronization and the trigger signal were recorded and stored for post processing and further analysis.

### Surgery

**1<sup>st</sup> Operation – Electrochemotherapy:** One month after the third cycle of chemotherapy (XELOX + bevacizumab), the patient was operated. Despite the downsizing which was visible on MRI images, intraoperative US assessment still showed direct contact of the metastasis with the IVC, and main hepatic veins at their origin, so the lesion was considered non-resectable. Due to the reasons explained earlier, RFA was not an option, so electrochemotherapy remained the only possibility. After the mobilization of the left liver, the area between IVC and the origin of the main hepatic veins was exposed. The electrodes were placed and electrochemotherapy was performed, as described. No single adverse effect was noted and blood loss was minimal. Postoperative course was uneventful and the patient was discharged from hospital on the day 10. After this operation patient did not receive any systemic treatment.

**2<sup>nd</sup> Operation – Excision of the Metastasis:** Due to changes visible on CT scan (homogeneously hypo dense lesion, without

**Table I**

Summary of planned voltages, number of pulses and predicted currents based on numerical model as well as the actually delivered voltages, number of pulses and measured currents.

Electrode pair	Voltage according to plan [V]	No. of pulses according to plan	Predicted current [A]	Delivered voltage [V]	Delivered No. of pulses	Measured current [A]
1-5	2100	8	31	1300	20	32.3
1-6	2100	8	26	2100	8	45.2
2-5	2100	8	26	1700	21	44.7
2-6	2100	8	25	2100	8	48.3
3-5	2100	8	25	2100	8	48.9
3-6	2100	8	29	1900	8	48.8
4-5	2100	8	28	2100	8	47.5
4-6	2100	8	33	1700	16	41.2
5-6	1700	8	40	1700	8	48.9
Total		72			105	

changes in size) the second operation was performed three months after the first one. Furthermore, intraoperative US scan showed that the metastasis was hypo-echogenic, which was interpreted as probable necrotic changes. The metastasis was found no longer firmly fixed to the surrounding structures, so it was decided to excise it. Postoperatively, a moderate subcutaneous wound infection occurred, which was treated with partial wound dehiscence. No other adverse effects were noted.

#### Histology

The excised tissue was fixed in 10% buffered formalin. After the macroscopic examination, the specimen was sectioned and entirely taken for microscopic examination. Tissue was embedded in paraffin; 3 µm thick sections were cut and stained using haematoxylin and eosin (H&E). Immunohistochemical studies were performed by peroxidase avidin-biotin method using the formalin fixed and paraffin embedded material. The following primary antibodies were used: against carcinoembryonic antigen (CEA) (DAKO, Denmark; polyclonal; dilution 1:8000) and CK20 (DAKO, Denmark; monoclonal; dilution 1:20) for staining tumor tissue and HEPAT (DAKO, Denmark; polyclonal; dilution 1:20) for staining liver tissue.

#### Results

##### Location of the Liver Metastasis

The metastasis treated with electrochemotherapy was confirmed by MRI using liver specific contrast Gd-EOB-DTPA before the operation (Figure 1). Twenty minutes after contrast application, a metastasis (34 mm × 15 mm) located in the paracaval region and caudate process, in contact with IVC and main hepatic veins was identified. No other lesions were seen in the liver.

#### Treatment Plan

Several treatment plans were prepared based on the MRI of the patient. The treatment plans were evaluated based on the quality of the predicted electric field distribution (for details see ref. 7) and on how difficult it would be for the surgeon to execute the plan. Finally, the setup with 6 electrodes presented in Figure 2 was selected for the treatment, with other treatment plans, including those with 4- and 5-electrode configurations (not presented) also prepared for back-up purposes. The final voltages and predicted currents, as well as actually delivered voltages and currents are shown in Table I with an overlay of the computational model and MRIs of the patient anatomy shown in Figure 3A. Two electrodes were positioned centrally in the tumor in order to provide sufficiently high electric field in the center of the tumor. The other 4 electrodes were positioned around the tumor in the normal liver tissue in order to provide the treatment of safety margins. These peripheral electrodes were positioned approximately 1-2 mm away from the tumor tissue.

#### Treatment Procedure

**Identification of Metastasis and Preparatory Procedures Needed Before Delivery of Electric Pulses:** During the operation in general anesthesia (December 2009) the left liver was mobilized, so that electrochemotherapy could be performed. The exact location of the tumor as well as the location of needle insertion according to the treatment plan was intraoperatively verified by US. Insertion of the needle electrodes was attempted to be as close as possible according to the treatment plan. The exact location of the electrodes was determined and was found later on to be in close match to the predetermined locations (Figure 2). Electrodes were inserted into the tumor and around it without any problem and without injury of any major blood vessel (Figure 3B).

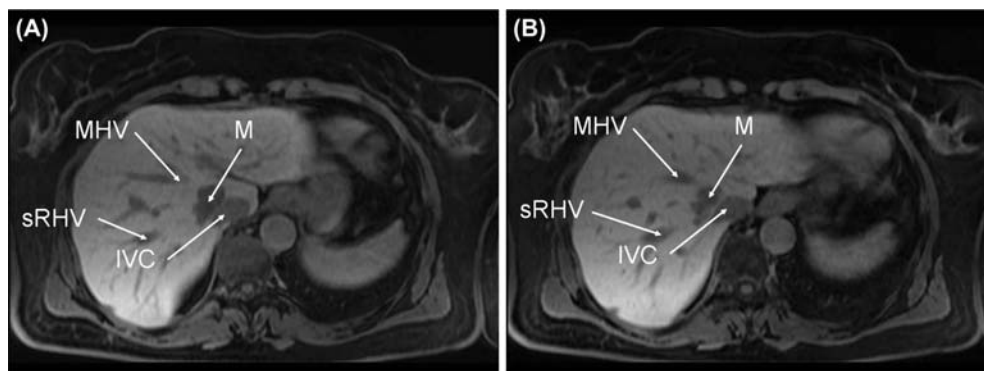


**Figure 1:** Axial T1W MRI image, showing a hypointense lesion (M) in between IVC and sRHV and MHV, in late liver phase, 20 min post Gd-EOB-DTPA. Images A and B are two consecutive images in 5 mm slice thickness.

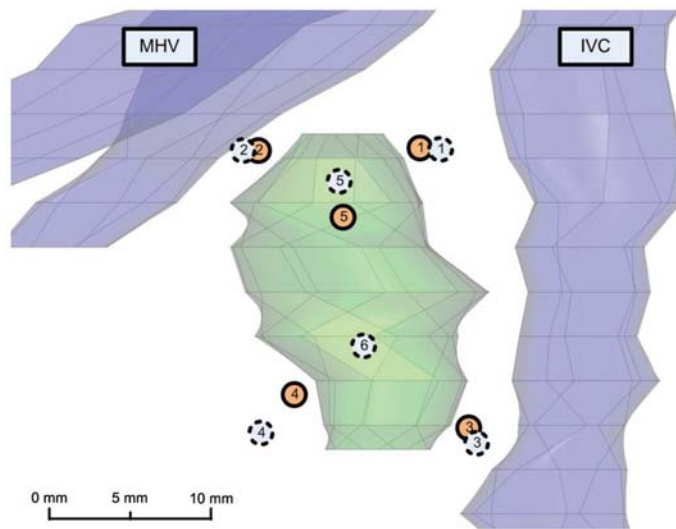


**Figure 2:** Design of treatment plan. The Figure shows the location of the tumor (green color) between the IVC and main hepatic veins (MHV, IVC, blue color). The solid circles represent electrode locations according to the original treatment plan and the dashed circles represent reconstructed electrode positions achieved *in situ*. The electrode 6 is in the same location in both cases.

After insertion into tissue the electrodes were connected to the Cliniporator *VITAE*, with special attention to correct wiring between the electrodes and the appropriate channel ports on the Cliniporator *VITAE*. Thereafter bleomycin (15000 U/m<sup>2</sup> of the patient) was injected intravenously in bolus. After 8 minutes, the time needed by the circulating bleomycin to

reach the pharmacological peak in the tumor, the preparations for delivery of electric pulses were completed.

**Delivery of Electric Pulses:** The generic electroporation procedure is described first. The delivery of electroporation pulses is always preceded by a sequence of low-voltage pre-pulses.

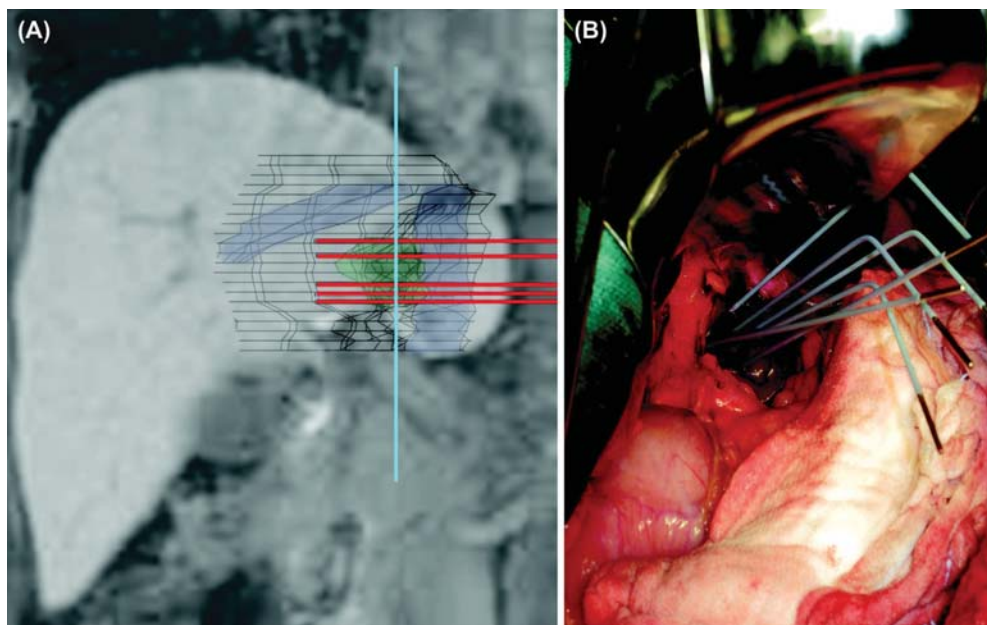


**Figure 3:** **A:** Overlay of the computational geometry and patient's anatomy. The red lines represent the direction of insertion of the electrodes, while the blue line represents the cross-section of Figure 2. **B:** Photograph of the surgical setup with electrodes penetrating into the tumor is clearly seen (cables not connected).

One pre-pulse is delivered to each pair of electrodes which is later to be used for actual electroporation according to the treatment plan. The purpose of pre-pulses is to verify the connections between the electrodes and Cliniporator *VITAE* outputs and also to predict (based on the current measured at low voltage) the current levels for the imminent electroporation pulses. For any pair of electrodes for which either a poor connection is found or the predicted current level exceeds 50 A (upper limit of the Cliniporator *VITAE*), the delivery of electroporation pulses is automatically suspended. Immediately after completion of the pre-pulse sequence, the high-voltage electric pulses, 8 per electrode pair, are delivered synchronized with the ECG (see the following subsection for details). The Cliniporator *VITAE* automatically suspends the delivery of electroporation pulses for: a) electrode pairs for which the pre-pulse sequence resulted in invalid values (current too low or too high); and b) for electrode pairs for which the actual current measured during electroporation itself exceeds the upper limit of 50 A, even though the predicted value based on the pre-pulse was below this limit. This completes the electroporation procedure. However, if needed, the procedure must then be repeated for all electrode pairs for which the delivery was suspended. Depending on the reason of suspension, the connections between the electrodes are checked and/or parameters of electroporation pulses are adjusted (voltage must be lowered if either the predicted or actual current exceeded 50 A). The whole electroporation procedure is then repeated just for the remaining electrode pairs. Sometimes more than one repetition may be required.

In our case, in the original treatment plan, 72 pulses were planned. However, a total of 105 electroporation pulses were delivered, because the electroporation procedure had to be repeated 5 times to complete delivery of all pulses. The larger number of actually delivered electroporation pulses is explained in the discussion. The entire electroporation procedure was finished 23.5 min after injection of bleomycin, *i.e.* within 15 minutes.

**ECG Synchronization:** The triggering of electric pulses was synchronized with ECG signals, through the ECG triggering device AccuSync, as described in previous section. The Cliniporator *VITAE* delivered one electroporation pulse per valid trigger pulse, which means that there was one pulse per heartbeat delivered. Whenever there was a transient loss of the ECG signal (due to ECG artifacts caused by muscle contractions after the previous pulse), the Cliniporator *VITAE* temporarily suspended pulse delivery until ECG and valid trigger pulse sequence were restored. The subsequent analysis of ECG signals showed that the synchronization procedure implemented in the Cliniporator *VITAE* resulted in safe and uneventful delivery of the pulses since all pulses were delivered outside the vulnerable period of the ventricles.

The preliminary evaluation of ECG signals recorded during the entire surgical procedure also revealed no heart arrhythmias or any other pathological morphological changes in any of the recorded signals either during or immediately after the application of pulses. However, some transient and statistically significant changes in the duration of some intervals in the PQRST complex were observed during the heartbeats coinciding with the delivery of electroporation pulses. Currently the practical significance of these changes (if there is any) is not clear and can only be elucidated when data from more patients treated in similar conditions become available.

#### *Safety of Treatment*

During and after the electrochemotherapy, there were no adverse effects which could be attributed to the procedure itself. Postoperative course was uneventful and the patient was released from the hospital on day 10.

#### *Post Treatment Follow-up and Treatment*

Two months after electrochemotherapy CT was performed. In the paracaval region toward the Sg 1 there was a homogeneous hypodense ovoid lesion (30 mm × 15 mm) without any new lesions (Figure 4).

There was no change in size of the metastasis treated with electrochemotherapy, however, CT image showed that margins were blurred, which demonstrated that treatment had some effect (Figure 4). At that time it was unclear what kind of the effect it was. The patient was suggested another exploration, which was accepted and the operation was performed three months after the first one. Intraoperative US examination showed hypo-echogenic changes, probably caused by necrosis. We mobilized left and right hemiliver and resected the part of paracaval region with Sg 1, preserving the main

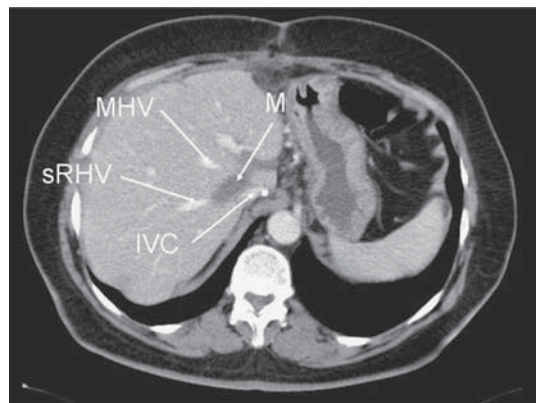


**Figure 4:** Axial CT image taken before the metastasis (M) was removed shows homogenous hypodense lesion in paracaval region toward Sg 1 (30 mm × 15 mm), with no signs of any new lesion.

## Electrochemotherapy of Liver Metastases

481

hepatic veins and IVC (Figure 5). Using ultrasound dissector the Sg 1 was easily resected from sRHV and common trunk. The walls of both vessels were firm and not as tender as usually. There was very little blood loss and no transfusion was needed during and after the operation.

Gross pathological examination of the excised specimen showed oval, relatively sharply demarcated area of amorphous and yellowish tissue in the liver parenchyma. Histologically, complete necrosis was found and, in the vicinity of it, focal necrosis of the narrow zone of the liver parenchyma was present. In the excised lesion there was no viable tumor tissue. Taking into account that etiology of necrosis can be different, immunohistochemical staining for CK20, CEA and Hepat was performed. CK20 is an intermediate filament (part of cytoskeleton) mainly expressed in gastrointestinal type epithelia and carcinomas deriving from it. CEA is found in a large variety of carcinomas of gastrointestinal, respiratory and genitourinary tract while Hepat stains normal human hepatocytes. Although CK20 and CEA are not entirely specific for colorectal carcinoma, vast majority of them are strongly positive for both markers. In our case, necrotic tissue was immunohistochemically positive for CK20 and CEA, and negative for Hepat in contrast to vital liver parenchyma which was positive for Hepat and negative for CEA and CK20 (Figure 6). Findings like that support that necrosis arose from the metastatic carcinoma. Although it was not possible to discriminate between necrosis induced by ECT or chemotherapy only, there was indirect evidence of the effect of electrochemotherapy and that is the presence of necrosis of the narrow zone of the liver parenchyma surrounding the tumor. On the border between necrotic tumor tissue and vital liver parenchyma, focal proliferation of fibroblastic tissue with some chronic inflammatory reaction, foamy macrophages and pigmentophages were observed. In the remaining liver parenchyma slight portal fibrosis was present.

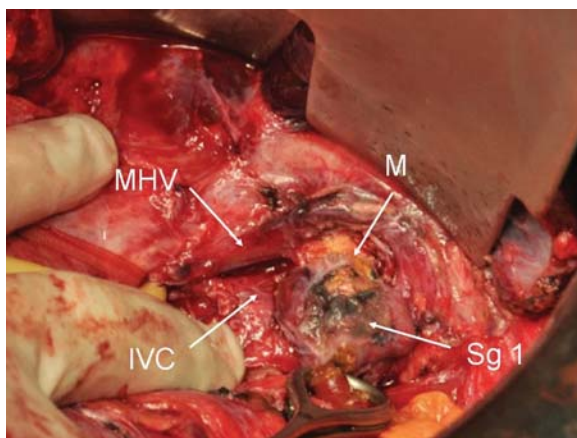


**Figure 5:** Resection of Sg 1 with common trunk and MHV exposed: Necrotic metastasis (M) is visible in Sg 1, close to the MHV and IVC.

### Discussion

The results of the study show that electrochemotherapy on liver metastases can be performed safely and effectively. Treatment procedure for electrochemotherapy of liver metastases is presented and described on a patient with CRLM in paracaval region extending to Sg 1. This single metastasis in difficult location was successfully treated, as evident by histological examination of the removed metastasis after the second operation. The described procedure demonstrates its complexity, where several specific steps have to be taken in consideration; exact treatment planning for electrode positioning and the delivery of electric pulses, positioning of the electrodes before injection of bleomycin, as well as synchronization of electric pulses delivery with ECG for safety reasons. The patient is disease free 16 months after the electrochemotherapy procedure.

Radical removal of any malignant tumor from the paracaval region and Sg 1, close to the main hepatic veins inflow to IVC is challenging. In the presented case, the radical resection of the metastasis would have been potentially possible by doing right trisectionectomy leaving probably too little liver remnant (lateral part of the left liver). Considering the specific location, RFA would not be effective because of the cooling effect of the veins. All possibilities of treatment had been presented to the patient who decided to be treated with electrochemotherapy. The treatment was performed following very closely the treatment plan, without post-treatment side effects.

Treatment planning is needed for the exact positioning of the electrodes, in order to predict successful electroporation of the whole tumor mass. As it is known, two conditions have to be met for effective electrochemotherapy: presence of the drug during the electroporation in the tissue and electroporation of the whole tumor mass. Based on the presumption that intravenous drug administration would adequately deliver bleomycin to the liver metastasis, emphasis was put on electroporation treatment plan. Several treatment plans were prepared, in order to satisfy all possible situations that might have occurred (7). According to the numerical model, it was decided that one or two electrodes should preferentially be inserted in the tumor to improve the electric field distribution and guarantee complete tumor coverage. This was reported previously (7), and we have shown that positioning of electrodes outside the tumor is very sensitive to errors in electrode placement and differences in tissue conductivities between the target (tumor) and surrounding tissue (8).

Despite the effort to precisely follow the treatment plan for the positioning of the electrodes, the final positions of the electrodes did not match the original treatment plan exactly. These deviations from the original treatment plan (see Figure 2 and Table I) were considered in the post-surgery numerical

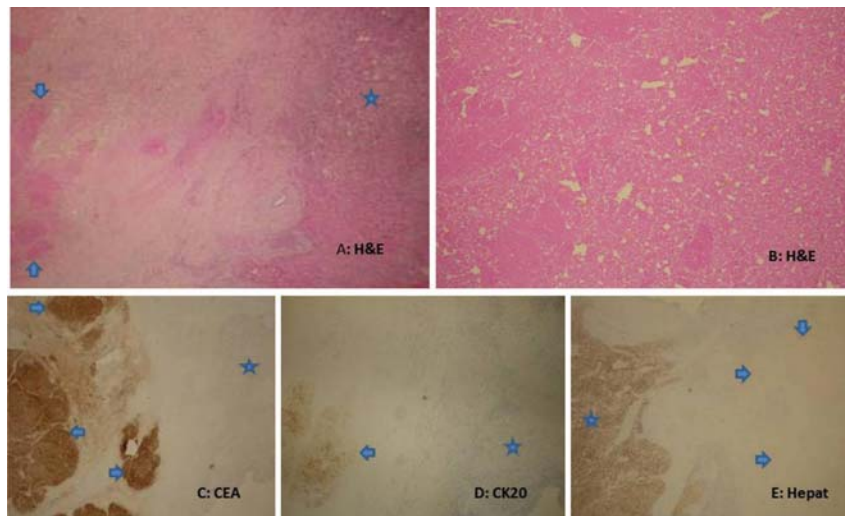


**Figure 6:** A: H&E, 4x; complete necrosis of the tumor tissue (arrows) and vital liver parenchyma (star). B: H&E, 10x; completely necrotic tumor tissue. C: IHC CEA 4x; CEA positive staining in the necrotic tumor tissue (arrows) and negative in the vital liver parenchyma (star). D: IHC CK20 4x; CK20 positive staining in necrotic tumor tissue (arrow) and negative in vital liver tissue (star). E: IHC Hepat 4x; positive staining for Hepat in the liver (star) and negative in the necrotic tumor tissue (arrows).

evaluation that used the same numerical model as in treatment planning. The calculations showed that the treatment plan was still followed closely enough and that the electric field distribution was adequate for the procedure, *i.e.* the entire tumor volume was exposed to the electric field above 450 V/cm, with 90% being higher than 900 V/cm.

In the delivery of pulses between electrodes 1-5, 2-5, 3-6 and 4-6 (see Table 1) the originally planned amplitude of voltage for pulses could not be used due to excessive current values experienced during the first attempt to deliver the pulses (more than 50 A – a limitation of the Cliniporator VITAE device). Therefore the amplitude was lowered and a greater number of pulses at decreased voltage were delivered. It is known that electroporation can be effectively carried out (and the desired effect achieved) if a weaker electric field is used but with a greater number of pulses (23, 24). For this reason the number of pulses delivered to some of the electrode pairs was increased.

In all reports on clinical use of electrochemotherapy for treatment of cutaneous or subcutaneous malignant tumors the method has been described as completely safe. No serious side effects for the patient have ever been reported. The minor side effects reported in the literature include localized transient lesions in normal tissue in immediate vicinity of the treated region and the acute pain associated with contraction of skeletal muscles in vicinity of the electrodes which was caused either by direct electrical stimulation of the

muscles or of the nerves innervating these muscles (25-27). The acute pain is the reason for use of either local or general anesthesia (depending on the location and number of tumors to be treated) during treatment of cutaneous or subcutaneous tumor lesions. Such electrochemotherapy treatment was shown to have no effect on the function of the heart apart from a transient and mild tachycardia attributed to anxiety of the patient in case of local anesthesia (10). This result was not surprising taking into account the high level of treatment localization (the electrodes are positioned close together and far away from the heart) and the very short duration of electric pulses. However, according to the results of the study on numerical calculations of electric field and current distribution for a tissue model it may be theoretically possible to affect functioning of the heart even in case of subcutaneous tumors located on the chest close to the heart and for deep insertion of needle electrodes (*e.g.* approximately 4 cm) (10). Under such extreme conditions the threshold value of current for induction of ventricular fibrillation (set at 100 mA for the given duration of electric pulses) could be exceeded (10). Furthermore, with recent development of new electrochemotherapy modalities for treatment of internal tumors using surgical procedures or endoscopic routes (28) to gain access to treatment area, could result in in the treated region located in close proximity of the heart. Due to the absence of protective barrier of the skin and relatively large electrical conductivity of internal tissues and organs the electrical current delivered during electrochemotherapy using invasive access, can propagate through a larger volume of

**Electrochemotherapy of Liver Metastases****483**

tissue surrounding the treated region. Therefore, an increased probability for electroporation pulses interfering with the heart function is present. In recently published studies on non-thermal irreversible electroporation, different minor and major hemodynamic and cardiologic changes due to unsynchronized irreversible electroporation pulse delivery were reported, such as systolic hypertension, supraventricular tachycardia, ventricular tachycardia with pressure drop, ventricular fibrillation, ST segment elevation and changes in T wave (11, 29). Deodhar *et al.* (11) showed that unsynchronized irreversible electroporation pulses delivered at less than or equal to 1.7 cm from the heart provoked fatal events (such as ventricular fibrillation) whereas pulses delivered more than 3 cm from the heart did not provoke any changes from baseline ECG (11). On the other hand, they reported that synchronized irreversible electroporation did not provoke any (fatal or minor) events at more than 1.7 cm distance from the heart. In the case reported here, the electroporation pulses were delivered at a location more than 10 cm away from the heart. Regardless of an unlikely event of serious consequences (such as induction of various arrhythmias or, in worst case, ventricular fibrillation), the synchronization of electroporation pulse delivery with the cardiac rhythm should be a prerequisite step for treatment of tumors in all internal organs, and especially those in close vicinity of the heart, to maximize the safety of the patient. The synchronization algorithm currently implemented in Cliniporator VITAE device coupled with the external triggering device AccuSync proved to be effective in preventing external stimulation of the heart during the so-called vulnerable period of the ventricles. As a result all electroporation pulses in our study were delivered outside the vulnerable period and no heart arrhythmias or any other pathological morphological changes were observed.

The safety of the treatment was demonstrated also by absence of side effects during and after electrochemotherapy. The use of electrochemotherapy did not extend hospital stay. Electrochemotherapy was performed in the vicinity of the big blood vessels (IVC, MHC, RHV), which may pose a specific problem. The electrodes are 1.2 mm in diameter and puncturing the vessels, specifically after retracting the electrodes may induce bleeding. However, also in this case, where electrodes were positioned nearby or even in or through the vessels no adverse events were recorded. No bleeding of the tissue after retraction of the electrodes was noticed. In the case of bleeding, the electrodes may be used as electrocoagulation tip by bringing them in contact with electrical surgical knife. This also has a preventive effect against bleeding. The mechanisms of action of electric pulses on vessels are known, for normal and tumor vessels (30-32). Electroporation induces immediate vasoconstrictive effect on vessels that is gradually

released after a few hours. This immediate effect can be continued by vascular disrupting effect when the drug is present leading also to cytotoxicity of endothelial cells and abrogation of perfusion for a long period of time. This vascular disrupting effect of electrochemotherapy may add substantial part to overall effectiveness of electrochemotherapy in treatment of well vascularized tumors (31). However, there was no damage observed on normal liver tissue in our case. The results are in agreement with the results on liver tissue with irreversible electroporation where safe use of electroporation on bigger vessels in the liver was described (33).

Based on histological analysis, electrochemotherapy treated metastasis underwent complete necrotization within two months after the treatment. However, we are aware, that this patient was not treated with electrochemotherapy solely. After the metastasis was diagnosed, the patient was treated with systemic chemotherapy (XELOX + bevacizumab), and 5 weeks later received electrochemotherapy; so it is hard to put all credits for good treatment result to electrochemotherapy only, although chemotherapy was discontinued 5 weeks before electrochemotherapy. Although full responses to systemic chemotherapy are rare, they do occur, but histologically these metastases tend to develop central fibrosis (34). The usual responses to electrochemotherapy are non-necrotic, however also necrotic responses were recorded, as in the case of treatment of brain metastases (35, 36). To clarify and evaluate the treatment effectiveness on larger number of patients, there is an ongoing phase I/II clinical trial at the Institute of Oncology Ljubljana. The trial is designed to evaluate the effectiveness, safety and toxicity of the electrochemotherapy with bleomycin in treatment of the liver metastases originating from colorectal cancer. After recruiting a sufficient number of patients, we will have a much clearer picture about effectiveness of electrochemotherapy in treatment of liver metastases. Therefore, we must await further experience with this technique to get proof of clinical efficacy.

In case of encouraging results of the on-going clinical trial, further clinical trials performed on other liver tumors or liver metastases will be performed. With well elaborated and tested treatment planning system even percutaneous treatment of tumors using a guided system could be performed, that would be considerable improvement over invasive procedure described here (37).

In conclusion, electrochemotherapy proved to be feasible technological approach for treatment of liver metastases. Due to absence of side effects and the first reported complete destruction of the treated tumor, electrochemotherapy in treatment of liver metastases proved to be safe with good treatment effectiveness even in a difficult-to-reach location.

**Conflict of Interest**

We certify that regarding this paper, no actual or potential conflict of interest exists; the work is original, has not been accepted for publication nor is concurrently under consideration elsewhere, and will not be published elsewhere without the permission of the Editor and that all the authors have contributed directly to the planning, execution or analysis of the work reported or to the writing of the paper.

**Acknowledgements**

The authors acknowledge the financial support of the state budget by Slovenian Research Agency (P3-0003 and P2-0249). Research was conducted in the scope of the EBAM European Associated Laboratory (LEA).

**References**

- Mir, L. M., Orlowski, S. Mechanisms of electrochemotherapy. *Adv Drug Deliv Rev* 35, 107-118 (1999).
- Gehl, J., Skovsgaard, T., Mir, L. M. Enhancement of cytotoxicity by electroporation: an improved method for screening drugs. *Anti-Cancer Drugs* 9, 319-325 (1998).
- Jaroszeski, M. J., Dang, V., Pottinger, C., Hickey, J., Gilbert, R., Heller, R. Toxicity of anticancer agents mediated by electroporation in vitro. *Anticancer Drugs* 11, 201-208 (2000).
- Sersa, G., Miklavcic, D., Cemazar, M., Rudolf, Z., Pucihar, G., Snoj, M. Electrochemotherapy in treatment of tumours. *EJSO* 34, 232-240 (2008).
- Testori, A., Tosti, G., Martinoli, C., Spadola, G., Cataldo, F., Verrecchia, F., Baldini, F., Mosconi, M., Soteldo, J., Tedeschi, I., Passoni, C., Pari, C., Di Pietro, A., Ferruchi, P. F. Electrochemotherapy for cutaneous and subcutaneous tumor lesions: a novel therapeutic approach. *Dermatol Ther* 23, 651-661 (2010).
- Todorovic, V., Sersa, G., Flisar, K., Cemazar, M. Enhanced cytotoxicity of bleomycin and cisplatin after electroporation in murine colorectal carcinoma cells. *Radiol Oncol* 43(3), 264-273 (2009).
- Miklavcic, D., Snoj, M., Zupanic, A., Kos, B., Cemazar, M., Kropivnik, M., Bracko, M., Pecnik, T., Gadzijevec, E., Sersa, G. Towards treatment planning and treatment of deep-seated solid tumors by electrochemotherapy. *Biomed Eng Online* 9, 10 (2010).
- Kos, B., Zupanic, A., Kotnik, T., Snoj, M., Sersa, G., Miklavcic, D. Robustness of treatment planning for electrochemotherapy of deep-seated tumors. *J Membrane Biol* 236, 147-153 (2010).
- Bertacchini, C., Margotti, P. M., Bergamini, E., Lodi, A., Ronchetti, M., Cadossi, R. Design of an irreversible electroporation system for clinical use. *Technol Cancer Res Treat* 6, 313-320 (2007).
- Mali, B., Jarm, T., Corovic, S., Paulin-Kosir, M. S., Cemazar, M., Sersa, G., Miklavcic, D. The effect of electroporation pulses on functioning of the heart. *Med Biol Eng Comput* 46, 745-757 (2008).
- Deodhar, A., Dickfeld, T., Single, G. W., Hamilton, W. C., Thornton, R. H., Sofocleous, C. T., Maybody, M., Gonen, M., Rubinsky, B., Solomon, S. B. Irreversible electroporation near the heart: ventricular arrhythmias can be prevented with ECG synchronization. *Am J Roentgenol* 196, 330-335 (2011).
- Capussotti, L., Polastri, R. Operative risks of major hepatic resections. *Hepato-Gastroenterol* 45, 184-190 (1998).
- Gonzales, H. D., Figueras, J. Practical questions in liver metastases of colorectal cancer: general principles of treatment. *HPB (Oxford)* 9, 251-258 (2007).
- Finch, R. J., Malik, H. Z., Hamady, Z. Z., Al-Mukhtar, A., Adair, R., Prasad, K. R., Lodge, J. P., Toogood, G. J. Effect of type of resection on outcome of hepatic resection for colorectal metastases. *Brit J Surg* 94, 1242-1248 (2007).
- Makuuchi, M., Hasegawa, H., Yamazaki, S., Takayasu, K. Four new hepatectomy procedures for resection of the right hepatic vein and preservation of the inferior right hepatic vein. *Surg Gynecol Obstet* 164, 68-72 (1987).
- Gleisner, A. L., Choti, M. A., Assumpcao, L., Nathan, H., Schulick, R. D., Pawlik, T. M. Colorectal liver metastases: recurrence and survival following hepatic resection, radiofrequency ablation, and combined resection-radiofrequency ablation. *Arch Surg* 143, 1204-1212 (2008).
- Elias, D., Baton, O., Sideris, L., Boige, V., Malka, D., Liberale, G., Pocard, M., Lasser, P. Hepatectomy plus intraoperative radiofrequency ablation and chemotherapy to treat technically unresectable multiple colorectal liver metastases. *J Surg Oncol* 90, 36-42 (2005).
- Elias, D., Goharin, A., El Otmany, A., Taieb, J., Duvillard, P., Lasser, P., de Baere, T. Usefulness of intraoperative radiofrequency thermoablation of liver tumours associated or not with hepatectomy. *Eur J Surg Oncol* 26, 763-769 (2000).
- Zupanic, A., Corovic, S., Miklavcic, D. Optimization of electrode position and electric pulse amplitude in electrochemotherapy. *Radiol Oncol* 42, 93-101 (2008).
- Sel, D., Macek-Lebar, A., Miklavcic, D. Feasibility of employing model-based optimization of pulse amplitude and electrode distance for effective tumor electroporation. *IEEE Trans Biomed Eng* 54, 773-781 (2007).
- Miklavcic, D., Beravs, K., Semrov, D., Cemazar, M., Demsar, F., Sersa, G. The importance of electric field distribution for effective in vivo electroporation of tissues. *Biophys J* 74, 2152-2158 (1998).
- Mir, L. M., Gehl, J., Sersa, G., Collins, C. G., Garbay, J. R., Billard, V., Geertsen, P., Rudolf, Z., O'Sullivan, G. C., Marty, M. Standard operating procedures of the electrochemotherapy: Instructions for the use of bleomycin or cisplatin administered either systemically or locally and electric pulses delivered by the Cliniporator (TM) by means of invasive or non-invasive electrodes. *EJC Suppl* 4, 14-25 (2006).
- Canatella, P. J., Karr, J. F., Petros, J. A., Prausnitz, M. A. Quantitative study of electroporation-mediated molecular uptake and cell viability. *Biophys J* 80, 755-764 (2001).
- Macek Lebar, A., Miklavcic, D. Cell electroporation to small molecules in vitro: control by pulse parameters. *Radiol Oncol* 35, 193-202 (2001).
- Mir, L. M., Glass, L. F., Sersa, G., Teissie, J., Domenge, C., Miklavcic, D., Jaroszeski, M. J., Orlowski, S., Reintgen, D. S., Rudolf, Z., Belehradec, M., Gilbert, R., Rols, M. P., Belehradec, J. Jr., Bachaud, J. M., DeConti, R., Stabuc, B., Cemazar, M., Coninx, P., Heller, R. Effective treatment of cutaneous and subcutaneous malignant tumors by electrochemotherapy. *Br J Cancer* 77, 2336-2342 (1998).
- Marty, M., Sersa, G., Garbay, J. R., Gehl, J., Collins, C. G., Snoj, M., Billard, V., Geertsen, P. F., Larkin, J. O., Miklavcic, D., Pavlovic, I., Paulin-Kosir, S. M., Cemazar, M., Morsli, N., Soden, D. M., Rudolf, Z., Robert, C., O'Sullivan, G. C., Mir, L. M. Electrochemotherapy – An easy, highly effective and safe treatment of cutaneous and subcutaneous metastases: Results of ESOPE (European Standard Operating Procedures of Electrochemotherapy) study. *EJC Suppl* 4, 3-13 (2006).
- Zupanic, A., Ribaric, S., Miklavcic, D. Increasing the repetition frequency of electric pulse delivery reduces unpleasant sensations that occur in electrochemotherapy. *Neoplasma* 54, 246-250 (2007).
- Soden, D. M., Larkin, J. O., Collins, C. G., Tangney, M., Aarons, S., Piggott, J., Morrissey, A., Dunne, C., O'Sullivan, G. C. Successful application of targeted electrochemotherapy using novel flexible electrodes and low dose bleomycin to solid tumours. *Cancer Lett* 232, 300-310 (2006).

**Electrochemotherapy of Liver Metastases****485**

29. Ball, C., Thomson, K. R., Kavnoudias, H. Irreversible electroporation: a new challenge in "out of operating theater" anesthesia. *Anesth Analg* 110, 1305-1309 (2010).
30. Gehl, J., Skovsgaard, T., Mir, L. M. Vascular reactions to in vivo electroporation: characterization and consequences for drug and gene delivery. *Biochim Biophys Acta Gen Subj* 1569, 51-58 (2002).
31. Sersa, G., Jarm, T., Kotnik, T., Coer, A., Podkrajsek, M., Sentjurc, M., Miklavcic, D., Kadivec, M., Kranjc, S., Secerov, A., Cemazar, M. Vascular disrupting action of electroporation and electrochemotherapy with bleomycin in murine sarcoma. *Br J Cancer* 98, 388-398 (2008).
32. Jarm, T., Cemazar, M., Miklavcic, D., Sersa, G. Antivascular effects of electrochemotherapy: implications in treatment of bleeding metastases. *Expert Rev Anticancer Ther* 10, 729-246 (2010).
33. Rubinsky, B., Onik, G., Mikus, P. Irreversible electroporation: A new ablation modality - clinical implications. *Technol Cancer Res Treat* 6, 37-48 (2007).
34. Ng, J. K. S., Urbanski, S. J., Mangat, N., McKay, A., Sutherland, F. R., Dixon, E., Dowden, S., Ernst, S., Bathe, O. F. Colorectal liver metastases contract centripetally with a response to chemotherapy. *Cancer* 112, 362-371 (2008).
35. Agerholm-Larsen, B., Iversen, H. K., Ibsen, P., Moller, J. M., Mahmood, F., Jensen, K. S., Gehl, J. Preclinical validation of electrochemotherapy as an effective treatment for brain tumors. *Cancer Res* 71, 3753-62 (2011).
36. Garcia, P. A., Pancotto, T., Rossmeisl, J. H. Jr., Henao-Guerrero, N., Gustafson, N. R., Daniel, G. B., Robertson, J. L., Ellis, T. L., Davalos, R. V. Non-thermal irreversible electroporation (N-TIRE) and adjuvant fractionated radiotherapeutic multimodal therapy for intracranial malignant glioma in a canine patient. *Technol Cancer Res Treat* 10, 73-83 (2011).
37. Crocetti, L., Lencioni, R., DeBeni, S., See, T. C., Della Pina, C., Bartolozzi, C. Targeting liver lesions for radiofrequency ablation: an experimental feasibility study using a CT-US fusion imaging system. *Invest Radiol* 43, 33-39 (2008).

Received: June 2, 2011; Revised: July 30, 2011;

Accepted: August 3, 2011

## Paper 7

**Title:** Treatment planning of electroporation-based medical interventions: electrochemotherapy, gene electrotransfer and irreversible electroporation

**Authors:** Županič Anže, Kos Bor, Miklavčič Damijan

**Publication:** Physics in Medicine and Biology

**DOI:** 10.1088/0031-9155/57/17/5425

**Year:** 2012

**Volume:** 57

**Number:** 17

**Pages:** 5425-5440

# Treatment planning of electroporation-based medical interventions: electrochemotherapy, gene electrotransfer and irreversible electroporation

Anze Zupanic<sup>1</sup>, Bor Kos<sup>1</sup> and Damijan Miklavcic

University of Ljubljana, Faculty of Electrical Engineering, Trzaska 25, 1000, Ljubljana, Slovenia

E-mail: [damijan.miklavcic@fe.uni-lj.si](mailto:damijan.miklavcic@fe.uni-lj.si)

Received 17 February 2012, in final form 4 July 2012

Published 3 August 2012

Online at [stacks.iop.org/PMB/57/5425](http://stacks.iop.org/PMB/57/5425)

## Abstract

In recent years, cancer electrochemotherapy (ECT), gene electrotransfer for gene therapy and DNA vaccination (GET) and tissue ablation with irreversible electroporation (IRE) have all entered clinical practice. We present a method for a personalized treatment planning procedure for ECT, GET and IRE, based on medical image analysis, numerical modelling of electroporation and optimization with the genetic algorithm, and several visualization tools for treatment plan assessment. Each treatment plan provides the attending physician with optimal positions of electrodes in the body and electric pulse parameters for optimal electroporation of the target tissues. For the studied case of a deep-seated tumour, the optimal treatment plans for ECT and IRE require at least two electrodes to be inserted into the target tissue, thus lowering the necessary voltage for electroporation and limiting damage to the surrounding healthy tissue. In GET, it is necessary to place the electrodes outside the target tissue to prevent damage to target cells intended to express the transfected genes. The presented treatment planning procedure is a valuable tool for clinical and experimental use and evaluation of electroporation-based treatments.

 Online supplementary data available from [stacks.iop.org/PMB/57/5425/mmedia](http://stacks.iop.org/PMB/57/5425/mmedia)

(Some figures may appear in colour only in the online journal)

## 1. Introduction

When cells are exposed to high electric fields of sufficient magnitude, the cell membrane becomes permeabilized. Electroporation, as the phenomenon has been named, results in inflow/outflow of various molecules that are otherwise unable to cross the membrane (Sale and Hamilton 1967). Usually, the electric fields are induced by electric pulses delivered to

<sup>1</sup> Both authors contributed equally to this work.

cells/tissues via needle or plate electrodes; by controlling the electric pulse parameters it is possible to control the level of electroporation, either reversible—caused by electric fields above the reversible but below the irreversible threshold—or irreversible that in time causes cell death (Neumann *et al* 1982). As electroporation is effective regardless of cell type—i.e. it works in prokaryotic and eukaryotic cells, mature neurons, as well as stem cells (Dunny *et al* 1991, Costa *et al* 2007, Jordan *et al* 2008)—it has become a ubiquitous biotechnological and biomedical tool for inducing molecular transport into and out of biological cells (Pakhomov *et al* 2010), with uses ranging from food processing (Morales-de la Peña *et al* 2011, Sack *et al* 2010) and *in utero* gene transfection (Garcia-Frigola *et al* 2007) to medical treatments, such as: (1) cancer electrochemotherapy (ECT) (Marty *et al* 2006, Mir *et al* 1991, Testori *et al* 2011), (2) gene electrotransfer for gene vaccination or gene therapy (GET) (Heller *et al* 2006, Luxembourg *et al* 2007) and (3) tissue ablation with irreversible electroporation (IRE) (Davalos *et al* 2005, Rubinsky *et al* 2007).

Although ECT, IRE and GET all utilize membrane electroporation, the nature of the desired effects requires that different electric pulse parameters be used for each of them. For ECT, it is necessary to reversibly electroporate tumour cells so that chemotherapeutic drugs can enter and cause cell death (Sersa *et al* 2008b). Although sufficient concentration of drugs in the cancer cells is the main cause of cell death, the contribution of irreversible electroporation can sometimes be substantial and is therefore tolerated. In GET, reversible electroporation is necessary to achieve DNA transfer and the resulting expression of therapeutic molecules. However, in contrast to ECT, irreversible electroporation has to be avoided as dead cells do not express the transferred genes; electric fields that generally produce the best results are far below the irreversible electroporation threshold (Gehl *et al* 1999). IRE requires the target tissue to be covered with an electric field above the irreversible electroporation threshold (Rubinsky *et al* 2007); however, the electric field has to be below magnitudes that would cause significant thermal damage (Shafiee *et al* 2009, Zupanic and Miklavcic 2011).

While electroporation of any cell type is possible, the exact parameters necessary for electroporation (i.e. the duration and magnitude of electric field that causes electroporation) of different cell types differ considerably, partly due to their different size and partly due to other cellular, or when electroporating tissues, extracellular biological differences (Kotnik *et al* 1997, Valic *et al* 2003, Kanthou *et al* 2006, Rols and Teissie 1992). Since tissues usually incorporate many different cell types, determining the optimal parameters for each application and for each tissue is both demanding and time consuming (Sel *et al* 2005). Furthermore, knowing the optimal parameters is not enough for successful medical application; it is also necessary to ensure that they are achieved in the whole target tissue and that damage to healthy tissue is kept at a minimum. This requires exact positioning of the electrodes around the target tissue and delivering electric pulses of appropriate amplitude, duration and number. For ECT and IRE, an optimal treatment would include reversible/irreversible electroporation of the whole target volume, while minimizing electroporation of healthy tissues (Miklavcic *et al* 2006). For GET, it is harder to define the exact target volume; however a recent study has demonstrated that it is possible to control the amount of gene expression after transfection by controlling the volume of electroporated tissue (Bureau *et al* 2010); therefore, if the relationship between gene expression and clinical response is known, it can be controlled by the electroporation parameters. It is worth noting that standard operating procedures have been defined for ECT of smaller skin tumours (below 3 cm diameter) that have so far been the main target of ECT, and they include exact guidelines for positioning of the electrodes and the amplitude of electric pulses (Mir *et al* 2006); however, these procedures do not provide guidelines for internal tumours, or tumours of larger dimensions and more complex shapes, which require a more involved pre-treatment planning.

In several recent studies, the utility of numerical modelling in predicting electroporation outcomes has been demonstrated (Miklavcic *et al* 2000, Pavselj *et al* 2005, Sel *et al* 2007, Edd and Davalos 2007, Garcia *et al* 2010, Mahmood and Gehl 2011). Our group is developing a treatment planning procedure for ECT of superficial and deep-seated tumours by combining medical image analysis, finite element modelling of electroporation and a genetic optimization algorithm (Zupanic *et al* 2008, Corovic *et al* 2008, Pavliha *et al* 2012). The genetic algorithm is used to change the location and electric potential of individual electrodes in the numerical models, until a good enough solution is obtained. Recently, we have used the treatment planning procedure for ECT of deep-seated tumours and also analysed the treatment planning robustness to errors in assigned tissue properties and errors in electrode positioning during treatment (Miklavcic *et al* 2010, Kos *et al* 2010). The procedure is currently being tested in a clinical trial of ECT of liver metastases at Institute of Oncology Ljubljana (EudraCT number 2008-008290-54; ClinicalTrials.gov (NCT01264952)) (Edhemovic *et al* 2011).

In this paper, we demonstrate that the treatment planning procedure that has been used before for ECT treatment planning can also be used for GET and IRE treatment planning. We can achieve this, by using the same mathematical model of electroporation and optimization procedures, but with the objective functions defined specifically for each treatment. We also propose several complementary ways of visually presenting the treatment planning data in the clinical environment. Furthermore, by comparing optimization results, we provide general guidance on positioning of the electrodes, including the number of required electrodes inserted in the target tissue.

## 2. Methods

### 2.1. How electroporation is performed in current electrochemotherapy clinical trials

The ECT procedure that is the base of the treatment planning algorithm presented in this paper depends on the properties of the equipment used to generate and measure electric pulses—Cliniporator Vitae (IGEA, Carpi, Italy). With Cliniporator Vitae, a train of high-voltage electric pulses is applied on two electrodes (one anode and one cathode) at a time. Currently, eight 100  $\mu$ s pulses with a repetition frequency of 1 Hz or 5 kHz are used; these are the parameters, for which electroporation thresholds have been determined in several tissues (Miklavcic *et al* 2000). The voltage can be adjusted by the user—medical doctor. If more than two electrodes are inserted into the tissue, trains of pulses can be applied on all possible pairs of electrodes, or only on particular pairs, defined by the treatment plan. In our study, we used 4, 5 or 6 electrodes inserted into the tissue. Electric pulses were applied to most possible pairs; in case of four electrodes, pulses were applied between electrodes 1–2, 1–3, 1–4, 2–3, 2–4 and 3–4. In case of five or six electrodes, more pairs are available and more pulses are thus applied. After all electric pulses are satisfactorily applied during a treatment, the electrodes are removed and the procedure is, for the electroporation part, over.

### 2.2. Model geometry

The model geometry used in the study was taken from a recent clinical case of ECT of a melanoma metastasis in the thigh of a patient. Briefly (for details, see Miklavcic *et al* (2010)), the model geometry was constructed from 32 CT images of the thigh (slice thickness 2.5 mm and pixel size 1.172 mm), with the tissues in the region of interest (tumour, muscle, fat) first delineated by an expert and then exported into COMSOL Multiphysics (version 3.5a, COMSOL, Sweden) with an algorithm written in Matlab (version 2009a, Mathworks,

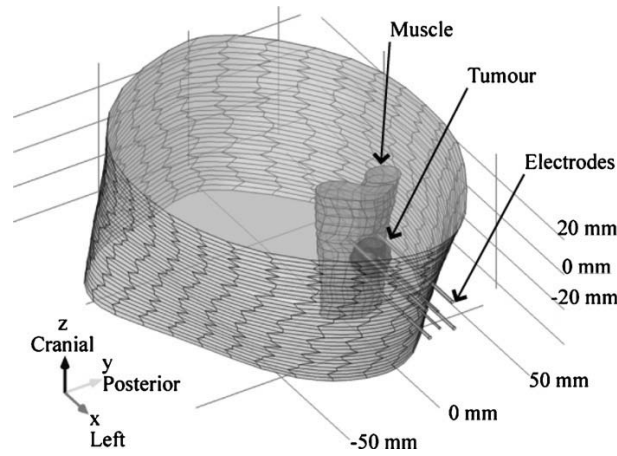


**Figure 1.** Orthographic representation of the model geometry. The model consists of three tissues and 4–6 electrodes. Given are the scale and the major axes used throughout the paper and the patient-centric directions.

USA). The resulting three-dimensional model, with added electrodes (1.8 mm in diameter and 10 cm in length, with a 4 cm conductive region at the top), is shown in figure 1. All tissues were considered isotropic and homogeneous, with conductivity values, before and during electroporation, and reversible electroporation thresholds the same as in Miklavcic *et al* (2010) and references therein, with the exception of muscle electroporation thresholds that were set lower as a result of recent measurements (Corovic *et al* 2010).

### 2.3. Mathematical model of electroporation

The sequential model of tissue electroporation that takes into account changes in electrical conductivity in the duration of electric pulses was used for all calculations (Pavselj *et al* 2005, Sel *et al* 2005). Details on the reasoning behind the sequential model and implementation in COMSOL Multiphysics can be found in Pavselj *et al* (2005). Briefly, the sequential model is superior to other current tissue level electroporation models in that it is able to accurately predict the electric current during the pulses and also better predicts the electroporated volume (Sel *et al* 2005). Mathematical simulation of electroporation with the sequential model includes: step 1—solving the Laplace equation for static electric currents:

$$-\nabla \cdot (\sigma \cdot \nabla V) = 0, \quad (2.1)$$

where  $\sigma$  is tissue conductivity and  $V$  is electric potential, and the boundary conditions are constant potential ( $V = \text{const.}$ ) on the surface of the active parts of the electrodes, continuity ( $\mathbf{n} \cdot (\mathbf{J}_1 - \mathbf{J}_2) = 0$ —normal current density is continuous on both sides of the boundary) on all other interior boundaries and insulation ( $\mathbf{n} \cdot \mathbf{J} = 0$ —normal current density across the boundary is zero) on the inactive parts of the electrodes and outer boundaries of the model, respectively; step 2—irreversibly changing electrical conductivity due to electric fields above the electroporation threshold:

$$\sigma(E) = \frac{\sigma_2 - \sigma_1}{E_{\text{irr}} - E_{\text{rev}}} \cdot E + \sigma_1, \quad (2.2)$$

where  $\sigma_1$  and  $\sigma_2$  are electrical conductivities of non-electroporated and electroporated tissues, respectively, and  $E_{\text{irr}}$  and  $E_{\text{rev}}$  are the thresholds of irreversible and reversible electroporation, respectively; step 3—sequentially repeating steps 1 and 2 until a steady state, when the conductivity does not change in sequential steps, is reached.

#### 2.4. Optimization

Optimization with a genetic algorithm (Holland 1992) was used to determine the optimum electrode positions and voltages between pairs of electrodes used to deliver the electroporation pulses. The genetic algorithm was written in Matlab and was run together with the finite element models using the link between Matlab and COMSOL Multiphysics. The details of the basic algorithm can be found in Zupanic *et al* (2008), while here we report the specific implementation and supplemental features. The genetic algorithm works by first defining an initial population of treatment plans (electrode number, positions and voltages applied between all pairs of adjacent electrodes). The quality of the treatment plans is then evaluated using a specifically defined fitness function (see equations (2.4)–(2.6) for the fitness functions used in this study). Treatment plans are, with a probability proportional to their quality, later selected for ‘reproduction’ by mathematical operations of mutation or cross-over. In this study, the population size was 30, in each generation all solutions except top three (elite) were replaced, and the algorithm ran for 300 iteration before stopping. The mutation rate was 50% (50% cross-over) in the first iteration and then dropped to 5% (95% cross-over) in the last iteration.

When choosing the electrode positions and voltages between the electrode pairs, the following constraints were used: electrodes penetrating the tumour were positioned in parallel, normal to the  $yz$  plane (figure 1), 1 cm apart, while electrodes positioned around the tumour had to be more than 0.5 mm and less than 3 cm from the tumour boundary; all electrodes were positioned so that the tip of the electrodes was at the same depth as the deepest part of the tumour; voltages between pairs of electrodes (in clinical ECT electric pulses are delivered sequentially between pairs of electrodes) ranged between 500 and 3000 V, which is the range of Cliniporator Vitae (IGEA, Carpi, Italy), the device currently being used to deliver electric pulses in clinical ECT at the Institute of Oncology in Ljubljana; there was also the option of 0 V between the electrodes, in which case the pair of electrodes was not included in the calculations. By using these constraints we avoided positioning the electrodes at the very edge of the tumour, which has been shown to be extremely difficult in clinical ECT (Miklavcic *et al* 2010) and also causes problem for the meshing algorithm used in COMSOL Multiphysics. At the same time, we avoided positioning electrodes too far from the tumour, which could not guarantee complete coverage of the tumour with an electric field of sufficiently high magnitude. Additional constraints were the maximum electric current allowed (50 A, Cliniporator Vitae)—when the current exceeded 50 A, the treatment plan’s fitness was changed to zero—and the number of used electrodes—limited to 4, 5 or 6. Because it is not possible to cross-over two treatment plans with different numbers of electrodes, the number of electrodes in the ‘offspring’ was determined randomly. Optimization was also performed using only sets of 4, 5 or 6 electrodes in a single optimization, to determine the efficiency of the algorithm of choosing the correct number of electrodes, but also to compare the optimum solutions in each specific case (it is wise to prepare more than one good enough treatment plan, in case insertion of some electrodes is not possible due to, e.g., the mobility of the tumour (Miklavcic *et al* 2010)). As the results of the combined optimization (4, 5 or 6 electrodes) did not significantly differ from best treatment plan of individual optimization, we only report the individual results here.

Separate fitness functions were defined for ECT, IRE and GET, after consulting with medical doctors involved in the ECT clinical trial at the Institute of Oncology, Ljubljana. For instance, fitness functions (equation (2.10)) for ECT were set according to the following reasoning:

$$F = \sum_t a_t E_{\text{rev}}^t - \sum_c b_c E_{\text{irr}}^c - \sum_t c_t E_{\text{irr}}^t - \sum_c d_c E_{\text{rev}}^c. \quad (2.3)$$

It is most important to cover all target tissues ( $t$ ) by an electric field above the reversible thresholds ( $_{\text{rev}}$ ); keeping healthy tissues ( $c$ ) (in our case, muscle and fat) from being damaged by irreversible electroporation is less important; keeping the tumour from being damaged by the electric field above the irreversible threshold ( $_{\text{irr}}$ ) even less important; and keeping the healthy tissues from being reversibly electroporated is the least important. Therefore the weights in equation (2.3) were set as  $a_t > b_c > c_t > d_c$ . Similar arguments lead to fitness functions for the optimization of IRE, as seen in the fitness function for ECT (2.4), GET (2.5) and IRE (2.6):

$$F_{\text{ECT}} = 100 V_{\text{rev}}^T - 10 V_{\text{irr}}^M - 5 V_{\text{irr}}^F \quad (2.4)$$

$$F_{\text{GET}} = 100(V_{\text{rev}}^T - V_{\text{irr}}^T) - 10 V_{\text{irr}}^M - 5 V_{\text{irr}}^F \quad (2.5)$$

$$F_{\text{IRR}} = 100 V_{\text{irr}}^T - 10 V_{\text{irr}}^M - 5 V_{\text{irr}}^F, \quad (2.6)$$

where ( $T$ ) is tumour, ( $M$ ) is muscle and ( $F$ ) is fat tissue. It should be stressed that the weights chosen for these fitness function are specific for this particular case, namely for a tumour on top muscle tissue, surrounded by fat. If the tumour was located near a vital tissue, such as the heart or the spine, the weights preventing damage to these tissues should be set higher. In general, the weights should be adjusted for each treatment and each patient.

### 2.5. Visualization

The first visualization approach is the overlay of the original CT images and the output of the model—the increases in tissue conductivity caused by electric field exceeding the electroporation thresholds (figure 2, supplementary file *Electroporation\_cross\_section\_images* available from [stacks.iop.org/PMB/57/5425/mmedia](https://stacks.iop.org/PMB/57/5425/mmedia)). The overlays were generated in Matlab using the built-in post-processing interpolation function of the COMSOL-Matlab link (*postinterp*). The function allows for interpolation of any result on an arbitrary three-dimensional grid. This allowed us to extract the results in a grid that corresponds on a pixel-by-pixel level with the original CT images.

The algorithm for extracting the results was as follows. For each subdomain in the COMSOL model (there were a total of two subdomains for the tumour tissue, five subdomains for the muscle tissue and one subdomain for the fat tissue), the interpolation was performed to determine where the conductivity increased. The increase of conductivity in the model is directly related to the maximum electric field strength and consequently also to the degree of electroporation (Pavlin *et al* 2005).

The other visualization approach is the cumulative coverage plot, which represents cumulative coverage of tissues by electric fields above the electroporation threshold after the complete sequence of pulses has been applied (cumulative coverage plot—figure 5). Together with the individual electrode-pair contributions presented in figure 6, these visualizations enable a quantitative means of comparing different treatment plans.

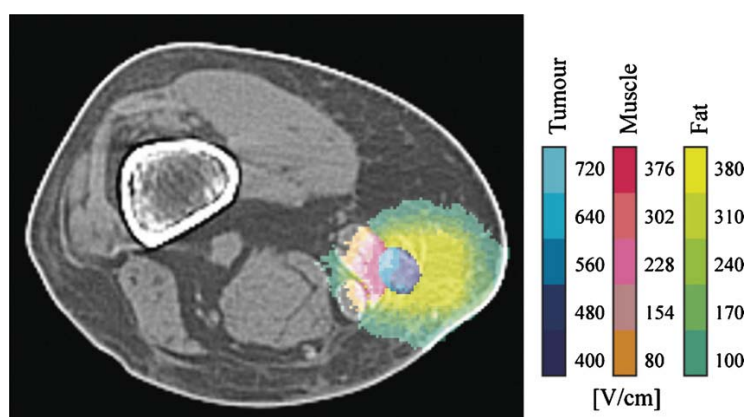


**Figure 2.** Cross-section plot of electroporation, slice 18 in the original CT images. The cross-section shows the degree of electroporation achieved by the proposed treatment plan for ECT with four electrodes, relative to the maximum reached electric field strength in the cross-section. The overlay consists of three colour progressions, with each colour indicating fields at or above the numerical value indicated in ( $\text{V cm}^{-1}$ ). The plot also gives an overview of the segmentation of the tissues and a qualitative means of evaluating the solution. Each pixel on the colour overlay represents a volume with dimensions of  $1.2 \times 1.2 \times 2.5$  mm.

### 3. Results

#### 3.1. Treatment plans for ECT, GET and IRE

In this study, we produced nine separate treatment plans, three each for ECT, GET and IRE. For each of the treatments, one treatment plan was prepared for four, one for five, and one for six electrodes inserted into and around the target tissue (in the following text referred to by the initials and number indicating the number of electrodes used, e.g. ECT4 for the four electrode electrochemotherapy). While complete tumour volume electroporation was achieved in all nine treatment plans, there were significant differences in both the optimal positions (figure 3) and voltages between the electrodes (table 1) as well as the total electric current (table 2). The fitness functions and coordinates of electrodes are reported in supplementary data table 1 (available from [stacks.iop.org/PMB/57/5425/mmedia](https://stacks.iop.org/PMB/57/5425/mmedia)).

For ECT, 100 % reversible electroporation of tumour was achieved regardless of the number of electrodes used; however, six electrodes proved to be better than five or four as their use caused the least healthy tissue damage (figure 4). The electric pulses delivered between the intratumoral electrodes already reversibly electroporate most of the tumour volume; therefore, lower voltage can be applied by the electrodes positioned around the tumour, causing less healthy tissue damage. With five electrodes, the penetrating electrode always has a partner electrode outside the tumour volume; because fat tissue surrounding the tumour has lower electrical conductivity than the tumour, a lot of the electric energy is 'lost' via the voltage drop across the fat and therefore higher voltages are needed for electroporation, leading to more healthy tissue damage. For the same reason, the four electrodes treatment plan was the worst of the three.

The IRE treatment plans follow the ECT plans closely, with six electrodes being better than five and four being the worst (in all three electrode configurations complete coverage of the tumour was achieved). The voltages required for IRE are significantly higher than for

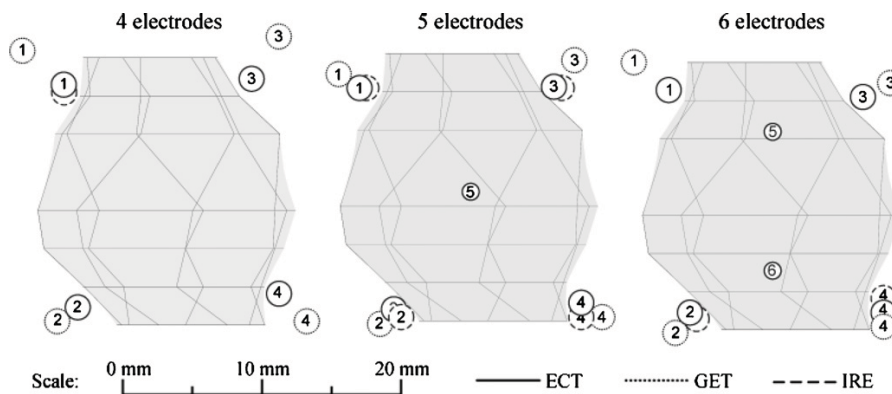


**Figure 3.** Positions of the electrodes with respect to the tumour for all nine treatment plans. The cross-section shows electrode positions in the  $y$ - $z$  plane. All elements of the figure are in scale.

**Table 1.** Voltages between electrode pairs for all nine treatment plans.  $U_{12}$  denotes voltage between electrodes 1 and 2; electrode numbering is shown in figure 3.

	4 electrodes			5 electrodes			6 electrodes		
	ECT	GET	IRE	ECT	GET	IRE	ECT	GET	IRE
$U_{12}$ [V]	1100	1500	2400	1100	1500	2300	600	1900	2300
$U_{13}$ [V]	1000	1500	2100	1000	1500	2000	600	1900	2000
$U_{24}$ [V]	1000	1400	2100	900	1500	1900	600	1900	2000
$U_{34}$ [V]	1100	1500	2100	1000	1700	2000	600	1900	1900
$U_{14}$ [V]	1400	1800	2500						
$U_{23}$ [V]	1300	1900	2500						
$U_{15}$ [V]				1000	600	1900	600	600	1600
$U_{25}$ [V]				900	600	1900			
$U_{35}$ [V]				1000	600	1800	500	600	1600
$U_{45}$ [V]				1000	600	1900			
$U_{26}$ [V]							600	600	1500
$U_{46}$ [V]							500	600	1600
$U_{56}$ [V]							1900	500	3000

ECT, with the voltages between the penetrating electrodes reaching 3000 V (table 1), the limit of Cliniporator Vitae. Higher voltages also cause more damage to healthy tissue compared to ECT (figure 4).

In contrast to ECT and IRE, six electrodes were the worst choice for GET, as their use lead to a large volume of the tumour irreversibly electroporated (supplementary file: cumulative coverage plots available from [stacks.iop.org/PMB/57/5425/mmedia](https://stacks.iop.org/PMB/57/5425/mmedia)), resulting in less gene expression, and four electrodes the best choice with the least tumour damage, but not the least healthy tissue damage (figure 5). In all three GET treatment plans, the four extratumoral electrodes were positioned further away from the tumour than for either ECT or IRE (figure 3). While this leads to less irreversible electroporation of the tumour tissue, the damage to healthy tissue was also bigger. For illustration of the differences, we have chosen to present the ECT 4, ECT 6, GET 4 and IRE 6 in figures 6 and 7 as examples of more and less damage to surrounding tissues.

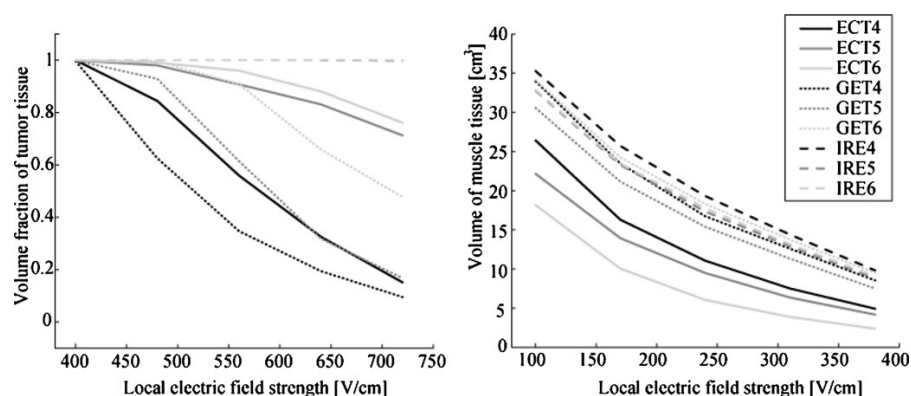


**Figure 4.** Cumulative coverage plot for the tumour and muscle in all nine treatment plans. Tumour coverage is shown as the fraction of the total volume of the tumour, while muscle is shown as total volume. A similar plot has been produced for the fat tissue, and is available in the supplementary data file—cumulative coverage plots available from [stacks.iop.org/PMB/57/5425/mmedia](https://stacks.iop.org/PMB/57/5425/mmedia).

**Table 2.** Computed currents in all nine treatment plans.  $I_{12}$  denotes current between electrodes 1 and 2. Electrode numbering is illustrated in figure 3, while the corresponding applied voltages are detailed in table 1.

	4 electrodes			5 electrodes			6 electrodes		
	ECT	GET	IRE	ECT	GET	IRE	ECT	GET	IRE
$I_{12}$ [A]	11.7	13.6	28.7	10.9	13.1	25.4	5.25	15.7	26.1
$I_{13}$ [A]	9.86	12.0	23.5	9.48	12.6	21.4	4.91	15.0	22.0
$I_{24}$ [A]	8.60	9.93	20.7	8.11	12.4	19.8	4.71	18.6	21.9
$I_{34}$ [A]	10.3	10.8	21.7	10.0	15.4	21.5	5.45	19.8	22.5
$I_{14}$ [A]	11.6	11.2	23.3						
$I_{23}$ [A]	12.3	16.5	27.1						
$I_{15}$ [A]				11.5	4.62	24.3	7.09	4.71	22.1
$I_{25}$ [A]				11.4	5.71	26.7			
$I_{35}$ [A]				13.3	5.65	25.7	6.41	6.34	24.5
$I_{45}$ [A]				11.1	4.48	22.3			
$I_{26}$ [A]							8.08	6.61	23.6
$I_{46}$ [A]							5.16	6.46	21.4
$I_{56}$ [A]							30.6	5.44	49.5

### 3.2. Visualization of the treatment plans

To enable a more visual and information rich comparison of the treatment plans, the modelling results can be overlaid over the original CT images (figure 5) and the coverage of the target and critical tissues by electroporation can be presented in the form of cumulative coverage plots (figures 6 and 7). The curves (figure 6) show the fraction of the tumour volume covered by at least a certain magnitude of electric field (similar to the dose–volume histogram used in radiotherapy (Bevilacqua *et al* 2007)). They can be used to relatively quickly evaluate the robustness of the treatment plan, but lack any spatial anatomical detail. Cumulative coverage curves for all nine treatment plans are available in the supplementary file—cumulative coverage plots available from [stacks.iop.org/PMB/57/5425/mmedia](https://stacks.iop.org/PMB/57/5425/mmedia).

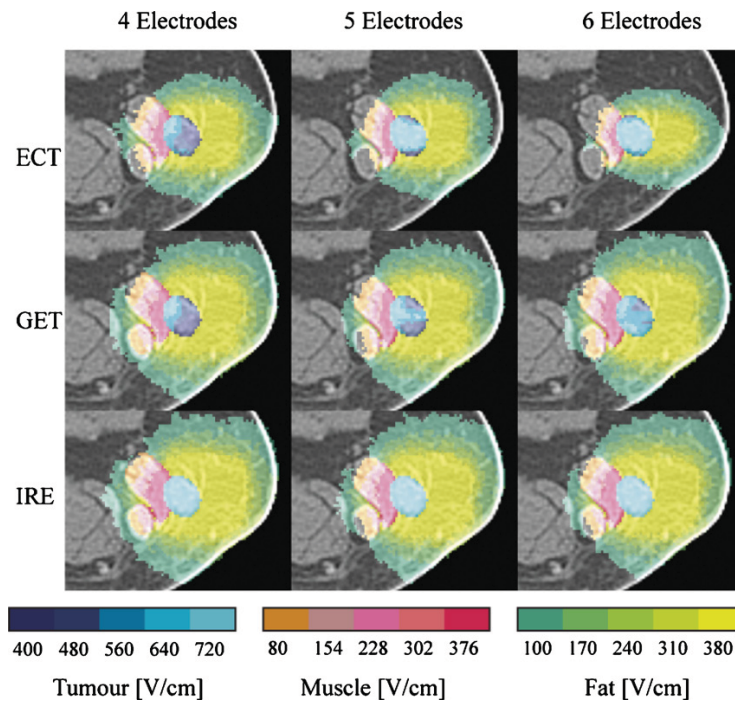


**Figure 5.** Comparison of the different treatment modalities and electrode configurations. The figure shows the region-of-interest on slice 18. The colour progressions indicate tissue where the electric fields exceed the indicated field strength corresponding to degrees of electroporation.

Additionally, the electrode pair contribution graphs indicate the extent of contribution of each electrode pair towards the total coverage of the target tissue. The CT and modelling overlay provides the spatial details and enables the attending physician to determine regions of the target and healthy tissue, where coverage needs to be improved. For example, in figure 5 it is easy to see that the edges of the tumour in ECT5 are covered by a lower electric field than in ECT6, and, in GET4, that the tumour volume closer to the muscle tissue is irreversibly electroporated, while the volume closer to the skin is reversibly electroporated.

#### 4. Discussion

In recent years electroporation-based treatments have made big steps from the lab into the clinic, with ECT already used for cancer treatment, with three thousand patients treated since SOP were published with success rates over 70% (Marty *et al* 2006, Sersa *et al* 2009, Campana *et al* 2008). As both IRE and GET are also coming closer to clinical use, it is important that the physical part of the treatments—the delivery of electric pulses—is as accurate as possible to give the best chance for complete therapy success. In this study, we demonstrate that the treatment planning procedure originally developed for clinical ECT (Zupanic *et al* 2008, Miklavcic *et al* 2010, Edhemovic *et al* 2011) is also suitable for treatment planning of IRE

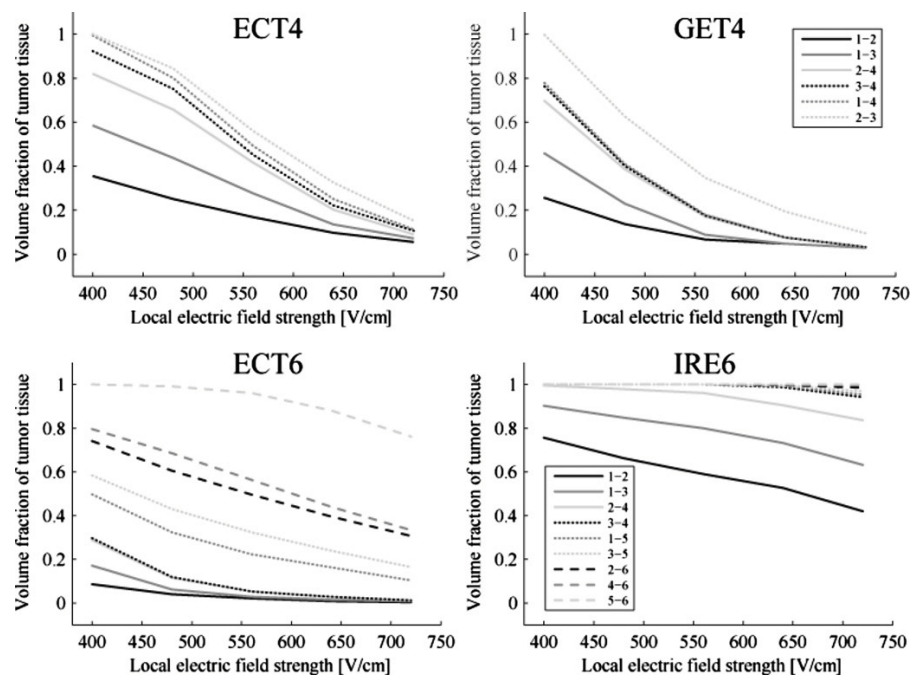


**Figure 6.** Cumulative coverage plots show the progression of total coverage of the tumour after the train of electric pulses is applied through each new electrode pair. The order in which the contributions were evaluated is the same as in the optimization. The numeral next to the name of the treatment indicates the number of electrodes used.

and GET, albeit with certain modifications in the form of the fitness function used in the optimization process.

By changing the factors and weights of the fitness function (see equations (2.2)–(2.6) in section 2) the treatment plans obtained for ECT, IRE and GET differ considerably. For both ECT and IRE, the best possible electrode configuration used six electrodes, two of them penetrating through the centre of the tumour. By having the entire source (the cathode and the anode) of the electric field inside the tumour the delivered electric energy stays in the tumour; thereby electroporation is limited almost entirely to the tumour volume. Although our study is limited by a single geometry, it is most probable that having two (or more) electrodes inserted into the tumour is the optimal electrode configuration for ECT or IRE of most large target tissues. The electrodes positioned outside the tumour (but still very close, see figure 3) can therefore be used with lower voltages (table 1) with their main function being electroporation of the tumour margins. When only one intratumoral electrode is used, the voltages used on the electrodes outside the tumour have to be higher thereby causing more tissue damage (table 1). Similar conclusions have been reached in a recent study of intracranial IRE, where positioning electrodes inside the target tissue produced better results (Garcia *et al* 2010).

The situation was reversed for GET, with four electrodes being the best option. This was mostly due to irreversible electroporation of the tumour being highly penalized in the fitness function (equation 2.5). A secondary effect of the high penalization was that the outside

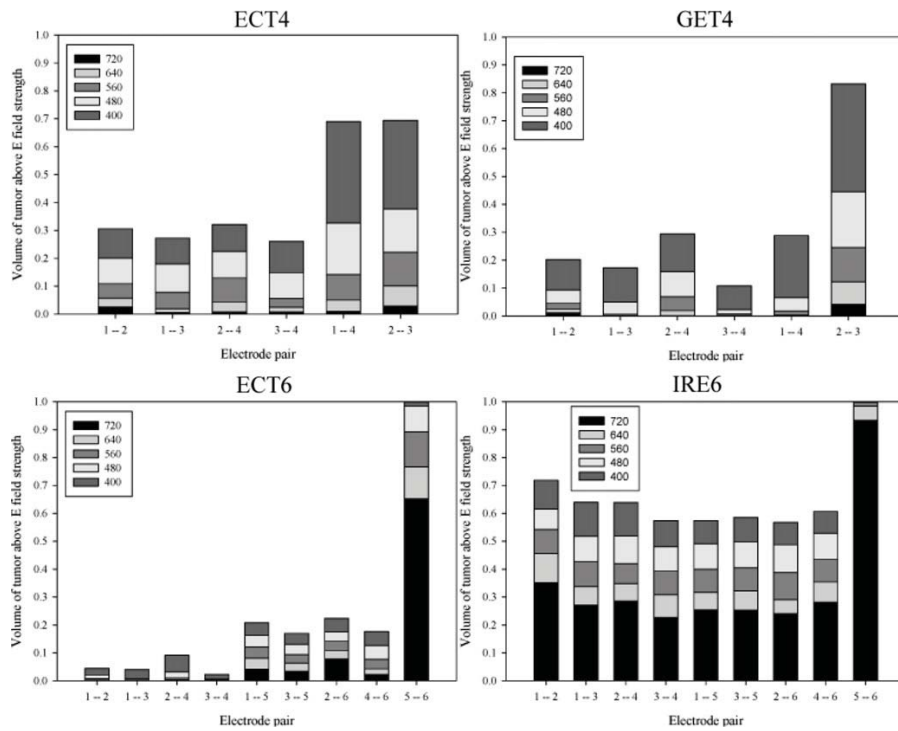


**Figure 7.** Individual electrode-pair contributions. This figure enables the viewer to discern the contribution of each electrode pair toward the success of the treatment. The values are given in  $V\text{ cm}^{-1}$ . The bars represent the volume fraction of tumour tissue above the respective electric field strength. The numeral next to the name of the treatment indicates the number of electrodes used.

electrodes were positioned further from the tumour than in ECT and IRE; such positioning caused more healthy tissue damage, but less damage to the tumour that was the designated tissue of transfected gene expression. Although the whole tumour volume is not the only possible target for cancer gene therapy (Heller and Heller 2010), the positioning of the electrodes further from the target tissue should remain valid in all cases, where the location of target cells can be volumetrically defined, e.g. stromal cell in the bone marrow (Van Damme *et al* 2002). In other cases, e.g. when muscle is the target tissue, controlling the volume of reversibly electroporated tissue can also control the amount of gene expression (Bureau *et al* 2010), while at the same minimizing damage to the healthy tissue (Zupanic *et al* 2010, Hojman *et al* 2011).

A second important contribution of this research is the presented visualization approach, which gives a new set of tools for the use in the clinical setting as well as for the electroporation research community. It lends itself to easy automation for high-throughput evaluation of treatment plans, and prepares the setting for the discussion on the fitness functions for a more formalized approach to treatment planning. Furthermore, the visualization tools will allow researchers to revisit the subject of robustness of the treatment plans.

The quality of the treatment plans, however, also depends on the validity of the mathematical model of electroporation used. While the current models take into account the

changes in electrical conductivity due to electroporation, and thus considerably improve the prediction of electroporated volumes (Sel *et al* 2005), all tissues are considered homogeneous, which might not be the case in reality. In particular, the viable and necrotic regions of large tumours might have different electrical conductivities. Nevertheless, we believe that a homogeneous representation of the tissues is a good approximation of reality and at the same time the best option currently available, as to the best of our knowledge an estimate of electrical heterogeneity of tumours, does not exist so far. It is, however, consistently reported in the literature that the electric conductivity of tumours is higher than that of the surrounding tissue and our previous investigation has shown that treatment planning depends more on the ratio between conductivities of the tumour and surrounding tissues than small variation of conductivity in the target tissue (Kos *et al* 2010).

Appropriate choice of weights in the fitness function can also significantly influence the quality of the treatment plan; therefore, the weights should be chosen in consultation with the treating medical doctor. When more data from more clinical studies become available, it will be possible to determine a formal way of selecting weights for different electroporation-based treatments, with a high degree of certainty about the quality of the treatment plan. At the moment, the data are not yet available; therefore, we have to rely (only) on critical thinking and knowledge about human physiology.

Our study shows that it is possible to use treatment planning for all three electroporation-based treatments; however, additional research will have to be done before it can be used in for clinical IRE and GET. Namely, the thresholds used in this study are valid only for the case of eight 100  $\mu$ s pulses (1 Hz repetition frequency) that are currently used in clinical ECT (Sel *et al* 2005), while the pulses used in IRE and GET are different: more pulses and higher/lower repetition frequencies are used in IRE (Rubinsky *et al* 2007, Onik *et al* 2007), while many different pulse configurations are used in GET (Gehl 2003, Rols and Teissie 1998, Bettan *et al* 2000, Satkauskas *et al* 2005, Tevz *et al* 2009, Scheerlinck *et al* 2004). Instead of using the maximum electric field achieved in the tissue as the measure of electroporation (figure 4), it would be better to calculate the probability of electroporation due to exposure to electric pulses. Some steps in this direction were taken in recent studies of the effects of pulse number and duration on electroporation (Golberg and Rubinsky 2010, Pucihar *et al* 2011). Also, since it has been shown several times that the direction of the field is also important—exposing cells or tissue to an electric field from two perpendicular directions and increasing the level of electroporation compared to a single direction (Faurie *et al* 2010, Rebersek *et al* 2007, Valic *et al* 2003)—it would be useful to add directionality to the calculation of the probability.

## 5. Conclusions

The method presented here enables accurate planning of the electroporation part of ECT, GET for gene therapy and DNA vaccination and IRE. While fixed-geometry electrodes and standard voltages can provide good guidelines in the treatment of smaller skin tumours (Sersa *et al* 2011), we believe that electric field distribution calculations or full treatment planning should be performed before each experiment or clinical treatment of larger target tissues. With all the confounding factors that are currently beyond clinical control, such as the effects of the vascularization on the drug distribution in the target tissues (Sersa *et al* 2008a, Brown *et al* 2004, Jain 1999) or the intrinsic ability of the cells to express the transfected construct (Herweijer and Wolff 2003), it is vital that the electroporation of the target tissues is achieved with certainty.

## Acknowledgments

This research was supported by the Slovenian Research Agency. Research was performed in the scope of LEA EBAM.

## References

- Bettan M, Ivanov M A, Mir L M, Boissiere F, Delaere P and Scherman D 2000 Efficient DNA electrotransfer into tumors *Bioelectrochemistry* **52** 83–90
- Bevilacqua V, Mastrorardi G and Piscopo G 2007 Evolutionary approach to inverse planning in coplanar radiotherapy *Image Vis. Comput.* **25** 196–203
- Brown E B, Boucher Y, Nasser S and Jain R K 2004 Measurement of macromolecular diffusion coefficients in human tumors *Microvasc. Res.* **67** 231–6
- Bureau M F, Juge L, Seguin J, Rager M-N, Scherman D and Mignet N 2010 Muscle transfection and permeabilization induced by electrotransfer or pluronic<sup>®</sup> L64: Paired study by optical imaging and MRI *Biochim. Biophys. Acta* **1800** 537–43
- Campana L G, Mocellini S, Basso M, Puccetti O, De Salvo G L, Chiarion-Sileni V, Vecchiato A, Corti L, Rossi C R and Nitti D 2008 Bleomycin-based electrochemotherapy: clinical outcome from a single institution's experience with 52 patients *Ann. Surg. Oncol.* **16** 191–9
- Corovic S, Zupanic A, Kranjc S, Al Sakere B, Leroy-Willig A, Mir L M and Miklavcic D 2010 The influence of skeletal muscle anisotropy on electroporation: *in vivo* study and numerical modeling *Med. Biol. Eng. Comput.* **48** 637–48
- Corovic S, Zupanic A and Miklavcic D 2008 Numerical modeling and optimization of electric field distribution in subcutaneous tumor treated with electrochemotherapy using needle electrodes *IEEE Trans. Plasma. Sci.* **36** 1665–72
- Costa M *et al* 2007 A method for genetic modification of human embryonic stem cells using electroporation *Nat. Protoc.* **2** 792–6
- Davalos R V, Mir L M and Rubinsky B 2005 Tissue ablation with irreversible electroporation *Ann. Biomed. Eng.* **33** 223–31
- Dunny G M, Lee L N and LeBlanc D J 1991 Improved electroporation and cloning vector system for Gram-positive bacteria *Appl. Environ. Microbiol.* **57** 1194–201
- Edd J F and Davalos R V 2007 Mathematical modeling of irreversible electroporation for treatment planning *Technol. Cancer Res. Treat.* **6** 275–86
- Edhemovic I *et al* 2011 Electrochemotherapy: a new technological approach in treatment of metastases in the liver *Technol. Cancer Res. Treat.* **10** 475–85
- Faurie C, Rebersek M, Golzio M, Kanduser M, Escoffre J-M, Pavlin M, Teissie J, Miklavcic D and Rols M-P 2010 Electro-mediated gene transfer and expression are controlled by the life-time of DNA/membrane complex formation *J. Gene Med.* **12** 117–25
- Garcia P A, Rossmesl J H, Neal R E, Ellis T L, Olson J D, Henao-Guerrero N, Robertson J and Davalos R V 2010 Intracranial nonthermal irreversible electroporation: *in vivo* analysis *J. Membr. Biol.* **236** 127–36
- Garcia-Frigola C, Carreres M I, Vegar C and Herrera E 2007 Gene delivery into mouse retinal ganglion cells by *in utero* electroporation *BMC Develop. Biol.* **7** 103
- Gehl J 2003 Electroporation: theory and methods, perspectives for drug delivery, gene therapy and research *Acta Physiol. Scand.* **177** 437–47
- Gehl J, Sorensen T H, Nielsen K, Raskmark P, Nielsen S L, Skovsgaard T and Mir L M 1999 *In vivo* electroporation of skeletal muscle: threshold, efficacy and relation to electric field distribution *Biochim. Biophys. Acta* **1428** 233–40
- Golberg A and Rubinsky B 2010 A statistical model for multidimensional irreversible electroporation cell death in tissue *Biomed. Eng. Online* **9** 13
- Heller L and Heller R 2010 Electroporation gene therapy preclinical and clinical trials for melanoma *Curr. Gene Ther.* **10** 312–7
- Heller R, Deconti R, Messina J, Andrews S, Urbas P, Ugen K, Puleo C, Sondak V, Riker A and Daud A 2006 Gene therapy with plasmid IL-12 delivered by electroporation in patients with malignant melanoma: results of first human Phase I trial *Eur. J. Cancer Suppl.* **4** 106–106
- Herweijer H and Wolff J A 2003 Progress and prospects: naked DNA gene transfer and therapy *Gene Ther.* **10** 453–8
- Hojman P, Brolin C and Gissel H 2011 Calcium influx and the muscular response to electrotransfer *Am. J. Physiol. Regul. Integr. Comp. Physiol.* **302** R446–53
- Holland J H 1992 *Adaptation in Natural and Artificial Systems: An Introductory Analysis with Applications to Biology, Control, and Artificial Intelligence* (Cambridge: MIT Press)

- Jain R K 1999 Transport of molecules, particles, and cells in solid tumors *Ann. Rev. Biomed. Eng.* **1** 241–63
- Jordan E T, Collins M, Terefe J, Ugozzoli L and Rubio T 2008 Optimizing electroporation conditions in primary and other difficult-to-transfect cells *J. Biomol. Tech.* **19** 328–34
- Kanthou C, Kranjc S, Sersa G, Tozer G, Zupanic A and Cemazar M 2006 The endothelial cytoskeleton as a target of electroporation-based therapies *Mol. Cancer Ther.* **5** 3145–52
- Kos B, Zupanic A, Kotnik T, Snoj M, Sersa G and Miklavcic D 2010 Robustness of treatment planning for electrochemotherapy of deep-seated tumors *J. Memb. Biol.* **236** 147–53
- Kotnik T, Bobanovic F and Miklavcic D 1997 Sensitivity of transmembrane voltage induced by applied electric fields—a theoretical analysis *Bioelectrochem. Bioenerg.* **43** 285–91
- Luxembourg A, Evans C and Hannaman D 2007 Electroporation-based DNA immunisation: translation to the clinic *Exp. Opin. Biol. Ther.* **7** 1647–64
- Mahmood F and Gehl J 2011 Optimizing clinical performance and geometrical robustness of a new electrode device for intracranial tumor electroporation *Bioelectrochemistry* **81** 10–6
- Marty M, Sersa G, Garbay J, Gehl J, Collins C, Snoj M, Billard V, Geertsen P, Larkin J and Miklavcic D 2006 Electrochemotherapy—an easy, highly effective and safe treatment of cutaneous and subcutaneous metastases: results of ESOPE (European standard operating procedures of electrochemotherapy) study *Eur. J. Cancer Suppl.* **4** 3–13
- Miklavcic D, Corovic S, Pucihar G and Pavselj N 2006 Importance of tumour coverage by sufficiently high local electric field for effective electrochemotherapy *Eur. J. Cancer Suppl.* **4** 45–51
- Miklavcic D, Semrov D, Mekid H and Mir L M 2000 A validated model of *in vivo* electric field distribution in tissues for electrochemotherapy and for DNA electrotransfer for gene therapy *Biochim. Biophys. Acta* **1523** 73–83
- Miklavcic D, Snoj M, Zupanic A, Kos B, Cemazar M, Kropivnik M, Bracko M, Pecnik T, Gadzijevec E and Sersa G 2010 Towards treatment planning and treatment of deep-seated solid tumors by electrochemotherapy *Biomed. Eng.* **9** 10
- Mir L M, Gehl J, Sersa G, Collins C G, Garbay J R, Billard V, Geertsen P F, Rudolf Z, O'Sullivan G C and Marty M 2006 Standard operating procedures of the electrochemotherapy: instructions for the use of bleomycin or cisplatin administered either systemically or locally and electric pulses delivered by the Cliniporator (TM) by means of invasive or non-invasive electrodes *Eur. J. Cancer Suppl.* **4** 14–25
- Mir L M, Orłowski S, Belehradek J and Paoletti C 1991 Electrochemotherapy potentiation of antitumor effect of bleomycin by local electric pulses *Eur. J. Cancer* **27** 68–72
- Morales-de la Peña M, Elez-Martínez P and Martín-Belloso O 2011 Food preservation by pulsed electric fields: an engineering perspective *Food Eng. Rev.* **3** 94–107
- Neumann E, Schaeferriider M, Wang Y and Hofschneider P H 1982 Gene-transfer into mouse lymphoma cells by electroporation in high electric-fields *EMBO J.* **1** 841–5
- Onik G, Mikus P and Rubinsky B 2007 Irreversible electroporation: implications for prostate ablation *Technol. Cancer Res. Treat.* **6** 295–300
- Pakhomov A G, Miklavcic D and Markov M S 2010 *Advanced Electroporation Techniques in Biology and Medicine* (Boca Raton, FL: CRC Press)
- Pavliha D, Kos B, Županič A, Marčan M, Serša G and Miklavčič D 2012 Patient-specific treatment planning of electrochemotherapy: procedure design and possible pitfalls *Bioelectrochemistry* [Epub ahead of print, doi:10.1016/j.bioelechem.2012.01.007]
- Pavlin M, Kanduser M, Rebersek M, Pucihar G, Hart F X, Magjarevic R and Miklavcic D 2005 Effect of cell electroporation on the conductivity of a cell suspension *Biophys. J.* **88** 4378–90
- Pavselj N, Bregar Z, Cukjati D, Batiuskaite D, Mir L M and Miklavcic D 2005 The course of tissue permeabilization studied on a mathematical model of a subcutaneous tumor in small animals *IEEE Trans. Biomed. Eng.* **52** 1373–81
- Pucihar G, Krmelj J, Rebersek M, Napotnik T and Miklavcic D 2011 Equivalent pulse parameters for electroporation *IEEE Trans. Biomed. Eng.* **58** 3279–88
- Rebersek M, Faurie C, Kanduser M, Xorovic S, Teissie J, Rols M P and Miklavcic D 2007 Electroporator with automatic change of electric field direction improves gene electrotransfer *in-vitro* *Biomed. Eng. Online* **6** 25
- Rols M P and Teissie J 1992 Experimental-evidence for the involvement of the cytoskeleton in mammalian-cell electropermeabilization *Biochim. Biophys. Acta* **1111** 45–50
- Rols M P and Teissie J 1998 Electropermeabilization of mammalian cells to macromolecules: control by pulse duration *Biophys. J.* **75** 1415–23
- Rubinsky B, Onik G and Mikus P 2007 Irreversible electroporation: a new ablation modality—clinical implications *Technol. Cancer Res. Treat.* **6** 37–48
- Sack M, Sigler J, Frenzel S, Eing C, Arnold J, Michelberger T, Frey W, Attmann F, Stukenbrock L and Müller G 2010 Research on industrial-scale electroporation devices fostering the extraction of substances from biological tissue *Food Eng. Rev.* **2** 147–56

- Sale A and Hamilton W 1967 Effects of electric fields on microorganisms I killing of bacteria and yeasts *Biochim. Biophys. Acta* **148** 781–8
- Satkauskas S, Andre F, Bureau M F, Scherman D, Miklavcic D and Mir L M 2005 Electrophoretic component of electric pulses determines the efficacy of *in vivo* DNA electrotransfer *Human Gene Ther.* **16** 1194–201
- Scheerlinck J P Y, Karlis J, Tjelle T E, Presidente P J A, Mathiesen I and Newton S E 2004 *In vivo* electroporation improves immune responses to DNA vaccination in sheep *Vaccine* **22** 1820–5
- Sel D, Cukjati D, Batuskaite D, Slivnik T, Mir L M and Miklavcic D 2005 Sequential finite element model of tissue electropermeabilization *IEEE Trans. Biomed. Eng.* **52** 816–27
- Sel D, Lebar A M and Miklavcic D 2007 Feasibility of employing model-based optimization of pulse amplitude and electrode distance for effective tumor electropermeabilization *IEEE Trans. Biomed. Eng.* **54** 773–81
- Sersa G, Cemazar M and Snoj M 2009 Electrochemotherapy of tumours *Curr. Oncol.* **16** 34–5
- Sersa G, Gehl J, Garbay J-R, Soden D M, O'Sullivan G C, Matthiessen L W, Snoj M and Mir L M 2011 *Electrochemotherapy of small tumors; the experience from the ESOPe (European standard operating procedures for electrochemotherapy) group* Clinical Aspects of Electroporation ed S T Kee, J Gehl and E W Lee (New York: Springer) pp 93–102
- Sersa G *et al* 2008a Vascular disrupting action of electroporation and electrochemotherapy with bleomycin in murine sarcoma *Br. J. Cancer* **98** 388–98
- Sersa G, Miklavcic D, Cemazar M, Rudolf Z, Pucihar G and Snoj M 2008b Electrochemotherapy in treatment of tumours *Eur. J. Surg. Oncol.* **34** 232–40
- Shafiee H, Garcia P A and Davalos R V 2009 A preliminary study to delineate irreversible electroporation from thermal damage using the arrhenius equation *Trans. ASME, J. Biomech. Eng.* **131** 5
- Testori A, Faries M B, Thompson J F, Pennacchioli E, Deroose J P, van Geel A N, Verhoef C, Verrecchia F and Soteldo J 2011 Local and intralesional therapy of in-transit melanoma metastases *J. Surg. Oncol.* **104** 391–6
- Tevz G, Kranjc S, Cemazar M, Kamensek U, Coer A, Krzan M, Vidic S, Pavlin D and Sersa G 2009 Controlled systemic release of interleukin-12 after gene electrotransfer to muscle for cancer gene therapy alone or in combination with ionizing radiation in murine sarcomas *J. Gene Med.* **11** 1125–37
- Valic B, Golzio M, Pavlin M, Schatz A, Faurie C, Gabriel B, Teissie J, Rols M P and Miklavcic D 2003 Effect of electric field induced transmembrane potential on spheroidal cells: theory and experiment *Eur. Biophys. J.* **32** 519–28
- Van Damme A, Vanden Driessche T, Collen D and Chuah M K L 2002 Bone marrow stromal cells as targets for gene therapy *Curr. Gene Ther.* **2** 195–209
- Zupanic A, Corovic S and Miklavcic D 2008 Optimization of electrode position and electric pulse amplitude in electrochemotherapy *Radiol. Oncol.* **42** 93–101
- Zupanic A, Corovic S, Miklavcic D and Pavlin M 2010 Numerical optimization of gene electrotransfer into muscle tissue *Biomed. Eng. Online* **9** 66
- Zupanic A and Miklavcic D 2011 Tissue heating during tumor ablation with irreversible electroporation *J. Electr. Eng. Comput. Sci.* **78** 42–7

## Discussion

---

### Discussion of EMF safety related papers

#### **Exposure to multi-band base station antennas**

In the first EMF safety paper we examined the case of occupational exposure to an example of a multi-band base-station antenna. This work was important in the context of the directive 2004/40/EC of the European Council on limiting occupational exposure to electromagnetic fields (EC 2004). The directive was first scheduled to come into force in the beginning of the year 2008, but its implementation was postponed until 2012 pending further review of possible negative effects on the economy. In 2012, the directive was again delayed, since the member states didn't manage to reach consensus as to what the minimum standards should be at the end of year 2011. At the time of writing it is still unclear what the eventual decision on the directive will be.

If the directive had come into action however, it would have required the occupational safety assessment of all workers for exposure to electromagnetic fields with the field levels and methodology taken from the 1998 ICNIRP guidelines. In most occupational settings, the electromagnetic fields are not a concern (and can be evaluated based on procedural standards, such as EN50499), but for some workplaces, the occupational exposure is significant and needs to be evaluated individually.

The case of base station antenna exposure is one such example. Although the simplest course of action for preventing overexposure when working near base stations is to shut the transmitters down, this is not always possible, since operators strive for maximum network availability, and can be complicated in case of urgent work at colocation sites, where several operators share the same antenna tower. There were several reports of determination of SAR in humans exposed to base station antennas in the literature before our paper (Martinez-Burdalo *et al* 2005, van Wyk *et al* 2005, Alanko *et al* 2008, Cooper *et al* 2002, Coray and Krahenbuhl 2003, Joseph and Martens 2005, Joseph *et al* 2008), but none of them considered the case of the simultaneous exposure to multi-band base station antennas.

Since multi-band base station antennas are often used in highly populated areas, where colocation and easy access to the antennas are quite common, we wanted to examine how the exposure to multi-band antennas should be determined. The ICNIRP guidelines provide the following criterion:

$$\sum_{i=1}^n \frac{SAR(f_i)}{SAR_L} \leq 1,$$

where  $SAR(f_i)$  is the specific absorption rate at frequency  $f_i$ , and  $SAR_L$  is the basic restriction of SAR. This ratio of SAR vs. the basic restriction should be summed over all frequencies present in the exposure scenario. Although the guidelines do not specify this explicitly, it is probable that the guidelines intended only the maximum values of SAR to be compared. With whole-body SAR this is the only possible interpretation, however with localized SAR, this could also potentially lead to high overestimation of combined exposure.

To illustrate this possibility of misclassification of exposure, let's consider a hypothetical case: the worker is exposed to two sources of different frequencies from opposite sides of the body. The maximum SAR from the first source is in the left hand, while the maximum SAR from the second source is in the right hand. The first source causes negligible exposure in the right hand and vice versa. If both SAR maxima are above one half of the basic restriction but still below the basic restriction, the classification according to the simple summation formula would indicate overexposure, even though there is no area on the body which is experiencing local SAR higher than the basic restriction. To avoid such cases we explored a voxel-by-voxel approach, wherein the summation and evaluation of the multiple-frequency formula is performed for each voxel in the human body. For the hypothetical case above, this approach would classify the exposure as compliant, since the sum of exposures from each source at any point wouldn't exceed the basic restriction.

To test these two approaches – simple summation and voxel-by-voxel summation – we first built a three dimensional model of a multi-band base station antenna and validated the electric fields and SAR values in a rectangular phantom exposed to this antenna with measured data reported in the literature (Toivonen *et al* 2009). The results of the validation (Paper 1 – Table 1) show a good agreement between the reported measurements and our numerical computations. Based on the validated model, we performed computations of exposure of a male human model in two different positions, as well as a female human model in front of the base station antenna at distances ranging from 10 mm from the front of the antenna radome to 1000 mm from the front of the radome. The results show that, for single frequency exposure, the highest investigated frequency (2100 MHz) caused the highest localized SAR. This is consistent with the fact that the penetration depth decreases with frequency, so the surface of the body absorbs a larger part of the whole delivered field energy.

Since different frequency components of the field cause different values of SAR, the final results of the combined exposure are also dependent on the ratio of radiated power from each of the studied frequencies. In the paper, we examined eight different power ratios. The results show (Paper 1 – Table 4) that the case of misclassification due to simple summation from the hypothetical case above is possible in reality even when several sources are affecting the body from the same direction. The highest overestimation percentage (of the simple summation versus the voxel-by-voxel summation) was found to be 55 %. This overestimation percentage shows that the voxel-by-voxel approach could be useful in some cases. However, the lowest percentage of overestimation was found to be only 2 %. This means that the local maxima occurred in essentially the same point. In this case it is wholly appropriate to use the simple summation approach, since the overestimation is negligible. The voxel-by-voxel approach also has an additional drawback: it requires keeping the whole computational voxel data for each human model, frequency, distance and antenna used in the evaluation. This means that it is much more practical to use the simple summation approach, even though it has the potential to cause some overestimation.

### **Exposure of children to magnetic fields from induction cookers**

The research on effects of human exposure to EMF has mostly focused on either the very low end of the frequency spectrum, where the power transmission and distribution frequencies are dominant (50 Hz in Europe and 60 Hz in North America), or at the higher frequency range where wireless communication devices are mostly located (900 MHz for GSM, 2170 MHz for 3G mobile telephony in Europe and 2450 MHz for Wi-Fi). Especially the frequency region between 1 kHz and 1 MHz remained largely uncovered by dosimetric studies. One technology operating in this frequency region is also becoming increasingly popular and common. These are induction cookers, which replace typical gas or electrical stovetops and have the additional benefits of higher efficiency and conveniently fast heating times. Although cooking is typically done by adults, it is not uncommon for children to use cooktops under supervision. This puts them into close proximity to the source of the stray magnetic fields generated by the induction cookers. Additionally, pregnant women might also use such cookers and the anatomical position of the foetus in the body, together with the standardized height of kitchen appliances puts the foetus in close proximity to the source (Paper 2 – Figure 1).

The primary aim of the paper was to find if there was any possibility of overexposure of the children or foetuses in terms of the basic restrictions of the new 2010 ICNIRP guidelines. Additionally, we wanted to investigate whether the change from the basic restriction on induced current density to the basic restriction on induced *in situ* electric fields affected the assessment and classification of exposure. The numerical model was built in SEMCAD X and validated with measurements of a commercially available

## Discussion

device (Paper 2 – Figure 2), and good agreement was obtained. The human models of two pregnant women and two children were then included in the simulation to determine the induced currents and *in situ* electric fields in the bodies. Special attention was given to the foetuses in the two pregnant women models and to the central nervous system of the 6- and 11-year old children. There were no cases of exceeded basic restrictions.

Since the rapid transitions of conductivities from one voxel to another can cause quite rapid changes in electric fields, the ICNIRP guidelines also foresee the provision for spatial averaging of the *in situ* electric fields. The fields should be averaged over a volume of  $2 \times 2 \times 2$  mm. Since this was the volume of voxels used in our simulations, averaging would yield the same number. Alternatively, the guidelines also mention the use of the 99<sup>th</sup> percentile of the *in situ* electric fields in contiguous tissues. We applied this metric to the tissues of the central nervous system of the children and the different tissues of the utero-foetal unit (including the amniotic fluid). The results (Paper 2 – Table 4) show that the 99<sup>th</sup> percentile is close to the maximum values in the internal tissues of the utero-foetal unit or the central nervous system. If it was applied to the whole body however, it would represent an excessive reduction in the field values, since the highest 1 % of the electric field exposure would include more than 0.5 kg of tissue, which is approximately one third of the adult brain. If such metric was used, it could lead to false negatives in terms of human exposure, i.e. some exposures would be classified as non-excessive, while they would in fact be above the basic restriction. To avoid this to some degree, we used the 999<sup>th</sup> per mille in the evaluation of the whole-body (as opposed to tissue-specific) exposure. This represents a more reasonable amount of tissue, while at the same time filtering some of the excessive values which are numerically determined in the skin, due to its extremely low conductivity. However, the 99<sup>th</sup> percentile and 999<sup>th</sup> per mille have the drawback that they are dependent on the volume (and consequently the number of representative voxels) of the original tissue as well as the discretization used in the simulations (Bakker *et al* 2012). To avoid this, other authors have also since proposed averaging the tissue conductivity values to smooth the rapid transitions and comparing the maximum values of the *in situ* electric field with the basic restrictions (Laakso and Hirata 2012).

Our work, while indicating that the basic restrictions were not exceeded in the cases investigated, highlighted that the device standards for induction cookers are rather lax, since they require measurements of fields at 30 cm from the front of the device. Although the appliance we used in our study passed the requirements of the standard easily, it doesn't exclude the possibility that devices with much stronger stray fields could be found on the market. The ergonomics of the typical cooking situation also require the person using the cooker to be close to the appliance in order to see into the pot

and to have a comfortable standing posture. The cases we investigated therefore do not represent the worst case, but a typical realistic usage scenario. If the users of the appliance would lean even more forward, or use inappropriate and off-centred cooking vessels, which increases the fields dramatically (Viellard *et al* 2007), they could realistically be exposed above the basic restrictions. Our results have also recently been confirmed by another research group, that reports similar values for induced electric fields in the body and shares our concerns about the industry standards (Christ *et al* 2012).

### **The role of spatial averaging of measured fields in exposure assessment**

The last EMF safety paper included in this thesis also focused on induction heating applications, albeit this time in the industrial setting. To our best of knowledge, there were no prior reports on the induced electric fields or currents in the human body exposed to such sources. One of the rare published papers in the considered frequency range gives only measured values of the external magnetic fields around induction furnaces (Floderus *et al* 2002). The power used by such machinery is often very high, and (Floderus *et al* 2002) reported measurements of furnaces in excess of 1 MW of working power. With such strong power, the magnetic fields generated can easily exceed the reference levels by one or more orders of magnitude. However, such equipment also poses other significant risks, such as dangerous fumes, risk of electric shock and very hot liquid metals, so movement in their immediate vicinity is strictly controlled. Consequently the EMF exposure is not of such concern, since the fields decrease rapidly with distance.

Our research focused on a moderately-powered application – an induction tempering furnace – with working power of only 10 kW. In contrast to high-power equipment, the studied furnace was compact and the workers have to perform their quality inspection tasks immediately next to the entrance of the tempering tunnel due to factory footprint constraints. Therefore the workers were exposed to fields which were in some places exceeding the reference levels, but highly inhomogeneous. We wanted to investigate the proposal of the 2010 ICNIRP guidelines, where spatial averaging of measurements is mentioned as an alternative to numerical dosimetry in such cases of inhomogeneous exposure (ICNIRP 2010, Jokela 2007).

Reference levels are defined in order to prevent any possibility of exceeding the basic restriction, and even though they do prevent overexposures in homogeneous fields (Bakker *et al* 2012) at low frequencies, they could be overly conservative when only parts of the body are exposed, or when exposure is inhomogeneous. In such cases, spatial averaging could be used to “relax” the reference levels, i.e. to use the spatially averaged fields for comparison with the reference levels instead of using the maximum measured values, or using numerical modelling to determine compliance with basic restrictions.

## Discussion

However, using spatial averaging introduces the risk that exposure can be misclassified. Misclassification can happen in two distinct ways. The first possible misclassification is a false positive, where exposure is classified as non-compliant (i.e. above the basic restrictions), when it is in reality compliant (i.e. below the basic restrictions). This does not present a risk, and should happen less often than with comparing the maximum measured value to the reference levels. The second possible exposure misclassification is a false negative. In such a case, the exposure is classified as compliant (i.e. safe for workers to work in) when it is in reality non-compliant (i.e. workers could experience adverse or perceptible effects).

We tested six different averaging schemes (Paper 3 – Figure 2), with different numbers of averaging points (ranging from 9 to 285) and covering either the whole body or only the torso. The averaging schemes were used to classify exposure in 15 different positions of the worker relative to the source – and therefore exposed in different parts of the body to different magnetic flux densities. The distances from the source ranged from 20 cm to 100 cm. These distances were chosen as they are the most likely distances at which spatial averaging of measured fields would be applicable. At even lower distances, spatial averaging could potentially miss important details and high exposures and could lead to too many false negatives. At distances higher than 100 cm, on the other hand, there is little need for spatial averaging as the fields are almost homogeneous, so reference levels can be used instead. The results show (Paper 3 – Table 3) that spatial averaging can reduce the measured fields by factors of up to 2 in cases of inhomogeneous exposure without causing false negatives. The averaging schemes with the most averaging points achieved reductions by factors over 5 (Paper 3 – Table 3), but on the other hand have a high likelihood of causing false negatives. This is especially pronounced in the whole-body dense averaging scheme, using arithmetic averaging, which produced false negatives in 10 % of cases. The torso reduced averaging scheme with the quadratic averaging algorithm produced no false negatives, but it did yield false positives in slightly more than 10 % of cases.

The presented work shows that spatial averaging of measured fields should not be applied indiscriminately to every measurement in the field. The averaging schemes with more than a hundred averaging points for each measurement location are in any case impractical without using some sort of automated measurement setup. This work has shown that the averaging schemes with fewer points are also more justified, since they carry a lesser risk of causing false positives. The practical application of spatial averaging would be in the cases where using administrative measures to reduce worker exposure is not possible due to technological issues. It could be used to resolve the question whether there is some possibility of overexposure in cases where measurements indicate that the maximum magnetic fields in the workers location are near or slightly above the reference levels. If the spatial average of fields in that

location is below the reference levels, the workplace can be classified as compliant. These measures could bring the benefits of reducing costs in determining workers exposure, while at the same time also reducing the industry opposition to applying binding regulations. The net result could be that workers' exposure would be more controlled even if some work would be permitted in areas with fields near the reference levels.

## Discussion of electroporation and treatment planning papers

### **Towards treatment planning**

The first paper in the electroporation treatment section presents a case where treatment planning was first developed for treatment of deep-seated tumours with electrochemotherapy. The patient had metastatic malignant melanoma, and a metastasis was detected in the thigh, so the patient was already scheduled for treatment with surgical resection. However, the patient developed high fever before the treatment and the operation had to be rescheduled. This left enough time to prepare a treatment plan and treat the patient with electrochemotherapy. Since the patient had undergone previous treatment for superficial metastases on the skin and had positive experience from the treatments, he consented to participating in the clinical study for ECT of deep seated tumours. The treatment plan was prepared by numerical computation of the electric fields in the tissue. The first feasibility studies of using numerical optimization and computation of electric fields needed to achieve successful ECT were already performed previously (Sel *et al* 2007, Corovic *et al* 2008, Županič *et al* 2008), so the main challenge was to translate the patient's medical image into a successful model and apply the optimization algorithms.

The model was built by segmenting the medical images, identifying the tumour, nearby muscles, and the surrounding adipose tissue. The skin was neglected in the model, since needle electrodes were used percutaneously, eliminating the skin boundary. The segmentation was then used to build planar contours of the tissues in every slice, by using splines with equal numbers of nodes on every slice. The contours were then vertically joined to create three-dimensional solids (Valic *et al* 2009). Electrodes were added into the model as cylinders with appropriate length and diameter. The optimization was then performed with a linear model employing no changes in conductivity for 4 and 5 electrodes. The treatment was then performed with ultrasonic guidance of electrode insertion. The surgeons encountered some issues with inserting the central electrode into the tumour, since the tumour was not firmly anchored and could not be penetrated. Therefore the treatment proceeded with only four electrodes inserted in the surrounding tissue. The treatment did achieve a partial success, with the tumour first shrinking to less

than half its original volume, but a regrowth was detected after two months, so the tumour was excised surgically.

The initial study showed that treatment of deep seated tumours with ECT was possible, and that the preparation of individualized treatment plans in short time-spans was feasible. Even before committing to it, the performing physicians can thus gain reasonable confidence in successful use of ECT for treatment of deep-seated tumours. The possibility of preparing treatment plans in a short time span between the acquisition of medical images and the treatment also allows being as accurate as possible and prevents the tumour to grow unexpectedly before the treatment.

After the treatment, we tried to identify the possible causes for the partial response of the tumour. We revisited the model and the documentation that was taken during treatment and identified that the possible cause of the tumour regrowth could be the non-complete coverage of the tumour by sufficiently high electric fields. The electrodes were inserted a few millimetres further apart than what was proposed in the treatment plan. Since the tumour was surrounded by low-conductivity adipose tissue, this likely caused the electric field in parts of the tumour to be below the reversible electroporation threshold (Paper 4 – Figure 8). These results were also one of the main motivations for the second paper in this section, where we evaluated the robustness of such treatment plans.

### **Robustness of treatment planning**

With the first applied treatment plan translated into the clinic (Paper 4), it became clear that a more detailed analysis of the robustness and practical feasibility of such treatment planning was necessary. There are several uncertainties present in the planning of the treatment, as well as errors, which can occur during implementation of the treatment. These possible errors are: uncertainties in the tissue electric properties; errors in the patient-specific model building; errors in the positioning of the electrodes during treatment; errors in the applied voltage amplitude; and finally the possibility of insufficient extracellular concentration of the chemotherapeutic drug. Electric properties of tissues are reported in the literature (Gabriel *et al* 1996, Haemmerich *et al* 2009, Gabriel *et al* 2009), albeit with the drawback that the measurements were in most cases performed on animal tissues. The data on tissue behaviour during application of electroporation pulses is even scarcer, with only few sources available (Cukjati *et al* 2007, Pavlin and Miklavcic 2008). Recently however, some very supportive data has also been published with imaging of conductivity during the application of electroporation pulses (Kranjc *et al* 2012). Errors in patient-specific model building depend on the quality of the imaging and segmentation technique and can therefore be controlled well. The errors in electrode positioning are to some degree inevitable when inserting electrodes by hand, but can be controlled by using image guidance during electrode insertion,

or could be even better controlled by using robotic equipment. The errors in applied voltage amplitude can occur due to normal tolerances of the voltage measurement circuitry in pulse generators. Another potential cause would be pulse interruptions due to unexpectedly high currents exceeding the maximum pulse generator current. In such cases, the voltage has to be reduced to allow the delivery of pulses. The concentration of the chemotherapeutic drug in the extracellular space of the tumour is also dependent on the concentration of the chemotherapeutic drug in the bloodstream and the vascularization of the tumour. The latter could be monitored pre-operatively with imaging perfusion assessments (Wang *et al* 2001, Taouli *et al* 2003).

To study the robustness, we used the same model geometry that was used in the treatment planning in of the first reported case. We upgraded the previously used numerical formulation (Paper 4) with electric field-dependent conductivity changes based on data available in published literature (Sel *et al* 2005, Cukjati *et al* 2007). The updated model was then used to check how the total coverage of the tumour is affected by small changes of each input parameter from the baseline value.

The parameter with the strongest influence on the tumour coverage was the tumour electroporation threshold (Paper 5 – Figure 4). This result is not unexpected, since the treatment plan was optimized for achieving a minimum electric field strength of 400 V/cm. If the electric field strength needed for successful electroporation is raised, large parts of the tumour will be below the threshold. However, the electric field applied by needle electrodes is highly inhomogeneous, so even with the threshold increased to 650 V/cm (an increase of over 60 %), the treatment would still achieve coverage of more than 50 % of the tumour volume. In reality, the reversible and irreversible electroporation thresholds are not discrete steps, but instead exhibit a more smoothed function of probability of electroporation versus the applied *in situ* electric field. This means that even if some areas are slightly below the electroporation threshold, a possibility that the treatment could be effective still exists.

The uncertainties in the electric conductivity of the tumour and the surrounding tissue are the second most influencing parameter. More precisely, the ratio between the conductivity of the tumour tissue versus the conductivity of the surrounding tissue is most important when electrodes are inserted also outside the tumour. This can be attributed to the voltage divider principle – since the tumours are typically much more conductive than the surrounding tissue (Haemmerich *et al* 2009), the surrounding tissue experiences a larger part of the voltage drop between the electrodes and therefore experiences stronger electric fields. The mechanism of increase of electrical conductivity during electroporation pulses mediates this effect to a certain degree, by increasing the conductivity of the surrounding tissue. To

## Discussion

mitigate the voltage divider effect to some degree, it is beneficial to insert one or more electrodes inside the tumour, since this improves the robustness, as will be shown in the final paper.

The effects of small errors in positioning of a single electrode do not have a very large impact on the total coverage of the tumour (Paper 5 – Figure 4), which is encouraging. However, when errors occur on all electrodes simultaneously, the tumour coverage drops significantly. This is caused by the increase of the surrounding layer of tissue around the tumour with lower conductivity that is treated with high fields. The requirement for accuracy of electrode insertion is therefore quite strict, requiring errors of less than 1 mm from the positions given by the treatment plan. Since it would be hard to achieve such precision without use of robotic assistants, an additional safety margin would need to be included in the treatment plans.

The final examined effects were from the uncertainty of applied voltage. The reduction of a single voltage by up to 300 volts does not cause a decrease in efficiency, while a reduction of all voltages by only 100 volts does. This is due to the fact that a majority of the tumour volume is covered by more than one set of electrodes (Paper 5 – Figure 2). Even though the baseline treatment plan used in this study was highly optimized, a small reduction in the voltage of one pair doesn't cause a dramatic drop in the effectiveness of the treatment. The usefulness of this fact has been confirmed in the following paper on the successful case of treatment of a colorectal carcinoma in the liver.

### **Treatment of liver metastasis with ECT**

The third paper in the electroporation section presents a synthesis of the work and lessons learned in the first two papers, with a successful application of patient-specific treatment planning and treatment of a metastasis in a different location – the liver. The metastasis was positioned between the *vena cava* and two main hepatic veins. Due to close proximity to the large blood vessels, surgical resection was not possible, and heat-based treatments, such as radiofrequency ablation would be defeated by the cooling effect of the large veins. The patient was treated in the scope of a clinical study (EudraCT number 2008-008290-54; ClinicalTrials.gov (NCT01264952)) at the Institute of Oncology in Ljubljana.

The treatment plan was prepared in accordance with previous work and the treatment was performed under general anaesthesia. The liver was mobilized (i.e. released from their fixed position), so the performing physician could access the metastasis from the planned direction. In contrast to the first treatment, reported in Paper 4, the treatment plan specified the insertion of two electrodes into the tumour and four electrodes around the tumour margins, but also other possibilities were considered in case the insertion of electrodes into the tumour would have turned out to be impossible. During the

operation, the insertion of two electrodes into the tumour and four electrodes in the surrounding liver tissue was successful, so electroporation pulses could be delivered. Some voltages had to be reduced, since the currents exceeded the maximum current capability of the pulse generator. Since the voltage was lowered by up to 800 V in some of the used electrode pairs, more pulses were applied to some electrode pairs. The reduction in voltage was also in part due to the electrodes being slightly closer together than given in the treatment plan and the tissue conductivity parameters being chosen very conservatively in the treatment planning stage. The final positioning of electrodes was documented photographically and by measuring the distances between them. The coverage of the tumour by electric fields was reconfirmed after the treatment also with reduced voltages and was found to have been adequate, with the entire tumour being exposed to electric fields in excess of 450 V/cm.

During the application of electroporation pulses, the pulse generator also records the real-time voltage and current waveforms. These measurements, together with the reconstructed model of the final electrode positioning and patient anatomy, allowed examining the data on the conductivity of tissues and the conductivity changes during pulse application. Although not published in the paper, the computed currents matched the measured currents to a high degree, when conductivity changes reported in earlier literature (Cukjati *et al* 2007) were used.

After a two month period, radiological examination still showed a presence of a (slightly smaller) lesion, although its viability was unknown. The patient was offered excision and accepted it. Upon histological examination, it was found that the lesion was completely necrotic, and no viable cancerous cells were found. The treatment proved that ECT can be an effective treatment in complicated difficult-to-reach cases, and can, supported by advanced treatment planning, offer a good choice for treatment of metastases.

### **Treatment planning of other electroporation based treatments and advanced visualizations**

The final paper in the electroporation section built on the previous work on numerical modelling of the electroporation phenomena and extended the algorithms and methods developed in the previous three papers. We used a model setup (Paper 7 – Figure 1) that was based on the case of the first reported patient (Paper 4). A genetic algorithm was used for optimizing electrode positions and voltages between electrodes. We also proposed different cost functions for the optimizer, which were defined to optimize either for electrochemotherapy (ECT), ablation by irreversible electroporation (IRE) or gene electrotransfer (GET).

## Discussion

For ECT, the most important part of the cost function was the coverage of the tumour with field above the *reversible* electroporation threshold, with small negative weights given to fields above the *irreversible* threshold in the tumour and in the surrounding fields. The choice of weights was based on the fact that irreversible electroporation of the tumour, while not the main endpoint, is also contributing to the final goal, namely, the destruction of the tumour. Irreversible electroporation of the surrounding tissue is inevitable to a certain extent, but can be tolerated if the neighbouring tissues are not critical. For IRE, the most important weight was given to the volume of tumour above the *irreversible* electroporation threshold.

In the case of IRE, there is no chemotherapeutic drug present that could aid in the destruction of the tumour, so the electric field needs to be strong enough to cause irreversible electroporation in the whole tumour, while still not causing the maximum currents of the electroporation device to be exceeded. As in the case of ECT, some irreversible electroporation in the surrounding tissue is inevitable, but the negative weight of the volume of external tissue meant that the optimizer favoured the reduction of the volume of healthy tissue being treated.

In the case of GET, the coverage of the entire tumour with fields above the *reversible* electroporation threshold was given the highest importance, however in this case the volume of tumour above the *irreversible* electroporation threshold was given a larger negative weight. The rationale is that the tumour cells need to take up the genes used by the therapy and survive in order to achieve gene expression. If too much of the tumour was damaged with irreversible electroporation, the gene expression could be too small to cause the desired response.

Although in this paper we considered that all treatment approaches would use the same values of pulse duration, repetition frequency and number of pulses between each electrode pair, this is not always true in practice. Particularly in the case of GET, the use of longer (5 ms to 50 ms duration) pulses is common (Andre and Mir 2004), as are combinations of high-voltage short pulses with low-voltage longer pulses (Bureau *et al* 2000, Kanduser *et al* 2009). It should be noted, that different pulse protocols have different electroporation thresholds (Pucihar *et al* 2011). The algorithms developed in this paper could also be modified to properly account for use of different electroporation protocols, without sacrificing any of the benefits of the proposed methods.

The automatic optimization of electrode positions and voltages gave very encouraging results, with the electrode positions being noticeably different between the different treatment approaches. For example, the electrodes for GET were much farther apart than electrodes for ECT and IRE (Paper 7 – Figure 3).

Although the electrode positions for ECT and IRE were very similar, the voltages were much higher in the case of IRE. In spite of that, even the highest voltages still achieved currents below the maximum current of 50 A. Although all combinations of electrodes (4, 5 or 6) managed to fulfil the main goal of the respective treatments, some electrode combinations were found to be more suitable in certain treatments than others. The differences in electric fields and electroporation achieved is best illustrated by Paper 7 – Figure 5, where it can be seen that ECT and IRE are most effective with six electrodes, where two electrodes are inserted into the tumour. These two solutions also show the smallest volume of surrounding tissue damage by irreversible electroporation. In contrast, for GET, four electrodes were the most effective at achieving uniform reversible electroporation in the tumour without causing irreversible electroporation. Due to the highly non-uniform fields around thin structures, some irreversible electroporation is inevitable around electrodes inserted into the tumour, and by moving the outside electrodes farther apart, the optimizer managed to achieve more uniform coverage of the tumour. However, by moving even farther apart, the negative weights of surrounding tissue damage would begin to dominate the cost function, so it was avoided by the algorithm.

With three-dimensional modelling, data visualization and presentation is often a challenge. The treatment planning modelling generates quite large data-sets where inter-comparison of different versions of the treatment plan is not trivial. Only giving the percentage of volume covered is a descriptive result which nevertheless loses too much information. To facilitate the presentation and human readability of the treatment plans produced by our methods, we devised several novel visualisation approaches for visualising the same data – the electric field in the target and surrounding tissues: electrode pair contribution graphs, cumulative coverage curves and electroporation cross-section images. Electrode pair contribution graphs (Paper 7 – Figure 7) show the volume fraction that each electrode pair contributes to the total coverage of the target tissue. The graphs show the relative importance of all electrode pairs included in the treatment. The cumulative coverage curves (Paper 7 – Figure 6) show the volume of each tissue covered above a certain electric field strength indicated by the horizontal axis. They enable a quick determination of volumes treated with fields above certain values and can also serve as quick references for the robustness of the treatment. Coverage progression from one electrode in the treatment is also visualized, with the coverage increasing with successive electrode pairs. The electroporation cross-section images are the most information-rich visualizations (Paper 7 – Figure 2). They represent a direct overlay of the degree of electroporation as indicated by the electric field strength with the original patient anatomical images. This visualization also allows a qualitative inter-comparison between different proposed treatment plans (Paper 7 – Figure 5). Since this visualization can be performed on each slice of the anatomical image, potential drawbacks or shortcomings of the treatment plan can be easily identified.



## Conclusion and future work

---

Numerical methods FDTD and FEM were used for determining electromagnetic fields in the human body for preventive and therapeutic applications. Human exposure to exogenous electromagnetic field has been steadily growing in the recent decades and exposure to some electromagnetic fields is inevitable. Close to the sources of electromagnetic fields, determination of the actual exposure is complicated by the complex geometries of the source, the complex patterns of electromagnetic fields in the near field and the inhomogeneity of the EMF spatial distribution. The work on safety of human exposure has built upon some issues that were not thoroughly defined in the exposure guidelines. The 2010 ICNIRP Guidelines have brought the change in the quantity used as a basic restriction at low frequencies (*in situ* electric field instead of current density used in the old Guidelines), and an increase in the reference levels for magnetic fields. Results show that the change in the basic restrictions and the reference levels didn't introduce the risk of overexposure, even where sensitive groups such as children and pregnant women are considered. Spatial averaging can also be used instead of more time- and cost-demanding numerical determination of exposure for determining exposure compliance in cases where the magnetic fields in free space are slightly above the reference levels and the magnetic fields are highly inhomogeneous. Future work will focus on determining exposures to as of now unexplored technologies, as well as on investigating exposures in different body postures. The forming of larger current loops by contact between hands and/or legs with the body is a topic that should be investigated further.

Numerical methods have also been successfully applied to the challenge of producing treatment plans for electroporation-based treatments. Numerical modelling allows for the production of robust treatment plans with automatic optimization of electrode voltages and positions, which allow the performing physicians to have confidence in the success of the treatment. This could eventually lead to more difficult cases being treated, where other options for efficacious treatment are limited. The developed methods and visualisations should also enable physicians to be less dependent on engineers and with appropriate software solutions should be able to prepare treatment plans themselves. Research on treatment planning algorithms will have to be augmented with more research into the electric properties of different tissues during the application of electroporation pulses, and into the reversible, as well as irreversible electroporation thresholds. Additionally, the goal is to progress from the threshold-based determination of electroporation to probability-based models. This should allow even more fine-tuning of the

## Conclusion

optimization algorithms and more precise prediction of treatment efficacy, and should enable the formal validation of the treatment planning approach.

## Original contributions

---

### Occupational exposure to multi-band base-station antennas

Although numerous studies investigating occupational exposure to base-station antennas have been published, none so far have specifically tackled the specifics of exposure assessment in the case of multi-band exposure from the same antenna. Multi-band base-station antennas are becoming increasingly common at transmitter sites, since they provide the network operators with a space- and cost-efficient means of operating several mobile telecommunication systems at once. I have determined the exposure due to a multi-band base station antenna at common mobile telephony frequencies (900, 1800 and 2100 MHz) using the FDTD method, and evaluated different approaches to determining the combined exposure due to the fields of different frequencies.

### Determination of exposure of sensitive groups to fields generated by induction cookers

Children in all stages of growth and development are more sensitive to various environmental factors than adults; in the case of EMFs, such sensitivity has not yet been conclusively proven, but it hasn't been disproven either. It is therefore essential that their exposure is thoroughly evaluated for different sources of EMFs, their frequencies and positions of the human body. To this end, I have performed an analysis of pre- and post-natal exposure of children to fields generated by induction cookers, which are becoming increasingly common. Using numerical modelling, induced electric fields and current densities have been determined in various tissues (the entire foetus, foetal central nervous system, uterus, placenta).

### Method for spatial averaging of measured magnetic fields

When measured values of magnetic fields in a workplace settings are above the reference levels given by the exposure guidelines, the workplace is not necessarily non-compliant. Compliance with the basic restrictions can be verified with numerical dosimetry and comparison of *in situ* induced electric fields with the basic restrictions. Since this is a difficult and time-consuming process, spatial averaging of measured fields could present a practical alternative. I have examined various spatial averaging schemes,

Original contributions

and compared their exposure classifications with computationally determined dosimetric evaluations. Results show that the use of spatial averaging in exposure assessment is justified with an appropriate choice of averaging schemes.

## Method for treatment planning of deep-seated tumours

Patient-specific anatomical models are used in electrochemotherapy treatment planning, which enables the calculation of electric field strength in the tumour and healthy surrounding tissues. To ensure treatment effectiveness, the entire target tissue needs to be covered with an electric field strength above the reversible electroporation threshold. Even when the target tissue is completely covered in the numerical model, several small errors and deviations from the plan inevitably occur during treatment delivery. Therefore it is necessary to ensure adequate robustness of the treatment plan, so that the treatment is successful despite the deviations from optimal parameters. In my work, I have evaluated the robustness of a treatment plan that has been used in a clinical setting. The sensitivity of the treatment plan to changes in the position of a single electrode, to changes in positions of all electrodes simultaneously, to the variability in electric conductivities of tissues and to errors in applied voltages have been determined and evaluated.

## Novel visualizations for electroporation-based treatment planning

Data visualization and presentation of complex three-dimensional data is challenging. Since the computational models for treatment planning of electroporation-based treatments produce such data, I have devised several novel approaches for visualising the electric fields in the target and surrounding tissues. The novel visualisations provide different points-of-view on the same data, allow easy comparisons between different solutions, and facilitate the detection of potential weaknesses of the proposed treatment plans.

## References

---

- Ackerman M J 1998 The visible human project *Proc IEEE* **86** 504–11
- Alanko T, Hietanen M and Von Nandelstadh P 2008 Occupational exposure to RF fields from base station antennas on rooftops *Ann Telecomm* **63** 125–32
- Alberts B, Bray D, Hopkin K, Johnson A, Lewis J, Raff M, Roberts K and Walter P 2009 *Essential Cell Biology* (Garland Science)
- Anderson W F 1998 Human gene therapy *Nature* **392** 25–30
- Andre F and Mir L M 2004 DNA electrotransfer: its principles and an updated review of its therapeutic applications *Gene Ther* **11** S33–S42
- Aydin D, Feychting M, Schüz J, Tynes T, Andersen T V, Schmidt L S, Poulsen A H, Johansen C, Prochazka M, Lannering B, Klæboe L, Eggen T, Jenni D, Grotzer M, Von der Weid N, Kuehni C E and Rööslı M 2011 Mobile phone use and brain tumors in children and adolescents: a multicenter case-control study *J Natl Cancer Inst* **103** 1264–76
- Bakker J F, Paulides M M, Christ A, Kuster N and Van Rhoon G C 2010 Assessment of induced SAR in children exposed to electromagnetic plane waves between 10 MHz and 5.6 GHz *Phys Med Biol* **55** 3115–30
- Bakker J F, Paulides M M, Neufeld E, Christ A, Chen X L, Kuster N and Van Rhoon G C 2012 Children and adults exposed to low-frequency magnetic fields at the ICNIRP reference levels: theoretical assessment of the induced electric fields *Phys Med Biol* **57** 1815–29
- Bibin L, Anquez J, De la Plata Alcalde J P, Boubekeur T, Angelini E D and Bloch I 2010 Whole-body pregnant woman modeling by digital geometry processing with detailed uterofetal unit based on medical images *IEEE Trans Biomed Eng* **57** 2346–58
- Bureau M F, Gehl J, Deleuze V, Mir L M and Scherman D 2000 Importance of association between permeabilization and electrophoretic forces for intramuscular DNA electrotransfer *Biochim. Biophys. Acta* **1474** 353–9
- Canè V, Botti P and Soana S 1993 Pulsed magnetic fields improve osteoblast activity during the repair of an experimental osseous defect *J Orthop Res* **11** 664–70
- Cemazar M, Jarm T and Sersa G 2010 Cancer electrogene therapy with interleukin-12 *Curr Gene Ther* **10** 300–11
- Christ A, Guldımann R, Bühlmann B, Zefferer M, Bakker J F, Van Rhoon G C and Kuster N 2012 Exposure of the human body to professional and domestic induction cooktops compared to the basic restrictions *Bioelectromagnetics* **33** 695–705

## References

- Christ A, Kainz W, Hahn E, Honegger K, Zefferer M, Neufeld E, Rascher W, Janka R, Bautz W, Chen J, Kiefer B, Schmitt P, Hollenbach H, Shen J, Oberle M, Szczerba D, Kam A, Guag J and Kuster N 2010 The Virtual Family-development of surface-based anatomical models of two adults and two children for dosimetric simulations *Phys Med Biol* **55** N23–N38
- Cooper J, Marx B, Buhl J and Hombach V 2002 Determination of safety distance limits for a human near a cellular base station antenna, adopting the IEEE standard or ICNIRP guidelines *Bioelectromagnetics* **23** 429–43
- Coray R and Krahenbuhl P 2003 EMF exposure in the vicinity of GSM - base stations *Electromagnetic Compatibility, 2003. EMC '03. 2003 IEEE International Symposium on Electromagnetic Compatibility, 2003. EMC '03. 2003 IEEE International Symposium on* vol 1 pp 398–401 Vol.1
- Corovic S, Zupanic A and Miklavcic D 2008 Numerical modeling and optimization of electric field distribution in subcutaneous tumor treated with electrochemotherapy using needle electrodes *IEEE Transactions on Plasma Science* **36** 1665–72
- Coster H G L 1965 A Quantitative Analysis of the Voltage-Current Relationships of Fixed Charge Membranes and the Associated Property of “Punch-Through” *Biophys J* **5** 669–86
- Courant R 1943 Variational methods for the solution of problems of equilibrium and vibrations *Bulletin (New Series) of the American Mathematical Society* **49** 1–23
- Cukjati D, Batiuskaite D, Andre F, Miklavcic D and Mir L 2007 Real time electroporation control for accurate and safe in vivo non-viral gene therapy *Bioelectrochemistry* **70** 501–7
- Curley S A, Izzo F, Delrio P, Ellis L M, Granchi J, Vallone P, Fiore F, Pignata S, Daniele B and Cremona F 1999 Radiofrequency ablation of unresectable primary and metastatic hepatic malignancies: results in 123 patients *Ann Surg* **230** 1–8
- Daniels C and Rubinsky B 2009 Electrical Field and Temperature Model of Nonthermal Irreversible Electroporation in Heterogeneous Tissues *Journal of Biomechanical Engineering-Transactions of the ASME* **131** Online: [http://apps.isiknowledge.com.nukweb.nuk.uni-lj.si/full\\_record.do?product=WOS&search\\_mode=GeneralSearch&qid=37&SID=R24hM5E8l0iD1FGiP51&page=1&doc=1](http://apps.isiknowledge.com.nukweb.nuk.uni-lj.si/full_record.do?product=WOS&search_mode=GeneralSearch&qid=37&SID=R24hM5E8l0iD1FGiP51&page=1&doc=1)
- Daud A, DeConti R, Andrews S, Urbas P, Riker A, Sondak V, Munster P, Sullivan D, Ugen K, Messina J and Heller R 2008 Phase I Trial of Interleukin-12 Plasmid Electroporation in Patients With Metastatic Melanoma *Journal of Clinical Oncology* **26** 5896–903
- Daz 2010 *Daz 3D Studio* (www.daz3d.com) Online: www.daz3d.com
- Dewey W 1994 Arrhenius Relationships from the Molecule and Cell to the Clinic *Int J Hyperthermia* **10** 457–83
- Donnelly J J, Ulmer J B, Shiver J W and Liu M A 1997 DNA vaccines *Annu Rev Immunol* **15** 617–48
- Duck F A 1990 *Physical properties of tissue: a comprehensive reference book* (Academic Press)

- EC 2004 Directive 2004/40/EC of the European Parliament and of the Council of 29 April 2004 on the minimum health and safety requirements regarding the exposure of workers to the risks arising from physical agents (electromagnetic fields) (18th individual Directive within the meaning of Article 16(1) of Directive 89/391/EEC) *Official Journal of the European Union* **47** 1–9
- Edhemovic I, Gadzijevec E M, Breclj E, Miklavcic D, Kos B, Zupanic A, Mali B, Jarm T, Pavliha D, Marcan M, Gasljevic G, Gorjup V, Music M, Vavpotic T P, Cemazar M, Snoj M and Sersa G 2011 Electrochemotherapy: a new technological approach in treatment of metastases in the liver *Technol Cancer Res Treat* **10** 475–85
- Floderus B, Stenlund C and Carlgren F 2002 Occupational exposures to high frequency electromagnetic fields in the intermediate range (>300 Hz-10 MHz) *Bioelectromagnetics* **23** 568–77
- Frei P, Poulsen A H, Johansen C, Olsen J H, Steding-Jessen M and Schüz J 2011 Use of mobile phones and risk of brain tumours: update of Danish cohort study *BMJ* **343** d6387
- Gabriel C, Peyman A and Grant E 2009 Electrical conductivity of tissue at frequencies below 1 MHz *Phys Med Biol* **54** 4863–78
- Gabriel S, Lau R and Gabriel C 1996 The dielectric properties of biological tissues: II. Measurements in the frequency range 10 Hz to 20 GHz *Phys Med Biol* **41** 2251–69
- Galvani L 1791 *De viribus electricitatis in motu musculari commentarius* (Bologna)
- Garcia P A, Rossmeisl J H Jr, Neal R E 2nd, Ellis T L and Davalos R V 2011 A Parametric Study Delineating Irreversible Electroporation from Thermal Damage Based on a Minimally Invasive Intracranial Procedure *Biomed Eng Online* **10** 34
- Garcia P A, Rossmeisl J H, Neal R E, Ellis T L, Olson J D, Henao-Guerrero N, Robertson J and Davalos R V 2010 Intracranial Nonthermal Irreversible Electroporation: In Vivo Analysis *J Membrane Biol* **236** 127–36
- Haemmerich D, Schutt D, Wright A, Webster J and Mahvi D 2009 Electrical conductivity measurement of excised human metastatic liver tumours before and after thermal ablation *Physiological Measurement* **30** 459–66
- Hamilton W A and Sale A J H 1967 Effects of high electric fields on micrororganisms II. Mechanism of action of the lethal effect *Biochimica et Biophysica Acta* **148** 789–800
- Hand J W 2008 Modelling the interaction of electromagnetic fields (10 MHz-10 GHz) with the human body: methods and applications *Phys Med Biol* **53** R243–R286
- Hardell L, Carlberg M and Hansson Mild K 2011 Re-analysis of risk for glioma in relation to mobile telephone use: comparison with the results of the Interphone international case-control study *Int J Epidemiol* **40** 1126–8
- Hardell L, Carlberg M, Söderqvist F, Mild K H and Morgan L L 2007 Long-term use of cellular phones and brain tumours: increased risk associated with use for > or =10 years *Occup Environ Med* **64** 626–32

## References

- Heller L and Heller R 2010 Electroporation Gene Therapy Preclinical and Clinical Trials for Melanoma *Current Gene Therapy* **10** 312–7
- Hirata A 2005 Temperature increase in human eyes due to near-field and far-field exposures at 900 MHz, 1.5 GHz, and 1.9 GHz *IEEE Trans. Electromagn. Compat.* **47** 68–76
- IARC In preparation *IARC MONOGRAPHS ON THE EVALUATION OF CARCINOGENIC RISKS TO HUMANS* vol 102 (Lyon, France: IARC Press)
- IARC 2002 *IARC MONOGRAPHS ON THE EVALUATION OF CARCINOGENIC RISKS TO HUMANS Non-Ionizing Radiation, Part 1: Static and Extremely Low-Frequency (ELF) Electric and Magnetic Fields* vol 80 (Lyon, France: IARC Press)
- ICNIRP 2010 Guidelines for limiting exposure to time-varying electric and magnetic fields (1 Hz to 100 kHz) *Health Phys* **99** 818–36
- ICNIRP 1998 Guidelines for limiting exposure to time-varying electric, magnetic, and electromagnetic fields (up to 300 GHz) *Health Phys* **74** 494–522
- ICNIRP 2009 Guidelines on limits of exposure to static magnetic fields *Health Phys* **96** 504–14
- IEEE 2006 IEEE standard for safety levels with respect to human exposure to radio frequency electromagnetic fields, 3 KHz to 300 GHz *IEEE Std C95.1-2005 (Revision of IEEE Std C95.1-1991)*
- IEEE 1992 IEEE Standard for Safety Levels With Respect to Human Exposure to Radio Frequency Electromagnetic Fields, 3 kHz to 300 GHz *IEEE Std C95.1-1991*
- IEEE 1999 IEEE Standard for Safety Levels With Respect to Human Exposure to Radio Frequency Electromagnetic Fields, 3 kHz to 300 GHz *1, 1999 Edition IEEE Std C95.1*
- INTERPHONE Study Group 2010 Brain tumour risk in relation to mobile telephone use: results of the INTERPHONE international case-control study *International Journal of Epidemiology* **39** 675 – 694
- Ivorra A, Al-Sakere B, Rubinsky B and Mir L 2009 In vivo electrical conductivity measurements during and after tumor electroporation: conductivity changes reflect the treatment outcome *Phys Med Biol* **54** 5949–63
- Jackson R 1970 Basic principles of electrosurgery: a review *Can J Surg* **13** 354–61
- Jokela K 2007 Assessment of complex EMF exposure situations including inhomogeneous field distribution *Health Phys* **92** 531–40
- Joseph W and Martens L 2005 Comparison of safety distances based on the electromagnetic field based on the SAR for occupational exposure of a 900-MHz base station antenna *IEEE Trans Electromagn Compat* **47** 977–85
- Joseph W, Verloock L and Martens L 2008 Accurate determination of the electromagnetic field due to WiMAX base station antennas *IEEE Transactions on Electromagnetic Compatibility* **50** 730–5

- Kanduser M, Miklavcic D and Pavlin M 2009 Mechanisms involved in gene electrotransfer using high- and low-voltage pulses--an in vitro study *Bioelectrochemistry* **74** 265–71
- Kheifets L, Ahlbom A, Crespi C M, Draper G, Hagihara J, Lowenthal R M, Mezei G, Oksuzyan S, Schüz J, Swanson J, Tittarelli A, Vinceti M and Wunsch Filho V 2010 Pooled analysis of recent studies on magnetic fields and childhood leukaemia *Br J Cancer* **103** 1128–35
- Kos B, Valič B, Kotnik T and Gajšek P 2011a Exposure assessment in front of a multi-band base station antenna *Bioelectromagnetics* **32** 234–42
- Kos B, Valič B, Kotnik T and Gajšek P 2012 Occupational exposure assessment of magnetic fields generated by induction heating equipment-the role of spatial averaging *Phys Med Biol* **57** 5943–53
- Kos B, Valič B, Miklavčič D, Kotnik T and Gajšek P 2011b Pre- and post-natal exposure of children to EMF generated by domestic induction cookers *Phys Med Biol* **56** 6149–60
- Kos B, Zupanic A, Kotnik T, Snoj M, Sersa G and Miklavcic D 2010 Robustness of treatment planning for electrochemotherapy of deep-seated tumors *J Membr Biol* **236** 147–53
- Kranjc M, Bajd F, Sersa I, Woo E J and Miklavcic D 2012 Ex vivo and in silico feasibility study of monitoring electric field distribution in tissue during electroporation based treatments *PLoS ONE* **7** e45737
- Laakso I 2009 Assessment of the computational uncertainty of temperature rise and SAR in the eyes and brain under far-field exposure from 1 to 10 GHz *Phys Med Biol* **54** 3393–404
- Laakso I and Hirata A 2012 Reducing the staircasing error in computational dosimetry of low-frequency electromagnetic fields *Phys Med Biol* **57** N25–34
- Levin G, Gershonowitz A, Sacks H, Stern M, Sherman A, Rudaev S, Zivin I and Phillip M 2005 Transdermal delivery of human growth hormone through RF-microchannels *Pharm Res* **22** 550–5
- Levin M 2012 Molecular bioelectricity in developmental biology: New tools and recent discoveries *BioEssays* **34** 205–17
- Mahmood F and Gehl J 2011 Optimizing clinical performance and geometrical robustness of a new electrode device for intracranial tumor electroporation *Bioelectrochemistry*
- Mali B, Jarm T, Snoj M, Sersa G and Miklavcic D 2013 Antitumor effectiveness of electrochemotherapy: A systematic review and meta-analysis *Eur J Surg Oncol* **39** 4–16
- Martinez-Burdalo M, Martin A, Anguiano M and Villar R 2005 On the safety assessment of human exposure in the proximity of cellular communications base-station antennas at 900, 1800 and 2170 MHz *Phys Med Biol* **50** 4125–37
- Maxwell J C 1873 *A Treatise on Electricity and Magnetism*
- Miklavcic D, Beravs K, Semrov D, Cemazar M, Demsar F and Sersa G 1998 The importance of electric field distribution for effective in vivo electroporation of tissues *Biophysical Journal* **74** 2152–8

## References

- Miklavčič D, Gajšek P and Vodovnik L 1999 *Vpliv neionizirnih elektromagnetnih sevanj na biološke sisteme* (Fakulteta za elektrotehniko)
- Miklavcic D, Snoj M, Zupanic A, Kos B, Cemazar M, Kropivnik M, Bracko M, Pecnik T, Gadzijevec E and Sersa G 2010 Towards treatment planning and treatment of deep-seated solid tumors by electrochemotherapy *Biomed Eng Online* **9** 8
- Mir L, Gehl J, Sersa G, Collins C, Garbay J, Billard V, Geertsen P, Rudolf Z, O'Sullivan G and Marty M 2006 Standard operating procedures of the electrochemotherapy: Instructions for the use of bleomycin or cisplatin administered either systemically or locally and electric pulses delivered by the Cliniporator (TM) by means of invasive or non-invasive electrodes *EJC Supplements* **4** 14–25
- Mir L M, Orlowski S, Belehradek J and Paoletti C 1991 Electrochemotherapy Potentiation of Antitumor Effect of Bleomycin by Local Electric Pulses *European Journal of Cancer* **27** 68–72
- Neumann E and Rosenheck K 1972 Permeability changes induced by electric impulses in vesicular membranes *Journal of Membrane Biology* **10** 279–90
- Neumann E, Schaeffer M, Wang Y and Hofschneider P H 1982 Gene-transfer into mouse lymphoma cells by electroporation in high electric-fields *EMBO J* **1** 841–5
- Pakhomov A G, Kolb J F, White J A, Joshi R P, Xiao S and Schoenbach K H 2007 Long-lasting plasma membrane permeabilization in mammalian cells by nanosecond pulsed electric field (nsPEF) *Bioelectromagnetics* **28** 655–63
- Pavliha D, Kos B, Županič A, Marčan M, Serša G and Miklavčič D 2012 Patient-specific treatment planning of electrochemotherapy: Procedure design and possible pitfalls *Bioelectrochemistry* **87** 265–73
- Pavlin M and Miklavcic D 2008 Theoretical and experimental analysis of conductivity, ion diffusion and molecular transport during cell electroporation--relation between short-lived and long-lived pores *Bioelectrochemistry* **74** 38–46
- Pelosi G 2007 The finite-element method, Part I: R. L. Courant [Historical Corner] *IEEE Antennas and Propagation Magazine* **49** 180–182
- Philips A and Lamburn G 2011 Updated study contains poor science and should be disregarded *BMJ* **343** d7899–d7899
- Piccolino M 1998 Animal electricity and the birth of electrophysiology: the legacy of Luigi Galvani *Brain Research Bulletin* **46** 381–407
- Polk C P and Postow E 1996 *Handbook of Biological Effects of Electromagnetic Fields, Second Edition* (CRC Press LLC)
- Pucihar G, Kotnik T, Miklavcic D and Teissie J 2008 Kinetics of transmembrane transport of small molecules into electropermeabilized cells *Biophys J* **95** 2837–48
- Pucihar G, Krmelj J, Reberšek M, Napotnik T B and Miklavčič D 2011 Equivalent pulse parameters for electroporation *IEEE Trans Biomed Eng* **58** 3279–88

- Reilly J P 2002 Neuroelectric mechanisms applied to low frequency electric and magnetic field exposure guidelines--part I: sinusoidal waveforms *Health Phys* **83** 341–55
- Roberts D C, Marcelli V, Gillen J S, Carey J P, Della Santina C C and Zee D S 2011 MRI magnetic field stimulates rotational sensors of the brain *Curr Biol* **21** 1635–40
- Saunders R D and Jefferys J G R 2007 A neurobiological basis for ELF guidelines *Health Phys* **92** 596–603
- Sel D, Cukjati D, Batiuskaite D, Slivnik T, Mir L M and Miklavcic D 2005 Sequential finite element model of tissue electropermeabilization *IEEE Trans Biomed Eng* **52** 816–27
- Sel D, Lebar A and Miklavcic D 2007 Feasibility of employing model-based optimization of pulse amplitude and electrode distance for effective tumor electropermeabilization *IEEE Trans Biomed Eng* **54** 773–81
- Sersa G, Miklavcic D, Cemazar M, Rudolf Z, Pucihar G and Snoj M 2008 Electrochemotherapy in treatment of tumours *European Journal of Surgical Oncology* **34** 232–40
- Setchell B P 1998 The Parkes Lecture - Heat and the testis *J Reprod Fertil* **114** 179–94
- Shi C and Xu X G 2004 Development of a 30-week-pregnant female tomographic model from computed tomography (CT) images for Monte Carlo organ dose calculations *Med Phys* **31** 2491–7
- Stämpfli R 1958 Reversible electrical breakdown of the excitable membrane of a Ranvier node *Ann Acad Brasil Ciens* **30** 57–63
- Taflove A and Brodwin M 1975 Computation of Electromagnetic-Fields and Induced Temperatures Within a Model of Microwave-Irradiated Human Eye *IEEE Trans Microw Theory Tech* **23** 888–96
- Taouli B, Vilgrain V, Dumont E, Daire J L, Fan B and Menu Y 2003 Evaluation of liver diffusion isotropy and characterization of focal hepatic lesions with two single-shot echo-planar MR imaging sequences: Prospective study in 66 patients *Radiology* **226** 71–8
- Toivonen T, Toivo T, Puranen L and Jokela K 2009 Specific Absorption Rate and Electric Field Measurements in the Near Field of Six Mobile Phone Base Station Antennas *Bioelectromagnetics* **30** 307–12
- Trock D H, Bollet A J and Markoll R 1994 The effect of pulsed electromagnetic fields in the treatment of osteoarthritis of the knee and cervical spine. Report of randomized, double blind, placebo controlled trials *J Rheumatol* **21** 1903–11
- Valic B, Gajsek P and Miklavcic D 2009 Current density in a model of a human body with a conductive implant exposed to ELF electric and magnetic fields *Bioelectromagnetics* **30** 591–9
- Viellard C, Romann A, Lott U and Kuster N 2007 *IT'IS Report: B-Field Exposure From Induction Cooking Appliances* (Zurich, Switzerland  
(<http://www.bag.admin.ch/themen/strahlung/00053/00673/03156/index.html>): IT'IS

## References

Foundation)

<http://www.bag.admin.ch/themen/strahlung/00053/00673/03156/index.html>

Online:

- Volta A 1800 On the Electricity Excited by the Mere Contact of Conducting Substances of Different Kinds. In a Letter from Mr. Alexander Volta, F. R. S. Professor of Natural Philosophy in the University of Pavia, to the Rt. Hon. Sir Joseph Banks, Bart. K. B. P. R. S. *Phil Trans R Soc Lond* **90** 403–31
- Wang Y X J, Hussain S M and Krestin G P 2001 Superparamagnetic iron oxide contrast agents: physicochemical characteristics and applications in MR imaging *Eur Radiol* **11** 2319–31
- Van Wyk M J, Bingle M and Meyer F J C 2005 Antenna modeling considerations for accurate SAR calculations in human phantoms in close proximity to GSM cellular base station antennas *Bioelectromagnetics* **26** 502–9
- Yee K 1966 Numerical solution of initial boundary value problems involving maxwell's equations in isotropic media *IEEE Trans Ant Prop* **14** 302–7
- Županič A, Čorović S and Miklavčič D 2008 Optimization of electrode position and electric pulse amplitude in electrochemotherapy *Radiol Oncol* **42** 93–101
- Zupanic A, Kos B and Miklavcic D 2012 Treatment planning of electroporation-based medical interventions: electrochemotherapy, gene electrotransfer and irreversible electroporation *Phys Med Biol* **57** 5425–40

## **Declaration**

The author hereby declares that the content of the thesis is a result of his own research work supervised by prof. Tadej Kotnik and dr. Peter Gajšek. The results, which were collected in collaboration with other colleagues, are published in the presented papers. The assistance from other colleagues is stated in the Acknowledgements. The published results of other authors are presented in the literature.

Bor Kos

## **Izjava**

Izjavljam, da sem doktorsko disertacijo izdelal sam, pod mentorstvom izr. prof. dr. Tadeja Kotnika in somentorstvom doc. dr. Petra Gajška. Rezultati, ki so nastali v sodelovanju z drugimi sodelavci, so bili objavljeni v predstavljenih člankih. Izkazano pomoč ostalih sodelavcev sem v celoti navedel v zahvali. Že objavljeni dosežki drugih avtorjev so navedeni v spisku literature.

Bor Kos